Mixed-Valency in Confacial Bioctahedral Complexes of Ruthenium and Osmium

A thesis submitted for the degree of Doctor of Philosophy of

The Australian National University

by

Brett Darren Yeomans

October 1995

Declaration

Except where specific reference is made to other sources, the work presented in this thesis is the work of the author. It has not been submitted, in whole or in part, for any other degree.

Brett Darren Yeomans

Acknowledgments

I would firstly like to thank my supervisor, Dr. Graham Heath, for his seemingly endless enthusiasm and encouragement over the past three and a half years. I would also like to thank Dr. Lucjan Dubicki for many helpful discussions and Dr. David Hockless for solving the X-ray structures. Thanks also to Dr. Richard Bramley, Dr. Paul Prenzler and Dr. Sue Boyd for recording EPR spectra, Dr. Ray Colton for the electrospray mass spectra and Stefan Lee for his help with some of the synthesis.

I am extremely grateful to Angela, John, Lynne, Paul, Rowena and Stuart for the proof reading, to Nick for keeping the computers going, and Angela and Rowena deserve special mention for all their help with bringing this thesis together in the past few days. Thanks also to everyone in the Heath group and in the RSC who have helped to make this time enjoyable, and thanks to all the members of the Total Vacuum indoor cricket team for keeping me amused on Monday nights.

Finally, I would like to thank Angela for all of her help and support, particularly in the last few weeks.

Abstract

This thesis is devoted to the synthesis, electrochemical and spectroelectrochemical characterisation of confacial bioctahedral complexes of ruthenium and osmium. The systems under study are of the form $[M_2(\mu\text{-}X)_3L_6]^z$ (z = 1+, 2+, 3+), where M_2 = Ru_2, Os_2 or RuOs, while X = Cl, Br and L = PR_3 or AsR_3. Particular emphasis is placed on characterisation of the mixed-valence state ($M_2^{II,III}$), where in principle it is possible for the unpaired electron to be shared equally between the two metal centres (delocalised) or reside preferentially on one metal (localised).

A brief introduction to mixed-valency is given in Chapter 1. Attention is then focussed on four mixed-valence systems based on this $\{M(\mu\text{-}X)_3M\}^{2+}$ (d^5d^6) core (M = Ru, Os). In particular, the confacial ruthenium "blues", $[Ru_2(\mu\text{-}X)_3L_6]^{2+}$ (L = H_2O, NH_3) are valence-delocalised systems where the visible region contains an intense $\sigma\rightarrow\sigma^*$ band (the source of the intense blue colour) together with a weaker, near-infrared $\delta_\pi\rightarrow\sigma^*$ band, where the degree of metal-metal interaction may be monitored by $\nu_{\sigma\rightarrow\sigma^*}$. The unusual spectroscopic properties of phosphine-capped diruthenium and diosmium complexes compared with their delocalised ammine-capped diruthenium "blue" analogues are highlighted.

Chapter 2 details the preparation of starting materials and the instrumental methods used to characterise products. Electrochemical and spectro-electrochemcial techniques, which are used extensively throughout this thesis, are emphasised.

Chapter 3 describes the characterisation of a series of six tertiary-arsine capped binuclear complexes, $[M_2(\mu\text{-}X)_3(AsR_3)_6]CF_3SO_3$ and a wide range of PR_3-capped analogues. A general route to these complexes from $K_3[Ru_2Cl_9]$ or $K_3[Ru_2Br_9]$ is described. Voltammetric studies show that stepwise reversible one-electron oxidations connect the

$Ru_2^{II,II}$ (d^6d^6 = 12-e) resting state with the d^5d^6 (11-e) and d^5d^5 (10-e) levels. The mixed-valence $[Ru_2(\mu\text{-}X)_3L_6]^{2+}$ species may be characterised by electrogeneration in CH_2Cl_2 at -60 °C. Unexpectedly, the AsR_3-capped complexes are found to be in the same electronic and optical mould as classical ruthenium "blues", where L = NH_3 or H_2O. The distinctly different spectral appearance of the familiar PR_3-capped mixed-valence compounds has been a long-standing puzzle, but the present investigation reveals that the entire family of binuclear systems with various PR_3 or AsR_3 terminal ligands are delocalised and belong within a continuum of electronic behaviour, with the metal-metal interaction decreasing progressively ($\nu_{\sigma\rightarrow\sigma^*}$ varies from 18 000 cm^{-1} to 5000 cm^{-1}) in the $\{Ru(\mu\text{-}X)_3Ru\}^{2+}$ series.

Chapter 4 describes the properties of the 12-e, 11-e and 10-e states of the analogous PR_3-capped diosmium complexes, $[Os_2(\mu\text{-}X)_3(PR_3)_6]^z$. In addition, a series of mixed-metal $[RuOs(\mu\text{-}X)_3(PR_3)_6]^+$ compounds have been prepared, which can be oxidised to the valence-trapped $\{Ru^{II}Os^{III}\}^{2+}$ state. The spectroscopic properties of the mixed-valence $\{Os_2\}^{2+}$ complexes resemble those of the $\{Ru^{II}Os^{III}\}^{2+}$ complexes and are in sharp contrast to their diruthenium analogues, leading us to assign the diosmium complexes as electronically trapped $\{Os^{II}Os^{III}\}^{2+}$ systems.

A series of monomeric complexes, $[MX_{6-n}L_n]^z$ (L = PR_3, AsR_3; n = 2-5), are described in Chapter 5. These complexes are important because of their relationship to the binuclear complexes, and are also of interest in their own right, particularly in terms of the concept of ligand additivity. This is the first report of $[MClL_5]^+$ (M = Ru, Os; L = $AsMe_3$). Trends in the electronic properties (redox and optical behaviour) are discussed, and the limitations of current ligand-additivity models are examined.

Table of Contents

List of Tables

List of Figures

CHAPTER ONE

Introduction

1.1 GENERAL

This study involves the synthesis, and the electrochemical and spectro-electrochemical characterisation of confacial bioctahedral complexes of ruthenium and osmium. Binuclear complexes of the type $[M_2(\mu\text{-}X)_3(PR_3)_6]^+X^-$ (M = Ru, Os; X = Cl, Br) (Fig. 1.1) were first recognised and reported in 1961 by Chatt and Hayter.[1] A variety of complexes of the same basic structure have since been prepared.[2] These complexes consist of two octahedra sharing one face, hence the metal centres are bridged by three groups. For ruthenium in particular, a wide family of compounds with this basic structure exists. These bridging groups are usually small anionic moieties such as halide (X^-), OH^- or OR^-. Complexes with terminal ligands (L) such as X^-, NH_3, H_2O, PR_3 and AsR_3 have been prepared, as well as complexes with a mixed set of six terminal ligands, with one or more CO, CS or halide ligands replacing PR_3, *e.g.* $[M_2(\mu\text{-}X)_3X_{6-n}(PR_3)_n]^z$.

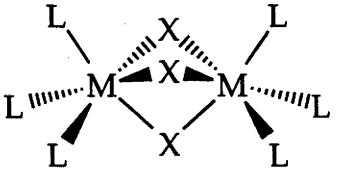

Figure 1.1 *General structure of a confacial bioctahedral complex,* $[M_2(\mu\text{-}X)_3L_6]^z$.

Complexes where the terminal ligands are X^-, NH_3 and H_2O tend to stabilise the $\{M(\mu\text{-}X)_3M\}^z$ unit in higher oxidation states, whereas ligands such as PR_3, AsR_3, CO,

CS and arenes stabilise the core in the closed-shell (d^6d^6) bis-divalent $\{M(\mu\text{-}X)_3M\}^+$ state. The systems under study in this thesis are of the form $[M_2(\mu\text{-}X)_3L_6]^z$ (z = 1+, 2+, 3+), where $M_2 = Ru_2$, Os_2 or RuOs, while X = Cl, Br and L = PR_3 or AsR_3.

These confacial bioctahedral systems are one of many diverse types of binuclear complexes. Some examples of the range of binuclear coordination include: complexes with unsupported metal-metal bonds, such as $[Re_2Cl_8]^{2-}$,[3] metal-metal bonded complexes held together by bidentate "strapping ligands", such as $[Cr_2(O_2CCH_3)_4]$,[4] complexes linked by a single bridging ligand, such as the pyrazine-bridged Creutz-Taube ion, $[(NH_3)_5Ru(\mu\text{-pz})Ru(NH_3)_5]^{5+}$ (pz = pyrazine),[5] and complexes with two metal centres linked by two or three monatomic ligands, such as edge-sharing $[Os_2X_{10}]^{2-}$ [6,7] and face-sharing M_2X_9 complexes.[8]

Many binuclear complexes display rich redox chemistry and unusual optical and magnetic properties, much of which can be attributed to the interaction of the metal centres. Some binuclear complexes have found uses as catalysts (such as $[Ru_2(\mu\text{-}Cl)_3Cl_2(PP)_2]$ complexes, where PP is a bidentate phosphine ligand, which have been investigated as hydrogenation catalysts)[9] and as models for active sites of enzymes (such as manganese, iron, iron-sulfur and copper proteins).[10-15] Importantly, their bimetallic constitution is at least partially responsible for the chemistry of these different systems and in many cases, the interesting electronic properties arise in the mixed-valence state.

1.2 MIXED-VALENCY

A significant aspect of the chemistry of bimetallic complexes is mixed-valency, which is the term used to describe compounds containing ions of the same element in two different formal oxidation states. This includes systems where individual ions are present

in distinct, different oxidation states and complexes where ions have an averaged valency due to electron delocalisation. The properties of mixed-valence compounds include those of the individual constituents and those emanating from the interaction of the metal centres. The most obvious effect of metal-metal interaction is the intense colour of many mixed-valence compounds, a phenomenon which cannot be attributed to a combination of the individual absorption spectra of the mononuclear species. An example of this, and one of the first man-made mixed-valence compounds, is "Prussian Blue", $K[Fe^{III}Fe^{II}(CN)_6]$, which was used in pigments and inks since its synthesis early in the 18th Century.[16] Prussian Blue is formed by mixing aqueous solutions of ferric and ferrocyanide ions[17] and contains the Fe^{III}-NC-Fe^{II} linkage.[18] Its intense blue colour is a property which cannot be attributed to the individual Fe^{II} or Fe^{III} complexes.

In 1967 separate articles by Allen and Hush[19] and Robin and Day[20] reviewed the physical properties of mixed-valence compounds, and mixed-valency has been the subject of several subsequent reviews.[21-23] Robin and Day developed a classification scheme based upon the symmetry and strength of the ligand fields about the metal ions.[20] This scheme divides mixed-valence compounds into three classes depending on the degree of mixing of the states:

• Class I systems have trapped valencies, *e.g.* $A^{II}B^{III}$. Sites A and B experience different symmetries and ligand field environments, and conversion from one state to the other requires substantial reorganisation of the structure about both ions. Compounds of this kind have properties which are essentially a superposition of those of A^{II} and B^{III} taken separately. One example of a class I material is $GaCl_2$, which contains a mixture of non-interacting Ga^{I} and Ga^{III} centres.[24]

• Class III systems are delocalised. In such complexes the symmetry and ligand environment of the two states are identical, and such complexes usually have different properties from the component monomers. The Creutz-Taube ion, $[(NH_3)_5Ru(\mu\text{-pz})Ru(NH_3)_5]^{5+}$, despite differing opinions as to whether it is a class II or

class III system, has ultimately proved to be an example of a delocalised mixed-valence complex.[23]

• Class II is an intermediate classification. Delocalisation does occur to some extent, but the two types of site (A and B) are still physically distinguishable on some specified experimental timescale. An example of a class II complex is Prussian Blue.[25]

The most conspicuous property of many mixed-valence compounds is the low energy optical absorption bands responsible for their colour. These transitions are not observed in the spectra of individual monomer units, and in electronically trapped systems they are attributed to an electron transfer from one metal site to another in an intervalence charge-transfer (IVCT) process, as shown in Fig. 1.2:

$$e.g.\ [A^{II}B^{III}]_o \rightarrow [A^{III}B^{II}]^*$$

where the photogenerated $[A^{III}]^*$ centre is in the environment of $[A^{II}]_o$ (and similarly $[B^{II}]^*$ retains the $[B^{III}]_o$ environment).

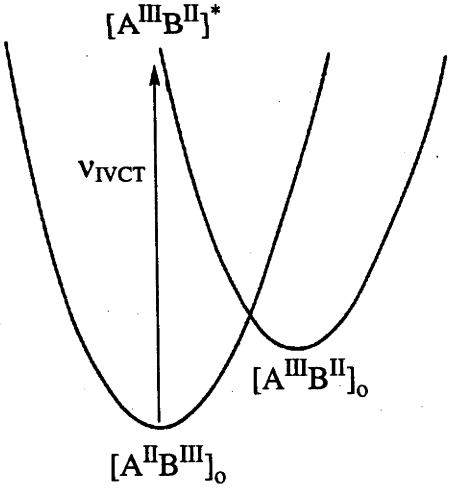

Figure 1.2 *Potential energy curves for an asymmetric mixed-valence complex showing the intervalence charge-transfer transition (ν_{IVCT}) which transfers an electron from A to B. The horizontal axis represents the reaction coordinate connecting $[A^{II}B^{III}]$ and $[A^{III}B^{II}]$ states.*

For class I species, this process is likely to be high in energy as each coordination site is distinctly unsuited to the metal ion of altered valency (*i.e.* $[A^{III}B^{II}]_o$ lies at higher energy than $[A^{II}B^{III}]_o$). In addition, the lateral displacement of the potential energy

curves means that the vertical transition is strongly augmented by the "reorganisation energy" that will be released thermally as $[A^{III}B^{II}]^*$ relaxes to $[A^{III}B^{II}]_o$. In other words, the IVCT transition leads to a strongly vibronically excited $[A^{III}B^{II}]^*$ state.

Class II species have two metal ions in similar environments, which in the limiting case of identical ligand sets for sites A and B may be differentiated only by the valency of the metal ion (*e.g.* A^{II} or B^{III}) and by the associated difference in coordination geometry for these sites. This leads to a smaller or zero energy difference between $[A^{II}B^{III}]_o$ and $[A^{III}B^{II}]_o$, hence a lower energy IVCT band results, generally in the visible/near-IR range, which gives the colour to many mixed-valence complexes.

For class III compounds, where the two metal sites are indistinguishable and strongly interacting, a molecular orbital approach is appropriate. The characteristic spectral features now arise from transitions within the binuclear molecular orbital manifold. Each of these orbitals is distributed symmetrically over A and B so the optical transitions no longer involve literal charge-transfer from site A to site B. Nevertheless, in many descriptions the term "IVCT" persists.

The IVCT absorption process for class II systems was discussed in a qualitative model proposed by Hush,[26,27] in which the Marcus theory of intermolecular electron transfer[28-30] was applied to intervalence transitions. Subsequent models for mixed-valence systems have also been developed by Piepho, Krausz and Schatz.[31,32] For weakly interacting systems these models are able to account for characteristic features of IVCT bands, such as their shift in energy depending upon solvent properties and their broad, low-intensity Gaussian profile.

As noted at the outset, the binuclear ruthenium and osmium compounds studied in this thesis have two octahedra fused by a face (the triple-halide bridge) and bearing six terminal "capping" ligands (Fig. 1.1). A survey follows (§1.3 to 1.6) of mixed-valency

in four distinct families of complexes based on this 11-e (d^5d^6) $\{M(\mu\text{-}X)_3M\}^{2+}$ structural core.

1.3 RUTHENIUM "BLUES", $[Ru_2(\mu\text{-}X)_3L_6]^{2+}$ (L = H_2O, NR_3)

Blue solutions of ruthenium have been observed since 1804,[33,34] when de Fourcroy and Vaquelin observed that a blue solution formed when certain solutions of known platinum metals were treated with zinc, although the metal "ruthenium" was not known at the time. In 1846, Claus, after discovering ruthenium metal earlier the same decade, demonstrated that the blue colour observed in 1804 was characteristic of ruthenium chemistry.[35]

The blue solutions have since been formed by the reduction of aqueous or ethanolic solutions of Ru^{III} or Ru^{IV} halides.[36-39] In 1959, Russian workers suggested that the blue colours obtained upon reduction of solutions of Ru^{IV} were due to Ru^{III} in the presence of lower oxidation states of ruthenium,[40] but later Ru^{II} chloride complexes were implicated.[41,42] Rose and Wilkinson obtained a precipitate formulated as $[Ru_5Cl_{12}]^{2-}$ from blue ruthenium solutions,[43] however the authors were unable to account for the paramagnetism and EPR signal observed for this complex, and stated the formulation was not consistent with a complex containing only Ru^{II}.

It was not until 1971 that Mercer and Dumas separated three blue complexes, of stoichiometry $Ru_2Cl_3^{2+}$, $Ru_2Cl_4^{+}$ and Ru_2Cl_5, from electrochemical reduction of $K_2[RuCl_5(H_2O)]$ in acidic solution.[44] The visible spectra of all three species were remarkably similar in band shape and position, with absorption maxima of the bands responsible for the blue colour ranging from 15 500 cm^{-1} to 16 600 cm^{-1}. Potentiometric titrations and polarography confirmed that the blue complexes contained both Ru^{II} and Ru^{III}, and magnetic data were consistent with one unpaired electron per two ruthenium

centres. On the basis of their experimental data, and comparisons with known $\{Ru(\mu\text{-}Cl)_3Ru\}^{2+}$ complexes such as $[Ru_2Cl_5(PR_3)_4]$,[45,46] Mercer and Dumas correctly formulated the blue complexes as triply-chloro bridged mixed-valence (2 x $Ru^{2.5+}$) complexes, with H_2O ligands completing the octahedral coordination about each metal (Fig. 1.3).†

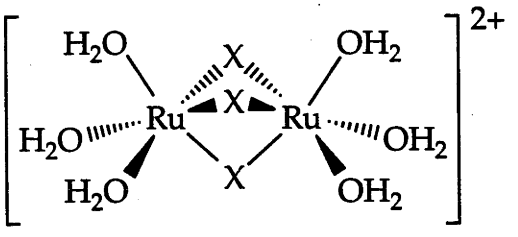

Figure 1.3 *Structure of the simplest of three "blue" ruthenium-aquo complexes (x = 0).*

Blue solutions have also been formed by the action of concentrated acid on Ru^{II} complexes containing nitrogen donor ligands. Lever and Powell isolated a blue solid from the reaction of $[Ru^{II}(NH_3)_6][ZnCl_4]$ with HCl, which they formulated as a monomeric species, $[Ru^{III}Cl_2(NH_3)_3(H_2O)]Cl$,[47] but suggested that a polynuclear species was responsible for the blue colour. Bottomley and Tong isolated the same compound by this procedure and showed evidence of halide-bridging and mixed oxidation states.[48] They suggested a binuclear complex with a single halide bridge, $[(NH_3)_3Cl_2Ru(\mu\text{-}Cl)RuCl(NH_3)_3(H_2O)]Cl$.

However, recognising the relationship with $[Ru_2(\mu\text{-}Cl)_3(H_2O)_6]^{2+}$, Mercer and Gray formulated the blue solid as $[Ru_2(\mu\text{-}Cl)_3(NH_3)_6]^{2+}$,[49] in accord with comprehensive analytical, electrochemical, magnetic and spectroscopic data. Supporting evidence for the postulated structure included the observation that the chloride complex decomposed to *fac*-$[RuCl_3(NH_3)_3]$,[49,50] identification of the 2+ charge by ion-exchange, isolation of salts with anions $2I^-$,[50] $[ZnCl_4]^{2-}$ [50] and $[ZnBr_4]^{2-}$,[51] and analysis of vibrational spectra based on D_{3h} symmetry.[51] The X-ray structures of the chloro[52] and

† The three aquo complexes were $[Ru_2(\mu\text{-}Cl)_3Cl_x(H_2O)_{6-x}]^{(2-x)+}$, where x = 0 to 2.

bromo[53] bridged complexes have since been determined, confirming the triply-bridged confacial bioctahedral structure (Fig. 1.4).

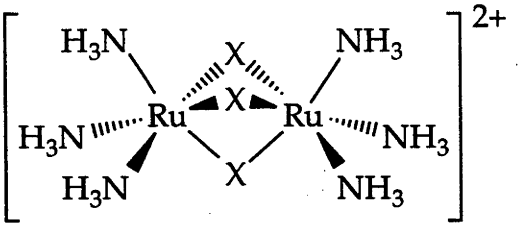

Figure 1.4 *Structure of "blue" ruthenium-ammine complexes,* $[Ru_2(\mu\text{-}X)_3(NH_3)_6]^{2+}$.

The electrochemical properties of these complexes were first investigated using polarography,[49] where an oxidation wave was found for $[Ru_2Cl_3(NH_3)_6]Cl_2$ in aqueous solution. The preparation of an organo-soluble salt of the dication has since permitted voltammetry in thf and CH_3CN.[54] Two redox processes were observed, these being a one-electron oxidation to $\{Ru^{III}(\mu\text{-}Cl)_3Ru^{III}\}^{3+}$, reversible at low temperatures, and a one-electron reduction to the $\{Ru^{II}(\mu\text{-}Cl)_3Ru^{II}\}^{+}$ state, which was not fully reversible, even at reduced temperatures. The separation between these two couples was relatively large (see below) at 1.23 V.

The spectroscopic properties of $[Ru_2X_3(NH_3)_6]^{2+}$ have been extensively studied, including UV/Vis/near-IR,[55] magnetic circular dichroism,[56] EPR[56] and Resonance Raman[57,58] measurements. The most striking feature of the complexes is the presence of a strong electronic band in the visible region, the source of their intense blue colour. A less intense band has also been detected in the near-infrared region. These two bands have been assigned to transitions between binuclear molecular orbitals resulting from the interaction of the t_{2g}-derived orbitals of the two ruthenium centres. The appropriate molecular orbital scheme for a confacial bioctahedral structure of D_{3h} symmetry is shown in Fig. 1.5.[59-62] The two allowed optical features have been assigned as an intense z-polarised $\sigma \rightarrow \sigma^*$ transition occurring near 18 000 cm^{-1}, and a less intense xy-polarised

$\delta_\pi^* \rightarrow \sigma^*$ transition near 7000 cm^{-1}.[55-58] The significance of the δ_π, δ_π^* terminology[8] is that the orbitals have 2/3 δ bonding character and 1/3 π character (Fig. 1.5).

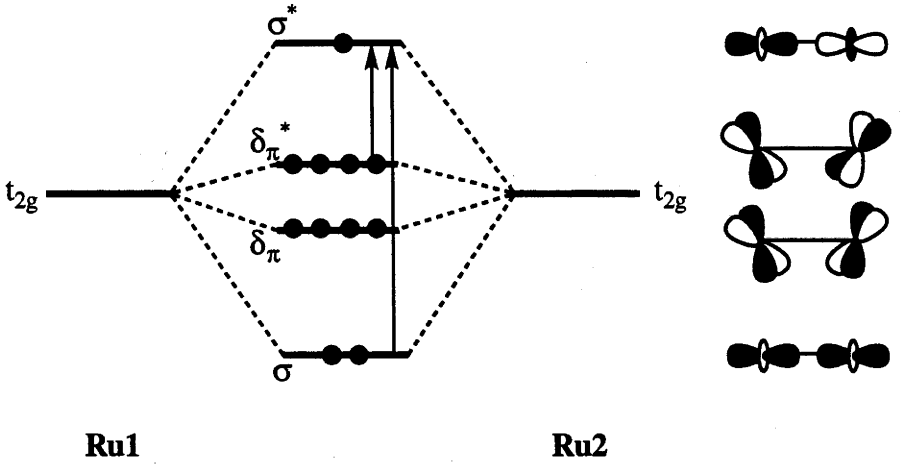

Figure 1.5 *MO scheme and expected transitions for a D_{3h} confacial bioctahedral complex.*

Similar complexes have been prepared by Wieghardt *et al*, using the cyclic tri-amines 1,4,7-triazacyclononane (tacn)[63] and 1,4,7-trimethyl-1,4,7-triazacyclononane (Me_3tacn)[64] as facial tridentate ligands (*e.g.* $[Ru_2(\mu\text{-}Cl)_3(Me_3tacn)_2]^{2+}$). These mixed valence systems are electronically delocalised with very similar properties to their NH_3 analogues. These highly characteristic bands for a typical "blue" complex are shown in Fig. 1.6.

In addition, Armstrong and Clucas have recently undertaken a systematic structural study of a series of tacn and Me_3tacn complexes, recording the electronic and Resonance Raman spectra, and obtaining X-ray crystal structures of $[Ru_2(\mu\text{-}X)_3(tacn)_2]^{2+}$ (X = Cl, Br, I) and $[Ru_2(\mu\text{-}X)_3(Me_3tacn)_2]^{2+}$ (X = Cl, Br).[65]

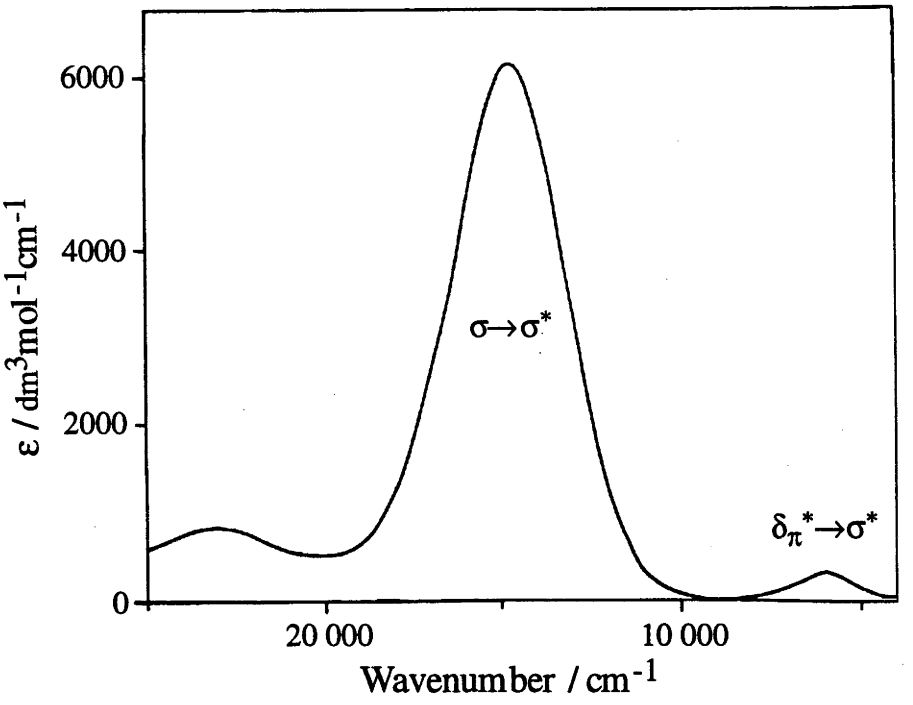

Figure 1.6 *Visible/near-IR spectrum of* $[Ru_2(\mu\text{-}Cl)_3(Me_3tacn)_2]^{2+}$, *with* $\sigma\rightarrow\sigma^*$ *and* $\delta_\pi{}^*\rightarrow\sigma^*$ *bands.*

1.4 MIXED-VALENCE NONAHALIDES, $[Ru_2(\mu\text{-}X)_3X_6]^{4-}$

Unlike the ruthenium blues described above, the diruthenium nonahalides, $[Ru_2(\mu\text{-}X)_3X_6]^{3-}$ (X = Cl, Br; Fig. 1.7),[66-70] are naturally found in the $Ru_2^{III,III}$ state and initially isolated as acid-soluble potassium salts. Their chemical development commenced with conversion to alkyl ammonium and phosphonium salts which are soluble in organic solvents.

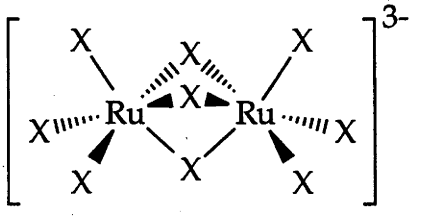

Figure 1.7 *Structure of the ruthenium nonahalides,* $[Ru_2(\mu\text{-}X)_3X_6]^{3-}$.

In 1983 Coombe *et al* investigated the electrochemistry of the nonahalides, observing two oxidations and one reduction, and electrogenerated the oxidised $\{Ru_2^{III,IV}\}^{2-}$ and $\{Ru_2^{IV,IV}\}^{-}$ states.[67] Since then, Kennedy, Heath and Khoo[69], using *in situ* spectro-electrochemical techniques, have reduced $[Ru_2Cl_9]^{3-}$ and $[Ru_2Br_9]^{3-}$ at low temperatures in CH_2Cl_2, leading to the formation of intense blue solutions of the $[Ru_2X_9]^{4-}$ ions, whose UV/Vis/near-IR spectra could be recorded. These electronic spectra of the mixed-valence (d^5d^6) species are dominated by two strong bands in the visible region ~15 000 cm^{-1} (containing the $\sigma \rightarrow \sigma^*$ transition) and a much weaker near-IR absorption near 5000 cm^{-1} ($\delta_\pi^* \rightarrow \sigma^*$), as seen in Fig. 1.8. The second feature, near 15 000 cm^{-1}, was assigned as a d-d type ($\sigma^* \rightarrow \pi^*$) transition. The resemblance to the ammine "blues" (Fig. 1.6) is evident.

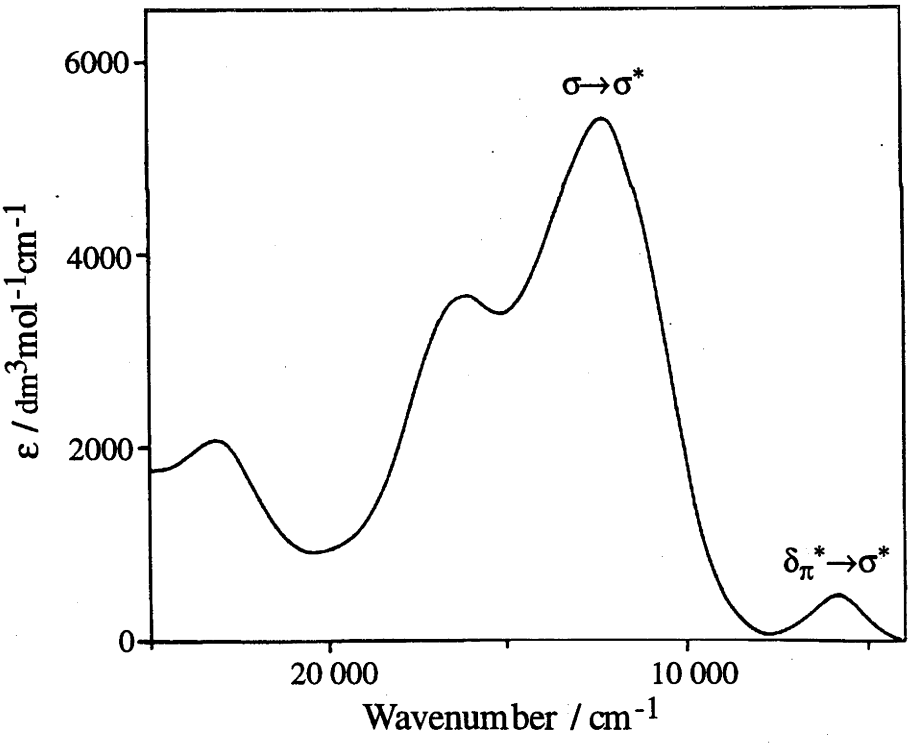

Figure 1.8 *Visible/near-IR spectrum of* $[Ru_2(\mu\text{-}Cl)_3Cl_6]^{4-}$, *showing the* $\sigma \rightarrow \sigma^*$ *and* $\delta_\pi^* \rightarrow \sigma^*$ *bands.*

1.5 MIXED-VALENCE $[Ru_2(\mu\text{-}X)_3(PR_3)_6]^{2+}$ COMPLEXES

Well before there was any knowledge of the existence of the $[Ru_2X_9]^{3-}$ ($Ru_2^{III,III}$) or "blue" $[Ru_2(\mu\text{-}X)_3(NH_3)_6]^{2+}$ ($Ru_2^{II,III}$) complexes, triply-chloride bridged phosphine-capped complexes of the form $[Ru_2(\mu\text{-}Cl)_3(PR_3)_6]^{+}$ (Fig. 1.9) were recognised by Chatt and Hayter.[1]

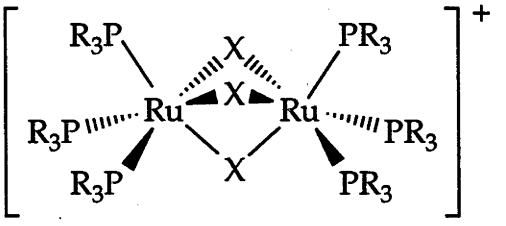

Figure 1.9 *Structure of $[Ru_2(\mu\text{-}X)_3(PR_3)_6]^{+}$ complexes.*

When isolated initially as chloride salts, the compounds had stoichiometry $RuCl_2(PR_3)_3$, but the confacial bioctahedral structure was deduced unerringly from molecular weight and conductivity measurements. It was also found that only 1/4 of the chlorides in these diamagnetic complexes could be readily exchanged for BPh_4^- or ClO_4^-. These observations were not consistent with possible alternative structures for the binuclear stoichiometry, such as edge-sharing $[Ru_2Cl_4(PR_3)_6]$ itself, $[Ru(PR_3)_6][RuCl_4]$ or $[Ru(PR_3)_4][RuCl_4(PR_3)_2]$. There have since been numerous preparations of complexes of this type with terminal phosphine or phosphite-type ligands (Fig. 1.10).

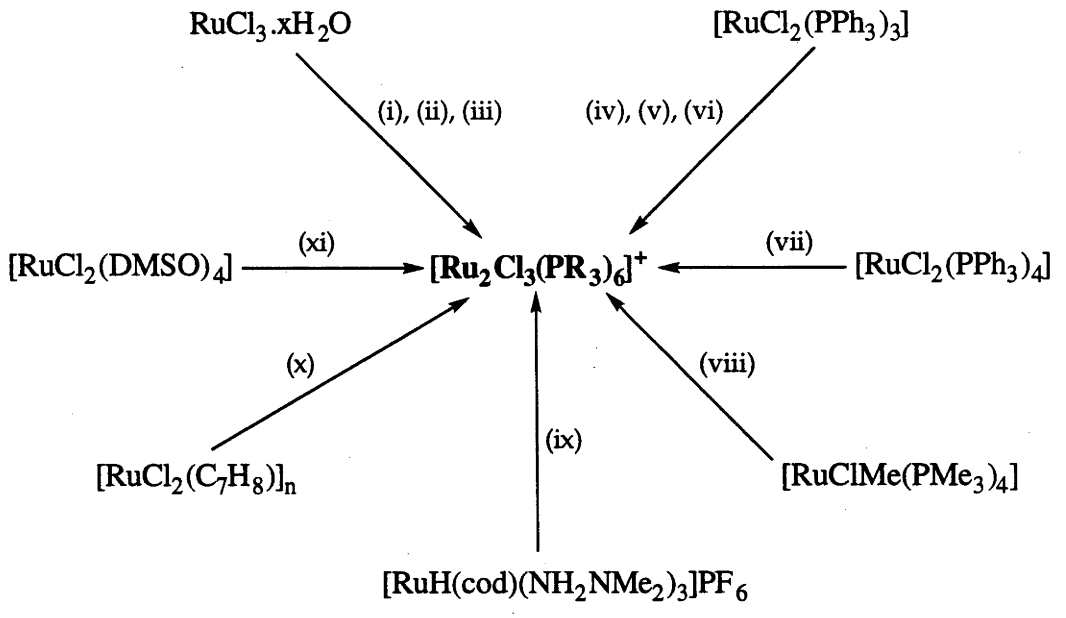

Figure 1.10 *Literature Routes to $[Ru_2(\mu\text{-}Cl)_3(PR_3)_6]^+$ Complexes: (i) Boiling MeOH; PR_3 = PMe_2Ph, PEt_2Ph, $PMePh_2$, $PEtPh_2$.*[1] *(ii) Boiling 2-MeOEtOH; PR_3 = PEt_3, PPr_2Ph, PBu_2Ph.*[71] *(iii) Boiling EtOH; PR_3 = $P(OEt)_3$, $P(OEt)_2Ph$.*[72] *(iv) Boiling hexane to prepare $[RuCl_2(PR_3)_4]$, then dissolved in polar solvent; PR_3 = $P(OMe)_2Ph$, $P(OMe)Ph_2$, $P(OEt)Ph_2$.*[73] *(v) Boiling benzene; $(PR_3)_3$ = ETP (bis(2-(diphenylphosphino)ethyl)phenylphosphine).*[74] *(vi) Boiling EtOH; PR_3 = PMe_2Ph, PEt_3, PEt_2Ph, $PEtPh_2$, $P(OMe)Ph_2$; $(PR_3)_3$ = triphos (1,1,1-tris((diphenylphosphino)methyl)ethane).*[75] *(vii) Boiling EtOH or CH_2Cl_2; PR_3 = PMe_2Ph, PEt_2Ph, $PEtPh_2$.*[76] *(viii) +$AgBF_4$ in thf; PR_3 = PMe_3.*[77] *(ix) $CHCl_3$ or EtOH; PR_3 = PMe_2Ph.*[78] *(x) Boiling MeOH; PR_3 = $P(OMe)_2Ph$, $P(OEt)_2Ph$, $P(OMe)Ph_2$, $P(OEt)Ph_2$.*[79] *(xi) Boiling toluene; $(PR_3)_3$ = triphos,*[80] *ETP.*[74]

Heath and Stephenson first investigated the redox activity of the $[L_3Ru(\mu\text{-}X)_3RuL_3]^z$ assembly, examining complexes containing soft terminal ligands such as phosphines and arsines.[81] They proposed that as a class such systems may undergo two successive metal-based one-electron transfers. Subsequent work has established a wealth of redox activity associated with the $\{Ru(\mu\text{-}X)_3Ru\}^z$ core, with oxidation states ranging from $Ru^{II}Ru^{II}$ (d^6d^6) to $Ru^{IV}Ru^{IV}$ (d^4d^4).[67,75,82-85] The relationship of the $[Ru_2(\mu\text{-}X)_3(PR_3)_6]^+$ complexes to the diruthenium nonahalides and to intermediate complexes $[Ru_2(\mu\text{-}Cl)_3Cl_{6-n}L_n]^z$ (L = PEt_2Ph, As(*p*-tol)$_3$)[83] is shown in Fig. 1.11, where the $Ru_2^{(III,III\rightarrow II,III)}$ and $Ru_2^{(II,III\rightarrow II,II)}$ redox processes (and their mean) are plotted against stoichiometry. Replacing the six terminal halides by phosphines has the effect of shifting the redox processes by ~2.5 V. The separation between the two

oxidations for $[Ru_2(\mu\text{-}X)_3(PEt_2Ph)_6]^+$ (on the extreme right of Fig. 1.11) is less than half the 1.2 V observed for the ruthenium "blues".

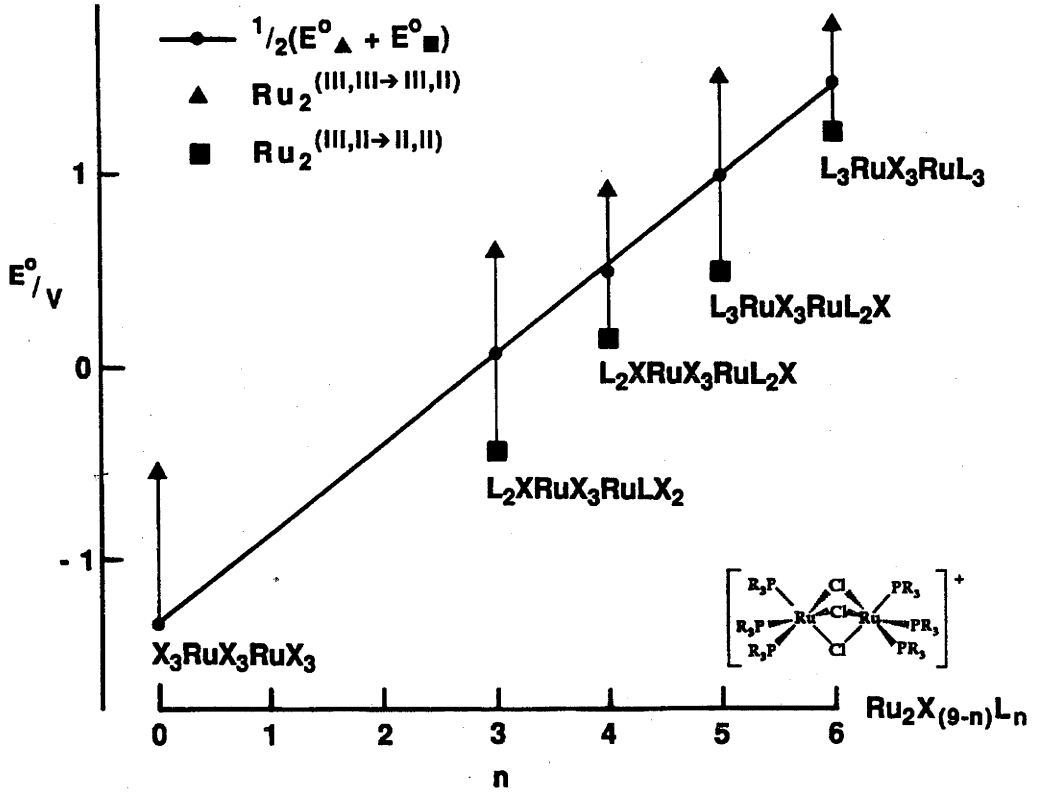

Figure 1.11 *A plot of the mean of the $d^5d^5 \rightarrow d^5d^6$ and $d^5d^6 \rightarrow d^6d^6$ redox processes vs n, in $[Ru_2(\mu\text{-}Cl)_3Cl_{6-n}L_n]^z$* complexes. *The indicated "mean" for the nonahalide arises only by extrapolation, as the second reduction has not been detected.*

In 1982 Heath *et al* electrogenerated a series of $[L_{3-x}Cl_xRuCl_3RuCl_yL_{3-y}]^z$ (L = soft neutral ligand) complexes in successive oxidation states and recorded the UV/Vis/near-IR spectra.[83] At the mixed-valence $Ru^{II}Ru^{III}$ level, for species such as $[Ru_2Cl_3(PEt_2Ph)_6]^{2+}$, they observed characteristic near-IR bands which were absent in the $Ru^{II}Ru^{II}$ and $Ru^{III}Ru^{III}$ systems, and pointed out the link with the classical "blue" complexes. For the asymmetrically halide-substituted complexes ($y \neq x$), the mixed-valence state is a localised $Ru^{II}Ru^{III}$ system, with the Ru^{III} centre being the one bearing the most halide ligands. The mixed-valence near-IR bands correspond to an IVCT process, *i.e.* $[Ru_a^{II}Ru_b^{III}] \rightarrow [Ru_a^{III}Ru_b^{II}]^*$. For the symmetrically substituted complexes ($y = x$) two bands were observed in the near-IR region, an "intervalence" band

and a second band at higher energy whose position appeared to parallel the degree of interaction between the metal centres.

A large number of $[Ru_2(\mu\text{-}X)_3(PR_3)_6]^{2+}$ complexes have since been electrochemically generated and their near-IR spectra recorded.[75,86] In all of these complexes two bands (ν_1 and ν_2 in Fig. 1.12) have been observed at low energy, typically in the region 4000 - 8000 cm^{-1}.

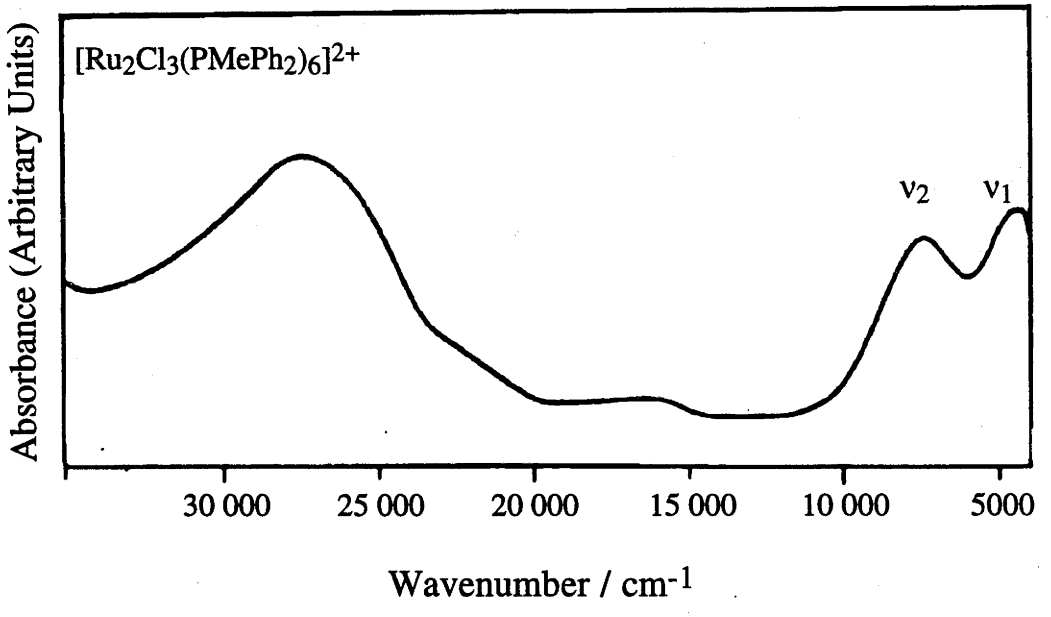

Figure 1.12 *Visible/near-IR spectrum of* $[Ru_2(\mu\text{-}Cl)_3(PMePh_2)_6]^{2+}$, *recorded in* CH_2Cl_2 *containing* $[Bu^n_4N][BF_4]$ *(0.5 mol* dm^{-3}*) at 213 K.*

The two near-IR bands have been assigned as the $\sigma \rightarrow \sigma^*$ and $\delta_\pi^* \rightarrow \sigma^*$ transitions associated with a delocalised mixed-valence structure and the associated MO scheme (Fig. 1.5).[75,86] However, the very different appearance of the spectra (Figs. 1.6 and 1.12), and especially the low frequency of ν_1 and ν_2 and their relative intensities, led us to wonder whether a localised structure prevails for the mixed-valence state in the phosphine systems.

1.6 DIOSMIUM COMPLEXES, $[Os_2(\mu\text{-}X)_3(PR_3)_6]^{2+}$

Analogous diosmium complexes were also first prepared by Chatt and Hayter[1] by reaction of $[OsCl_6]^{2-}$ with PR_3 in aqueous ethanol. Several synthetic routes have since been established, as shown in Fig. 1.13.

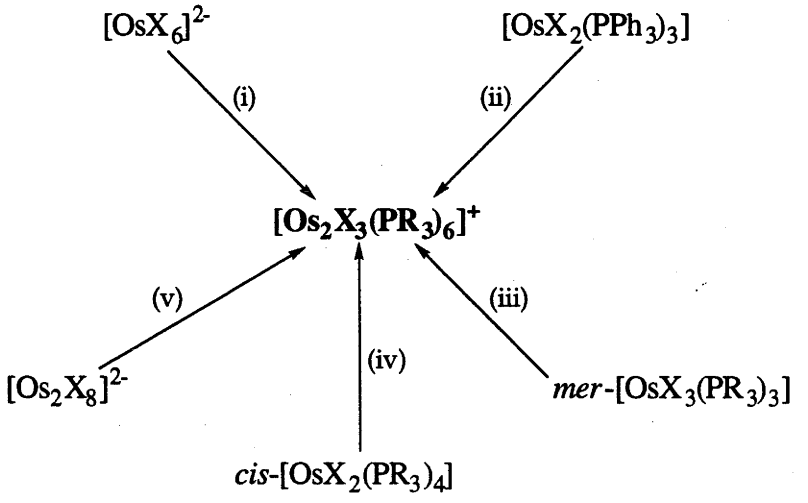

Figure 1.13 *Preparative Routes to $[Os_2(\mu\text{-}X)_3(PR_3)_6]X$ Complexes: (i) Boiling aqueous EtOH; X = Cl, PR_3 = PMe_2Ph, $PMePh_2$, PEt_2Ph, $PEtPh_2$.*[1] *(ii) Boiling EtOH; X = Cl, PR_3 = PEt_3, PEt_2Ph, $(PR_3)_3$ = triphos.*[75] *(iii) Treatment with Zn/Hg under Ar at room temperature in thf; X = Cl, PR_3 = PMe_2Ph, PEt_2Ph, $PEtPh_2$;*[87] *X = Cl, PR_3 = PMe_2Ph, via electrochemical reduction in CH_2Cl_2;*[88] *Boiling 2-MeOEtOH; X = Br, PR_3 = PMe_2Ph.*[75] *(iv) Refluxing Bu^iOH; X = Cl, PR_3 = PMe_2Ph.*[88] *(v) Boiling EtOH; X = Cl, Br, PR_3 = $PMePh_2$, PEt_3.*[89]

Several of these complexes have been electrochemically oxidised to the $[Os_2(\mu\text{-}X)_3(PR_3)_6]^{2+}$ state[75,86] and the X-ray structure of $[Os_2(\mu\text{-}Cl)_3(PEt_3)_6]^{2+}$, prepared by chemical oxidation of $[Os_2(\mu\text{-}Cl)_3(PEt_3)_6]^{+}$, has been reported.[86] The near-IR spectra of the mixed-valence complexes show several bands at low energy (Fig. 1.14), but are seemingly more complicated than the spectra of the corresponding diruthenium complexes.

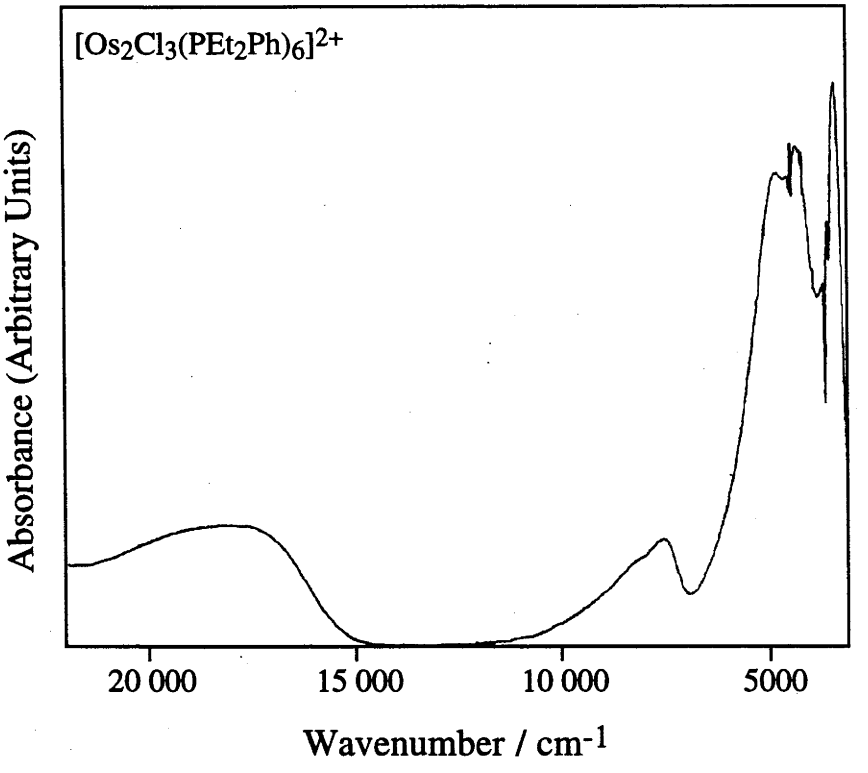

Figure 1.14 *Visible/near-IR spectrum of* $[Os_2(\mu\text{-}Cl)_3(PEt_2Ph)_6]^{2+}$, *recorded in* CH_2Cl_2 *containing* $[Bu^n_4N][BF_4]$ *(0.5 mol* dm^{-3}*) at 213 K.*

These spectra have been assigned elsewhere in terms of the familiar delocalised model and it has been implicitly assumed that the diosmium species are equivalent to their diruthenium analogues. This is consistent with the general belief that 5d metals can engage in stronger metal-metal interaction. In addition, solvent dependence studies[86] found the near-IR bands to be invariant with solvent, which is usually indicative of a delocalised (class III) system. However, we believe that the difference between the $[Os_2(\mu\text{-}X)_3(PR_3)_6]^{2+}$ and the classical "blues", which is even more marked than for their diruthenium analogues, means that the electronic nature of the $[Os_2(\mu\text{-}X)_3(PR_3)_6]^{2+}$ complexes is far from resolved.

1.7 PURPOSE OF THIS WORK

The work described in this thesis involves the synthesis, and the electrochemical and spectro-electrochemical characterisation of a wide range of triply halide-bridged bioctahedral complexes of ruthenium and osmium. These compounds are of interest because of their range of accessible oxidation states and their intriguing electronic spectra. A central objective in this work was to characterise in detail the mixed-valence state ($M_2^{II,III}$) of the phosphine- and arsine-capped complexes, where it is possible for the unpaired electron to be shared equally between the two metal centres (delocalised) or reside preferentially on one metal (localised). Near-IR and EPR spectra, voltammetry and structural data are all probes to the nature of the mixed-valence state and the degree of metal-metal interaction, and these techniques were employed extensively in this work.

The unusual characteristics of known mixed-valence $[M_2(\mu\text{-}X)_3(PR_3)_6]^{2+}$ complexes led us to extend the range of phosphine-capped complexes and investigate for the first time the properties of analogous mixed-valence $[Ru_2(\mu\text{-}X)_3(AsR_3)_6]^{2+}$ systems. In addition, related mononuclear complexes $[RuX_{6-n}(AsR_3)_n]^z$ have been studied, which are important in terms of their relationship to the binuclear complexes as well as being of interest in their own right.

1.8 REFERENCES

1. J. Chatt and R.G. Hayter, *J. Chem. Soc. (A)*, 1961, 896.
2. E.A. Seddon and K.R. Seddon, *The Chemistry of Ruthenium*, Elsevier, Amsterdam, 1984.
3. F.A. Cotton and C.B. Harris, *Inorg. Chem.*, 1965, **4**, 330.
4. F.A. Cotton, *Chem. Soc. Rev.*, 1975, **4**, 27.
5. C. Creutz and H. Taube, *J. Am. Chem. Soc.*, 1973, **95**, 1086.
6. F.A. Cotton, S.A. Duraj, C.C. Hinckley, M. Matusz and W.J. Roth, *Inorg. Chem.*, 1984, **23**, 3080.
7. B. Krebs, M. Bruns, M. Dartmann, G. Henkel, and W. Preetz, *Z. Naturforsch.*, 1984, **39b**, 843.
8. S.F. Gheller, G.A. Heath, D.C.R. Hockless, D.G. Humphrey and J.E. McGrady, *Inorg. Chem.*, 1994, **33**, 3986.
9. D.E. Fogg, B.R. James and M. Kilner, *Inorg. Chim. Acta*, 1994, **222**, 85, and references therein.
10. S.J. Lippard, *Angew. Chem., Int. Ed. Engl.*, 1988, **27**, 344.
11. L. Que, Jr. and A.E. True, *Prog. Inorg. Chem.*, 1990, **38**, 97.
12. K. Wieghardt, *Angew. Chem., Int. Ed. Engl.*, 1989, **28**, 1153.
13. G. Christou, *Acc. Chem. Res.*, 1989, **22**, 328.
14. R.H. Holm, S. Ciurli, and J.A. Weigel, *Prog. Inorg. Chem.*, 1990, **38**, 1.
15. T.D. Westmoreland, D.E. Wilcox, M.J. Baldwin, W.B. Mims and E.I. Solomon, *J. Am. Chem. Soc.*, 1989, **111**, 6106.
16. H.M. Powell, *Proc. Chem. Soc.*, 1959, 73.
17. M.B. Robin, *Inorg. Chem.*, 1962, **1**, 337.
18. H.J. Buser, D. Schwarzenbach, W. Petter and A. Ludi, *Inorg. Chem.*, 1977, **16**, 2704.
19. G.C. Allen and N.S. Hush, *Prog. Inorg. Chem.*, 1967, **8**, 357.
20. M.B. Robin and P. Day, *Adv. Inorg. Chem. Radiochem.*, 1967, **10**, 247.

21. C. Creutz, *Prog. Inorg. Chem.*, 1983, **30**, 1.

22. D.E. Richardson and H. Taube, *Coord. Chem. Rev.*, 1984, **60**, 107.

23. R.J. Crutchley, *Adv. Inorg. Chem.*, 1994, **41**, 273.

24. G. Garton and H.M. Powell, *J. Inorg. Nucl. Chem.*, 1957, **4**, 84.

25. A. Ludi, in *Mixed-Valence Compounds*, ed. D.B. Brown, Reidel Publishing Co., Dordrecht, 1980, pp. 25-47.

26. N.S. Hush, *Prog. Inorg. Chem.*, 1967, **8**, 391.

27. N.S. Hush, *Electrochim. Acta*, 1968, **13**, 1005.

28. R.A. Marcus, *J. Chem. Phys.*, 1956, **24**, 966.

29. R.A. Marcus, *J. Chem. Phys.*, 1957, **26**, 867.

30. R.A. Marcus, *J. Chem. Phys.*, 1957, **26**, 872.

31. S.B. Piepho, E.R. Krausz and P.N. Schatz, *J. Am. Chem. Soc.*, 1978, **100**, 2996.

32. K.Y. Wong and P.N. Schatz, *Prog. Inorg. Chem.*, 1981, **28**, 369.

33. A.F. de Fourcroy and N.L. Vaquelin, *Ann. Chim. (Paris)*, 1804, **49**, 188.

34. A.F. de Fourcroy and N.L. Vaquelin, *Ann. Chim. (Paris)*, 1804, **50**, 5.

35. C. Claus, *Justus Liebigs Ann. Chem.*, 1846, **59**, 283.

36. J.L. Howe, *J. Am. Chem. Soc.*, 1901, **23**, 775.

37. J.L. Howe, J.L. Howe, Jr. and S.C. Ogburn, Jr., *J. Am. Chem. Soc.*, 1924, **46**, 335.

38. L.W.N. Godward and W. Wardlaw, *J. Chem. Soc.*, 1938, 1422.

39. G.A. Rechnitz, *Inorg. Chem.*, 1962, **1**, 953.

40. I.E. Starlik and Yu. A. Barbanel', *Russ. J. Inorg. Chem.*, 1961, **6**, 109.

41. M.G. Adamson, *Aust. J. Chem.*, 1967, **20**, 2517.

42. M.G. Adamson, *J. Chem. Soc. (A)*, 1968, 1370.

43. D. Rose and G. Wilkinson, *J. Chem. Soc. (A)*, 1970, 1791.

44. E.E. Mercer and P.E. Dumas, *Inorg. Chem.*, 1971, **10**, 2755.

45. J.K. Nicholson, *Angew. Chem., Int. Ed. Engl.*, 1967, **6**, 264.

46. G. Chioccola and J.J. Daly, *J. Chem. Soc. (A)*, 1968, 1981.

47. F.M. Lever and A.R. Powell, *J. Chem. Soc. (A)*, 1969, 1477.

48. F. Bottomley and S.B. Tong, *Can. J. Chem.*, 1971, **49**, 3739.

49. E.E. Mercer and L.W. Gray, *J. Am. Chem. Soc.*, 1972, **94**, 6426.

50. F. Bottomley, *Can. J. Chem.*, 1977, **55**, 2788.

51. J.R. Durig, Y. Omura and E.E. Mercer, *J. Mol. Struct.*, 1975, **29**, 53.

52. M.N. Hughes, D. O'Reardon, R.K. Poole, M.B. Hursthouse and M. Thornton-Pett, *Polyhedron*, 1987, **6**, 1711.

53. J.K. Beattie, P. Del Favero, T.W. Hambley and N.S. Hush, *Inorg. Chem.*, 1988, **27**, 2000.

54. V.T. Coombe, Ph.D. Thesis, University of Edinburgh, 1985.

55. N.S. Hush, J.K. Beattie and V.M. Ellis, *Inorg. Chem.*, 1984, **23**, 3339.

56. L. Dubicki and E.R. Krausz, *Inorg. Chem.*, 1985, **24**, 4461.

57. R.S. Armstrong, J.K. Beattie, P. Del Favero, V.M. Ellis and N.S. Hush, *Inorg. Chim. Acta*, 1984, **89**, L33.

58. R.S. Armstrong, W.A. Horsfield and K.W. Nugent, *Inorg. Chem.*, 1990, **29**, 4551.

59. R. Saillant and R.A.D. Wentworth, *J. Am. Chem. Soc.*, 1969, **91**, 2174.

60. J.L. Templeton, W.C. Dorman, J.C. McClardy and R.E. McCarley, *Inorg. Chem.*, 1978, **17**, 1263.

61. R.H. Summerville and R. Hoffmann, *J. Am. Chem. Soc.*, 1979, **101**, 3821.

62. W.C. Trogler, *Inorg. Chem.*, 1980, **19**, 697.

63. K. Wieghardt, W. Herrmann, M. Köppen, I. Jibril and G. Huttner, *Z. Naturforsch.*, 1984, **39b**, 1335.

64. P. Neubold, B.S.P.C. Della Vedova, K. Wieghardt, B. Nuber and J. Weiss, *Inorg. Chem.*, 1990, **29**, 3355.

65. R.S. Armstrong and W.A. Clucas, personal communication;
see also W. A. Clucas, Ph.D. Thesis, University of Sydney, 1994.

66. J.E. Fergusson and A.M. Greenaway, *Aust. J. Chem.*, 1978, **31**, 497.

67. V.T. Coombe, G.A. Heath, T.A. Stephenson and D.K. Vattis, *J. Chem. Soc., Dalton Trans.*, 1983, 2307.

68. D. Appleby, P.B. Hitchcock, C.L. Hussey, T.A. Ryan, J.R. Sanders, K.R. Seddon, J.E. Turp and J.A. Zora, *J. Chem. Soc., Dalton Trans.*, 1990, 1879.

69. B.J. Kennedy, G.A. Heath and T.J. Khoo, *Inorg. Chim. Acta*, 1991, **190**, 265.

70. G.A. Heath and J.E. McGrady, *J. Chem. Soc., Dalton Trans.*, 1994, 3759.

71. M.S. Lupin and B.L. Shaw, *J. Chem. Soc. (A)*, 1968, 741.

72. G. Albertin, S. Antoniutti and E. Bordignon, *J. Chem. Soc., Dalton Trans.*, 1987, 1813.

73. W.J. Sime and T.A. Stephenson, *J. Organomet. Chem.*, 1977, **124**, C23.

74. A. Albinati, Q. Jiang, H. Rüegger and L.M. Venanzi, *Inorg. Chem.*, 1993, **32**, 4940.

75. D.G. Humphrey, Ph.D. Thesis, Australian National University, 1992.

76. P.W. Armit, A.S.F. Boyd and T.A. Stephenson, *J. Chem. Soc., Dalton Trans.*, 1975, 1663.

77. J.A. Statler, G. Wilkinson, M. Thornton-Pett and M.B. Hursthouse, *J. Chem. Soc., Dalton Trans.*, 1984, 1731.

78. M. Laing and L. Pope, *Acta Crystallogr., Sect. B*, 1976, **32**, 1547.

79. D.A. Couch and S.D. Robinson, *Inorg. Chem.*, 1974, **13**, 456.

80. L.F. Rhodes, C. Sorato, L.M. Venanzi and F. Bachechi, *Inorg. Chem.*, 1988, **27**, 604.

81. G.A. Heath, G. Hefter, D.R. Robertson, W.J. Sime and T.A. Stephenson, *J. Organomet. Chem.*, 1978, **152**, C1.

82. T. Arthur, R. Contreras, G.A. Heath, G. Hefter, A.J. Lindsay, J.A. Riach and T.A. Stephenson, *J. Organomet. Chem.*, 1979, **179**, C49.

83. G.A. Heath, A.J. Lindsay, T.A. Stephenson and D.K. Vattis, *J. Organomet. Chem.*, 1982, **233**, 353.

84. T. Easton, G.A. Heath, T.A. Stephenson and M. Bochmann, *J. Chem. Soc., Chem. Commun.*, 1985, 154.

85. R.M. Christie, G.A. Heath, S.A. Macgregor, M.A. Schröder and L.J. Yellowlees, *J. Chem. Soc., Chem. Commun.*, 1990, 1445.

86. S.A. Macgregor, E. McInnes, R.J. Sorbie and L.J. Yellowlees, in *Molecular Electrochemistry of Inorganic, Bioinorganic and Organometallic Compounds*, eds. A.J.L. Pombeiro and J.A. McCleverty, Kluwer Academic Publishers, Dordrecht, 1993, pp. 503-507.

87. J. Chatt, D.P. Melville and R.L. Richards, *J. Chem. Soc. (A)*, 1971, 1169.

88. V.T. Coombe, G.A. Heath, T.A. Stephenson, J.D. Whitelock and L.J. Yellowlees, *J. Chem. Soc., Dalton Trans.*, 1985, 947.

89. P.E. Fanwick, I.F. Fraser, S.M. Tetrick and R.A. Walton, *Inorg. Chem.*, 1987, **26**, 3786.

CHAPTER TWO

General Experimental Procedures

2.1 INTRODUCTION

A number of common starting materials and experimental techniques have been employed in the course of this work. This chapter groups the details of preparation of starting materials and the instrumental methods used to characterise products. Most attention is given to electrochemical and spectro-electrochemical techniques, which are relied on throughout this thesis.

2.2 PREPARATION OF STARTING MATERIALS

2.2.1 Basic Materials

"$RuCl_3.xH_2O$" and $Na_2[OsCl_6]$ were purchased from Johnson-Matthey, $[NH_4]_2[OsCl_6]$, $[NH_4]_2[OsBr_6]$ and $NOPF_6$ from Strem Chemicals Inc., $[Bu^n_4N]OH$ from Aldrich Chemical Co. and HBF_4 was purchased from Ajax Chemicals. Trifluoromethanesulphonic acid (triflic acid, CF_3SO_3H) was vacuum-distilled before use. All reactions were carried out using deoxygenated analytical grade solvents under an atmosphere of N_2, however the isolated solids were handled in air.

2.2.2 Arsine and Phosphine Ligands

$AsMePh_2$,[1] PMe_3 [2] and $PMePh_2$ [3] were prepared according to literature methods. Other monodentate arsine and phosphine ligands were purchased from Aldrich Chemical Co. and Organometallics Inc. Tridentate 1,1,1-tris(diphenylphosphinomethyl)ethane (triphos) was obtained from Strem Chemicals Inc.

2.2.3 Ruthenium Complexes

$K_3[Ru_2Cl_9].KCl$

Prepared by the method of Coombe,[4] heating $K_2[RuCl_5(H_2O)]$ (prepared by the method of Buckley and Mercer[5]) in an evacuated tube at 260 °C for one week. Typical yield: 98%.

$K_3[Ru_2Br_9]$

Prepared by the method of Coombe *et al*,[6] heating "$RuCl_3.xH_2O$" in a 1:1 mixture of EtOH and HBr (48 %) followed by addition of KBr. The black microcrystalline product precipitated upon concentrating and cooling the solution. The solid $K_3[Ru_2Br_9]$ was washed with ethanol, diethyl ether and dried *in vacuo*. Typical yield: 60%.

$[Bu^n_4N]_3[Ru_2X_9]$ (X = Cl, Br)

Prepared in quantitative yield by addition of excess $[Bu^n_4N]X$ to aqueous solutions of $K_3[Ru_2Cl_9].KCl$ or $K_3[Ru_2Br_9]$. The $[Bu^n_4N]_3[Ru_2X_9]$ salts precipitated and were washed with distilled water and dried *in vacuo*.

$[RuCl_2(PPh_3)_3]$

Prepared by the method of Stephenson and Wilkinson,[7] by heating "$RuCl_3.xH_2O$" and excess PPh_3 in methanol for 6 h. The red-brown microcrystalline precipitate was collected and washed with methanol and diethyl ether. Typical yield: 90%.

$[RuBr_2(PPh_3)_3]$

Prepared according to the method described by Lindsay,[8] using $[Bu^n_4N]_3[Ru_2Br_9]$ in place of $[P(CH_2Ph)Ph_3]_3[Ru_2Br_9]$. For example, $[Bu^n_4N]_3[Ru_2Br_9]$ (3.13 g, 1.9 mmol) was dissolved in methanol (150 cm^3) and heated at reflux for 0.5 h. The solution was filtered through celite into a flask containing PPh_3 (6.0 g, 22.9 mmol). The mixture was heated at reflux for 1 h. The red-brown precipitate was collected and washed with methanol and diethyl ether. Yield of $[RuBr_2(PPh_3)_3]$: 1.7 g (43 %).

2.2.4 Osmium Complexes

$[Bu^n_4N]_2[OsX_6]$ (X = Cl, Br)

$[Bu^n_4N]_2[OsCl_6]$ was prepared in quantitative yield by the addition of a solution containing an excess of $[Bu^n_4N]Cl$ in dilute HCl (0.5 mol dm^{-3}) to $[NH_4]_2[OsCl_6]$ in 0.5 mol dm^{-3} HCl. The yellow $[Bu^n_4N]_2[OsCl_6]$ precipitate was collected, washed with water and dried *in vacuo* at 100 °C for 8h. The red coloured $[Bu^n_4N]_2[OsBr_6]$ was prepared in a similar manner.

$[OsX_2(PPh_3)_3]$ (X = Cl, Br)

Prepared by the method of Goeden and Haymore,[9] by heating $[Bu^n_4N]_2[OsX_6]$† and an excess of PPh_3 in a mixture of Bu^tOH and H_2O (1:3) for 48 h. The green $[OsX_2(PPh_3)_3]$ precipitates were collected, washed with n-hexane and dried. Typical yields: 90% (X = Cl), 85% (X = Br).

† The preparation of $[OsBr_2(PPh_3)_3]$ fails if other salts such as $[NH_4]_2[OsBr_6]$ are used in place of $[Bu^n_4N]_2[OsBr_6]$.

2.3 INSTRUMENTAL TECHNIQUES

2.3.1 Elemental Analyses

Analyses for C, H, N, Cl and Br were performed by the Microanalytical Unit, Research School of Chemistry, Australian National University.

2.3.2 ^{1}H and ^{31}P-$\{^{1}H\}$ NMR

^{1}H and ^{31}P-$\{^{1}H\}$ NMR spectra were recorded using a Varian Gemini 300 MHz (BB) instrument, with chemical shifts in ppm referred to internal $SiMe_4$ (^{1}H) or external H_3PO_4 (85% in D_2O) for ^{31}P-$\{^{1}H\}$ spectra. Chemical shifts quoted are positive to higher frequency (lower shielding) than the reference.

2.3.3 Mass Spectra

Electrospray mass spectrometry (ESMS) is a technique which allows pre-existing ions to be very gently transferred to the gas phase and then examined by conventional mass spectrometric techniques. The widest application of ESMS has been in the field of biological chemistry,[10] where the observation of ions usually depends upon protonation of the substrate by the mobile phase used in the spectrometer (typically H_2O/MeOH/HOAc = 50:50:1%). This technique has since been applied to inorganic and organometallic systems which are usually already ionic and for which observation of ions does not depend upon reaction with the mobile phase. In studies with solutions containing single species,[11-16] the intact ion is almost invariably observed, often as the only significant peak in the mass spectrum. It has also been discovered that if solutions containing several rapidly exchanging species are examined using ESMS, then individual species are observed.[17-20]

The electrospray mass spectra were recorded by Dr Ray Colton at La Trobe University, with a VG Bio-Q triple quadrupole mass spectrometer using a water/methanol/acetic acid (50:50:1%) mobile phase. Solutions of the compounds (2 x 10^{-3} mol dm^{-3}) in dichloromethane were diluted 1:10 with methanol. The diluted

solutions of the compounds were injected directly into the spectrometer *via* a Rheodyne model 7125 injector using a Phoenix 20 micro LC syringe pump to deliver the solution to the vaporisation nozzle of the electrospray ion source. The compounds described in this thesis gave strong signals in their ES mass spectra and typically 4-8 averaged spectra were required to give a good signal to noise ratio. Measurements were made at an ion-source energy (B1) voltage of 40 V unless stated otherwise.

Positive-ion Fast Atom Bombardment (FAB) mass spectra of compounds dissolved in dichloromethane were obtained on a ZAB2-SEQ mass spectrometer, using 4-nitrobenzylalcohol (NBA) as the liquid matrix.

The ES and FAB mass spectra of complexes showed a range of m/z values corresponding to the isotopic mass distribution for the particular complex. In all cases there was good agreement between the experimental and calculated isotopic mass distribution, and the most intense m/z values have been quoted.

2.4 ELECTROCHEMICAL TECHNIQUES

2.4.1 Experimental Conditions

Electrochemical measurements and electrosyntheses were carried out in CH_2Cl_2 containing 0.5 mol dm^{-3} $[Bu^n_4N][BF_4]$ or CH_3CN containing 0.1 mol dm^{-3} $[Bu^n_4N][BF_4]$. The electrolyte, $[Bu^n_4N][BF_4]$, was prepared by neutralising $[Bu^n_4N]OH$ (40 % in water) with HBF_4 to pH 6. The precipitate was collected by filtration, washed with large amounts of distilled water, recrystallised twice from methanol/water (4:1) and dried *in vacuo* at 100 °C for 8 h or until an acceptable electrochemical background was attained. Dichloromethane was pre-dried over KOH pellets before distilling from CaH_2 just before use. Acetonitrile was purified by the method described by Walter and Ramaley:[21] in succession, analytical grade acetonitrile was heated at reflux over, then distilled from (i) anhydrous $AlCl_3$, (ii) alkaline $KMnO_4$, (iii) $KHSO_4$ and (iv) finally distilled from CaH_2 just before use.

Cyclic voltammetry (CV) and alternating current voltammetry (acV) measurements were carried out using a PAR model 170 electrochemical system, linked where appropriate to a Macintosh LC630 computer *via* an AD Instruments MacLab interface system. A standard three-electrode configuration was used. The working electrode was a platinum disc (1 mm diameter) and a platinum rod was used as the counter electrode. The reference electrode was a Ag/AgCl electrode (Metrohm), separated from the solution by two porous glass frits. The internal compartment of the reference electrode was filled with 0.05 mol dm^{-3} $[Bu^n_4N]Cl$ / 0.45 mol dm^{-3} $[Bu^n_4N][BF_4]$ in CH_2Cl_2 (or with both $Bu^n_4N^+$ salts 0.05 mol dm^{-3} for CH_3CN). The external compartment was filled with the standard electrolyte solution, 0.50 mol dm^{-3} $[Bu^n_4N][BF_4]$ in CH_2Cl_2 (or 0.10 mol dm^{-3} in CH_3CN). Under these conditions ferrocene was oxidised at +0.55 V in CH_2Cl_2 and +0.41 V in CH_3CN at room temperature. Linear stirred voltammetry employed a Tacussel EDI rotating platinum disc working electrode operating in the range 1000 - 6000 rpm. Typical scan rates were 100 mV s^{-1} (CV) and 10 mV s^{-1} (acV). The latter

were recorded with positive feedback resistance compensation and phase-sensitive detection. The sinusoidal modulation was set at 10 mV and the frequency, ω, was 205 Hz.

The electrochemical cell was a jacketted glass cell (10 cm^3) incorporating the above electrodes. The electrolyte solutions were purged with either N_2 or Ar and the cell maintained under an inert atmosphere. Low temperature measurements were recorded by connecting the jacketted glass cell to a Lauda RL6 circulating alcohol cooling bath. The temperature was monitored to within 0.2 °C by a digital thermometer with the probe located directly in the electrochemical solution.

Bulk electrolyses were performed at low temperature using a jacketted three compartment H-cell, with a platinum mesh basket working electrode, double-fritted non-aqueous Ag/AgCl reference electrode and platinum wire counter electrode separated from the bulk solution by two glass frits. A platinum disc voltammetric electrode (1 mm diameter) was used to monitor the electrolysis.

2.4.2 Cyclic Voltammetry (CV)

Cyclic voltammetry involves the use of a static working electrode in an unstirred ("quiet") solution. The potential of the working electrode is varied at a constant rate, ν (typically 50 - 1000 mV s^{-1}), between two pre-set values in a cyclic fashion.

The solution is quiet, hence diffusion of reactants and products between the bulk solution and the solution/electrode interface is the only means of mass transport. As the redox potential of the substrate is passed, the current rises to a maximum and, then, as the substrate around the electrode is depleted, the current declines, producing the observed asymmetric peak. On reversal of the potential ramp the electron-transfer process can be reversed, with a corresponding depletion of the species previously generated at the electrode surface, giving the characteristic voltammogram (Fig. 2.1). Only the small

portion of the substrate near the electrode surface is actually oxidised or reduced, hence the bulk solution undergoes negligible electrolysis. The timescale of the process is determined by the scan rate, ν.

Four measurable parameters can be be obtained for a reversible process: the net current (i_pf) and potential (E_pf) of the forward curve and the corresponding parameters for the reverse curve (i_pr and E_pr). The value of $E_{1/2}$ for a reversible process is determined from the mean of E_pf and E_pr. These four parameters can be used to determine whether the redox process is reversible, quasi-reversible or irreversible. A voltammetrically "reversible" process means that the charge-transfer process occurs considerably faster than the rate of diffusion. A reaction in which the electron-transfer process is not effectively instantaneous and is controlled by both diffusion and charge-transfer kinetics is termed "quasi-reversible", and a reaction in which the product formed at the electrode is not returned to the starting species at a significant rate on the reverse scan is termed "irreversible". A "partially-reversible" process has an irreversible chemical reaction following charge-transfer. The criteria for voltammetric reversibility or otherwise are outlined in Table 2.1.[22-24]

High solution resistance in non-aqueous media can produce non-ideal responses for voltammetrically reversible systems, especially at low temperature.[25] The ferrocinium/ferrocene (Fc^+/Fc) couple is known to satisfy the criteria for a reversible diffusion-controlled redox process.[26,27] Redox processes which gave an equivalent response to the Fc^+/Fc couple under the same conditions were regarded as electrochemically reversible in the present work, whether this response was exactly Nernstian or not. Ferrocene was added to the solution at the conclusion of an experiment both for this purpose, and as an internal reference. Ferrocene was oxidised at +0.55 V in CH_2Cl_2 at room temperature, and at +0.55 ± 0.02 V at 213 K. The invariance of the Fc/Fc^+ couple presumably arises through accidental cancellation of opposing factors.

Table 2.1 *Criteria for reversible, quasi-reversible, partially-reversible and irreversible charge transfer processes for cyclic voltammetry at 298 K.*[*]

Reversible E_p is independent of ν $E_pf - E_pr = 59/n$ mV (42/n mV at 213 K) and is independent of ν $1/2[E_pf + E_pr] = E_{1/2}$, independent of concentration $i_p/\nu^{1/2}$ is independent of ν i_pr/i_pf is unity, independent of ν
Quasi-reversible (*i.e.* electron transfer sluggish, product stable) E_p shifts with ν $E_pf - E_pr$ increases as ν increases $1/2[E_pf + E_pr] = E_{1/2}$, independent of concentration $i_p/\nu^{1/2}$ is virtually independent of ν i_pr/i_pf generally = 1 (so long as $\alpha \sim 0.5$)
Partially reversible (product unstable, electron transfer may be fast) E_p increases by 30/n mV (21/n mV at 213 K) for a tenfold increase in ν, at low ν $i_p/\nu^{1/2}$ is independent of ν i_pr/i_pf increases toward 1 as ν increases
Irreversible (product unstable or grossly altered structurally, electron transfer is slow) E_p shifts with ν $i_p/\nu^{1/2}$ is independent of ν no current on reverse scan
ν = scan rate (mV s^{-1}); α = charge-transfer coefficient (ideally 0.5) n = number of electrons involved in redox process E_pf and i_pf = potential and net current at the maximum of the forward wave E_pr and i_pr = potential and net current at the maximum of the reverse wave

*See especially E.R. Brown and R.F Large, Tables 6.2, 6.3, 6.4 & 6.8 in *Physical Methods of Chemistry* (A. Weissberger and B.W. Rossiter, Editors), Vol 1, *Part IIA, Electrochemical Methods*, Ch. 6, Wiley, New York, 1971

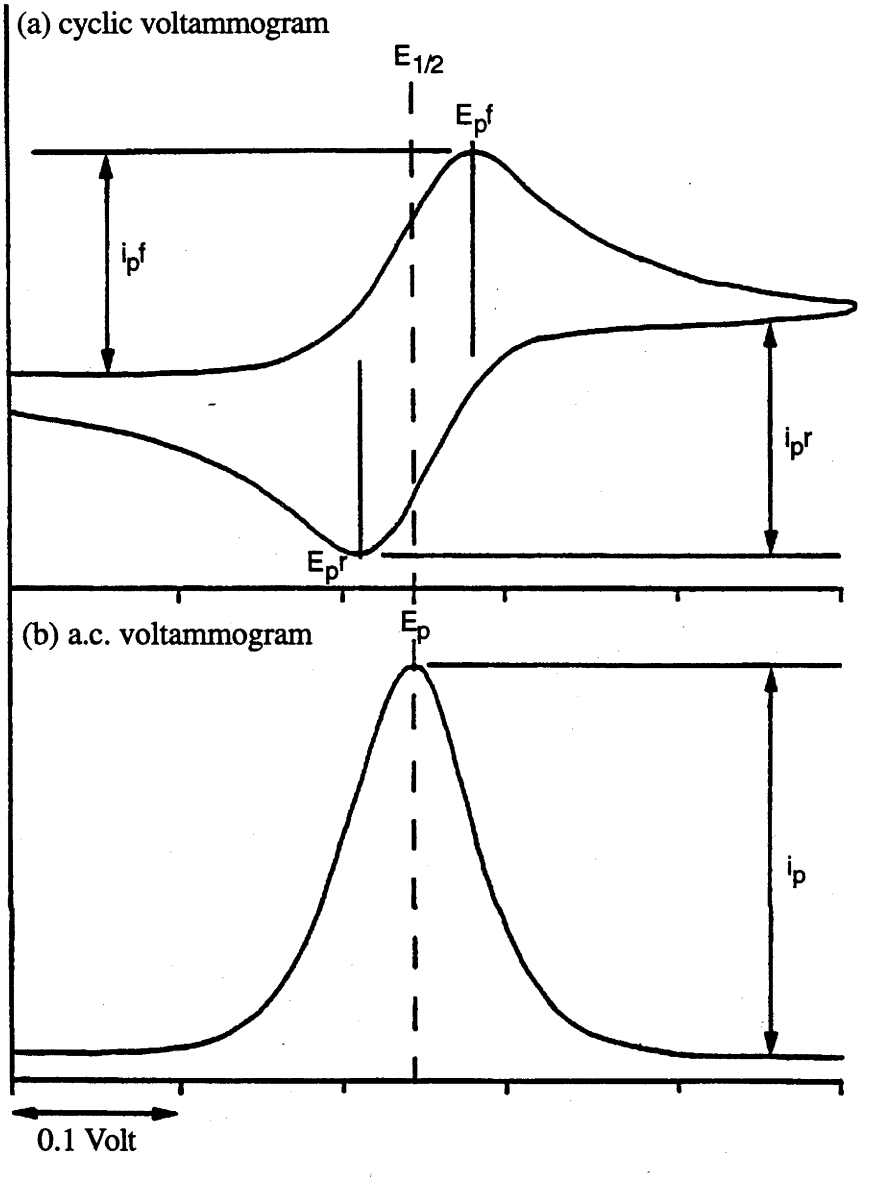

Figure 2.1 *Form of (a) cyclic voltammogram and (b) a.c. voltammogram for a reversible process.*

2.4.3 Alternating Current Voltammetry (acV)

The alternating current voltammetry technique involves the superposition of a small alternating potential upon a linearly ramped d.c. potential. The d.c. potential is varied at a constant rate (10 mV s^{-1}) and the alternating current only is measured. The superimposed voltage (ΔV = 10 mV in our work) is generally sinusoidal in form, and a range of frequencies, ω, from *ca.* 10 - 1000 Hz may be employed. For a reversible redox process the output signal in the i *vs* E trace is a symmetric peak centred on $E_{1/2}$ of the

corresponding cyclic voltammogram (Fig. 2.1). Focussing on the "faradaic" current (*i.e.* the resultant current from the oxidation-reduction process at the electrode) of a redox process,

$$Ox + ne \rightleftharpoons Red \qquad (2.1)$$

it is necessary to have both an oxidisable and reducible species at the electrode surface for such an alternating current to exist. At potentials prior to $E_{1/2}$, significant concentrations of "Red" are present only when the potential corresponds to the steeply rising portion of the cyclic voltammogram (where [Ox] > [Red] > 0), and the magnitude of the alternating current is determined by [Red] at the electrode surface. Similarly, at potentials just beyond $E_{1/2}$, [Red] > [Ox] > 0 and the magnitude of the alternating current is dependent upon [Ox]. The faradaic current is at a maximum when [Ox] = [Red] (*i.e.* at $E_{1/2}$). For non-reversible processes, rapid decay of "Red" prevents the system oscillating with applied voltage modulation, leading to collapse of the a.c. signal. For irreversible processes no a.c. peak is observed, and for quasi-reversible processes the magnitude of the a.c. current is dependent upon the frequency of the a.c. source, ω. The timescale of the experiment is effectively controlled by ω, rather than ν, and provides a stringent test of electrochemical reversibility. The criteria for reversibility in the a.c. mode are shown below:

$E_p = E_{1/2}$ (d.c.) independent of concentration and ω.

The wave is highly symmetric with a width at half height of 90 mV (64 mV at 213 K).

i_p gives a linear plot *vs* $\omega^{1/2}$ which passes through the origin.

(ω = a.c. frequency; i_p = peak current; E_p = peak potential)

A major advantage of a.c. voltammetry is the ability to discriminate against the "capacitative" background current (arising from the charging of the double layer surrounding the electrode) in favour of the faradaic current. The faradaic and capacitative current components have different phase relationships with the sinusoidal applied voltage.

Phase-sensitive detection allows the relevant faradaic current to be measured exclusively, leading to an increase in sensitivity and often assists the definition of waves that would be concealed at the d.c. voltammetric positive or negative limits. Another advantage is that two adjacent waves can be resolved with a difference in $E_{1/2}$ of 0.08 V, compared with 0.15 V in cyclic voltammetry. Alternating current voltammetry also contains information about the reversibility of the process as outlined above.

2.4.4 Stirred Linear Voltammetry (S-V)

This S-V technique involves scanning (10 mV s^{-1}) to increasingly anodic or cathodic potentials whilst stirring the solution (preferably by employing a purpose-built rotating disc electrode), which continually renews the solution in contact with the electrode. Resulting currents are positive (above the i = 0 line) for reductive and negative (below the i = 0 line) for oxidative processes. As the species under investigation undergoes electron-transfer, the current reaches a maximum or minimum value (the diffusion current i_d), determined by the rate of transport of the species to the electrode surface by diffusion and forced convection. For an ideally reversible system, the midpoint of the wave, $E_{1/2}$, coincides with the standard E° potential defined by the Nernst equation as long as the oxidised and reduced species have similar diffusion coefficients.

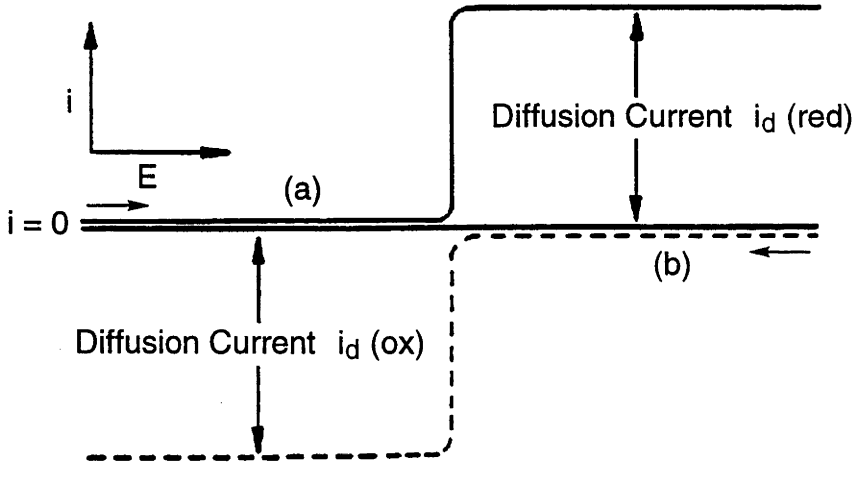

Figure 2.2 *Linear stirred voltammograms for (a) oxidised form, and (b) reduced form of a given complex. $E_{1/2}$ is coincident for the two traces but the i/E trace is displaced with respect to the i = 0 line.*

This technique can be used to determine whether a particular process is a reduction or oxidation (the "oxidation level" of a solution), and hence to monitor the progress of a bulk electrolysis (see §2.4.5). At a molecular level, the number of electrons transferred in the electrode precess can be determined by comparison of the diffusion current with i_d of known charge-transfer processes under the same conditions.

2.4.5 Bulk Electrolysis

Bulk electrolysis experiments were carried out in a three compartment cell with a large Pt mesh basket working electrode. Solutions (10 cm^3) generally contained ~10^{-2} mol dm^{-3} of the complex undergoing electrolysis. The potential of the working electrode is held constant beyond $E_{1/2}$ for the redox process in question whilst the solution is stirred. As the starting material is consumed the current decays exponentially toward i = 0. The three compartment design allows the counter electrode to be separated from the bulk solution by two porous glass frits, ensuring species generated at the counter electrode do not contaminate the bulk solution. A separate 1 mm Pt disc electrode was used for *in situ* voltammetric measurements, and stirred linear-sweep voltammetry (§2.4.4) was used at intervals to determine the percentage completion of the electrolysis, from the ratio of oxidised to reduced material.

2.5 SPECTRO-ELECTROCHEMISTRY

2.5.1 UV/Vis/Near-Infrared Spectro-Electrochemistry

Electronic spectra in the range 45 000 - 3125 cm^{-1} were recorded using a Perkin-Elmer λ9 double-beam UV/Vis/near-IR spectrophotometer with digital background subtraction capability. The spectra of electrogenerated species were collected *in situ*, by the use of an optical semi-thin layer electrochemical (OSTLE) cell, with a path-length of 0.5 mm, mounted within the sample compartment of the spectrophotometer.

The electrolyte ($[Bu^n_4N][BF_4]$) and solvents (CH_2Cl_2 or CH_3CN) were prepared as described previously. Solutions for spectro-electrochemical experiments were made up as for other electrochemical experiments, *i.e.* 0.5 mol dm^{-3} $[Bu^n_4N][BF_4]$ in CH_2Cl_2, and contained *ca.* 10^{-3} mol dm^{-3} of the complex under investigation.

The OSTLE cell (Fig. 2.3), placed in the sample beam of the spectrophotometer, was a flat rectangular fused silica (Suprasil W) cell of path length 0.5 mm, constructed to our design and widened at the top to accommodate the reference and counter electrodes. The working electrode was a rectangular piece of fine platinum gauze (70% transmittance) located in the lower section of the cell, and placed centrally in the optical beam. Spot-welded to the platinum gauze was a section of platinum wire passing to the top of the cell, where it was connected to the potentiostat. The wire was sheathed by poly(tetrafluoroethylene) (PTFE) tubing, to ensure electrolysis occurred only at the platinum gauze. The wide part of the cell, above the flat section, contained a platinum wire auxiliary electrode and non-aqueous Ag/AgCl reference electrode as described above, both separated from the solution by salt bridges containing electrolyte solution. The cell placed in the reference beam was of similar profile, and contained a matching section of platinum gauze.

The cells (sample and reference) were cryostatted in gas-tight, double-glazed (Suprasil W windows) PTFE cell blocks, enabling both the cells and their contents to be cooled by cold N_2 gas. The N_2 gas was chilled by passing it through a copper coil immersed in liquid N_2. It was then passed over a heater element in a Dewar tube (15 cm x 1 cm) and maintained at the desired temperature by a Bruker NMR temperature controller, piped into the cell compartment and through the sample and reference cell blocks. The thermocouple for the temperature controller was positioned at the point of gas outflow from the cell block. A known difference between gas outflow temperature and solution temperature within the cells allowed the required temperature to be accurately

established and maintained. To prevent fogging of the cell-block windows, room temperature N_2 gas was passed between the inner and outer windows.

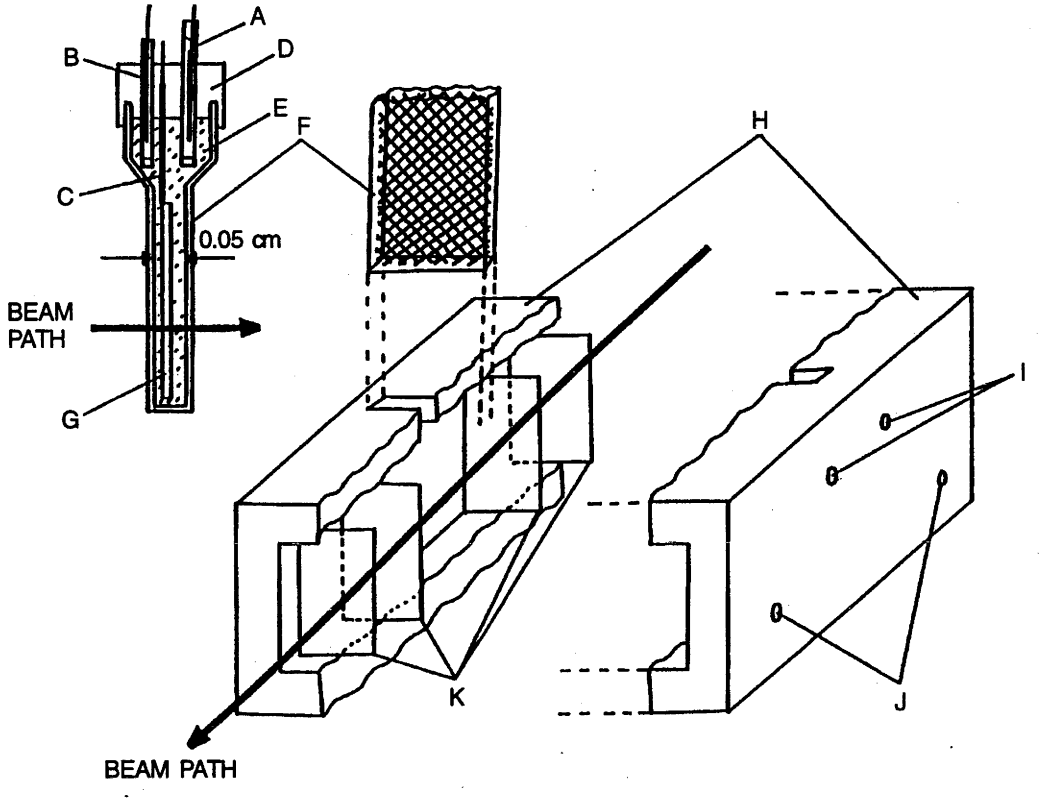

KEY

A Counter electrode
B Reference electrode
C Working electrode connection protected from bulk solution by PTFE sleeve
D Cell cap
E Sample solution, degassed with N_2 or Ar
F 0.05 cm Suprasil W quartz cell containing Pt gauze working electrode
G Pt gauze working electrode
H PTFE cell block
I Cold N_2 inlet ports
J Dry (298 K) N_2 inlet ports (to prevent fogging of inner quartz windows)
K Supasil W quartz cell block windows

Figure 2.3 *Components of the Optical Semi-Thin Layer Electrochemical (OSTLE) cell.*

Initially a background scan was recorded with pure electrolyte solution (0.5 mol dm^{-3} $[Bu^n_4N][BF_4]$) and platinum gauze in both sample and reference cells. The sample solution was prepared (*ca.* 10^{-3} mol dm^{-3} of compound in 2 cm^3 electrolyte solution), purged with either N_2 or Ar and transferred *via* syringe into the sample cell.

The working, auxiliary and reference electrodes were added to the sample cell and connected to a Thompson E-series Ministat potentiostat. The temperature, usually -60 °C (CH_2Cl_2) or -30 °C (CH_3CN), was stabilised to ± 0.3 °C before commencing electrolysis. The electrolysis was typically carried out at a potential 200 mV past $E_{1/2}$ of the redox process in question, and continued until the spectrum ceased to change and the current decayed to a constant minimum. The potential was then reset and the spectrum of the starting complex regenerated. The observation of stable isosbestic points and regeneration of starting spectra, without loss or gain of any features, were taken as evidence for chemical reversibility for the process. For systems with more than one redox process, this procedure was repeated for each step before continuing to subsequent processes.

2.5.2 Electron Paramagnetic Resonance Spectra

The majority of the EPR spectra recorded in this thesis required oxidation of the compound to the $M_2^{II,III}$ odd-electron state. Unlike the optical spectra which were electrogenerated *in situ*, solutions for EPR experiments were prepared externally, by bulk electrolysis of diamagnetic precursors, or by chemical oxidation (using $NOPF_6$ as the oxidant), and transferred to quartz EPR tubes. The concentration of complex in solution was typically 10^{-2} mol dm^{-3} in freshly distilled CH_2Cl_2 containing 0.5 mol dm^{-3} electrolyte . The oxidations were carried out under an atmosphere of N_2 and the solutions were transferred to deoxygenated EPR tubes *via* syringe, then frozen to a glass and stored in liquid N_2. EPR spectra of frozen solutions (glasses) were recorded at 20 K using a Varian X-band spectrometer fitted with an Oxford Instruments helium flow cryostat. Species generated by chemical oxidation were checked by comparison of their UV/Vis/near-IR spectra with those obtained in the OSTLE cell. For systems generated chemically, the EPR spectra of several typical complexes were confirmed by the electrochemical preparation. It is worth noting that the electrolyte medium is a superior solvent than pure CH_2Cl_2 for forming EPR glasses at 20 K, even when no electrogeneration is required.

2.6 REFERENCES

1. G.J. Burrows and E.E. Turner, *J. Chem. Soc.*, 1920, **117**, 1373.
2. M.L. Luetkens, A.P. Sattelberger, H.H. Murray, J.D. Basil and J.P. Fackler, *Inorg. Synth.*, 1989, **26**, 7.
3. V.D. Bianco and S. Doronzo, *Inorg. Synth.*, 1976, **16**, 155.
4. V.T. Coombe, Ph.D. Thesis, University of Edinburgh, 1985.
5. E.E. Mercer and R.R. Buckley, *Inorg. Chem.*, 1965, **4**, 1692.
6. V.T. Coombe, G.A. Heath, T.A. Stephenson and D.K. Vattis, *J. Chem. Soc., Dalton Trans.*, 1983, 2307.
7. T.A. Stephenson and G. Wilkinson, *J. Inorg. Nucl. Chem.*, 1966, **28**, 945.
8. A.J. Lindsay, Ph.D. Thesis, University of Edinburgh, 1982.
9. G.V. Goeden and B.L. Haymore, *Inorg. Chim. Acta*, 1983, **71**, 239.
10. R.D. Smith, J.A. Loo, R.R. Ogorzalek Loo, M. Busman and H.R. Udseth, *Mass Spectrom. Rev.*, 1991, **10**, 359.
11. R. Colton and J.C. Traeger, *Inorg. Chim. Acta*, 1992, **201**, 153.
12. R. Colton, V. Tedesco and J.C. Traeger, *Inorg. Chem.*, 1992, **31**, 3865.
13. R. Colton, J. Harvey and J.C. Traeger, *Org. Mass Spectrom.*, 1992, **27**, 1030.
14. I. Ahmed, A.M. Bond, R. Colton, M. Jurcevic, J.C. Traeger and J.N. Walter, *J. Organomet. Chem.*, 1993, **447**, 59.
15: A.J. Canty, R. Colton and I.M. Thomas, *J. Organomet. Chem.*, 1993, **455**, 283.
16: A.J. Canty, P.R. Traill, R. Colton and I.M. Thomas, *Inorg. Chim. Acta*, 1993, **210**, 91.
17: R. Colton, J.C. Traeger and V. Tedesco, *Inorg. Chim. Acta*, 1993, **210**, 193.
18: R. Colton and D. Dakternieks, *Inorg. Chim. Acta*, 1993, **208**, 173.
19: R. Colton, B.D. James, I.D. Potter and J.C. Traeger, *Inorg. Chem.*, 1993, **32**, 2626.
20: T.J. Cardwell, R. Colton, N. Lambropoulos, J.C. Traeger and P.J. Marriott, *Anal. Chim. Acta*, 1993, **280**, 239.

21. M. Walter and L. Ramaley, *Anal. Chem.*, 1973, **45**, 165.

22. D.T. Sawyer and J.R Roberts, *Experimental Electrochemistry for Chemists*, Wiley, New York, 1974.

23. F.C. Anson, *Electroanalytical Chemistry*, Sound Recording and Manual, American Chemical Society, Washington D.C., 1976.

24. A.J. Bard and L.R. Faulkner, *Electrochemical Methods: Fundamentals and Applications*, Wiley, New York, 1980.

24. M. Kony, A.M. Bond and A.G. Wedd, *Inorg. Chem.*, 1990, **29**, 4521.

26. R.R. Gagné, C.A. Koval and G.C. Lisensky, *Inorg. Chem.*, 1980, **19**, 2854.

27. G. Gritzner and J. Kuta, *Pure. Appl. Chem.*, 1982, **54**, 1527.

CHAPTER THREE

Diruthenium Complexes, $[Ru_2(\mu\text{-}X)_3L_6]^{+/2+/3+}$: Synthesis, Electrochemistry and Spectro-electrochemistry.

3.1 SYNTHESIS

Since Chatt and Hayter's first recognition of $[Ru_2(\mu\text{-}Cl)_3(PR_3)_6]Cl$ complexes,[1] there have been numerous reported syntheses of such compounds, as detailed in §1.5.[2-10] In contrast, there are only infrequent scattered accounts of the preparation of analogous tertiary arsine complexes (Fig. 3.1).[8,11,12]

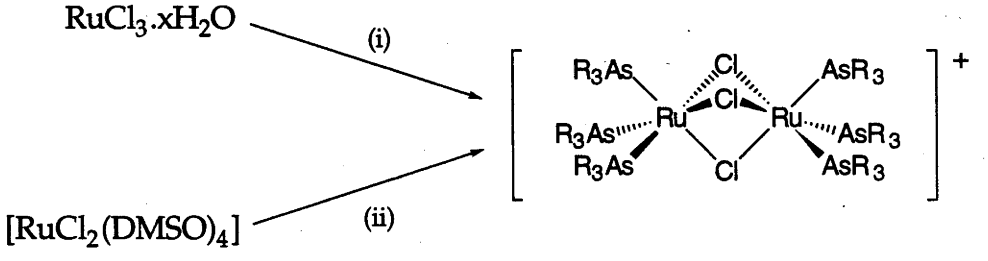

Figure 3.1 *Literature methods for the preparation of $[Ru_2(\mu\text{-}Cl)_3(AsR_3)_6]Cl$ complexes: (i) Boiling EtOH; AsR_3 = $AsRPh_2$ (R = Me, Et, Pr^n, Bu^n).*[11,12] *(ii) Boiling toluene, then methanol; $(AsR_3)_3$ = triars (1,1,1-tris(diphenylarsino)methylethane).*[8]

Reddy *et al* obtained the series $[Ru_2Cl_3(AsRPh_2)_6]Cl$ (R = Me, Et, Pr^n, Bu^n),[11,12] in a manner seemingly specific to alkyl diphenyl arsine derivatives. This involved heating "$RuCl_3.xH_2O$" in ethanol in the presence of $AsRPh_2$, as in the original synthesis of $[Ru_2Cl_3(PR_3)_6]Cl$.[1] Our attempts to prepare the corresponding $AsMe_3$ and

$AsMe_2Ph$ complexes under similar conditions yielded *trans*-$[RuCl_2(AsR_3)_4]$ instead. Neutral phosphine complexes of the form $[RuCl_2(PR_3)_n]$ (n = 3 or 4) are known to condense spontaneously to $[Ru_2Cl_3(PR_3)_6]Cl$ in polar solvents,[4] and *trans*-$[RuCl_2(AsMePh_2)_4]$ dimerises in the same fashion when warmed in ethanol with a small amount of $AsMePh_2$.[12] In contrast, we have established that neither *trans*-$[RuCl_2(AsMe_3)_4]$ nor *trans*-$[RuCl_2(AsMe_2Ph)_4]$ transform to $[Ru_2Cl_3(AsR_3)_6]^+$ under these mild conditions, and this is clearly connected with the failure of Reddy's method in the more general case.

Given the somewhat variable composition of $RuCl_3.xH_2O$,[13] we turned to well characterised tervalent $K_3[Ru_2Cl_9]$ as a convenient starting material.[14,15] In absolute ethanol, the product of the reaction of $K_3[Ru_2Cl_9]$ with AsR_3 is again *trans*-$[RuCl_2(AsR_3)_4]$, however, deliberate inclusion of water (H_2O/EtOH, 1/4) led to formation of a measurable proportion of $[Ru_2Cl_3(AsR_3)_6]Cl$ (Fig. 3.2). The emergence of the ionic product is perhaps attributable to the increase in solvent polarity. The products were easily separated since neutral *trans*-$[RuCl_2(AsR_3)_4]$ compounds tend to precipitate from the reaction mixture, leaving $[Ru_2Cl_3(AsR_3)_6]Cl$ in solution. Upon work-up, this method gave moderate yields of $[Ru_2Cl_3(AsR_3)_6]Cl$ complexes for AsR_3 = $AsMe_3$, $AsMe_2Ph$ and $AsMePh_2$. Moreover, the analogous bromide-bridged complexes $[Ru_2Br_3(AsR_3)_6]Br$, unreported prior to this study, can be prepared conveniently by the equivalent procedure from known $K_3[Ru_2Br_9]$.[14,16]

The binuclear products, initially isolated as halide salts, were routinely converted to the corresponding redox-inert 'triflates' (*i.e.* $CF_3SO_3^-$ salts). This involved gentle heating of dichloromethane solutions of $[Ru_2X_3(AsR_3)_6]X$ in the presence of CF_3SO_3H (added as a dilute solution in methanol). Following evaporation of the solvent, the residues were recrystallised from dichloromethane/diethyl ether to give yellow crystalline products, $[Ru_2X_3(AsR_3)_6]CF_3SO_3$. The $[Ru_2Br_3(AsMePh_2)_6]CF_3SO_3$ complex was obtained in relatively low yield (four independent preparations) and gives reproducible

but disappointing microanalytical data despite manifest evidence of its correct constitution and intrinsic purity (including NMR and mass spectra, voltammetric and spectro-electrochemical studies).

$$K_3[Ru_2X_9] \xrightarrow{AsMe_3,\ EtOH,\ \Delta} [Ru_2X_3(AsR_3)_6]X + [RuX_2(AsR_3)_4]$$

$$[Ru_2X_3(AsR_3)_6]X \xrightarrow[MeOH/CH_2Cl_2]{CF_3SO_3H\ (0.1M),} [Ru_2X_3(AsR_3)_6]CF_3SO_3$$

Figure 3.2 *Synthesis of* $[Ru_2(\mu\text{-}X)_3(AsR_3)_6]CF_3SO_3$ *complexes.*

It is worth noting that returning to "$RuCl_3.xH_2O$" in the mixed ethanol/water solvent gave similar results, although a lower yield resulted. In another effort to prepare $[Ru_2Cl_3(AsMe_3)_6]^+$, we attempted the reaction of "$RuCl_3.xH_2O$" with $AsMe_3$ in a mixture of ethanol/concentrated HCl (10:1). Whereas the same reaction in ethanol gave *trans*-$[RuCl_2(AsMe_3)_4]$ as the only isolable product, and in ethanol/water produced a mixture of *trans*-$[RuCl_2(AsMe_3)_4]$ and $[Ru_2Cl_3(AsMe_3)_6]^+$, the ethanol/HCl mixture produced a mixture of *cis*- and *trans*-$[RuCl_2(AsMe_3)_4]$, and the desired binuclear complex (Fig. 3.3). As with other preparations, the *trans* isomer precipitated from the reaction solution. The *cis* isomer was separated from the remaining mixture by extracting into diethyl ether, leaving $[Ru_2Cl_3(AsMe_3)_6]Cl$, which could then be converted to its triflate salt. The three complexes were each isolated in ~25% yield.

$$\text{"}RuCl_3.xH_2O\text{"} \xrightarrow{AsMe_3,\ EtOH/HCl,\ \Delta} \begin{array}{l} \textit{trans}\text{-}[RuCl_2(AsMe_3)_4] \\ + \textit{cis}\text{-}[RuCl_2(AsMe_3)_4] \\ + [Ru_2Cl_3(AsMe_3)_6]Cl \end{array}$$

$$[Ru_2Cl_3(AsMe_3)_6]Cl \xrightarrow[MeOH/CH_2Cl_2]{CF_3SO_3H\ (0.1M),} [Ru_2Cl_3(AsMe_3)_6]CF_3SO_3$$

Figure 3.3 *Preparation of* $[Ru_2(\mu\text{-}Cl)_3(AsMe_3)_6]CF_3SO_3$ *from "*$RuCl_3.xH_2O$*".*

The only product isolated from the reaction of "$RuCl_3.xH_2O$" with $AsMe_2Ph$ in the ethanol/HCl mixture was *cis*-$[RuCl_2(AsMe_2Ph)_4]$. The diosmium complex $[Os_2(\mu\text{-}Cl)_3(PMe_2Ph)_6]Cl$ has been prepared by heating *cis*-$[OsCl_2(PMe_2Ph)_4]$ for a prolonged period in a high-boiling alcoholic solvent.[17] Similarly, $[Ru_2(\mu\text{-}Cl)_3(AsMe_2Ph)_6]CF_3SO_3$ was isolated in low yield by heating *cis*-$[RuCl_2(AsMe_2Ph)_4]$ in *iso*-butanol, followed by treatment with CF_3SO_3H (Fig. 3.4). Unfortunately, this does not appear to be a generally applicable reaction, as *cis*-$[RuCl_2(AsMe_3)_4]$ did not react at all when heated in *iso*-butanol. As mentioned above, many *trans*-$[RuX_2(AsR_3)_4]$ complexes resist transformation to $[Ru_2X_3(AsR_3)_6]^+$ under mild conditions. Efforts to prepare the binuclear complexes by using harsher conditions, such as prolonged heating in high boiling solvents (*e.g. iso*-butanol or 1,2-dichlorobenzene), or treatment with concentrated CF_3SO_3H solutions, have shown the *trans*-$[RuCl_2(AsR_3)_4]$ complexes to be either unreactive or to be oxidised to the corresponding Ru^{III} monomer cation instead. While these reactions from commercial "$RuCl_3.xH_2O$" were interesting, the general conclusion is that the $K_3[Ru_2Cl_9]$ / ethanol / water preparative route is the preferred strategy.

$$\text{"}RuCl_3.xH_2O\text{"} \xrightarrow{AsMe_2Ph,\ EtOH/HCl,\ \Delta} \textit{cis}\text{-}[RuCl_2(AsMe_2Ph)_4]$$

$$\textit{cis}\text{-}[RuCl_2(AsMe_2Ph)_4] \xrightarrow[\text{(ii) } CF_3SO_3H,\ MeOH/CH_2Cl_2]{\text{(i) } Bu^iOH,\ \Delta} [Ru_2Cl_3(AsMe_2Ph)_6]CF_3SO_3$$

Figure 3.4 *Preparation of* $[Ru_2(\mu\text{-}Cl)_3(AsMe_2Ph)_6]CF_3SO_3$ *from cis-*$[RuCl_2(AsMe_2Ph)_4]$.

At an earlier stage, we had attempted to synthesise $[Ru_2Cl_3(AsR_3)_6]Cl$ complexes from mixtures of $[RuCl_2(PPh_3)_3]$ and AsR_3, since a similar procedure has been widely used to prepare $[Ru_2Cl_3(PR_3)_6]Cl$ complexes in high yield through the ready replacement of PPh_3 (see below). Extended heating of an ethanol mixture of $[RuCl_2(PPh_3)_3]$ and $AsMe_3$ gave a yellow product of stoichiometry $[Ru_2Cl_3(AsMe_3)_4(PPh_3)_2]CF_3SO_3$ after treatment with triflic acid and normal work-up. Several isomers are possible for a

complex of this formula. However, the $^{31}P-\{^1H\}$ NMR spectrum revealed a single peak at +53.2 ppm and the ^1H NMR spectrum contained an aryl multiplet at 7.35 ppm and singlets at 0.66 and 1.16 ppm, corresponding to PPh_3:$AsMe_3$:$AsMe_3$ in the ratio 1:1:1. This suggests a "symmetrically ligated" binuclear complex, $[(PPh_3)(AsMe_3)_2Ru(\mu\text{-}Cl)_3Ru(AsMe_3)_2(PPh_3)]^+$, but with staggered PPh_3 ligands as shown in Figure 3.5. Attempts to displace the remaining PPh_3 by prolonged heating with excess $AsMe_3$ gave no evidence of further substitution.

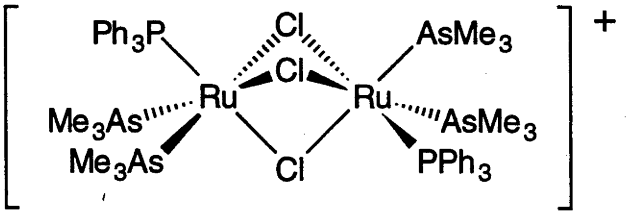

Figure 3.5 *Structure of the mixed-ligand complex $[Ru_2(\mu\text{-}Cl)_3(AsMe_3)_4(PPh_3)_2]^+$.*

In contrast to the arsine complexes, the $[Ru_2Cl_3(PR_3)_6]^+$ complexes investigated in the course of this work have all been prepared previously by a number of procedures. Humphrey's method[18] was used to prepare $[Ru_2(\mu\text{-}Cl)_3(PR_3)_6]^+$ complexes (PR_3 = PMe_2Ph, PEt_3, PEt_2Ph, $PEtPh_2$, $P(OMe)Ph_2$, or 3 x PR_3 = triphos[†]). This involved boiling absolute ethanol suspensions of $[RuCl_2(PPh_3)_3]$ and the appropriate phosphine for an extended period (Fig. 3.6). In the present work, the chloride counter-ions in the $[Ru_2Cl_3(PR_3)_6]Cl$ salts were invariably displaced by triflate as described above for $[Ru_2Cl_3(AsR_3)_6]CF_3SO_3$.

$$2\,[RuX_2(PPh_3)_3] + 6PR_3 \xrightarrow{EtOH,\ \Delta} [Ru_2X_3(PR_3)_6]X + 6PPh_3$$

$$[Ru_2X_3(PR_3)_6]X \xrightarrow[MeOH/CH_2Cl_2]{CF_3SO_3H\ (0.1M),} [Ru_2X_3(PR_3)_6]CF_3SO_3$$

Figure 3.6 *Synthesis of $[Ru_2(\mu\text{-}Cl)_3(PR_3)_6]CF_3SO_3$ complexes.*

[†] triphos = 1,1,1-tris((diphenylphosphino)methyl)ethane.

Bromide-bridged $[Ru_2Br_3(PR_3)_6]^+$ complexes are, however, far less common in the literature than their chloride analogues. An early preparation of $[Ru_2Br_3(PMe_2Ph)_6]^+$, from $RuCl_3.xH_2O$, PMe_2Ph and excess LiBr,[2] was later shown to yield a mixture of $[Ru_2(\mu\text{-}Cl)_x(\mu\text{-}Br)_{3-x}(PMe_2Ph)_6]^+$ complexes (x = 0-3). Authentic $[Ru_2Br_3(PMe_2Ph)_6]Br$ has since been prepared from $[RuBr_2(PPh_3)_3]$.[19] In addition, in the present work, $[Ru_2Br_3(PMe_2Ph)_6]^+$ and $[Ru_2Br_3(PEt_3)_6]^+$ were prepared using Humphrey's method of heating $[RuBr_2(PPh_3)_3]$ with an excess of phosphine in ethanol. Likewise, $[Ru_2Br_3(triphos)_2]^+$ was prepared by heating $[RuBr_2(PPh_3)_3]$ and triphos in 2-methoxyethanol.

$[Ru_2Cl_3(PMePh_2)_6]CF_3SO_3$ and $[Ru_2Br_3(PEt_2Ph)_6]CF_3SO_3$ were obtained in poor yield and purity from $[RuX_2(PPh_3)_3]$, possibly due to competition between the incoming phosphine and PPh_3. Better yields of $[Ru_2Cl_3(PMePh_2)_6]CF_3SO_3$ were achieved by heating $K_3[Ru_2Cl_9]$ with $PMePh_2$ in ethanol. The residue after solvent removal contained $[Ru_2Cl_3(PMePh_2)_6]Cl$, which was converted to the triflate salt as outlined above. Similarly, $K_3[Ru_2Br_9]$ provided a superior route to $[Ru_2Br_3(PEt_2Ph)_6]CF_3SO_3$.

The vitally important $[Ru_2X_3(PMe_3)_6]X$ compounds could not be prepared at all by the $[RuX_2(PPh_3)_3]$ route. Reaction of $[RuX_2(PPh_3)_3]$ (X = Cl, Br) and PMe_3 in ethanol gave only *trans*-$[RuX_2(PMe_3)_4]$. As with the $AsMe_3$ analogues, these neutral monomers resisted condensation to the triply-bridged structure. However, $[Ru_2X_3(PMe_3)_6]CF_3SO_3$ (X = Cl, Br) dimers were readily isolated by reaction of PMe_3 in ethanol/water with $K_3[Ru_2Cl_9]$ or $K_3[Ru_2Br_9]$ as appropriate, followed by triflic acid metathesis.

In summary, the ruthenium nonahalides, $K_3[Ru_2Cl_9]$ and in particular $K_3[Ru_2Br_9]$, have proven to be important starting points for the preparation of triply-halide bridged complexes. Although some of the desired arsine-capped complexes could

be prepared from "$RuCl_3.xH_2O$", the successful preparation of $[Ru_2(\mu\text{-}Cl)_3(AsR_3)_6]^+$ from $K_3[Ru_2Cl_9]$ foreshadowed a general synthetic route to both chloro- and bromo-bridged complexes. Previously, $[Ru_2(\mu\text{-}Br)_3(PR_3)_6]^+$ complexes had been prepared from $[RuBr_2(PPh_3)_3]$,[18] which in itself is prepared from $K_3[Ru_2Br_9]$ *via* an organo-soluble salt of $[Ru_2Br_9]^{3-}$.[19] The potassium salt of $[Ru_2Br_9]^{3-}$ is easily prepared[16] from "$RuCl_3.xH_2O$" and provides a convenient and more direct route to both phosphine- and arsine-capped systems (Fig. 3.7).

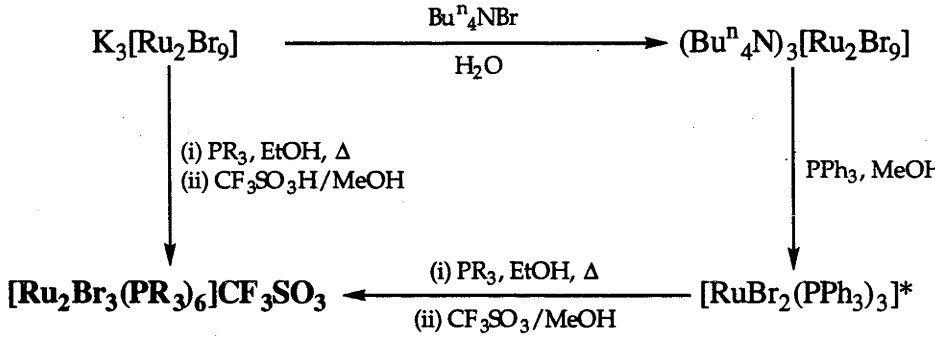

Figure 3.7 *Preparation of $[Ru_2(\mu\text{-}Br)_3(PR_3)_6]CF_3SO_3$ complexes. *Alternatively derived from "$RuCl_3.xH_2O$", PPh_3 and excess LiBr,*[20] *but shown to contain a mixture of $[RuCl_xBr_{2-x}(PPh_3)_3]$ (x = 0-2).*[21]

3.2 ELECTROCHEMISTRY

This is the first account of the voltammetric response of the hexakis arsine dimers. In company with their phosphine-capped predecessors, they display two stepwise reversible oxidations when examined in $CH_2Cl_2/[Bu^n_4N][BF_4]$ (0.5 mol dm^{-3}), as illustrated in Figure 3.8.

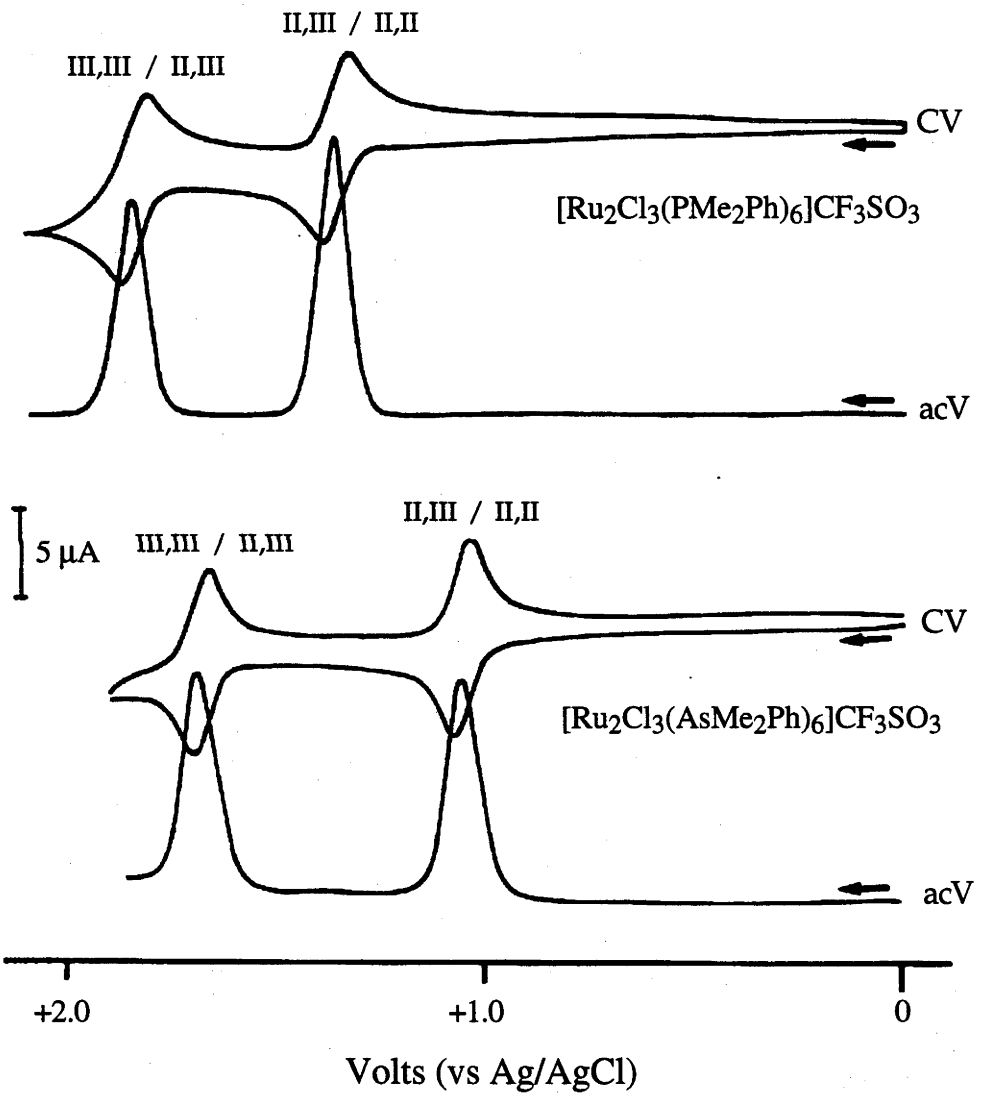

Figure 3.8 *Cyclic and alternating current voltammograms of* $[Ru_2(\mu\text{-}Cl)_3L_6]CF_3SO_3$ *(L =* PMe_2Ph, $AsMe_2Ph$*) in 0.5 mol* dm^{-3} $[Bu^n_4N][BF_4]/CH_2Cl_2$*; scan rates 100 mV* s^{-1} *(CV) and 10 mV* s^{-1} *(acV).*

Bulk coulometry for the first step and steady-state voltammetry employing a rotating platinum electrode establish that both steps are one-electron processes, in accord with Fig. 3.9.

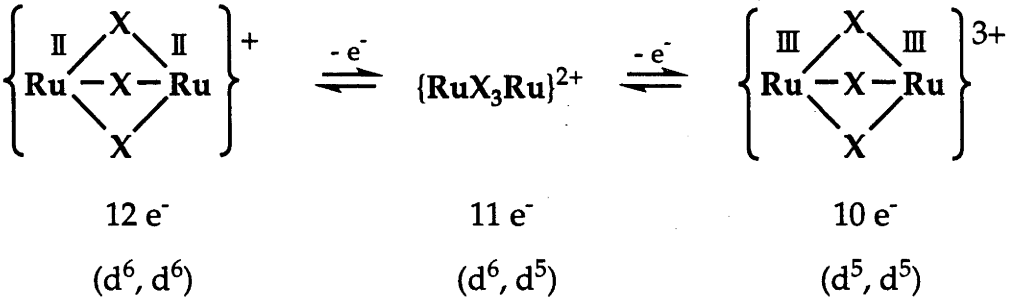

Figure 3.9 *Electron counting scheme for* $[Ru_2(\mu\text{-}X)_3L_6]^{z+}$ *complexes.*

The electrogenerated $\{Ru_2^{III,III}\}^{3+}$ ions are very reactive and tend to degrade in an unspecified way at room temperature. Accordingly, the electrode potentials for all compounds collected in Table 3.1 have been measured at -60 °C. Under these conditions, in the presence of a suitably polarised electrode, there is conclusive spectro-electrochemical evidence that all the singly-oxidised species and even some of the doubly-oxidised species persist unchanged in solution over several hours (see later).

At first sight, there is little in Table 3.1 to suggest a distinction in electronic properties between the arsine and phosphine dimers. The most obvious aspect of these measurements is the general similarity in redox behaviour of corresponding AsR_3 and PR_3 complexes.

Table 3.1 *Electrochemical Data for $[Ru_2X_3L_6]^+$ Complexes.*

Complex	$E_{1/2}$ / V vs Ag/AgCl [a] $E_{ox}(1)$	$E_{ox}(2)$	E_{av} / V [b]	$\Delta E_{1/2}$ / V [c]
$[Ru_2Cl_3(AsMe_3)_6]^+$	+0.95	+1.63	+1.29	0.68
$[Ru_2Br_3(AsMe_3)_6]^+$	+0.95	+1.56	+1.26	0.61
$[Ru_2Cl_3(AsMe_2Ph)_6]^+$	+1.07	+1.70	+1.39	0.63
$[Ru_2Br_3(AsMe_2Ph)_6]^+$	+1.06	+1.62	+1.34	0.56
$[Ru_2Cl_3(AsMePh_2)_6]^+$	+1.19	+1.85	+1.52	0.66
$[Ru_2Br_3(AsMePh_2)_6]^+$	+1.20	+1.76	+1.48	0.56
$[Ru_2Cl_3(AsMe_3)_4(PPh_3)_2]^+$	+1.18	+1.80	+1.49	0.62
$[Ru_2Cl_3(PMe_3)_6]^+$	+1.18	+1.72	+1.45	0.54
$[Ru_2Br_3(PMe_3)_6]^+$	+1.20	+1.69	+1.45	0.49
$[Ru_2Cl_3(PMe_2Ph)_6]^+$ [d]	+1.31	+1.87	+1.59	0.56
$[Ru_2Br_3(PMe_2Ph)_6]^+$ [d]	+1.32	+1.87	+1.60	0.55
$[Ru_2Cl_3(PMePh_2)_6]^+$	+1.38	+1.92	+1.65	0.54
$[Ru_2Cl_3(PEt_3)_6]^+$ [d]	+1.09	+1.71	+1.40	0.62
$[Ru_2Br_3(PEt_3)_6]^+$ [d]	+1.11	+1.68	+1.40	0.57
$[Ru_2Cl_3(PEt_2Ph)_6]^+$ [d]	+1.19	+1.71	+1.45	0.52
$[Ru_2Br_3(PEt_2Ph)_6]^+$	+1.18	+1.70	+1.44	0.52
$[Ru_2Cl_3(PEtPh_2)_6]^+$ [d]	+1.21	+1.80 [e]		
$[Ru_2Cl_3(triphos)_2]^+$ [d]	+1.46	+1.94	+1.70	0.48
$[Ru_2Br_3(triphos)_2]^+$	+1.47	+1.91	+1.69	0.44
$[Ru_2Cl_3(P(OMe)Ph_2)_6]^+$ [d]	+1.46 [e]	+1.97 [f]		
$[Ru_2Cl_3(Me_3tacn)_2]^{2+}$ [d]	-0.09	+1.10	+0.51	1.19
$[Ru_2Br_3(Me_3tacn)_2]^{2+}$ [d]	+0.04	+1.09	+0.57	1.05

[a] *Recorded in CH_2Cl_2 containing 0.5 mol dm^{-3} $[NBu^n_4][BF_4]$ at 213K; ferrocene is oxidised at +0.55 V vs Ag/AgCl under these conditions.* [b] $E_{av} = 1/2(E_{ox}(1) + E_{ox}(2))$. [c] $\Delta E_{1/2} = (E_{ox}(2) - E_{ox}(1))$. [d] *Data from Ref. 18.* [e] *Quasi-reversible.* [f] *Irreversible.*

Rather than focussing on the successive couples themselves, it is appropriate to consider their *mean* ($E_{av} = 1/2(E_{ox}(1) + E_{ox}(2))$ and their *separation* ($\Delta E_{1/2} = E_{ox}(2) - E_{ox}(1)$) in each case, since this separation varies in a characteristic way from one complex to another. For example, for the Me_3tacn/μ-Cl dimer $\Delta E_{1/2}$ is exceptionally large at 1.2 V and E_{av} = +0.5 V, while for the $AsMe_3/\mu$-Cl dimer $\Delta E_{1/2}$ is only 0.7 V and E_{av} = +1.3 V, and the underlying shift in E_{av} is 0.8 V, rather than the shifts of 1.0 or 0.5 V suggested by $E_{ox}(1)$ or $E_{ox}(2)$ respectively..

Considered in this light, the electrochemical data in Table 3.1 invite a number of empirical generalisations:

- Within either the AsR_3 or PR_3 series, variation of R (mainly by substituting aryl by alkyl) is capable of shifting the couples by up to 0.25 V.
- The AsR_3 complexes are characteristically easier to oxidise than their exact PR_3 analogues by about 0.2 V (the mean shift in E_{av} is 190 mV).
- The AsR_3 complexes display distinctly greater separation between successive couples than their PR_3 counterparts (the mean difference in $\Delta E_{1/2}$ = 90 mV).
- Considering the AsR_3 series, the μ-Br dimers tend to display smaller $E_{1/2}$ values (by ~70 mV) and are collectively easier to oxidise (E_{av} shifting by ~40 mV) than their exact μ-Cl analogues.
- When μ-Br replaces μ-Cl in the $[(PR_3)_3Ru(\mu\text{-}X)_3(PR_3)_3]^+$ complexes, $\Delta E_{1/2}$ contracts by only ~30 mV, on average, while E_{av} shifts by a marginal 5 mV.
- The mixed-ligand complex, $[Ru_2Cl_3(AsMe_3)_4(PPh_3)_2]^+$, is unexceptional in its voltammetric properties; compared to $[Ru_2Cl_3(AsMe_3)_6]^+$, retention of one PPh_3 ligand in place of $AsMe_3$ on each Ru centre leads to an increase of 200 mV in E_{av} and a decrease in $\Delta E_{1/2}$ of 60 mV.

These small differences have been pursued in detail because of circumstantial evidence that they underlie and determine mixed-valence behaviour, as discussed overleaf. Figure 3.10 shows that the E_{av} and $\Delta E_{1/2}$ terms are mutually correlated, despite experimental scatter among the present twenty closely related Ru_2 compounds.

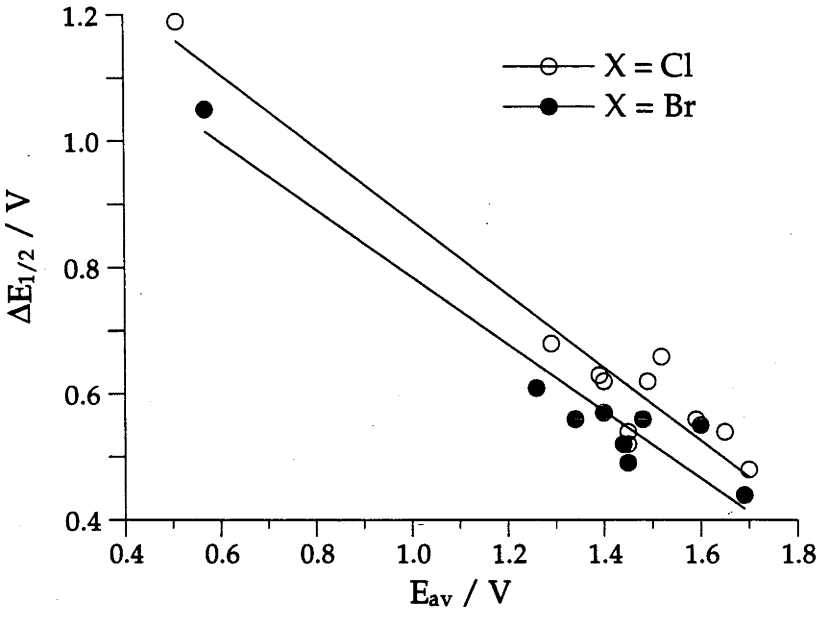

Figure 3.10 *Correlation of $\Delta E_{1/2}$ with E_{av} for $[Ru_2(\mu\text{-}X)_3L_6]^+$ complexes listed in Table 3.1.*

3.3 SPECTRO-ELECTROCHEMISTRY - UV/VIS/NEAR-INFRARED

3.3.1 General Features of the Optical Spectra

As ordinarily isolated, the $[(AsR_3)_3Ru(\mu\text{-}X)_3Ru(AsR_3)_3]^+$ complexes and their PR_3 analogues exist in the relatively uninformative closed-shell oxidation state, in contrast to the archetypal ruthenium ammine "blues" found naturally in the II,III form. Optical spectro-electrochemistry plays a key role in this work; firstly, because it gives access to the numerous mixed-valence species $[L_3Ru(\mu\text{-}X)_3RuL_3]^{2+}$ and establishes their individual stability, and secondly, because near-infrared spectroscopy is the first-choice probe of electronic behaviour for such systems. The optical data (45 000 to 3125 cm^{-1}) for the successive II,II, II,III and III,III states are collected in Tables 3.2, 3.3 and 3.4, respectively.

Figure 3.11 shows the stepwise electro-oxidation of $[Ru_2Cl_3(AsMe_2Ph)_6]^+$, with typical time-dependent progressions to the successive II,III and III,III states monitored in an optical semi-thin-layer electrochemical (OSTLE) cell at low temperature. A separate family of isosbestic points prevails at each step. Three strict requirements applied in the present work are: integrity of all isosbestic points; checks for 100% electrolysis; full retrieval of the starting spectrum upon electrochemical regeneration.

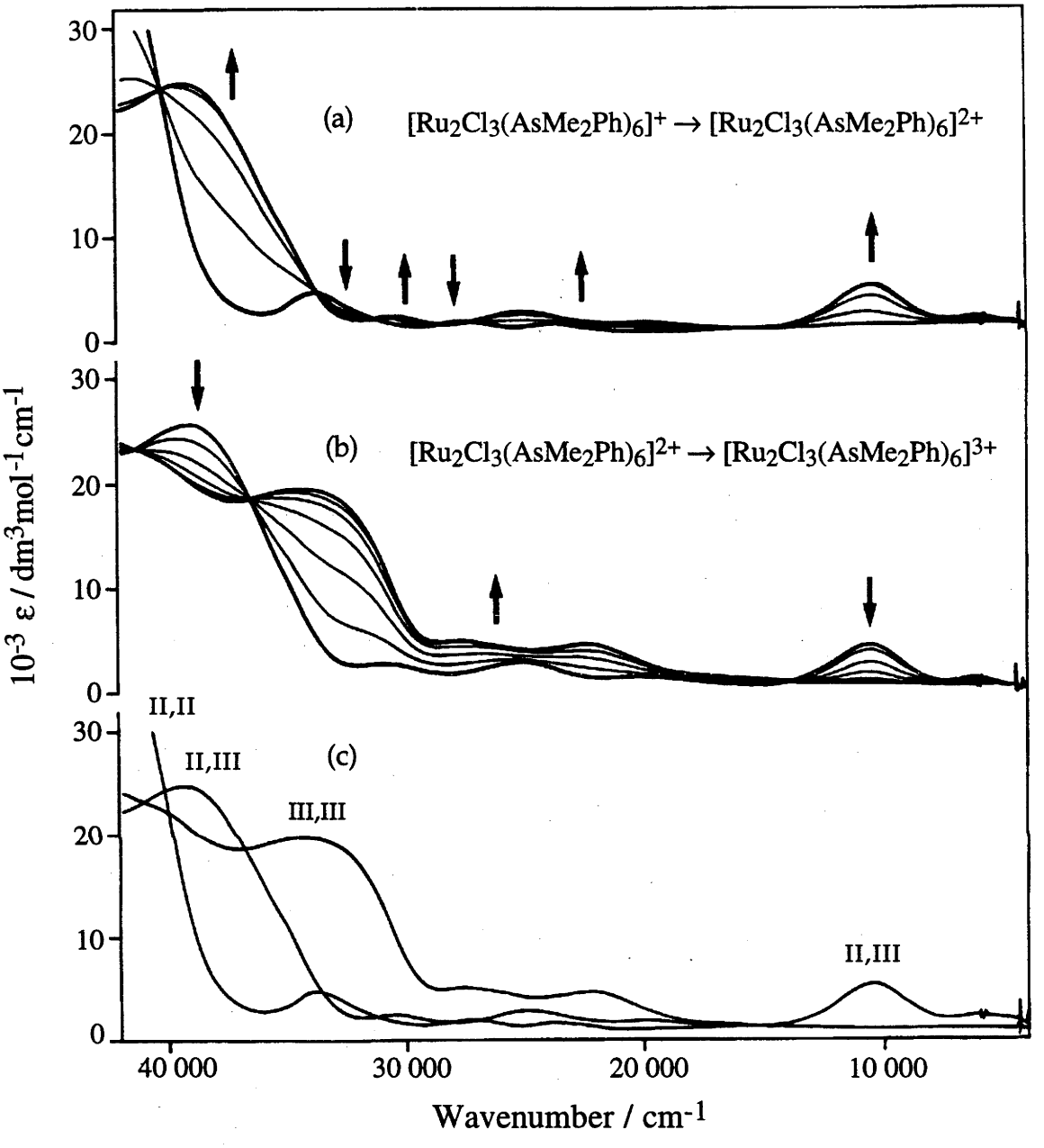

Figure 3.11 *Spectral progressions upon oxidation of (a) $[Ru_2(\mu\text{-}Cl)_3(AsMe_2Ph)_6]^+$, and (b) $[Ru_2(\mu\text{-}Cl)_3(AsMe_2Ph)_6]^{2+}$ in the OSTLE cell. The limiting traces of the II,II, II,III and III,III oxidation states are shown superimposed in (c).*

The $Ru_2^{II,II}$ (12-e) dimers are featureless throughout the visible/near-infrared range, and particularly transparent below ~ 15 000 cm^{-1}, which helps the definition of the emerging near-IR bands in the II,III state. Upon further oxidation these bands collapse again, confirming they are specific to the 11-e configuration rather than being

characteristic single-ion (Ru^{3+}) features. This holds true for the PR_3 compounds as well, despite the complexities in their near-IR spectra mentioned in §1.4.

One distinctive aspect of the II,III and III,III states is the spectral similarity of the μ-Cl and μ-Br forms throughout the UV/visible region. Here one might anticipate obvious features associated with X→Ru(III) CT, which should be red-shifted by 6000 cm^{-1} or more for the bromo complex (see §5.4). This unexpected spectral convergence is also seen for the corresponding μ-Cl and μ-Br ammines - it has a cogent explanation resting on topological exclusion of bridging halide ligands from participation in charge transfer to low-lying acceptor orbitals.[22]

3.3.2 $\{Ru_2^{II,II}\}^+$ Spectra

All the $Ru_2^{II,II}$ compounds in Table 3.2 show an intense absorption near 40 000 cm^{-1} associated with $L(\sigma)\rightarrow Ru(e_g)$ charge-transfer from AsR_3 or PR_3 (where $Ru(e_g)$ is related to the e_g-derived binuclear molecular orbitals, as shown in the molecular orbital scheme in Fig. 3.12). These strong ligand-to-metal charge-transfer bands persist in red-shifted form in the II,III and III,III states, as expected for a LMCT process.

Two low-intensity bands below, and one moderately intense band above 30 000 cm^{-1}, are observed for most AsR_3 and PR_3 complexes. Comparison of corresponding μ-Cl and μ-Br complexes shows that the bands lie at lower energy (500 - 2000 cm^{-1}) for the μ-Br complexes. These bands, likely to arise from transitions between the t_{2g}- and e_g-derived orbitals, should be ligand-field dependent, hence transitions for the μ-Br complexes are at marginally lower energy than their μ-Cl analogues, in accord with the lower single-ion ligand field associated with bromide.[23]

Table 3.2 *UV/Vis/near-IR Spectral Data For $[Ru_2X_3L_6]^+$ Complexes.*

Complex	ν_{max} / cm^{-1} (ε / $dm^3\ mol^{-1}\ cm^{-1}$) [a]
$[Ru_2Cl_3(AsMe_3)_6]CF_3SO_3$	25 090 (1030), 29 000 (950), 35 700 (3830)
$[Ru_2Br_3(AsMe_3)_6]CF_3SO_3$	24 300 (1460), 28 000 (740), 34 000 (5200), 40 800 (32 900)
$[Ru_2Cl_3(AsMe_2Ph)_6]CF_3SO_3$	24 000 (2960), 27 560 (3940), 33 720 (9550), 41 630 (78 200)
$[Ru_2Br_3(AsMe_2Ph)_6]CF_3SO_3$	23 100 (2490), 26 600 (3270), 32 200 (6390), 38 500 (sh), 40 900 (56 600)
$[Ru_2Cl_3(AsMePh_2)_6]CF_3SO_3$	23 400 (1010), 26 600 (1370), 32 320 (4550), 40 450 (43 400)
$[Ru_2Br_3(AsMePh_2)_6]CF_3SO_3$	22 500 (2020), 31 000 (3460), 40 100 (42 100)
$[Ru_2Cl_3(AsMe_3)_4(PPh_3)_2]CF_3SO_3$	24 760 (2500), 33 630 (8150)
$[Ru_2Cl_3(PMe_3)_6]CF_3SO_3$	28 900 (1710), 31 900 (1520), 38970 (3570)
$[Ru_2Br_3(PMe_3)_6]CF_3SO_3$	28 000 (1430), 36 710 (2690), 43 250 (20 800)
$[Ru_2Cl_3(PMe_2Ph)_6]CF_3SO_3$ [b]	29 450 (3730)
$[Ru_2Br_3(PMe_2Ph)_6]CF_3SO_3$ [b]	28 520 (3740)
$[Ru_2Cl_3(PMePh_2)_6]CF_3SO_3$	25 200 (2150), 27 550 (2680), 32 950 (4870)
$[Ru_2Cl_3(PEt_3)_6]CF_3SO_3$ [b]	27 150 (1740), 30 270 (2290), 36 230 (5460)
$[Ru_2Br_3(PEt_3)_6]CF_3SO_3$ [b]	26 180 (2100), 29 380 (2800), 34 380 (5440)
$[Ru_2Cl_3(PEt_2Ph)_6]CF_3SO_3$ [b]	28 800 (3130), 34 300 (6340)
$[Ru_2Br_3(PEt_2Ph)_6]CF_3SO_3$	28 490 (3300), 33 380 (6090), 41 320 (98 600)
$[Ru_2Cl_3(PEtPh_2)_6]CF_3SO_3$ [b]	27 440 (3180)
$[Ru_2Cl_3(triphos)_2]CF_3SO_3$ [b]	27 230 (6020)
$[Ru_2Br_3(triphos)_2]CF_3SO_3$	26 100 (6320)
$[Ru_2Cl_3(P(OMe)Ph_2)_6]CF_3SO_3$ [b]	27 810 (4430)

[a] *Recorded in CH_2Cl_2 containing 0.5 mol dm^{-3} $[NBu^n_4][BF_4]$ at 213K.* [b] *Data from Ref. 18.*

3.3.3 $\{Ru_2^{II,III}\}^{2+}$ Spectra

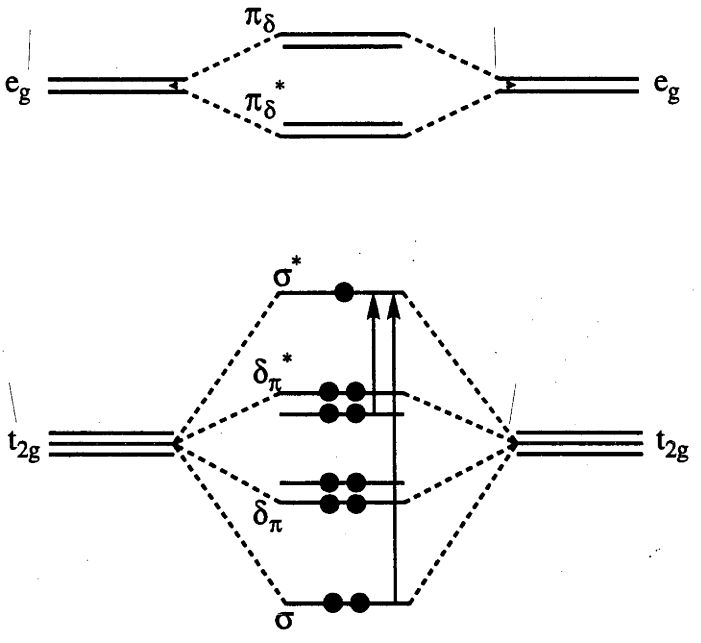

Figure 3.12 *Molecular orbital scheme for D_{3h} confacial bioctahedral geometry. The $\sigma \rightarrow \sigma^*$ and $\delta_\pi^* \rightarrow \sigma^*$ transitions, which dominate the visible/near-IR spectra of the 11-e complexes, are shown. The positioning of the π_δ^* orbital at lower energy than π_δ has recently been reported,[24] however the reverse ordering has been used to assign spectra of, for example, $[Ru_2X_3(NH_3)_6]^{2+}$.[25]*

The dominant features of the mixed-valence 11-e complexes are the two near-IR bands, which will be discussed below. In addition, both AsR_3 and PR_3 complexes display a number of weak bands at higher energy (> 20 000 cm^{-1}). Similar weak bands (between 23 000 and 36 000 cm^{-1}) in the classical "blues" have been assigned as promotions between t_{2g}/e_g-based levels, *e.g.*, using Armstrong's notation[25], $\sigma^* \rightarrow \pi^*$, $\delta,\delta^* \rightarrow \pi$ and $\delta,\delta^* \rightarrow \pi^*$. Comparisons between analogous μ-Cl and μ-Br species show that in all three cases (capping ligands NR_3, AsR_3 and PR_3) these bands are at marginally lower energy for the μ-Br complexes. There is also the possibility of LMCT bands transitions for the AsR_3- and PR_3-capped systems, *e.g.* $As(\sigma) \rightarrow Ru_2(\sigma^*)$. Many monomeric Ru^{III} complexes studied in this work have displayed $As(\sigma)$ or $P(\sigma) \rightarrow Ru^{III}(t_{2g})$ charge-transfer bands in the region 15-20 000 cm^{-1} (§5.4). The broad bands at 20 000 cm^{-1} in the AsR_3- and PR_3-capped binuclear complexes are likely to be composed of a combination of LMCT and d-d type transitions.

We now turn to closer examination of the near-IR spectra of the present complexes, which are of primary importance because of their direct bearing on metal-metal bonding in the mixed valence $[L_3Ru(\mu\text{-}X)_3RuL_3]^{2+}$ state. Figures 3.13 and 3.14 show how the arsine-capped dimers (L = $AsMe_3$, $AsMe_2Ph$; X = Cl, Br) all share the classical band envelope of the established "blues", despite the $\sigma\rightarrow\sigma^*$ band being shifted to substantially lower energies (between 10 000 and 12 000 cm^{-1}). Notably, the mixed-ligand $\{(AsMe_3)_2PPh_3\}$-capped system falls clearly into the same category (Fig. 3.15).

The spectral envelopes for the corresponding family of tertiary-phosphine complexes are much more variable. Figure 3.16 shows the "orthodox" near-IR region of $[Ru_2(\mu\text{-}Cl)_3(AsMePh_2)_6]^{2+}$ compared with the unusual spectrum of the $PMePh_2$ analogue. Figures 3.17 and 3.18 reveal that, among the many hexakis-phosphine complexes we have characterised, only the PMe_3 derivatives lend a classical appearance to the near-IR spectrum. With the benefit of these examples, one can see clearly that the phosphine systems form a series in which the near-infrared spectra still contain discernible $\sigma\rightarrow\sigma^*$ and $\delta_\pi{}^*\rightarrow\sigma^*$ components but become progressively less orthodox in appearance as the manifold shifts ever lower in energy. The anomaly then rests in the dramatic intensity transfer between the two bands as they begin to converge. An alternative reading in which the two bands cross over, so that the $\sigma\rightarrow\sigma^*$ falls to lower frequency but retains the greater intensity, can be dismissed on several grounds (see later).

The comparatively low intensity recorded for the $\delta_\pi{}^*\rightarrow\sigma^*$ band of the $AsMe_3$-capped complexes (the first two entries in Table 3.3) supports the view that these are indeed the complexes most closely resembling the ammine "blues", as depicted in Figure 3.13.

Table 3.3 *UV/Vis/Near-IR spectral data for $[Ru_2X_3L_6]^{2+}$ Complexes.*

Complex	ν_{max} / cm^{-1} (ε / dm^3 mol^{-1} cm^{-1}) [a]		
	$\delta_\pi^* \rightarrow \sigma^*$	$\sigma \rightarrow \sigma^*$	Other bands
$[Ru_2Cl_3(AsMe_3)_6]^{2+}$	6400 (720)	11 800 (5600)	21 200 (720), 27 700 (2300), 31 500 (1240)
$[Ru_2Br_3(AsMe_3)_6]^{2+}$	6470 (1130)	11 150 (6600)	19 700 (540), 25 100 (1890), 27 100 (2480), 31 000 (2030)
$[Ru_2Cl_3(AsMe_2Ph)_6]^{2+}$	6250 (2140)	10 510 (8680)	20 000 (2800), 25 100 (5520), 30 600 (5050), 38 970 (48 100)
$[Ru_2Br_3(AsMe_2Ph)_6]^{2+}$	5900 (1800)	10 100 (4800)	23 900 (3970), 20 000 (sh), 37 900 (43 100)
$[Ru_2Cl_3(AsMePh_2)_6]^{2+}$	6200 (1930)	9700 (4580)	23 740 (7500), 26 500 (7230), 37 040 (29 000)
$[Ru_2Br_3(AsMePh_2)_6]^{2+}$	5800 (2020)	8700 (3170)	20 100 (1730), 22 200 (2890), 36 900 (33 200)
$[Ru_2Cl_3(AsMe_3)_4(PPh_3)_2]^{2+}$	4900 (2630)	8600 (5290)	25 100 (4370)
$[Ru_2Cl_3(PMe_3)_6]^{2+}$	5800 (2360)	9350 (7500)	19 660 (220), 24 200 (sh), 28 490 (2510), 33 800 (1540)
$[Ru_2Br_3(PMe_3)_6]^{2+}$	5590 (2430)	8870 (5080)	16 600 (150), 23 100 (sh), 27 060 (2220), 31 900 (1630)
$[Ru_2Cl_3(PMe_2Ph)_6]^{2+}$ [b]	5100 (2390)	7950 (3330)	17 000 (730), 28 000 (4400)
$[Ru_2Br_3(PMe_2Ph)_6]^{2+}$ [b]	4700 (3440)	7400 (2480)	17 600 (950), 26 800 (4660)
$[Ru_2Cl_3(PMePh_2)_6]^{2+}$	4050 (3300)	4950 (2780)	15 930 (930), 25 200 (3480)
$[Ru_2Cl_3(PEt_3)_6]^{2+}$ [b]	4600 (3000)	7460 (2580)	16 500 (350), 27 000 (3830)
$[Ru_2Br_3(PEt_3)_6]^{2+}$ [b]	4140 (4200)	6500 (1600)	14 230 (420), 26 020 (4350)
$[Ru_2Cl_3(PEt_2Ph)_6]^{2+}$ [b]	4500 (2800)	6250 (1500)	16 900 (720), 25 960 (3510)
$[Ru_2Br_3(PEt_2Ph)_6]^{2+}$	4100 (3980)	4700 (sh)	13 100 (720), 16 800 (990), 25 600 (3900)
$[Ru_2Cl_3(PEtPh_2)_6]^{2+}$ [b]	4900 (2700)	6980 (1610)	16 920 (990), 24 100 (3140)
$[Ru_2Cl_3(triphos)_2]^{2+}$ [b]	4100 (1580)	5300 (1700)	17 000 (800), 27 460 (6200)
$[Ru_2Br_3(triphos)_2]^{2+}$	4360 (3140)	5400 (3000)	22 800 (14 000)
$[Ru_2Cl_3(P(OMe)Ph_2)_6]^{2+}$ [b]	4900 (1720)	8420 (1760)	14 740 (920), 27 270 (4100)

[a] *Recorded in CH_2Cl_2 containing 0.5 mol dm^{-3} $[NBu^n_4][BF_4]$ at 213K. Spectra were obtained by in situ electrogeneration as described in the text.*

[b] *Data from Ref. 18.*

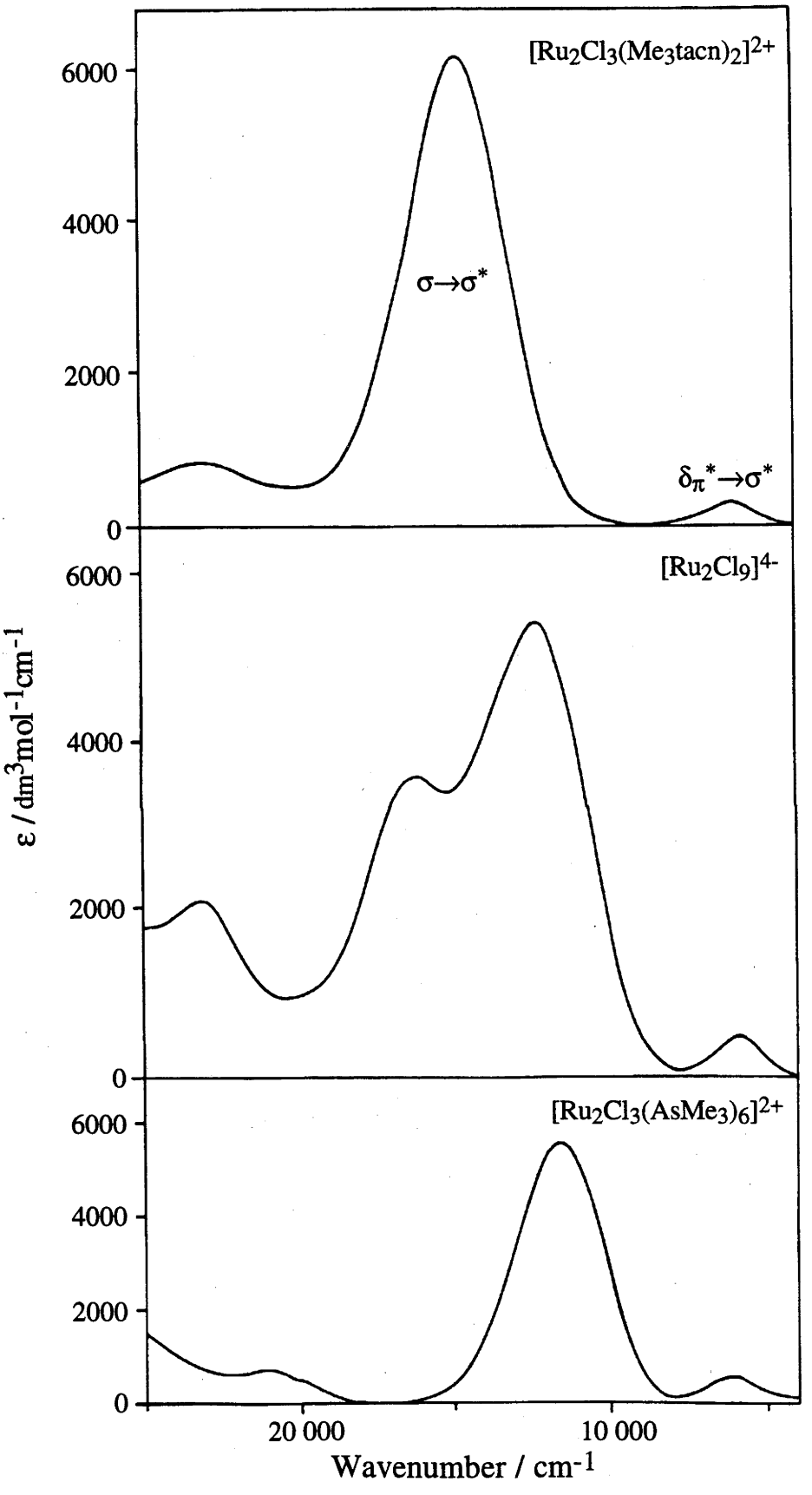

Figure 3.13 *Comparison of the visible/near-IR band envelopes of* $[Ru_2(\mu\text{-}Cl)_3L_6]^z$ *complexes.*

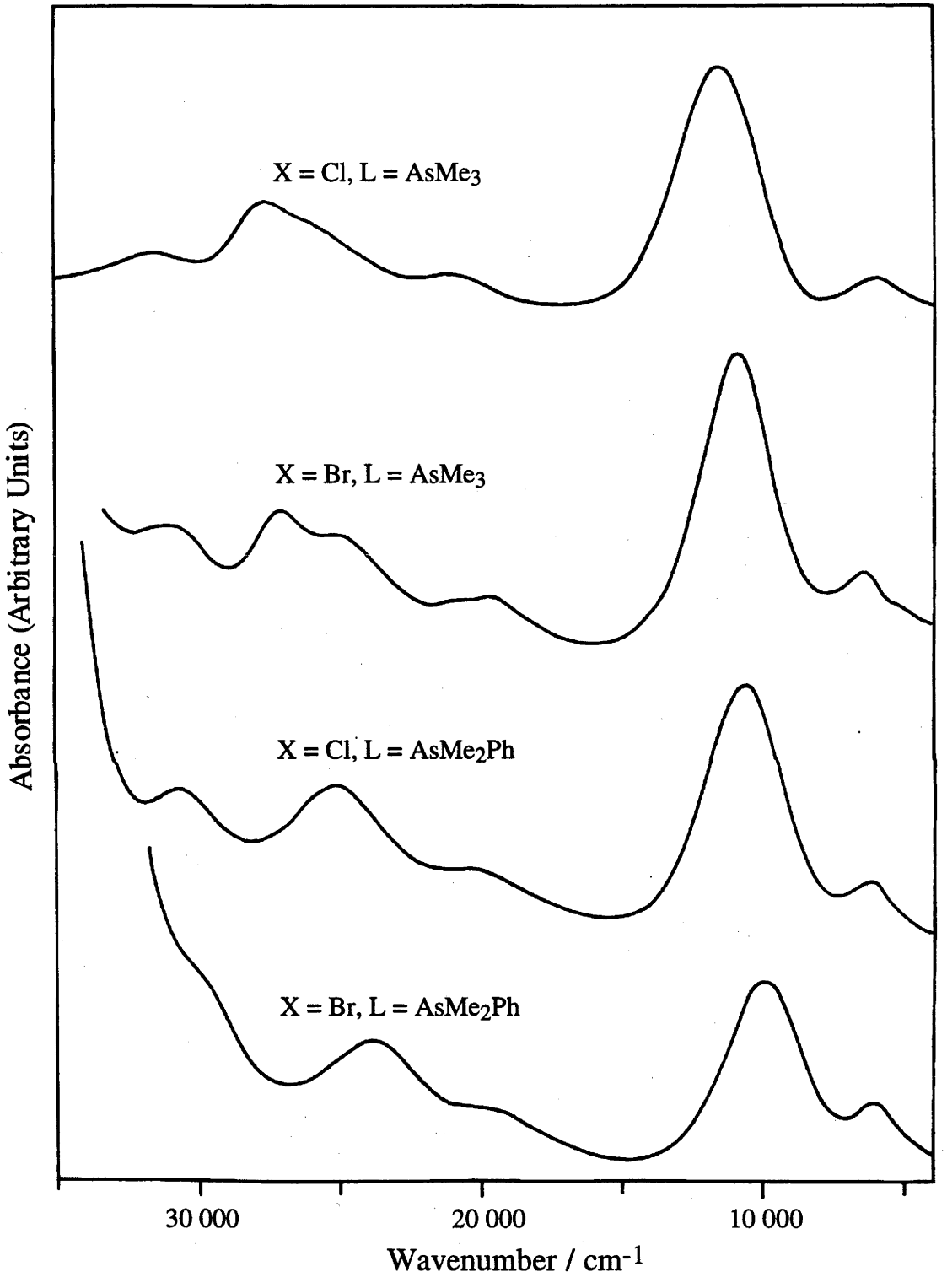

Figure 3.14 *Visible/near-IR spectra of* $[Ru_2(\mu\text{-}X)_3(AsR_3)_6]^{2+}$ *complexes.*

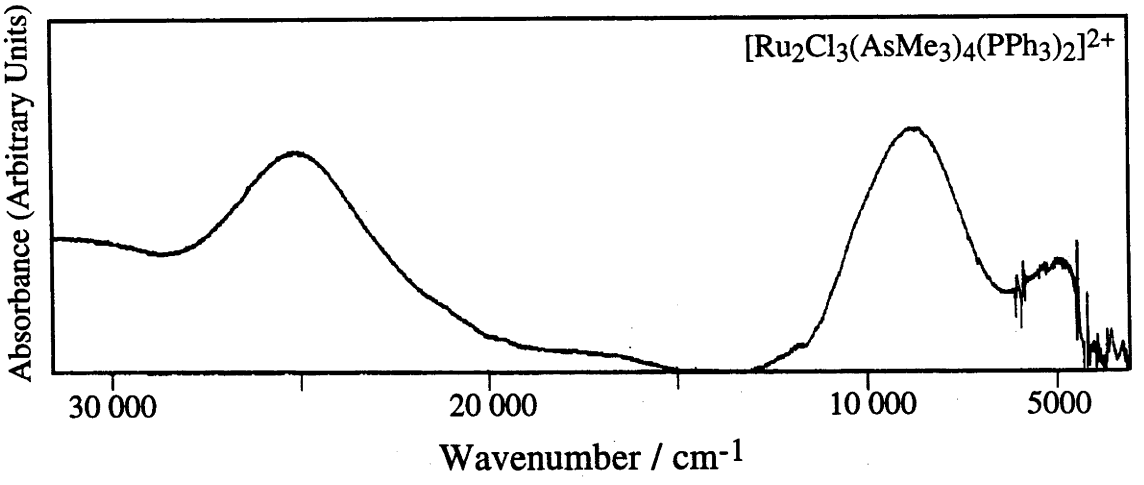

Figure 3.15 *Visible/near-IR spectrum of* $[Ru_2(\mu\text{-}Cl)_3(AsMe_3)_4(PPh_3)_2]^{2+}$.

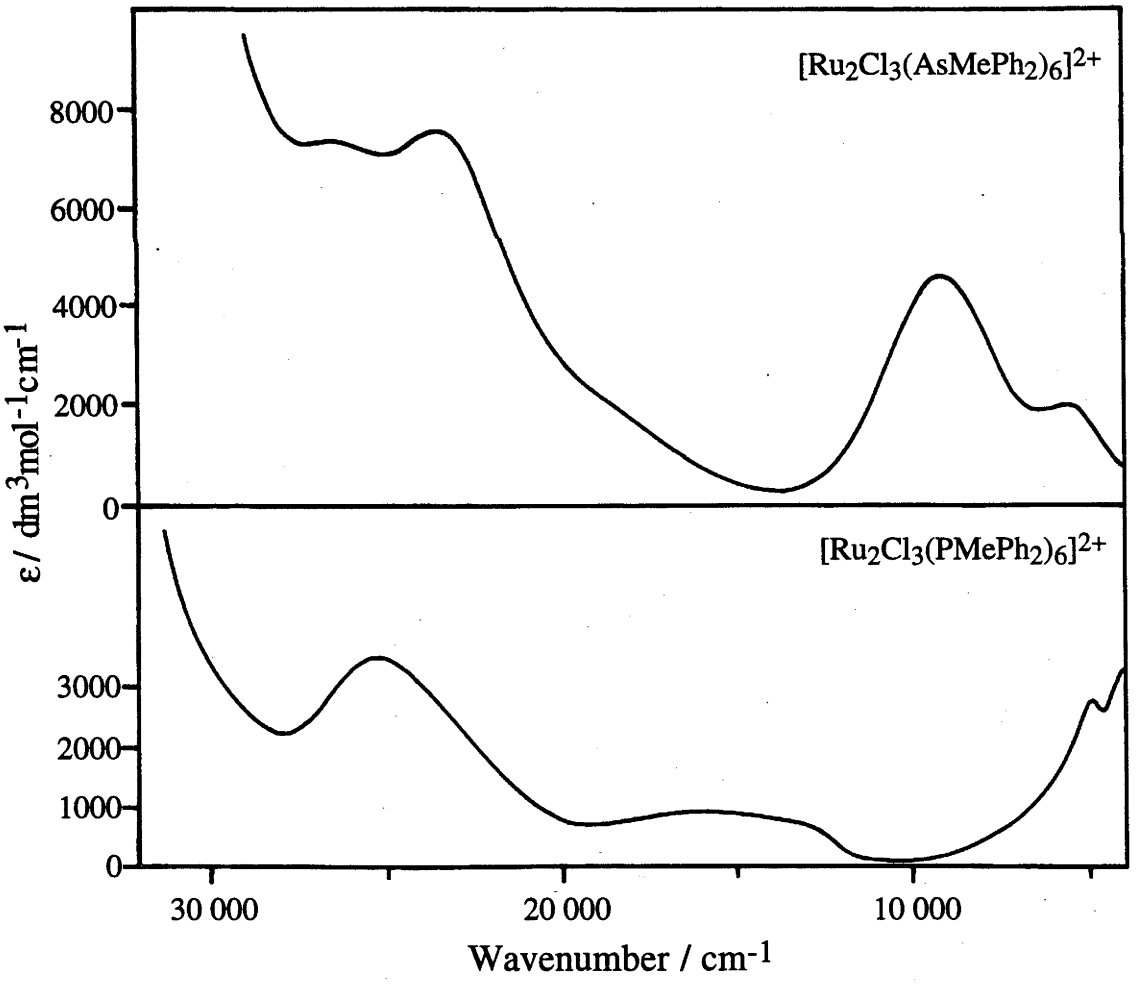

Figure 3.16 *Comparison of the visible/near-IR spectra of* $[Ru_2(\mu\text{-}Cl)_3(EMePh_2)_6]^{2+}$ *(E = P, As).*

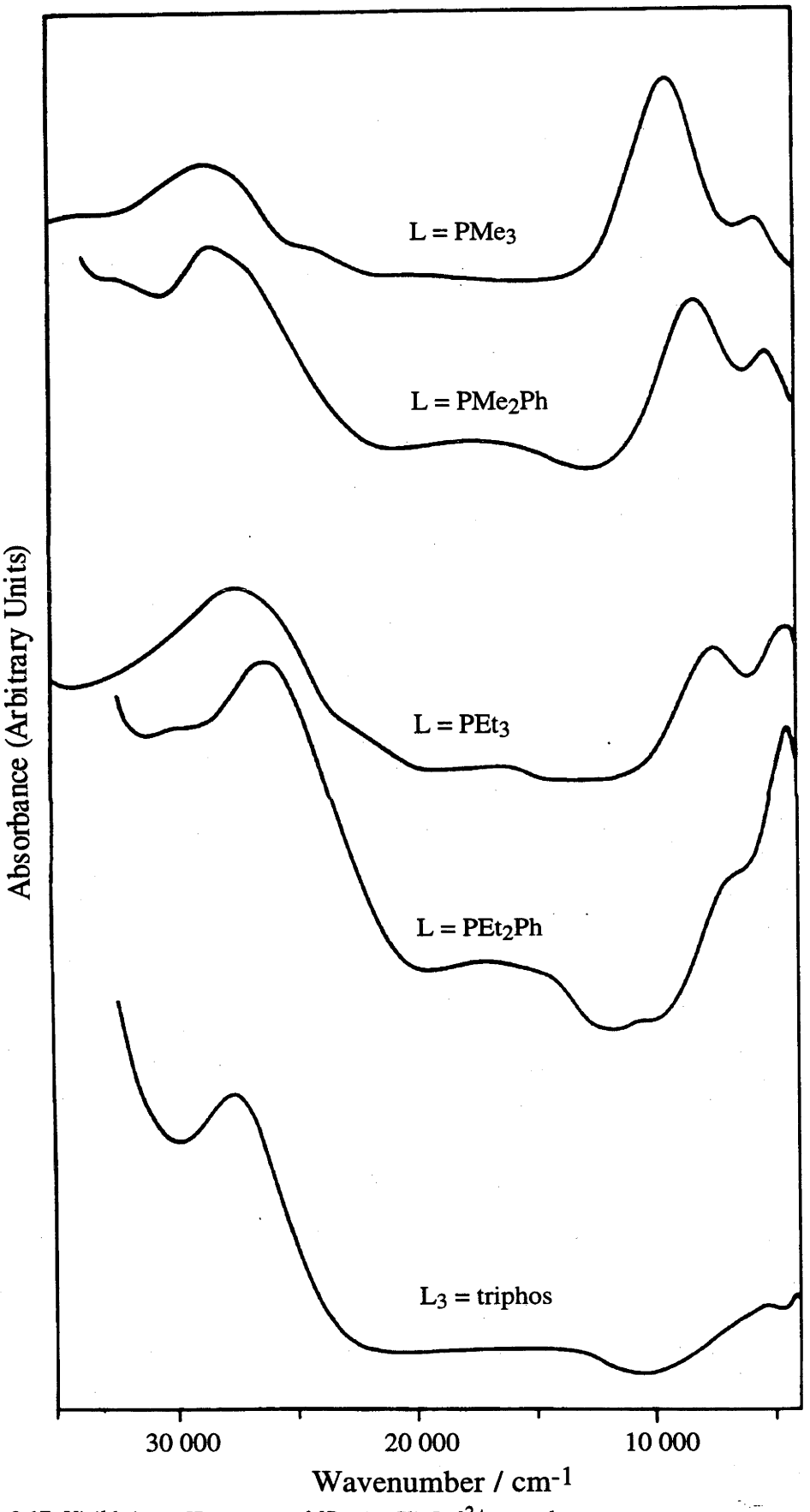

Figure 3.17 *Visible/near-IR spectra of* $[Ru_2(\mu\text{-}Cl)_3L_6]^{2+}$ *complexes.*

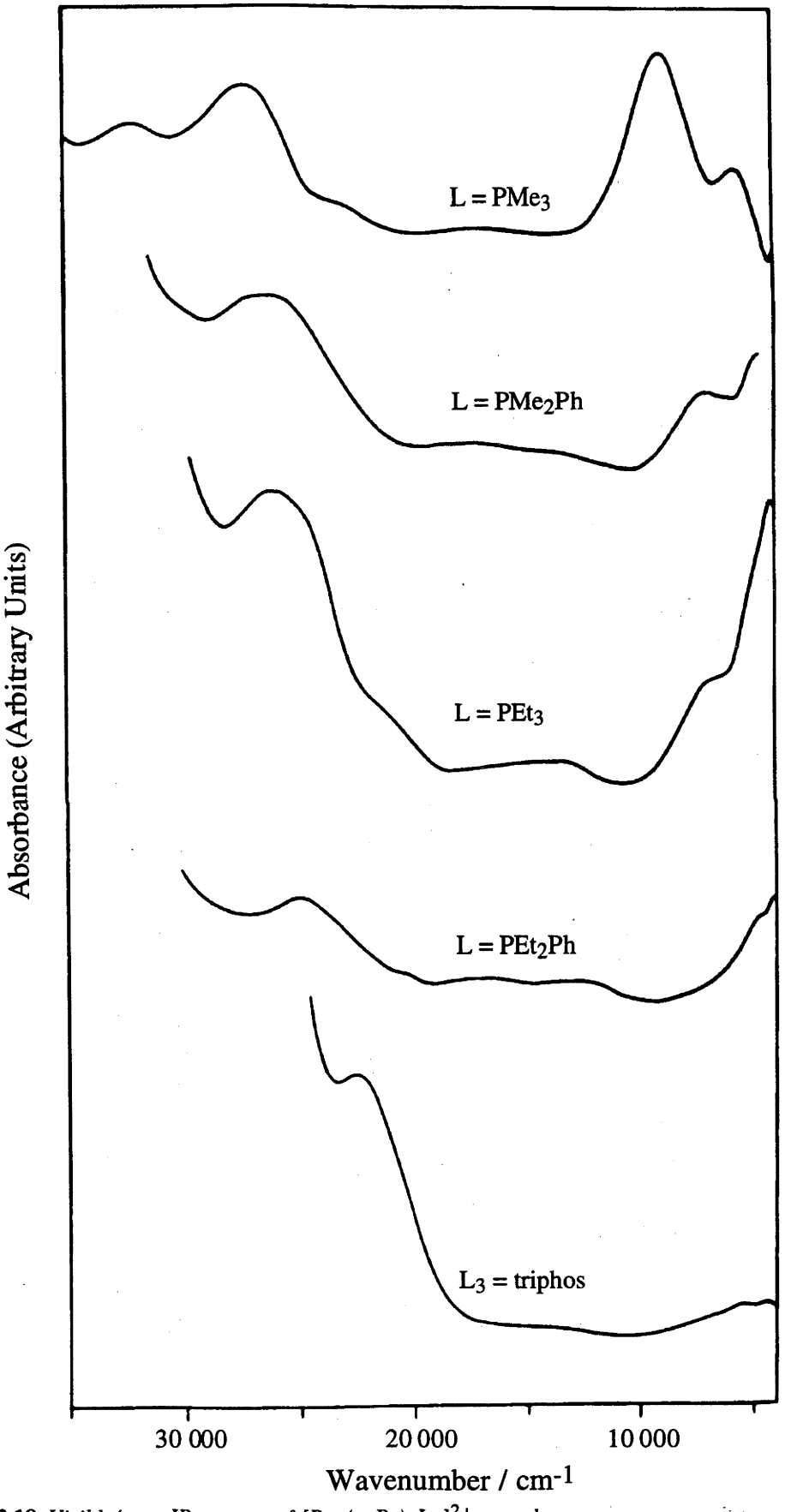

Figure 3.18 *Visible/near-IR spectra of* $[Ru_2(\mu\text{-}Br)_3L_6]^{2+}$ *complexes.*

Some years ago, in studying the more general class $[Cl_x(PR_3)_{3-x}Ru(\mu\text{-}Cl)_3Ru(PR_3)_{3-y}Cl_y]^{2-x-y}$, Heath, Stephenson and colleagues noted that in addition to a weak, low-energy inter-valence charge-transfer band (now identified as the $\delta_\pi \rightarrow \sigma^*$ band), the fully symmetric systems (y = x) displayed a characteristic higher-energy band whose position seemed to reflect the degree of delocalisation.[26] This is, in retrospect, an apt description of the $\sigma \rightarrow \sigma^*$ band.

The EPR data in the next section offer strong supporting evidence that the symmetric AsR_3 and PR_3 complexes collectively represent a continuum of delocalised 11-e electronic structures. We conclude that the non-classical appearance of some of the near-IR spectra is a consequence of complexities in optical behaviour in the limit of ever-diminishing confacial σ/σ^* splitting in the M.O. diagram (Fig. 3.12), and not due to a dichotomy in bonding in the ground-state. A more embracing treatment[27] suggests that the simple picture of a strong $\sigma \rightarrow \sigma^*$ band and a less intense $\delta_\pi^* \rightarrow \sigma^*$ band, with $\nu_{\delta\pi^* \rightarrow \sigma^*}$ roughly half $\nu_{\sigma \rightarrow \sigma^*}$, is bound to collapse in the domain of weaker, but still delocalised, metal-metal coupling which prevails in the phosphine systems. In brief, as the energy of the $\sigma \rightarrow \sigma^*$ band diminishes (and $\sigma \rightarrow \sigma^*$ and $\delta_\pi^* \rightarrow \sigma^*$ converge), spin-orbit coupling promotes an intensity-stealing mechanism effective only in this special domain.

The large number of complexes investigated here makes it possible to rank the orderly progress of the crucial $\sigma \rightarrow \sigma^*$ band over the whole body of twenty compounds. To a good theoretical approximation,† the frequency of this band is equal to twice the energy of the one-electron separation of the σ and σ^* orbitals (W_σ) and provides a direct measure of metal-metal coupling (including both direct and bridge-mediated contributions). Moreover, a correlation between the electrochemical and optical data is readily discerned, such that those binuclear compounds which are relatively electron-deficient (higher E_{av}) and less closely coupled (smaller $\Delta E_{1/2}$) are precisely the ones to

† Thus, in Fig. 3.12 and 3.28, the σ and σ^* orbitals are separated by $2W\sigma$; see also refs 37, 39.

emerge with lower $\sigma \rightarrow \sigma^*$ promotion energies. Further comment is deferred until the complementary EPR data for the same 11-e systems have been considered.

3.3.4 $\{Ru_2^{III,III}\}^{3+}$ Spectra

The UV/Vis/near-IR data for diruthenium complexes oxidised to the $Ru_2^{III,III}$ (10-e) state are listed in Table 3.4. These seven complexes displayed exceptional stability compared to the majority of complexes which were unstable when oxidised to the $\{Ru_2^{III,III}\}^{3+}$ state, even at -60 °C.

Table 3.4 *UV/Vis/Near-IR Spectral Data for* $[Ru_2X_3L_6]^{3+}$ *Complexes*

Complex	ν_{max} / cm^{-1} (ε / dm^3 mol^{-1} cm^{-1}) [a]
$[Ru_2Cl_3(AsMe_2Ph)_6]^{3+}$	22 370 (8600), 27 600 (9300), 33 900 (37 600)
$[Ru_2Br_3(AsMe_2Ph)_6]^{3+}$	21 700 (4300), 24 600 (4600), 33 000 (31 900), 42 700 (46 600)
$[Ru_2Cl_3(AsMePh_2)_6]^{3+}$	22 000 (7290), 240900 (8860), 32 960 (45 000), 39 340 (37 400)
$[Ru_2Cl_3(PEt_3)_6]^{3+}$ [b]	**11 100 (4550)**, 16 200 (1100), 25 480 (3540), 27 800 (3540)
$[Ru_2Br_3(PEt_3)_6]^{3+}$ [b]	4200 (300), **10 090 (3110)**, 16 800 (2340)
$[Ru_2Cl_3(PEt_2Ph)_6]^{3+}$ [b]	4500 (170), **10 100 (3850)**, 12 600 (1800)
$[Ru_2Br_3(PEt_2Ph)_6]^{3+}$	9 800 (5150), **12 500 (2570)**, 340410 (60 100)

[a] *Recorded in* CH_2Cl_2 *containing 0.5 mol* dm^{-3} $[NBu^n_4][BF_4]$ *at 213K. Spectra were obtained by in situ electrogeneration. The suggested pairwise transition (see text) in* PR_3 *complexes is shown in bold.* [b] *Data from Ref. 18.*

In the III,III complexes, the absence of halide to ruthenium charge-transfer absorption noted above (together with the relatively high local ligand-field strength which should displace the "crystal field" transitions above 25 000 cm^{-1}) means that the near-UV and visible spectrum is dominated by the $\sigma \rightarrow \sigma^*$ and $\delta_\pi^* \rightarrow \sigma^*$ transitions within the binuclear manifold, uncomplicated by other features. The iso-electronic hexa-arsino complexes have "orthodox" visible/near-IR spectra much as measured previously[15,18] for their ammine counterparts. The well-defined leading band near 22 000 cm^{-1} (Fig 3.19 and Table 3.4) is provisionally assigned to the $\sigma \rightarrow \sigma^*$ band without any implication that

the underlying W_σ term has increased from the Ru_2(II,III) value (see below). It is uncertain whether the metal-metal interaction would be greater in the 10-e two-electron "single-bond" system or the 11-e single-electron "hemi-bond" case, despite the formal increase in bond order. The increase in electrostatic repulsion of the two 3+ metal centres and orbital contraction of the single-ion d orbitals are effects that could negate the influence of the potential two-electron bond.

The energy of the $\sigma\rightarrow\sigma^*$ band is increased in the 10-e systems due to electron-electron correlation. In the odd-electron systems, to a first approximation, electron-electron correlation terms do not need to be considered, and the energy of the $\sigma\rightarrow\sigma^*$ transition can be assumed to be representative of the energy difference between the σ and σ^* orbitals, whereas in the 10-e case, the $\sigma\rightarrow\sigma^*$ band is expected to be strongly displaced to higher energy, due to the unpairing of two electrons. This effect can displace the $\sigma\rightarrow\sigma^*$ absorption band to higher energy by as much as 10 000 cm^{-1} relative to the underlying σ/σ^* orbital separation.[22]

The PR_3-capped III,III complexes in Table 3.4 contain a remarkable, intense feature near 10 000 cm^{-1} as shown in Fig. 3.19. For the purpose of this work, it is important to note that the AsR_3 complexes exhibiting "orthodox" mixed-valence (11-e) spectra (similar to the classical "blues") also show "orthodox" spectra for the 10-e species. The intense band near 10 000 cm^{-1} in the PR_3 complexes resembles a feature in the spectrum of the isoelectronic $[Ir_2Cl_9]^-$, which has been assigned as a pairwise transition‡ associated with the localised $d^5\cdots d^5$ system.[28] Unfortunately the PMe_3 complexes, which we believe may lie near the crossover of these two situations, have not yet been stabilised at the 10-e level.

‡ A concerted transition arising from each centre, at twice the energy of the single-ion transition. These bands are characteristically intense and narrow in profile.

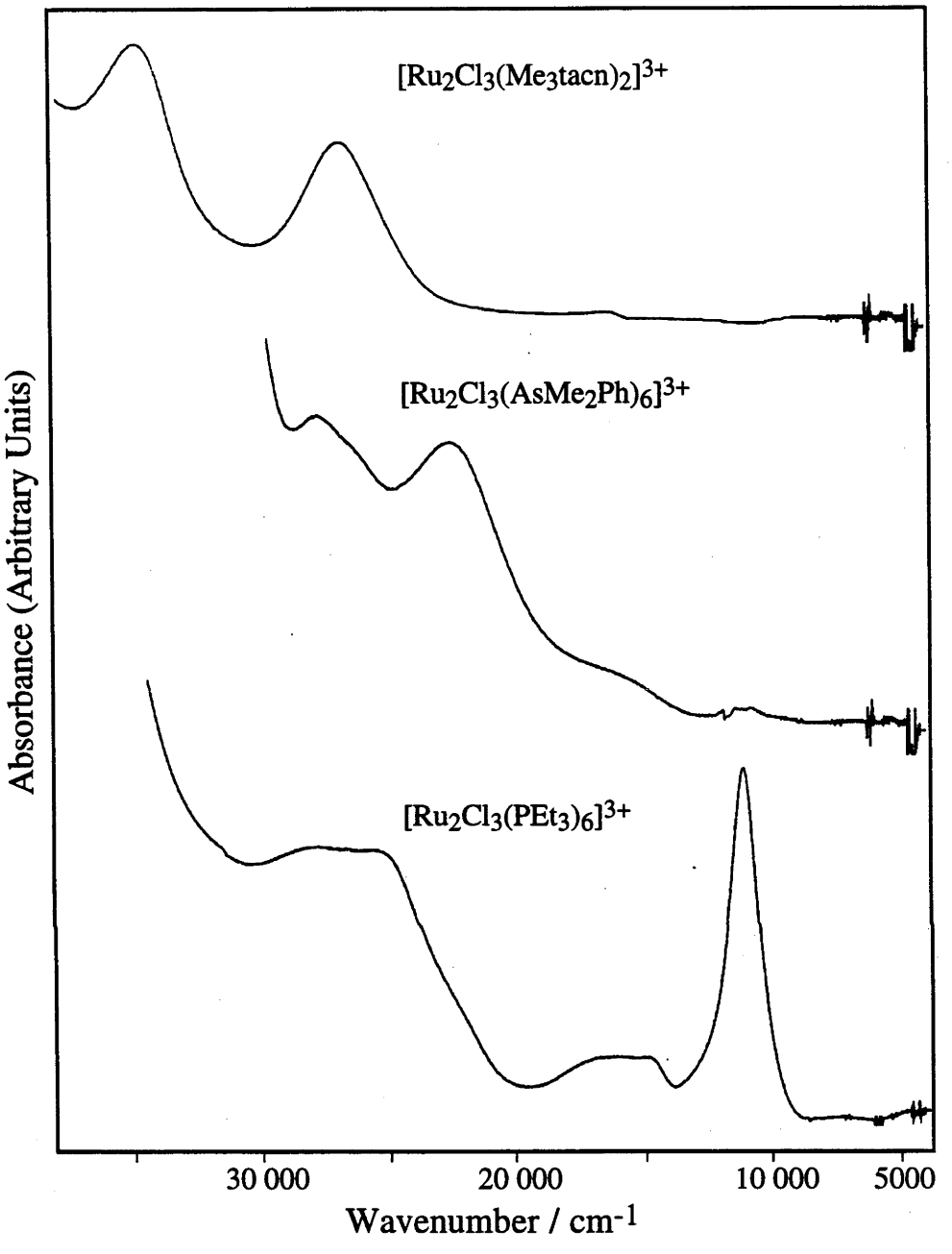

Figure 3.19 *UV/Vis/near-IR spectra of* $[Ru_2(\mu\text{-}Cl)_3L_6]^{3+}$ *complexes.*

3.4 EPR SPECTRA OF $\{Ru_2^{II,III}\}^{2+}$ COMPLEXES

3.4.1 Introduction

For an isolated electron, characterised by the quantum number s = 1/2, there are two possible spin states, $m_s = \pm 1/2$, which differ in energy in the presence of an applied magnetic field (Zeeman splitting). Transitions between these levels occur with the absorption of microwave radiation, in accord with the selection rule $\Delta m_s = \pm 1$, and are measured in the EPR spectrum. Absorption of energy will occur when the microwave frequency matches the energy separation between the two states. The energy difference between the $m_s = +1/2$ and -1/2 states, is given by:

$$\Delta E = h\nu = g\mu_B B \qquad (3.1)$$

where the value of g depends on the electron's environment, μ_B is the Bohr magneton and B is the magnitude of the applied magnetic field. The value for an isolated electron, g_e, is 2.0023.

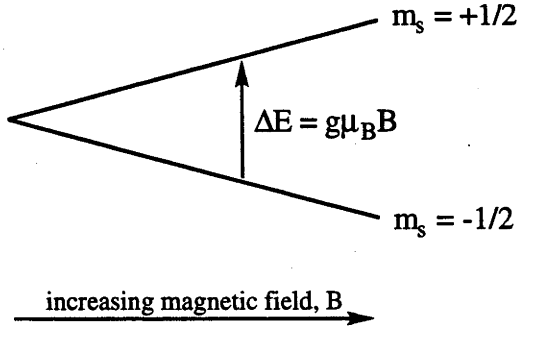

Figure 3.20 *Splitting of the spin states of an electron in a magnetic field.*

For a paramagnetic transition metal complex, the unpaired d-electrons of the central ion may possess orbital angular momentum, in addition to spin angular momentum. The quantised orbital and spin momenta (labelled L and S respectively) can interact with one another ("spin-orbit coupling"), and also with any external magnetic field. This spin-orbit interaction has its origin in relativistic theory, where the nucleus is considered from the electron's reference frame/coordinate system. Spin-orbit coupling

may be viewed as the interaction of the magnetic moment of an electron spin with the magnetic field induced by the motion of the charged nucleus around the electron. The net orbital and spin momenta couple to give a total angular momentum, represented by the quantum number J (= L + S). The effectiveness of the spin-orbit coupling is identified by the spin-orbit coupling constant, λ, which measures the energy separation within the L/S multiplet, usually specified in units of cm^{-1}, and is characteristic of each metal ion.

The Zeeman operator, H_Z, in its simplest first-order version then reflects the orbital contribution by taking the form:

$$H_Z = \mu_B B(g_1 S + L) \qquad (3.2)$$

where $g_1 = 2$. The Zeeman energy splitting may still be expressed much as for the isolated electron except that, in the multi-electron/molecular situation, $h\nu = g_{eff}\mu_B B$ and the effective g-tensor (g_{eff}) becomes a complex parameter which includes both spin and the influence of the orbital angular momentum contribution. This arises because of the artificial but convenient assumption that the transition is governed by $\Delta M_S = \pm 1$, the so-called "spin-only Hamiltonian" approach, rather than by $\Delta M_J = \pm 1$. For this reason, g_{eff} can be anisotropic when the molecular symmetry departs from cubic, and can take values differing markedly from 2.0023. The behaviour of the g-tensor then becomes a sensitive probe of molecular symmetry, electronic configuration and bond type.

For an axially distorted system (be it tetragonal or trigonal), g will have one component (g_z) parallel to the principal symmetry axis, which is called $g_{\parallel}$, and two equivalent components ($g_x = g_y$) along the x and y axes, referred to collectively as $g_{\perp}$. Because of this, the magnetic resonance condition is dependent upon the alignment of the molecule with respect to the magnetic field. In a population of randomly oriented molecules (*e.g.* in a frozen solution or "glass") both resonances will be separately observable at different, characteristic energies.¶

¶ In the EPR experiment we maintain constant frequency and sweep the magnetic field, B.

In a six-coordinate metal complex, lowering the molecular symmetry below O_h will differentiate between the t_2 orbitals. For example, in *fac*-$[RuCl_3(PR_3)_3]$ the t_2 orbitals are split into non-degenerate x_o and doubly-degenerate $x_\pm$ orbitals, where we use the trigonal wavefunctions as defined by Sugano *et al.*[29] Here the subscripts 0 and +/- refer to the quantised angular momentum with respect to the trigonal axis, z. The trigonal field splitting of one-electron t_2 orbitals is then defined as $v = E(x_o) - E(x_\pm)$.

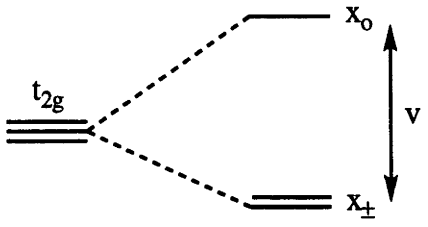

Figure 3.21 *Splitting of octahedral t_2 orbitals with axial distortion.*

For a low spin d^5 (t_2^5) configuration with orbital splitting as shown in Fig. 3.21, where the $x_\pm$ orbitals are assumed to be stabilised to a greater extent than x_o, two electronic states result. In this case the $x_\pm^4x_o^1$ state, $^2A_1$, will lie at lower energy than the $x_\pm^3x_o^2$ state, ^2E. The two states are separated by an energy difference Δ_t, which approximately equals v, defined in Fig. 3.21, although there are significant second-order corrections.[27] This trigonal-field parameter, Δ_t, is defined as positive when the $^2A_1$ state lies at lower energy than the ^2E state,[30] as shown in Fig. 3.22. Similarly, if the x_o orbital lies lower than $x_\pm$, then the ^2E state ($x_o^2x_\pm^3$) is more stable than $^2A_1$ ($x_o^1x_\pm^4$), and Δ_t is negative.

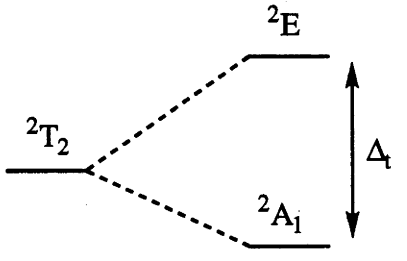

Figure 3.22 *Splitting of the $^2T_2$ term in a trigonally distorted t_2^5 octahedral complex.*

In trigonally distorted S = 1/2 systems, such as those discussed in this thesis, the quantitative relationship between the effective g-tensor and the axial field parameter, Δ_t, has been derived from crystal field theory.[31-33] Application of the Zeeman operator H_Z (3.2) to the components of the $^2T_2$ multiplet described above leads to first order expressions for the $g_{||}$ and $g_\perp$ values:

$$g_{||} = 2\,|\,(1+K)\cos^2\alpha - \sin^2\alpha\,| \qquad (3.3)$$

$$g_\perp = 2\,|\,\sqrt{2}\,K\cos\alpha\sin\alpha + \sin^2\alpha\,| \qquad (3.4)$$

where $\tan 2\alpha = \sqrt{2}\,(1/2-\Delta_t/\lambda)^{-1}$. Here, the multi-electron parameter K is introduced, rather than the more familiar k, as the "effective orbital reduction" or "electron delocalisation" factor. The value of K is likely to approach unity, as the tendency of covalency to reduce k is compensated by configurational interaction between ground and excited states.[34] For example, quite typically k = 0.7, but K = 125% k.

The $g_\perp$ and $g_{||}$ expressions detailed above can then be plotted against the ratio Δ_t/λ, as shown in Fig. 3.23. In these expressions, λ is the effective spin-orbit coupling for the $^2T_2(t_2^5)$ multiplet. To the first order, $\lambda = \zeta$, the one-electron spin-orbit coupling constant, and takes a positive sign.

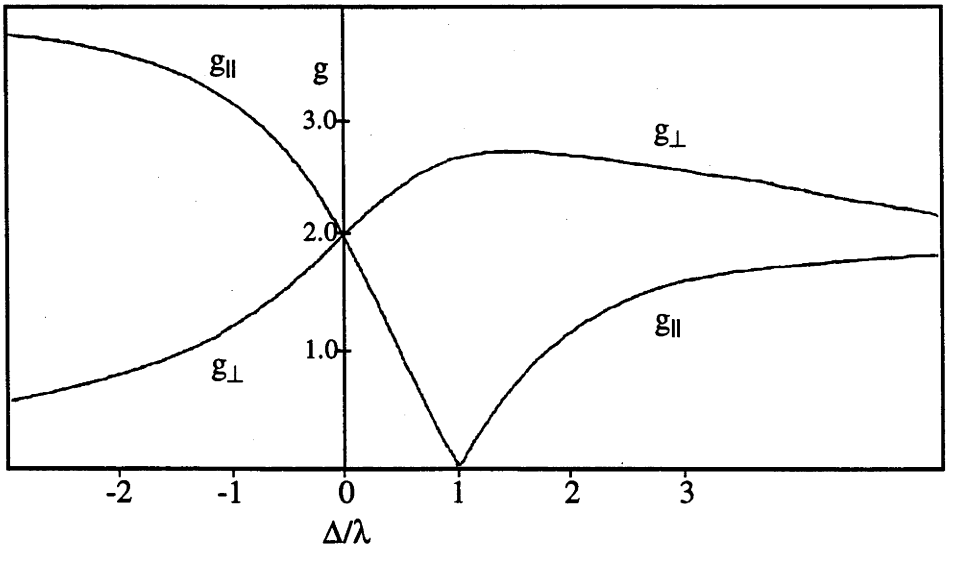

Figure 3.23 *General form of the plot of g-values vs Δ/λ, from equations 3.3 and 3.4, for K = 1 (λ positive).*

There is nothing in the derivation of these equations restricting them to monomer paramagnets. It has been shown by Hush[35] and others[36,37] that expressions 3.3 and 3.4 can be applied to delocalised (S = 1/2) binuclear systems. For example, in the trigonally distorted D_{3h} binuclear complexes under investigation in this thesis, the σ and σ^* orbitals arise expressly by interaction of the x_o wavefunctions of each metal centre, and likewise δ_π and δ_π^* are formed from the two sets of $x_\pm$ wavefunctions.

3.4.2 EPR Spectra of $[Ru_2(\mu\text{-}X)_3L_6]^{2+}$ Complexes

Other than the EPR analysis of $[Ru_2(\mu\text{-}X)_3(NH_3)_6]^{2+}$ complexes,[37] reports of EPR spectra of triply halide-bridged $Ru_2^{II,III}$ systems have been rather scattered, and no particular significance has been attached to them except to establish the S = 1/2 nature and overall symmetry of the complexes in question. In general, only compounds found naturally in the II,III state have been examined elsewhere.[15,38] The one exception is the early study in Edinburgh on the electrogenerated series $[Cl_xL_{3-x}RuCl_3RuL_{3-y}Cl_y]^{2-x-y}$ (L mostly PR_3 or AsR_3), where the level of terminal chloride ligation (x+y) ranged from 0 to 3.[26] Table 3.5 lists the EPR data of a number of $[Ru_2(\mu\text{-}X)_3L_6]^{2+}$ complexes, from both the present work and elsewhere. In our laboratory the L = AsR_3 and PR_3 complexes were either chemically or electrochemically oxidised to the mixed-valence state, and the EPR spectra were recorded as frozen $CH_2Cl_2/[Bu^n_4N][BF_4]$ (0.5 mol dm^{-3}) solutions at 20 K. The diverse conditions reported for the other complexes listed in Table 3.5 should be noted. In particular, values for $[Ru_2(\mu\text{-}Br)_3(Me_3tacn)_3]^{2+}$ seem elevated with $g_{||}$ unexpectedly greater than 2.0 (though converging with $g_\perp$ as expected; see overleaf).

The present EPR spectra were sharply defined and invariant in form between 10K and 30 K. Diminished signal strength with decreasing Curie susceptibility prevented accurate measurements above 40 K. The signals generally disappeared altogether before 100 K, but could be fully recovered on cooling. Failure to observe EPR spectra for $[Ru_2(\mu\text{-}X)_3(PR3)_6]^{2+}$ complexes in the range 120 - 290 K has been reported elsewhere,[26] and this is the first time these axial signals have been uncovered.

Table 3.5 *EPR Data For* $[Ru_2X_3L_6]^{2+}$ *Complexes.*

Complex	$\nu_{\sigma\rightarrow\sigma^*}$ / cm^{-1} [a]	EPR [b] $g_\perp$	EPR [b] $g_{\|\|}$
$[Ru_2Cl_3(NH_3)_6]^{2+}$ [c]	17 100	2.10	1.95
$[Ru_2Br_3(NH_3)_6]^{2+}$ [c]	15 700	2.16	1.95
$[Ru_2Cl_3(Me_3tacn)_2]^{2+}$ [d]	14 700	2.12	1.90
$[Ru_2Br_3(Me_3tacn)_2]^{2+}$ [d]	13 240	2.23	2.03
$[Ru_2Cl_3(H_2O)_6]^{2+}$ [e]	16 500	2.08	1.96
$[Ru_2Cl_3(AsMe_3)_6]^{2+}$	11 600	2.16	1.90
$[Ru_2Br_3(AsMe_3)_6]^{2+}$	10 800	2.22	1.85
$[Ru_2Cl_3(AsMe_2Ph)_6]^{2+}$	10 510	2.18	1.87
$[Ru_2Br_3(AsMe_2Ph)_6]^{2+}$	10 100	2.24	1.77
$[Ru_2Cl_3(PMe_3)_6]^{2+}$	9350	2.23	1.82
$[Ru_2Br_3(PMe_3)_6]^{2+}$	8800	2.28	1.65
$[Ru_2Cl_3(AsMe_3)_4(PPh_3)_2]^{2+}$	8700	2.26	1.73
$[Ru_2Cl_3(PMe_2Ph)_6]^{2+}$	7950	2.29	1.68
$[Ru_2Cl_3(PEt_3)_6]^{2+}$	7460	2.32	1.65
$[Ru_2Br_3(PMe_2Ph)_6]^{2+}$	7400	2.34	*f*
$[Ru_2Cl_3(PEtPh_2)_6]^{2+}$	6980	2.32	1.50
$[Ru_2Br_3(PEt_3)_6]^{2+}$	6500	2.35	*f*
$[Ru_2Cl_3(PEt_2Ph)_6]^{2+}$	6250	2.32	1.40
$[Ru_2Cl_3(PMePh_2)_6]^{2+}$	4950	2.35	*f*
$[Ru_2Br_3(PEt_2Ph)_6]^{2+}$	4800	2.35	*f*

[a] Recorded in CH_2Cl_2 at 213 K unless stated otherwise. [b] Recorded in frozen glass CH_2Cl_2 solutions containing $[Bu^n_4N][BF_4]$ (0.5 mol dm^{-3}) at 20 K, unless stated otherwise. [c] Visible spectrum recorded in DMSO,[39] EPR recorded in DMSO/glycerol glass at 60 K.[37] [d] EPR recorded as DMSO glass at 10 K.[38] [e] Visible spectrum recorded in aqueous solution, EPR recorded as aqueous glass at 150 K.[15] [f] $g_{||}$ too broad and weak to assign.

Figure 3.24 illustrates the range of EPR behaviour spanned by the present electrogenerated hexakis arsine and phosphine compounds. These delocalised, binuclear S = 1/2 paramagnets display an axially symmetric g-tensor, as expected. That is, $g_{||} = g_z$ and $g_\perp = g_x, g_y$, where z coincides with the Ru-Ru axis and so with the principal alignment of the singly occupied σ^* orbital. In all AsR_3 and PR_3 complexes $g_\perp > 2$ and $g_{||} < 2$, and the numerically greater component is associated with the more intense EPR

signal. At one extreme, where the axial perturbation provided by metal-metal bonding greatly exceeds local spin-orbit coupling, $g_{\perp}$ and $g_{\parallel}$ should both approach 2.0,[40] and this is seen for "blues" such as $[Ru_2X_3(Me_3tacn)_2]^{2+}$. There is a systematic technical difficulty in tracking the $g_{\parallel}$ resonance as it diminishes in value because it becomes broad and weak, and is ultimately undetectable when $g_{\parallel} < ca.$ 1.4.

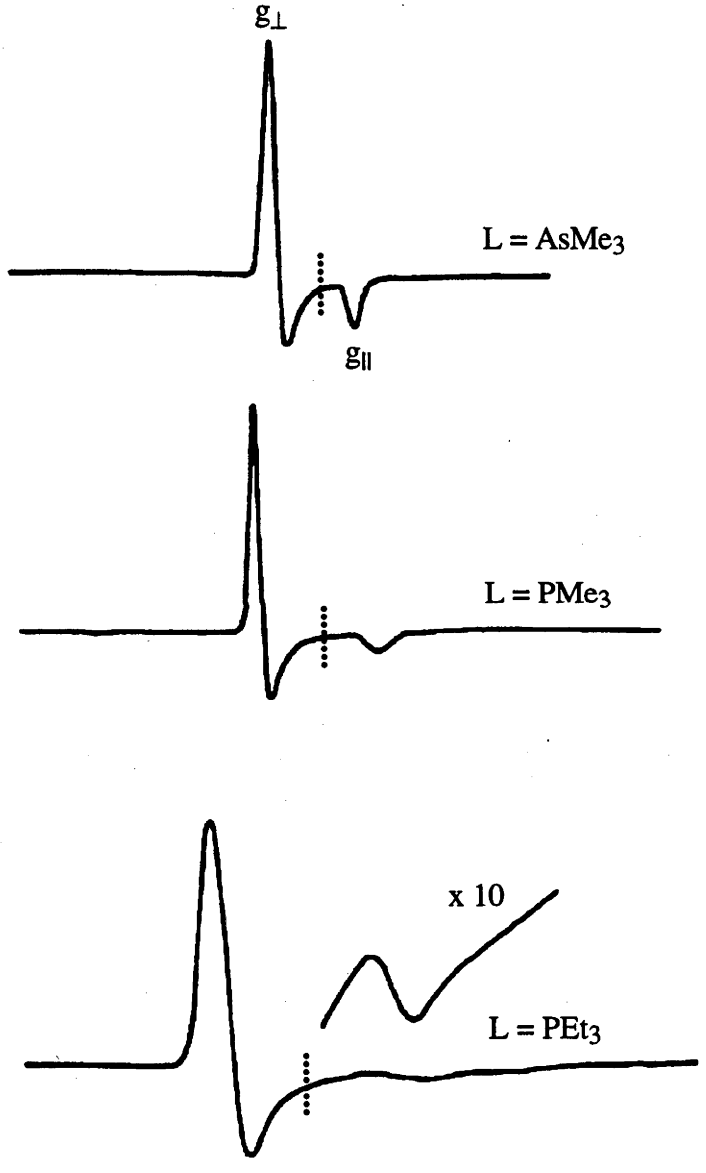

Figure 3.24 *EPR spectra of* $[Ru_2(\mu\text{-}Cl)_3L_6]^{2+}$ *complexes. The dotted line represents a g value of 2.0. All spectra were recorded at 20 K in frozen* $CH_2Cl_2/[Bu^n_4N][BF_4]$ *solutions.*

By inspection, the present tertiary arsine and phosphine complexes form a continuous series with progressively diverging $g_{\perp}$ and $g_{\parallel}$ values. The mixed-ligand complex falls smoothly in the sequence with no evidence of its lower formal symmetry. Descending Table 3.5, $g_{\perp}$ increases to ~2.35 and then levels off, whereas $g_{\parallel}$ decreases, slowly at first and then increasingly steeply from its initial value of 1.90. This bimodal trend, as shown in Fig. 3.25, follows the classical model discussed above. Given that the energy of the $\sigma \rightarrow \sigma^*$ transition is a measure of the metal-metal interaction, and assuming comparable metal-centred spin-orbit coupling over the range of 11-e complexes studied, the striking similarity between the theoretical plot of g-values vs Δ_t/λ (Fig. 3.23), and experimental g-values vs $\nu_{\sigma \rightarrow \sigma^*}$ (Fig. 3.25) implies that the trigonal field distortion parameter, Δ_t, is dominated by the degree of interaction between the two metal centres.

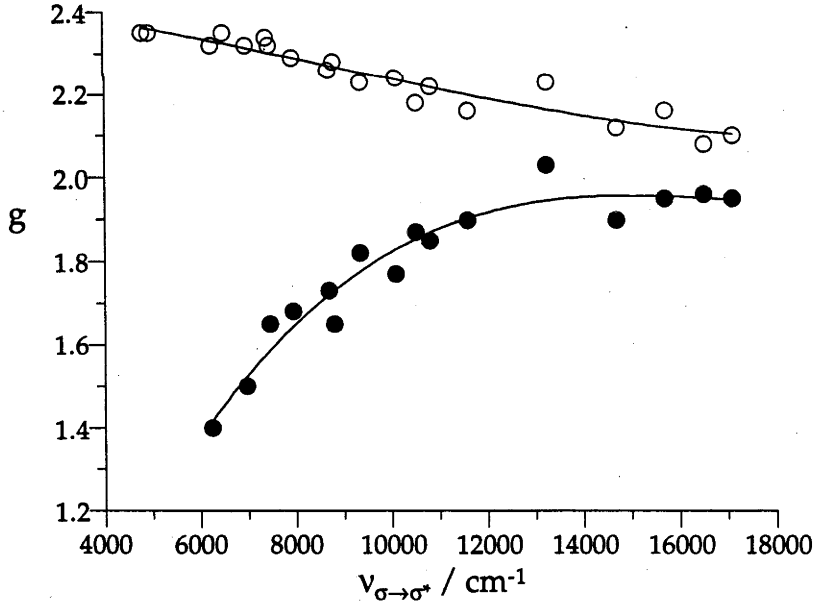

Figure 3.25 *Plot of g values vs* $\nu_{\sigma \rightarrow \sigma^*}$. $g_{\perp}$ *and* $g_{\parallel}$ *are represented by open and closed circles respectively. The smooth curves are computer-generated lines of best fit, to 3rd order polynomials. Data taken from Table 3.5.*

3.4.3 Conclusions from EPR Spectra

The detailed ligand-field analysis of the axial g-tensor for this body of compounds and the fundamental, quantitative correlation with the associated metal-metal σ-bonding is under theoretical development in our laboratory.[27] Here we wish merely to stress our qualitative observations. Firstly, the smooth progression in EPR parameters independently confirms the overall ranking of compounds within the family. Despite the marked contrast between the first and last members, there is no evidence of a dichotomy in electronic ground state. We believe a very different g-tensor would emerge in the so-far hypothetical situation of a trapped ($Ru^{2+}Ru^{3+}$) ground state. Accordingly, an empirical correlation exists whether the strength of electronic coupling is judged by voltammetry ($\Delta E_{1/2}$), near-IR spectroscopy ($\nu_{\sigma\rightarrow\sigma^*}$), or electron paramagnetic resonance ($g_\perp$ and $g_\parallel$). It is worth noting that if a cross-over assignment were adopted, with $\nu_{\sigma\rightarrow\sigma^*}$ lower than $\nu_{\delta\pi^*\rightarrow\sigma^*}$ for the majority of phosphine complexes (see above), then the optical aspect of this correlation would break down.

In summary, the metal-metal interaction, as measured by $\nu_{\sigma\rightarrow\sigma^*}$, dominates the axial ligand-field distortion and this is reflected in the g-tensor. For this reason the EPR spectra are particularly deserving of rigorous analysis, which is beyond the scope of this thesis, and will be the subject of ongoing study. The body of EPR data collected in this work, in conjunction with previously unexploited data, has helped place both PR_3 and AsR_3 complexes in context with their "blue" analogues.

3.5 STRUCTURAL DATA

3.5.1 Ru_2(II,II) Complexes

As part of this study, we have obtained the first X-ray crystallographic measurements on the confacial hexa-arsino di-ruthenium cations, $[Ru_2X_3(AsMe_3)_6]^+$ (X = Cl and Br) and $[Ru_2Cl_3(AsMe_2Ph)_6]^+$, patterned on the earlier confacial phosphine-capped compounds. In addition we have obtained structures of the $[Ru_2X_3(PMe_3)_6]^+$ (X = Cl and Br) complexes. The dimensions of $[Ru_2Cl_3(PMe_3)_6]^+$ have been reported elsewhere,[7] and is remarkable for the relatively short Ru···Ru non-bonding distance of 3.27 Å (see below). We collected our own data on the triflate salt of this cation so that detailed comparisons between the four ($AsMe_3$/PMe_3, Cl/Br) structures could be as reliable as possible. Our structure of $[Ru_2Cl_3(PMe_3)_6]CF_3SO_3$ is notably different from that reported for the $[Ru_2Cl_3(PMe_3)_6][BF_4]$,[7] with a difference in the crucial Ru···Ru distance of 0.1 Å longer in the newly discovered structure. Figure 3.26 illustrates the molecular structure of the relatively uncluttered $AsMe_3$ compound. In both cases coordination in the triply-bridged cations approaches regular trigonal symmetry. Selected bond lengths and angles for the cations are listed in the Appendices 3.1 - 3.5.

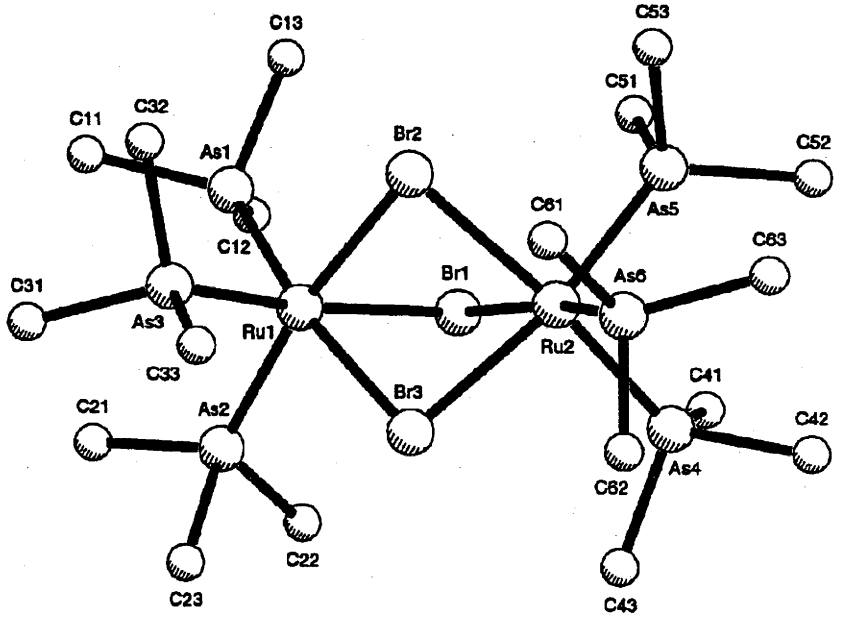

Figure 3.26 *Molecular structure of* $[Ru_2(\mu\text{-}Br)_3(AsMe_3)_6]^+$.

Mean values of the most pertinent dimensions are collected in Table 3.6, where the μ-Cl/$AsMe_2Ph$ compound is compared directly with its μ-Cl/PMe_2Ph congener and also with a wider range of tertiary phosphine analogues.

Table 3.6 *Structural Parameters for Triple Halide-Bridged Diruthenium Complexes*

	Ru-Ru /Å	Ru-X [a] /Å	Ru-L [a] /Å	Ru-X-Ru [a] /°	L-Ru-L [a] /°	ref [b]
$[Ru_2Cl_3(AsMe_3)_6]^+$	3.263(1)	2.48	2.37	82.4	95.0	tw
$[Ru_2Cl_3(AsMe_2Ph)_6]^+$	3.275(1)	2.46	2.40	83.5	95.4	tw
$[Ru_2Cl_3(PMe_3)_6]^+$	3.374(6)	2.50	2.26	85.1	95.2	tw
$[Ru_2Cl_3(PMe_3)_6]^+$ [c]	(3.27$_5$)	(2.48)	(2.25)	(82.9)	(95.4)	7[c]
$[Ru_2Cl_3(PMe_2Ph)_6]^+$	3.39	2.49	2.29	86.0	96	5
$[Ru_2Cl_3(PEt_2Ph)_6]^+$	3.44	2.48	2.32	87.9	96.9	41
$[Ru_2Cl_3(PBu_3)_6]^+$	3.39	2.49	2.30	86.2	96.6	42
$[Ru_2Cl_3(triphos)_2]^+$	3.455	2.49	2.31	87.8	88.3	8
$[Ru_2Br_3(AsMe_3)_6]^+$	3.413(1)	2.61	2.38	81.8	94.6	tw
$[Ru_2Br_3(PMe_3)_6]^+$	3.5365(8)	2.64	2.27	84.2	95.0	tw

[a] *Averaged values.* [b] *tw = this work.* [c] *Less appropriate comparison (see text); this structure has highly disordered BF_4^- counter-ions whose spatial relationship to the cation is uncertain. No special cation/anion contacts are apparent in the unit-cell organisation of the present family of $CF_3SO_3^-$ derivative.*

These X-ray data refer to the $Ru_2^{II,II}$ oxidation state which of course has no net metal-metal bonding. The wide separation of the metal centres, ranging from above 3.25 to 3.45 Å, confirms this and presumably reflects the effect of the underlying cation/cation repulsion. Remarkably however, the $Ru_2^{II,II}$ arsine complexes have a distinctly smaller bridgehead angle than typical phosphine systems, by 3° or more, with a corresponding contraction of at least 0.1 Å in the non-bonding Ru-Ru separation. It is most instructive that the structural differences between the binuclear arsine and phosphine complexes are encountered at the closed-shell II,II level, because it makes it clear that we require an explanation that does not rely on the operation of metal-metal bonding. The source of this discriminatory effect on the geometry of the $\{Ru(\mu\text{-}X)_3Ru\}^+$ core is not immediately obvious, since the μ-Cl/$AsMe_2Ph$ complex and its μ-Cl/PMe_2Ph analogue exhibit very similar exterior cone angles in the RuL_3 face (95.4° vs 96°) and also a similar *trans*

influence on the bridging Ru-Cl bond length (2.46 vs 2.49 Å). Similar differences between phosphine and arsine derivatives are observed between the μ-Cl/$AsMe_3$ and μ-Cl/PMe_3, and μ-Br/$AsMe_3$ and μ-Br/PMe_3 complexes. In all of these examples a geometric distinction between AsR_3 and PR_3 complexes is observed, with Ru···Ru distances extended by ~0.12 Å in the phosphine derivatives, which also have a larger bridgehead angle. The Cl/PMe_3 complex has the shortest Ru···Ru distance and the sharpest bridgehead angle of all the phosphines, in accord with its near-classical optical spectrum. The AsR_3/PR_3 distinction revealed here may reflect the extended Ru-As bonds (longer by ~0.12 Å) reducing contact of the bulky ligands with the bridging $\{X_3\}$ array.

3.5.2 Ru_2(II,III) Complexes

With respect to the geometry of the *oxidised* (11-e) systems $[L_3Ru(\mu\text{-}X)_3RuL_3]^{2+}$, no crystal structures are available for L = AsR_3 or PR_3. However, it is important to have some guidance since the electronic properties of these systems form the main focus of this thesis. Recent SCF-Xα computations in our laboratory have established a faithful quantitative match between the observed and calculated $\nu_{\sigma\rightarrow\sigma^*}$ energies for seven ruthenium ammine and tacn "blues" of known structure.[43] An orderly near-linear relationship emerges between the calculated $\nu_{\sigma\rightarrow\sigma^*}$ energy and the parameter r(Ru-Ru), when the latter is made to vary between 2.6 and 3.1 Å. Extension of this methodology led to six separate correlation curves (constructed for L = NH_3, AsH_3, and PH_3; X = Cl or Br) by which the observed $\nu_{\sigma\rightarrow\sigma^*}$ energies could be linked to the implied equilibrium separation, r(Ru-Ru), in each case. This work suggests, for example, that whereas r(Ru-Ru) is known crystallographically to equal 2.76 Å for the μ-Cl/NH_3 system[44] it expands distinctly to 2.92 Å for μ-Cl/$AsMe_3$, and to 3.00 Å for μ-Cl/PMe_3. For the corresponding bromides, on the evidence of the $\nu_{\sigma\rightarrow\sigma^*}$ band energies, r(Ru-Ru) expands from 2.85 Å in the μ-Br/NH_3 system,[45] to 3.00 Å for μ-Br/$AsMe_3$ and 3.09 Å for μ-Br/PMe_3 respectively. Further computation suggests that, between 3.1 and 3.2 Å, r(Ru-Ru) is approaching the limit for sustaining a meaningful t_{2g}-based M-M hemi bond.[43] The new structural and optical data amassed for seven ammine blues (Ch.1, ref. 65) were crucial in the "calibration" of these predictions.

In summary, the new structural data gathered for the closed-shell systems reveal an unexpected but distinctive capacity for the tertiary organo-arsine ligands so far studied ($AsMe_3$ and $AsMe_2Ph$) to promote closer Ru···Ru contact. Independent computational advances allow estimation of the hemi-bonded Ru-Ru separation from the observed near-IR $\sigma \rightarrow \sigma^*$ transition in all cases, and this implies progressive lengthening in the sequence $L = NR_3 > AsR_3 > PR_3$. Empirical confirmation of these structural predictions is provided by the related neutral mixed-valence dimer $[(PMe_3)_2ClRu(\mu\text{-}Cl)_3RuCl(PMe_3)_2]$ with eclipsed terminal phosphine ligands; this has a crystallographically determined Ru-Ru separation[42] of 2.992(1) which should, if anything, be shorter than in the hexa-PMe_3 μ-Cl analogue.

3.6 OVERALL TRENDS IN STRUCTURE, BONDING AND SPECTROSCOPY

The data surveyed above can now be confidently understood to reflect a *three or fourfold* variation overall in metal-metal interaction within this isostructural family. As the energy of identified $\sigma \rightarrow \sigma^*$ band (Table 3.3) is equal to $2W_\sigma$ (where W_σ is the one-electron separation of the σ and σ* orbitals), then W_σ increases from ~2500 cm^{-1} in $[Ru_2Cl_3(PMePh_2)_6]^{2+}$ to ~6000 cm^{-1} in $[Ru_2Cl_3(AsMe_3)_6]^{2+}$, with a parallel trend in the μ-Br series. This trend smoothly connects with isostructural ammine systems where W_σ rises to ~8000 cm^{-1} in $[Ru_2Cl_3(NH_3)_6]^{2+}$. As noted above, this is fully consistent with the non-linear but coherent progression in the experimentally determined g-tensor (and of course with the estimated change in the interatomic Ru-Ru separation).

This sequence ($PR_3/AsR_3/NR_3$) is all the more interesting because it is non-periodic, and because it follows the order of increasing ease of oxidation as measured empirically by E_{av}. There is also a scattered but unmistakable correlation of $\sigma \rightarrow \sigma^*$ band energy with the gap in oxidation potentials, $\Delta E_{1/2}$. These two progressions are

compared in Fig 3.27. Their complementary nature follows naturally from the underlying relationship between E_{av} and $\Delta E_{1/2}$ presented in Fig. 3.10.

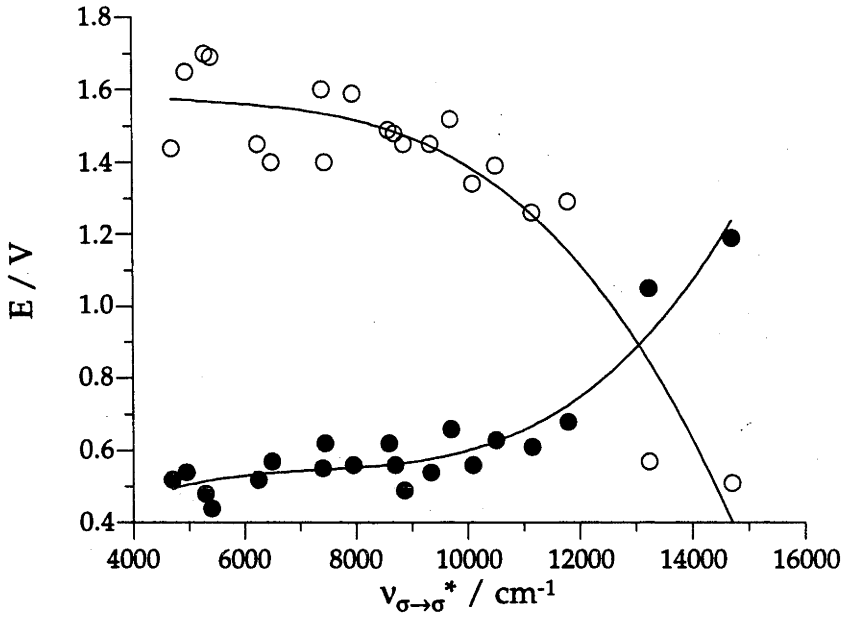

Figure 3.27 *Plot of E_{av} (open circles) and $\Delta E_{1/2}$ (closed circles) vs $\nu_{\sigma\rightarrow\sigma^*}$. The smooth curves are computer-generated lines of best fit, to 3rd order polynomials.*

3.7 COMPROPORTIONATION ENERGY, ΔG

It is often said that increased metal-metal interaction in redox-active binuclear complexes should be accompanied by increasing separation of the successive couples ($\Delta E_{1/2}$). This axiom was originally developed in the context of weakly coupled (class II) mixed-valence systems,[46,47] in which the contribution of the potential 2-electron bond in the accompanying 10-e state could be discounted.[46] For fully delocalised (class III) systems, the proposition seems to us neither self-evident nor inevitable, despite being nicely exemplified by the present $[L_3Ru(\mu\text{-}X)_3RuL_3]^z$ family (Fig 3.10). The physical significance of the $\Delta E_{1/2}$ parameter, which ranges widely from 0.45 to 1.2 V in the present compounds, is therefore examined below.

It is rigorously true that $\Delta E_{1/2}$ is thermodynamically equivalent to ΔG_c, the free energy of comproportionation of $M_2^{II,II} + M_2^{III,III}$ to form two moles of $M_2^{II,III}$; *i.e.* $\Delta G_c = -nF\Delta E_{1/2}$. So the question becomes: "Under what circumstances will variations in the comproportionation energy, ΔG_c, reflect variations in M-M bond strength of the mixed-valence state, within a family of electronically and structurally related binuclear compounds?"

$$(II,II) + (III,III) \overset{\Delta G_c}{\rightleftharpoons} 2(II,III) \qquad (3.5)$$

For three-electron hemibonded systems,[48] the comproportionation is bound to be strongly exothermic, since $[\{\sigma^2\sigma^{*1}\} + \{\sigma^2\sigma^{*1}\}]$ is greatly favoured over $[\{\sigma^2\sigma^{*2}\} + \{\sigma^2\sigma^{*0}\}]$ as the preferred distribution of six frontier electrons between two molecules, with less net electron-electron repulsion and a more symmetric charge distribution overall. Clearly however, this universal effect will not in itself lead to *differences* in $\Delta E_{1/2}$ in a series of similar binuclear compounds.

Upon oxidation from the 11-e to 10-e state, it is possible that the σ/σ^* splitting (i) remains approximately constant, (ii) decreases or (iii) increases. These three possibilities may be considered in turn:

(i) On the simplest assumption of constant splitting between the σ and σ^* orbitals across the three successive oxidation states, as shown in Fig. 3.28, the gap in successive oxidation potentials owes nothing to the W_σ contributions, which cancel out, and $\Delta E_{1/2}$ depends rather on the mutual repulsion experienced by electrons occupying the redox-active, σ^* orbital. This term might be expected not to vary significantly within the series of isostructural $\{Ru(\mu\text{-}X)_3Ru\}^z$ dimers. However there is the possibility that the correlation energy associated with filling σ^* (Fig. 3.12) increases systematically as the quality of the σ bond increases and the electrons are more closely confined to a common region.

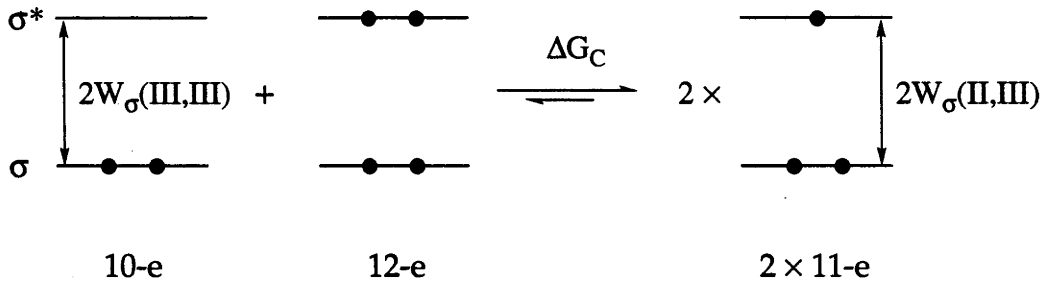

Figure 3.28 *Comproportionation energy for Ru_2(II,III) systems, showing constant splitting between σ and σ* orbitals (W_σ constant).*

(ii) If instead we assume the σ/σ* splitting diminishes upon oxidation to the 10-e state, then the connection between enhanced metal-metal bonding in the mixed-valence state and increased $\Delta E_{1/2}$ becomes straightforward. Comproportionation is made more exothermic to the extent that $W_\sigma(III,III) < W_\sigma(II,III)$ because 1x $\{\sigma^2\sigma^{*0}\}_{III,III}$ then carries less bond-energy overall than does 2x $\{\sigma^2\sigma^{*1}\}_{II,III}$. It is reasonable (though not inevitable) that the sequence from non-bonded $\sigma^2\sigma^{*2}$ through hemi-bonded $\sigma^2\sigma^{*1}$ to the $\sigma^2\sigma^{*0}$ configuration could culminate in a weakened two-electron bond because progressive oxidation of the binuclear core is accompanied by radial contraction of the single-ion d-orbitals, and by increased electrostatic repulsion between the two positive metal centres. These are strong effects which may outweigh the effect of increasing bond-order.[22,49]

(iii) As noted above, it is possible that in other systems the two-electron single bond "wins out" over the aforementioned effects, with synergistic establishment of a shorter M-M separation and thereby a *greater* W_σ in the 10-e state, notwithstanding the higher overall oxidation state. This would lead to inversion of the conventional ΔE/binuclear-interaction relationship. To evaluate these logical alternatives, (i) to (iii), one needs to assemble reliable information on the electronic σ/σ* splitting (= $2W_\sigma$) and the associated M-M distance in both hemi-bonded and singly bonded states.

In the present context of triply halide-bridged di-ruthenium complexes, the factual and circumstantial evidence is most complete for the $[Ru_2X_9]^z$ systems (X = Cl, Br), which are positioned neatly between the ammine "blues" and the analogous arsines according to their optical and voltammetric behaviour. The metal-metal distance has been estimated to contract by ~0.15 Å between the $Ru_2^{II,III}$ and $Ru_2^{III,III}$ nonahalides.[43] Overall, the estimated σ/σ^* splitting is almost unaltered upon oxidation to the III,III state (decreasing from 10 100 cm^{-1} in $[Ru_2Br_9]^{4-}$,[50] to 9 400 cm^{-1} in $[Ru_2Br_9]^{3-}$,[43] and stationary at 12 300 cm^{-1} for $[Ru_2Cl_9]^{4-}$ and $[Ru_2Cl_9]^{3-}$ [50]). These systems provide a clear example of important metal-metal bonding in the 10-e state, and approach the simple premise of a constant W_σ, presumably through the interplay of the formal doubling of bond-order with the countervailing influence of orbital contraction and increased cation/cation repulsion.

In summary, within a given family of binuclear compounds the observed increase in the electrode potential separation ($\Delta E_{1/2}$) may well be attributable to a parallel trend in the M-M bond strength, W_σ, at the mixed-valence level, but only if the W_σ term decreases distinctly and proportionately for each system upon oxidation. As yet, the evidence is incomplete for the present AsR_3- and PR_3-capped compounds because of the reactive nature of the 10-e state. However, we suspect that a pronounced decline in W_σ between the II,III and III,III levels plays a major role in the behaviour of $[Ru_2X_3(AsR_3)_6]^{2+}$ and $[Ru_2X_3(PR_3)_6]^{2+}$ systems.

3.8 CONCLUDING REMARKS

These studies, introducing AsR_3 capping ligands for the first time into the family of $[L_3Ru(\mu\text{-}X)_3RuL_3]^{2+}$ complexes, have placed the long-standing mixed-valence phosphino derivatives in a proper context and clarified the significance of their non-classical near-IR spectra. In contrast to the new AsR_3-capped ruthenium "blues", there is considerable circumstantial evidence that the hexa-phosphine complexes, while still delocalised, are close to the point where the driving force for forming the one-electron bond is marginal. This evidence includes the smooth progression in voltammetric behaviour connecting symmetric 11-e $[(PR_3)_3Ru(\mu\text{-}X)_3Ru(PR_3)_3]^{2+}$ and $[X(PR_3)_2Ru(\mu\text{-}X)_3Ru(PR_3)_2X]$ with compounds of the more general stoichiometry $[(PR_3)_{3-x}X_xRu(\mu\text{-}X)_3RuX_y(PR_3)_{3-y}]$,[26] even though the latter are localised whenever $y \neq x$.

It may be possible to induce electronic trapping in coordinatively symmetric Ru_2 systems if a pattern of terminal ligation is found for which W_σ is projected to diminish by a further 500 to 1000 cm^{-1} from its smallest present value. Naturally, the $Ru_2^{II,III}$ oxidation state becomes harder to reach as more electron-withdrawing ligands are introduced, but our projections (Figures 3.10 and 3.27) suggest the trapped state might be approached without an impossibly high electrogeneration potential. Given the enforced proximity of the two (halide-bridged) metal ions, the limiting physical properties of such notionally trapped confacial systems are of keen interest. Inevitably, there will be a domain which is transitional between the two clear-cut descriptions.

3.9 EXPERIMENTAL

Ruthenium starting materials were prepared as described in §2.2, except for *cis*-$[RuCl_2(AsMe_2Ph)_4]$, the preparation of which is given in §5.6. NMR data (^1H and ^{31}P-$\{^1H\}$), yields and reaction times are listed in Table 3.7, and Table 3.8 lists analytical and mass spectral data. All reactions were carried out under an atmosphere of N_2, but the products were handled in air. Details of electrochemical and spectro-electrochemical experiments are given in §2.4. Solutions of mixed-valence complexes for EPR studies were generated by bulk electrolysis (or alternatively by chemical oxidation, using $NOPF_6$) of solutions of *ca.* 10^{-2} mol dm^{-3} $[Ru_2(\mu\text{-}X)_3L_6]^+$ in CH_2Cl_2 containing 0.5 mol dm^{-3} $[NBu^n_4][BF_4]$. The UV/Vis/near-IR spectra of the electrogenerated and chemically oxidised complexes were compared with spectra obtained by *in situ* spectro-electrochemistry. Several examples were prepared by both methods to confirm that the EPR spectra of the mixed-valence complexes were unaffected by the use of the chemical oxidant.

Preparation of $[Ru_2(\mu\text{-}X)_3L_6]CF_3SO_3$ complexes from $K_3[Ru_2X_9]$

For example, a mixture of $K_3[Ru_2Cl_9]$ (0.15 g, 0.23 mmol) and $AsMe_3$ (0.25 g, 2.1 mmol) in ethanol (45 cm^3) and distilled water (15 cm^3) was heated at reflux for 24 h. The solvent was evaporated *in vacuo* to leave a yellow residue which was washed with diethyl ether, dissolved in dichloromethane, filtered and heated at reflux with 0.1 mol dm^{-3} CF_3SO_3H in methanol (3 cm^3, 0.3 mmol) for 16 h. The solvent was evaporated *in vacuo* and the residue recrystallised from dichloromethane/diethyl ether.

Preparation of $[Ru_2(\mu\text{-}X)_3L_6]CF_3SO_3$ complexes from $[RuX_2(PPh_3)_3]$

For example, to a suspension of $[RuBr_2(PPh_3)_3]$ (0.25 g, 0.24 mmol) in 2-methoxyethanol (30 cm^3) was added triphos (0.30g, 0.50 mmol). The mixture was heated at reflux for 26 h, producing a yellow solution. The solvent was removed *in vacuo* to give a yellow residue, which was stirred with a mixture of benzene (2 cm^3) and

diethyl ether (10 cm^3) to give a yellow precipitate ($[Ru_2(\mu\text{-}Br)_3(triphos)_2]Br$) which was collected and washed with diethyl ether. The bromide salt was dissolved in dichloromethane (10 cm^3) and 0.1 mol dm^{-3} CF_3SO_3H in methanol (2 cm^3, 0.2 mmol) added, and heated to reflux for 16 h. The solvent was evaporated *in vacuo* and the residue recrystallised from dichloromethane/diethyl ether.

Preparation of $[Ru_2(\mu\text{-}Cl)_3(AsMe_3)_6]CF_3SO_3$ from "$RuCl_3.xH_2O$"

Commercial "$RuCl_3.xH_2O$" (0.10 g, 0.42 mmol Ru) and $AsMe_3$ (0.30 g, 2.5 mmol) were dissolved in ethanol (20 cm^3) and conc. HCl (1 cm^3) added. The solution was heated at reflux for 48 h and the solvent reduced to about 3 cm^3. An orange powder (*trans*-$[RuCl_2(AsMe_3)_4]$) precipitated upon the addition of water. The powder was collected, and the filtrate evaporated to dryness to leave a yellow powder, consisting of *cis*-$[RuCl_2(AsMe_3)_4]$ and $[Ru_2Cl_3(AsMe_3)_6]Cl$. The *cis*- isomer was extracted into diethyl ether, leaving $[Ru_2Cl_3(AsMe_3)_6]Cl$ as a yellow powder. Yield: 60 mg (27%). The metathesis to the triflate ($CF_3SO_3^-$) salt was achieved by gentle heating of a solution of $[Ru_2Cl_3(AsMe_3)_6]Cl$ in CH_2Cl_2 (5 cm^3) with 0.1 mol dm^{-3} CF_3SO_3H in methanol (1 cm^3, 0.1 mmol) for 16 h. The solvent was evaporated to dryness and the yellow residue recrystallised from dichloromethane/diethyl ether. The yellow crystalline material was collected and washed with diethyl ether. Overall yield: 16 mg (6%).

Preparation of $[Ru_2(\mu\text{-}Cl)_3(AsMe_2Ph)_6]CF_3SO_3$ from cis-$[RuCl_2(AsMe_2Ph)_4]$

cis-$[RuCl_2(AsMe_2Ph)_4]$ (60 mg, 0.067 mmol) was heated at reflux in *iso*-butanol (5 cm^3) for 16 h. The solvent was removed *in vacuo*, the residue dissolved in dichloromethane (3 cm^3), 0.1 mol dm^{-3} CF_3SO_3H in methanol (1 cm^3, 0.1 mmol) added, and heated to reflux for 16 h. The solvent was evaporated *in vacuo* and the residue recrystallised from dichloromethane/diethyl ether to yield orange crystals of $[Ru_2(\mu\text{-}Cl)_3(AsMe_2Ph)_6]CF_3SO_3$: 5 mg (10 %).

Table 3.7 *Experimental Details for the Preparation of $[Ru_2(\mu\text{-}X)_3L_6]CF_3SO_3$ Complexes.*

Complex	Starting Material	Solvent	Reaction Time [a] (h)	Yield [b] (%)	NMR [c]		
					$^{31}P\text{-}\{^1H\}$	^1H (Me)	^1H (Ph)
$[Ru_2Cl_3(AsMe_3)_6]CF_3SO_3$	$K_3[Ru_2Cl_9]$ $RuCl_3.xH_2O$	EtOH/H_2O EtOH/HCl	24 48	22 6	-	1.35 (s)	-
$[Ru_2Br_3(AsMe_3)_6]CF_3SO_3$	$K_3[Ru_2Br_9]$	EtOH/H_2O	40	31	-	1.41 (s)	-
$[Ru_2Cl_3(AsMe_2Ph)_6]CF_3SO_3$	$K_3[Ru_2Cl_9]$ *cis*-$[RuCl_2(AsMe_2Ph)_4]$	EtOH/H_2O Bu^{i}OH	16 16	42 10	-	1.45 (6H, s)	7.15 (2H, d), 7.30 (2H, t), 7.40 (1H, t)
$[Ru_2Br_3(AsMe_2Ph)_6]CF_3SO_3$	$K_3[Ru_2Br_9]$	EtOH/H_2O	16	13	-	1.52 (6H, s)	7.12 (2H, d), 7.31 (2H, t), 7.41 (1H, t)
$[Ru_2Cl_3(AsMePh_2)_6]CF_3SO_3$	$K_3[Ru_2Cl_9]$	EtOH/H_2O	15	32	-	1.60 (3H, s)	7.00 (4H, d), 7.14 (4H, t), 7.34 (2H, t)
$[Ru_2Br_3(AsMePh_2)_6]CF_3SO_3$	$K_3[Ru_2Br_9]$	EtOH/H_2O	16	3	-	1.70 (3H, s)	6.97 (4H, d), 7.12 (4H, t), 7.30 (2H, t)
$[Ru_2Cl_3(AsMe_3)_4(PPh_3)_2]CF_3SO_3$	$[RuCl_2(PPh_3)_3]$	EtOH	16	74	+53.2	0.66 (3H, s), 1.16 (3H, s)	7.35 (5H, m)
$[Ru_2Cl_3(PMe_3)_6]CF_3SO_3$	$K_3[Ru_2Cl_9]$	EtOH/H_2O	40	49	+22.2		
$[Ru_2Br_3(PMe_3)_6]CF_3SO_3$	$K_3[Ru_2Br_9]$	EtOH/H_2O	16	38	+19.6		
$[Ru_2Cl_3(PMePh_2)_6]CF_3SO_3$	$K_3[Ru_2Cl_9]$	EtOH	72	58	+18.8		
$[Ru_2Br_3(PEt_2Ph)_6]CF_3SO_3$	$K_3[Ru_2Br_9]$	EtOH	16	60	+35.1		
$[Ru_2Br_3(triphos)_2]CF_3SO_3$	$[RuBr_2(PPh_3)_3]$	2-MeOEtOH	26	59	+32.6		

[a] *Reaction time for the initial reaction. All compounds were subsequently treated with CF_3SO_3H to obtain the triflate salts.* [b] *Yields of triflate salts after recrystallisation.*

[c] *Chemical shifts (δ) in ppm relative to $SiMe_4$ (^1H) or 85% H_3PO_4 ($^{31}P\text{-}\{^1H\}$). Spectra were recorded in CD_2Cl_2. All $^{31}P\text{-}\{^1H\}$ resonances are singlets.*

Table 3.8 *Analytical and Positive Ion Fast Atom Bombardment Mass Spectral (FAB MS) Data.*[a]

Complex	Analytical Data (%) C	H	Cl/Br	FAB MS (m/z)
$[Ru_2Cl_3(AsMe_3)_6]CF_3SO_3$	19.0 (19.4)	4.9 (4.6)	9.4 (9.0)	1037.2 (1028.1)
$[Ru_2Br_3(AsMe_3)_6]CF_3SO_3$	17.5 (17.4)	4.3 (4.15)	18.4 (18.3)	
$[Ru_2Cl_3(AsMe_2Ph)_6]CF_3SO_3$	37.8 (38.0)	4.5 (4.3)	6.8 (6.9)	
$[Ru_2Br_3(AsMe_2Ph)_6]CF_3SO_3$	34.5 (35.0)	4.0 (3.95)	14.1 (14.2)	
$[Ru_2Cl_3(AsMePh_2)_6]CF_3SO_3$	49.0 (49.35)	4.2 (4.1)	5.6 (5.5)	1774.8 (1773.5)
$[Ru_2Br_3(AsMePh_2)_6]CF_3SO_3$[b]	44.9 (46.15)	4.0 (3.8)	13.1 (11.7)	1906.9 (1906.9)
$[Ru_2Cl_3(AsMe_3)_4(PPh_3)_2]CF_3SO_3$	39.8 (40.25)	4.5 (4.55)	7.2 (7.3)	1315.9 (1313.2)
$[Ru_2Cl_3(PMe_3)_6]CF_3SO_3$	25.3 (25.0)	6.1 (5.95)	11.8 (11.6)	766.9 (765.0)
$[Ru_2Br_3(PMe_3)_6]CF_3SO_3$	21.9 (21.8)	5.3 (5.2)	22.8 (22.9)	
$[Ru_2Cl_3(PMePh_2)_6]CF_3SO_3$	56.6 (57.2)	4.7 (4.7)	6.3 (6.4)	
$[Ru_2Br_3(PEt_2Ph)_6]CF_3SO_3$	46.3 (46.1)	6.3 (5.7)	15.1 (15.1)	
$[Ru_2Br_3(triphos)_2]CF_3SO_3$	53.9 (54.2)	4.0 (4.3)	13.2 (13.0)	1693.1 (1691.2)

[a] *Calculated values in parentheses.* [b] *Unable to improve upon these analytical results despite numerous recrystallisations.*

3.10 REFERENCES

1. J. Chatt and R.G. Hayter, *J. Chem. Soc.*, 1961, 896.
2. M.S. Lupin and B.L. Shaw, *J. Chem. Soc. (A)*, 1968, 741.
3. D.A. Couch and S.D. Robinson, *Inorg. Chem.*, 1974, **13**, 456.
4. P.W. Armit, A.S.F. Boyd and T.A. Stephenson, *J. Chem. Soc., Dalton Trans.*, 1975, 1663.
5. M. Laing and L. Pope, *Acta Crystallogr., Sect. B*, 1976, **32**, 1547.
6. W.J. Sime and T.A. Stephenson, *J. Organomet. Chem.*, 1977, **124**, C23.
7. J.A. Statler, G. Wilkinson, M. Thornton-Pett and M.B. Hursthouse, *J. Chem. Soc., Dalton Trans.*, 1984, 1731.
8. L.F. Rhodes, C. Sorato, L.M. Venanzi and F. Bachechi, *Inorg. Chem.*, 1988, **27**, 604.
9. G. Albertin, S. Antoniutti and E. Bordignon, *J. Chem. Soc., Dalton Trans.*, 1987, 1813.
10. A. Albinati, Q. Jiang, H. Rüegger and L.M. Venanzi, *Inorg. Chem.*, 1993, **32**, 4940.
11. E.G. Leelamani and G.K.N. Reddy, *Inorg. Nucl. Chem. Lett.*, 1975, **11**, 5.
12. K.G. Srinivasamurthy, N.M. Nanje Gowda and G.K.N. Reddy, *J. Inorg. Nucl. Chem.*, 1977, **39**, 1977.
13. E.A. Seddon and K.R. Seddon, *The Chemistry of Ruthenium*, Elsevier, Amsterdam, 1984, p. 159.
14. J.E. Fergusson and A.M. Greenaway, *Aust. J. Chem.*, 1978, **31**, 497.
15. V.T. Coombe, Ph.D. Thesis, University of Edinburgh, 1985.
16. V.T. Coombe, G.A. Heath, T.A. Stephenson and D.K. Vattis, *J.Chem. Soc., Dalton Trans.*, 1983, 2307.
17. V.T. Coombe, G.A. Heath, T.A. Stephenson, J.D. Whitelock and L.J. Yellowlees, *J. Chem. Soc., Dalton Trans.*, 1985, 947.
18. D.G. Humphrey, Ph.D. Thesis, Australian National University, 1992.

19. A.J. Lindsay, Ph.D. Thesis, University of Edinburgh, 1982.

20. T.A. Stephenson and G. Wilkinson, *J. Inorg. Nucl. Chem.*, 1966, **28**, 945.

21. P.R. Hoffman and K.G. Caulton, *J. Am. Chem. Soc.*, 1975, **97**, 4221.

22. G.A. Heath and J.E. McGrady, *J. Chem. Soc., Dalton Trans.*, 1994, 3759.

23. A.B.P. Lever, *Inorganic Electronic Spectroscopy*, Elsevier, New York, 2nd edn., 1984, p. 751.

24. S.F. Gheller, G.A. Heath, D.C.R. Hockless, D.G. Humphrey and J.E. McGrady, *Inorg. Chem.*, 1994, **33**, 3986.

25. R.S. Armstrong, W.A. Horsfield and K.W. Nugent, *Inorg. Chem.*, 1990, **29**, 4551.

26. G.A. Heath, A.J. Lindsay, T.A. Stephenson and D.K. Vattis, *J. Organomet. Chem.*, 1982, **233**, 353.

27. L. Dubicki, unpublished work.

28. G.A. Heath and B.J. Kennedy, manuscript in preparation.

29. S. Sugano, Y. Tanabe and H. Kamimura, *Multiplets of Transition Metal Ions in Crystals*, Academic Press, New York, 1970.

30. B.N. Figgis, *Trans. Faraday Soc.*, 1961, **57**, 198.

31. K.W.H. Stevens, *Proc. R. Soc. London, Ser. A*, 1953, **219**, 542.

32. H. Kamimura, *J. Phys. Soc. Jpn*, 1956, **11**, 1171.

33. B. Bleany and M.C.M. O'Brien, *Proc. Phys. Soc., London, Sect. B*, 1956, **69**, 1216.

34. J.H.M. Thornley, *J. Phys. C*, 1968, **1**, 1024.

35. N.S. Hush, A. Edgar and J.K. Beattie, *Chem. Phys. Lett.*, 1980, **69**, 128.

36. L. Dubicki, J. Ferguson and E.R. Krausz, *J. Am. Chem. Soc.*, 1985, **107**, 179.

37. L. Dubicki and E.R. Krausz, *Inorg. Chem.*, 1985, **24**, 4461.

38. P. Neubold, B.S.P.C. Della Vedova, K. Wieghardt, B. Nuber and J. Weiss, *Inorg. Chem.*, 1990, **29**, 3355.

39. N.S. Hush, J.K. Beattie and V.M. Ellis, *Inorg. Chem.*, 1984, **23**, 3339.

40. N.S. Hush, in *Mixed-Valence Compounds*, ed. D.B. Brown, Reidel Publishing Co., Dordrecht, 1980, pp. 151-188.

41. K.A. Raspin, *J. Chem. Soc. (A)*, 1969, 461.

42. F.A. Cotton and R. Torralba, *Inorg. Chem.*, 1991, **30**, 2196.

43. J.E. McGrady, Ph.D. Thesis, Australian National University, 1994.

44. M.N. Hughes, D. O'Reardon, R.K. Poole, M.B. Hursthouse and M. Thornton-Pett, *Polyhedron*, 1987, **6**, 1711.

45. J.K. Beattie, P. Del Favero, T.W. Hambley and N.S. Hush, *Inorg. Chem.*, 1988, **27**, 2000.

46. J.E. Sutton, P.M. Sutton and H. Taube, *Inorg. Chem.*, 1979, **18**, 1017.

47. C. Creutz, *Prog. Inorg. Chem.*, 1983, **30**, 1.

48. P.M.W. Gill and L. Radom, *J. Am. Chem. Soc.*, 1988, **110**, 4931.

49. G.A. Heath, J.E. McGrady, R.G. Raptis and A.C. Willis, *Inorg. Chem.*, to be submitted for publication.

50. B.J. Kennedy, G.A. Heath and T.J. Khoo, *Inorg. Chim. Acta*, 1991, **190**, 265.

APPENDIX 3.1

X-RAY STRUCTURE OF $[Ru_2(\mu\text{-}Cl)_3(AsMe_3)_6]CF_3SO_3$

Crystal data. $C_{19}H_{54}As_6Cl_3F_3O_3Ru_2S$, M = 1177.72, monoclinic, space group $P2_1/n$ (#14), a = 9.767(2), b =26.699(2), c = 15.449(1) Å, β = 91.53(1) °, V = 4027.4(8) Å^3, Z = 4, D_{calc} = 1.942 g cm^{-3}, $F(000)$ = 2288, Cu-$K\alpha$ radiation, λ = 1.54178 Å, μ(Cu-$K\alpha$) = 141.70 cm^{-1}, T = 296 K, 6143 unique reflections (R_{int} = 0.037).

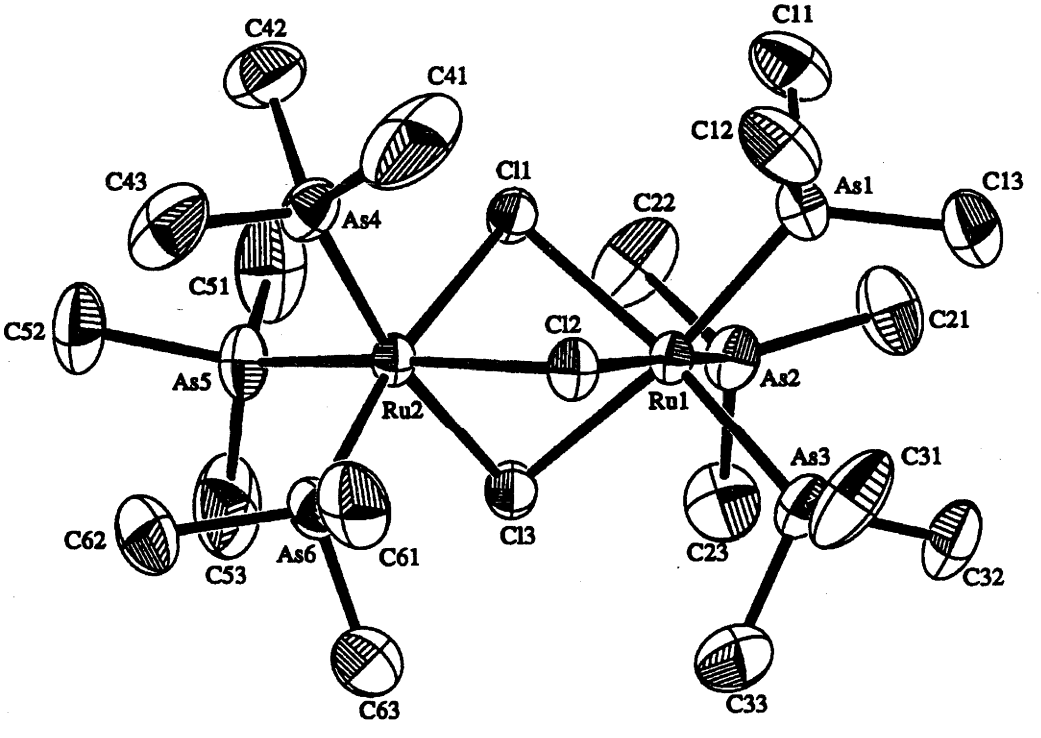

Figure A3.1 *View of the binuclear cation $[Ru_2(\mu\text{-}Cl)_3(AsMe_3)_6]^+$, showing atom numbering scheme. Ellipsoids are drawn at the 50 % probability level.*

Table A3.1 *Selected Bond Lengths (Å) and Angles (°) for* $[Ru_2(\mu\text{-}Cl)_3(AsMe_3)_6]CF_3SO_3$.

Ru(1)-As(1)	2.374(1)	Ru(2)-As(4)	2.368(1)
Ru(1)-As(2)	2.3730(9)	Ru(2)-As(5)	2.3770(9)
Ru(1)-As(3)	2.3713(9)	Ru(2)-As(6)	2.3651(9)
Ru(1)-Cl(1)	2.484(2)	Ru(2)-Cl(1)	2.475(2)
Ru(1)-Cl(2)	2.477(2)	Ru(2)-Cl(2)	2.476(2)
Ru(1)-Cl(3)	2.477(2)	Ru(2)-Cl(3)	2.471(2)
As(1)-Ru(1)-As(2)	94.25(3)	As(4)-Ru(2)-As(5)	94.90(4)
As(1)-Ru(1)-As(3)	94.61(4)	As(4)-Ru(2)-As(6)	95.66(4)
As(2)-Ru(1)-As(3)	95.33(3)	As(5)-Ru(2)-As(6)	95.01(4)
Cl(1)-Ru(1)-Cl(2)	80.97(6)	Cl(1)-Ru(2)-Cl(2)	81.18(6)
Cl(1)-Ru(1)-Cl(3)	81.39(6)	Cl(1)-Ru(2)-Cl(3)	81.68(6)
Cl(2)-Ru(1)-Cl(3)	81.23(6)	Cl(2)-Ru(2)-Cl(3)	81.37(6)
Ru(1)-Cl(1)-Ru(2)	82.31(5)	Ru(1)-Cl(2)-Ru(2)	82.54(6)
Ru(1)-Cl(3)-Ru(2)	82.44(5)		

Note also that the non-bonded Ru····Ru separation is 3.263(1) Å.

APPENDIX 3.2

X-RAY STRUCTURE OF $[Ru_2(\mu\text{-}Cl)_3(AsMe_2Ph)_6]CF_3SO_3$

Crystal data. $C_{49}H_{66}As_6Cl_3F_3O_3Ru_2S$, M = 1550.14, monoclinic, space group $P2_1/c$ (#14), a = 14.663(2), b =16.773(3), c = 24.441(3) Å, β = 97.30(1) °, V = 5962(1) Å^3, Z = 4, D_{calc} = 1.727 g cm^{-3}, $F(000)$ = 3056, Mo-$K\alpha$ radiation, λ = 0.71069 Å, μ(Mo-$K\alpha$) = 40.28 cm^{-1}, T = 296 K, 8164 unique reflections (R_{int} = 0.035).

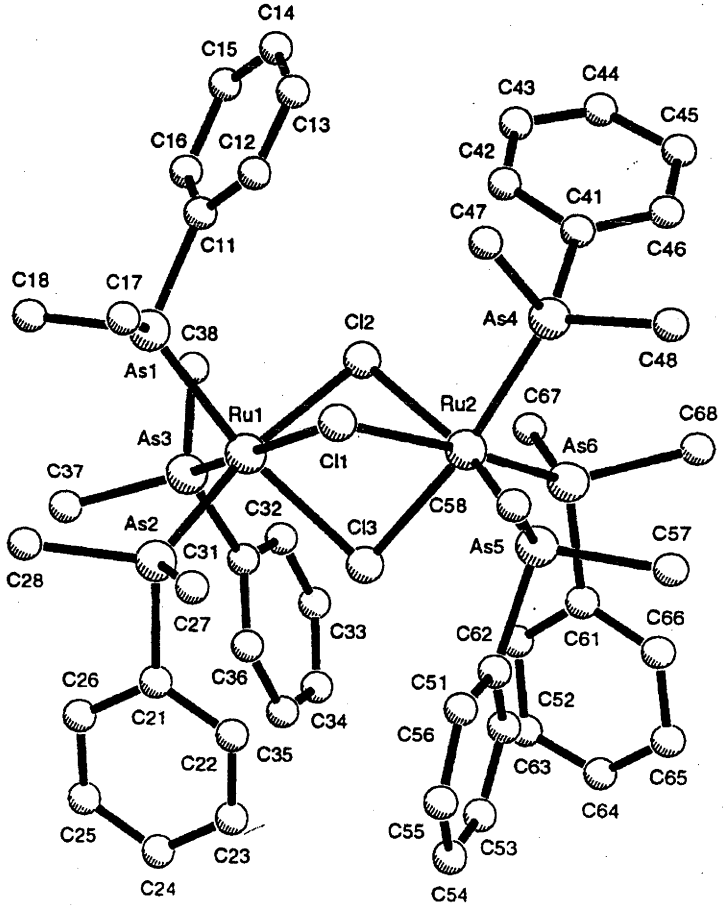

Figure A3.2 *Molecular structure of the binuclear cation* $[Ru_2(\mu\text{-}Cl)_3(AsMe_2Ph)_6]^+$, *showing atom numbering scheme.*

Table A3.2 *Selected Bond Lengths (Å) and Angles (°) for* $[Ru_2(\mu\text{-}Cl)_3(AsMe_2Ph)_6]CF_3SO_3$.

Ru(1)-As(1)	2.389(3)	Ru(2)-As(4)	2.405(3)
Ru(1)-As(2)	2.391(2)	Ru(2)-As(5)	2.386(3)
Ru(1)-As(3)	2.378(3)	Ru(2)-As(6)	2.388(3)
Ru(1)-Cl(1)	2.476(5)	Ru(2)-Cl(1)	2.484(5)
Ru(1)-Cl(2)	2.455(4)	Ru(2)-Cl(2)	2.474(5)
Ru(1)-Cl(3)	2.439(5)	Ru(2)-Cl(3)	2.427(5)
As(1)-Ru(1)-As(2)	94.06(8)	As(4)-Ru(2)-As(5)	94.51(10)
As(1)-Ru(1)-As(3)	94.93(9)	As(4)-Ru(2)-As(6)	93.79(9)
As(2)-Ru(1)-As(3)	97.59(8)	As(5)-Ru(2)-As(6)	97.61(9)
Cl(1)-Ru(1)-Cl(2)	80.0(2)	Cl(1)-Ru(2)-Cl(2)	79.5(2)
Cl(1)-Ru(1)-Cl(3)	81.3(2)	Cl(1)-Ru(2)-Cl(3)	81.3(2)
Cl(2)-Ru(1)-Cl(3)	80.5(2)	Cl(2)-Ru(2)-Cl(3)	80.3(2)
Ru(1)-Cl(1)-Ru(2)	82.7(1)	Ru(1)-Cl(2)-Ru(2)	83.3(2)
Ru(1)-Cl(3)-Ru(2)	84.6(2)		

Note also that the non-bonded Ru····Ru separation is 3.275(1) Å.

APPENDIX 3.3

X-RAY STRUCTURE OF $[Ru_2(\mu\text{-}Cl)_3(PMe_3)_6]CF_3SO_3$

Crystal data. $C_{19}H_{54}Cl_3F_3O_3P_6Ru_2S$, M = 914.03, monoclinic, space group $P2_1/n$ (#14), a = 9.523(3), b =26.549(2), c = 15.015(2) Å, β = 91.64(1) °, V = 3794(1) Å^3, Z = 4, D_{calc} = 1.600 g cm^{-3}, $F(000)$ = 1856, Cu-$K\alpha$ radiation, λ = 1.54178 Å, μ(Cu-$K\alpha$) = 116.17 cm^{-1}, T = 296 K, 5797 unique reflections (R_{int} = 0.036).

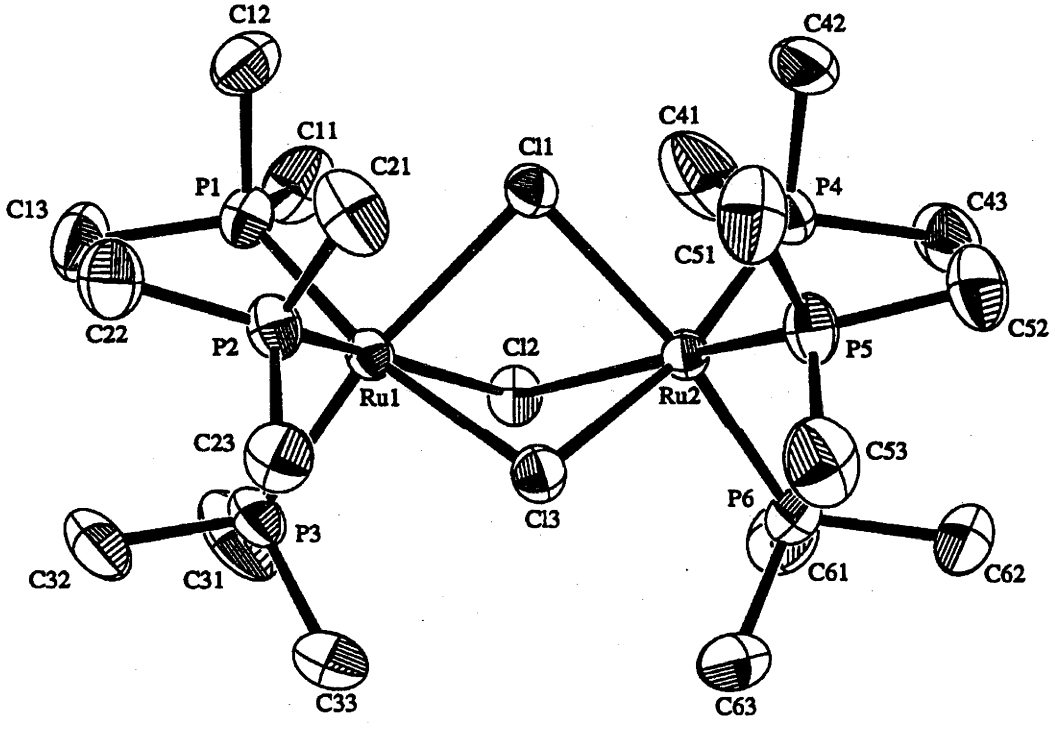

Figure A3.3 *View of the binuclear cation $[Ru_2(\mu\text{-}Cl)_3(PMe_3)_6]^+$, showing atom numbering scheme. Ellipsoids are drawn at the 50 % probability level.*

Table A3.3 *Selected Bond Lengths (Å) and Angles (°) for* $[Ru_2(\mu\text{-}Cl)_3(PMe_3)_6]CF_3SO_3$.

Ru(1)-P(1)	2.267(2)	Ru(2)-P(4)	2.261(2)
Ru(1)-P(2)	2.264(2)	Ru(2)-P(5)	2.269(2)
Ru(1)-P(3)	2.266(2)	Ru(2)-P(6)	2.257(2)
Ru(1)-Cl(1)	2.511(1)	Ru(2)-Cl(1)	2.501(1)
Ru(1)-Cl(2)	2.505(1)	Ru(2)-Cl(2)	2.503(1)
Ru(1)-Cl(3)	2.509(1)	Ru(2)-Cl(3)	2.498(1)
P(1)-Ru(1)-P(2)	94.66(6)	P(4)-Ru(2)-P(5)	95.20(6)
P(1)-Ru(1)-P(3)	94.99(6)	P(4)-Ru(2)-P(6)	95.58(6)
P(2)-Ru(1)-P(3)	95.48(6)	P(5)-Ru(2)-P(6)	95.28(6)
Cl(1)-Ru(1)-Cl(2)	79.07(4)	Cl(1)-Ru(2)-Cl(2)	79.30(4)
Cl(1)-Ru(1)-Cl(3)	79.64(5)	Cl(1)-Ru(2)-Cl(3)	80.03(5)
Cl(2)-Ru(1)-Cl(3)	79.38(5)	Cl(2)-Ru(2)-Cl(3)	79.63(5)
Ru(1)-Cl(1)-Ru(2)	84.74(4)	Ru(1)-Cl(2)-Ru(2)	84.82(4)
Ru(1)-Cl(3)-Ru(2)	85.85(5)		

Note also that the non-bonded Ru····Ru separation is 3.374(6) Å.

APPENDIX 3.4

X-RAY STRUCTURE OF $[Ru_2(\mu\text{-}Br)_3(AsMe_3)_6]CF_3SO_3$

Crystal data. $C_{19}H_{54}As_6Br_3F_3O_3Ru_2S$, M = 1311.07, monoclinic, space group $P2_1/c$ (#14), a = 10.670(4), b =14.742(4), c = 26.253(3) Å, β = 91.14(2) °, V = 4128(1) Å^3, Z = 4, D_{calc} = 2.109 g cm^{-3}, $F(000)$ = 2504, Mo-$K\alpha$ radiation, λ = 0.71069 Å, μ(Mo-$K\alpha$) = 85.01 cm^{-1}, T = 296 K, 5749 unique reflections (R_{int} = 0.049).

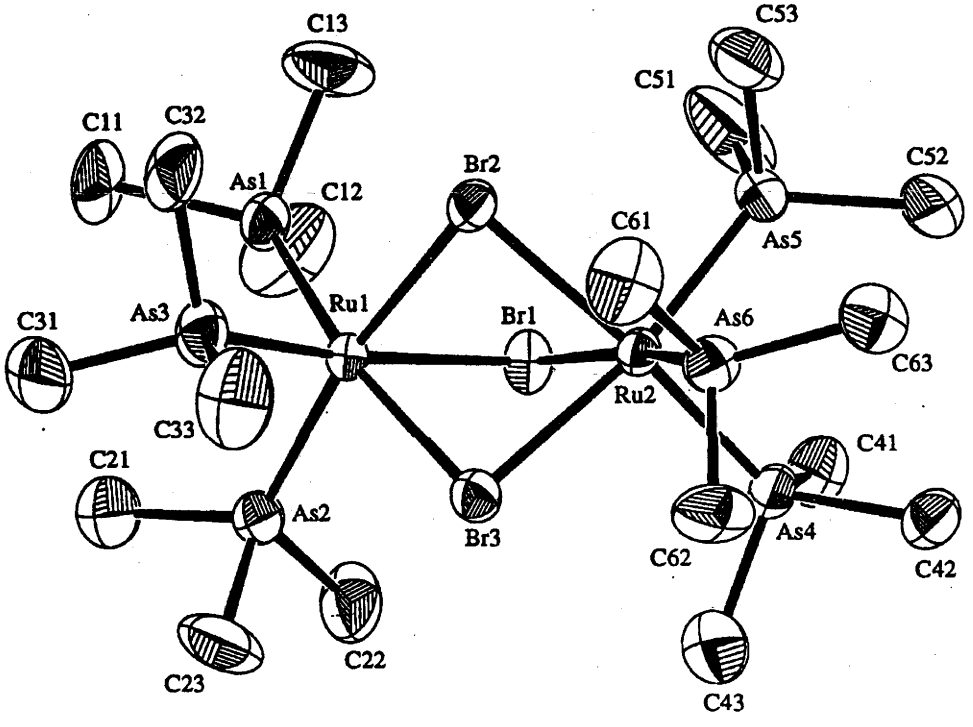

Figure A3.4 *View of the binuclear cation $[Ru_2(\mu\text{-}Br)_3(AsMe_3)_6]^+$, showing atom numbering scheme. Ellipsoids are drawn at the 50 % probability level.*

Table A3.4 *Selected Bond Lengths (Å) and Angles (°) for* $[Ru_2(\mu\text{-}Br)_3(AsMe_3)_6]CF_3SO_3$.

Ru(1)-As(1)	2.382(2)	Ru(2)-As(4)	2.373(2)
Ru(1)-As(2)	2.380(2)	Ru(2)-As(5)	2.380(2)
Ru(1)-As(3)	2.367(2)	Ru(2)-As(6)	2.385(2)
Ru(1)-Br(1)	2.594(2)	Ru(2)-Br(1)	2.611(2)
Ru(1)-Br(2)	2.616(2)	Ru(2)-Br(2)	2.606(2)
Ru(1)-Br(3)	2.606(2)	Ru(2)-Br(3)	2.606(2)
As(1)-Ru(1)-As(2)	95.18(7)	As(4)-Ru(2)-As(5)	94.06(6)
As(1)-Ru(1)-As(3)	94.80(7)	As(4)-Ru(2)-As(6)	94.47(7)
As(2)-Ru(1)-As(3)	93.82(6)	As(5)-Ru(2)-As(6)	95.11(7)
Br(1)-Ru(1)-Br(2)	82.27(5)	Br(1)-Ru(2)-Br(2)	82.13(5)
Br(1)-Ru(1)-Br(3)	81.79(5)	Br(1)-Ru(2)-Br(3)	81.47(6)
Br(2)-Ru(1)-Br(3)	81.39(5)	Br(2)-Ru(2)-Br(3)	81.58(5)
Ru(1)-Br(1)-Ru(2)	81.96(5)	Ru(1)-Br(2)-Ru(2)	81.63(5)
Ru(1)-Br(3)-Ru(2)	81.82(5)		

Note also that the non-bonded Ru····Ru separation is 3.413(1) Å.

APPENDIX 3.5

X-RAY STRUCTURE OF $[Ru_2(\mu\text{-}Br)_3(PMe_3)_6]CF_3SO_3$

Crystal data. $C_{19}H_{54}Br_3F_3O_3P_6Ru_2S$, M = 1047.38, monoclinic, space group $P2_1/c$ (#14), a = 10.411(6), b =14.272(6), c = 26.018(4) Å, β = 91.20(3) °, V = 3865(2) Å^3, Z = 4, D_{calc} = 1.800 g cm^{-3}, $F(000)$ = 2072, Mo-$K\alpha$ radiation, λ = 0.71069 Å, μ(Mo-$K\alpha$) = 42.29 cm^{-1}, T = 296 K, 7135 unique reflections (R_{int} = 0.024).

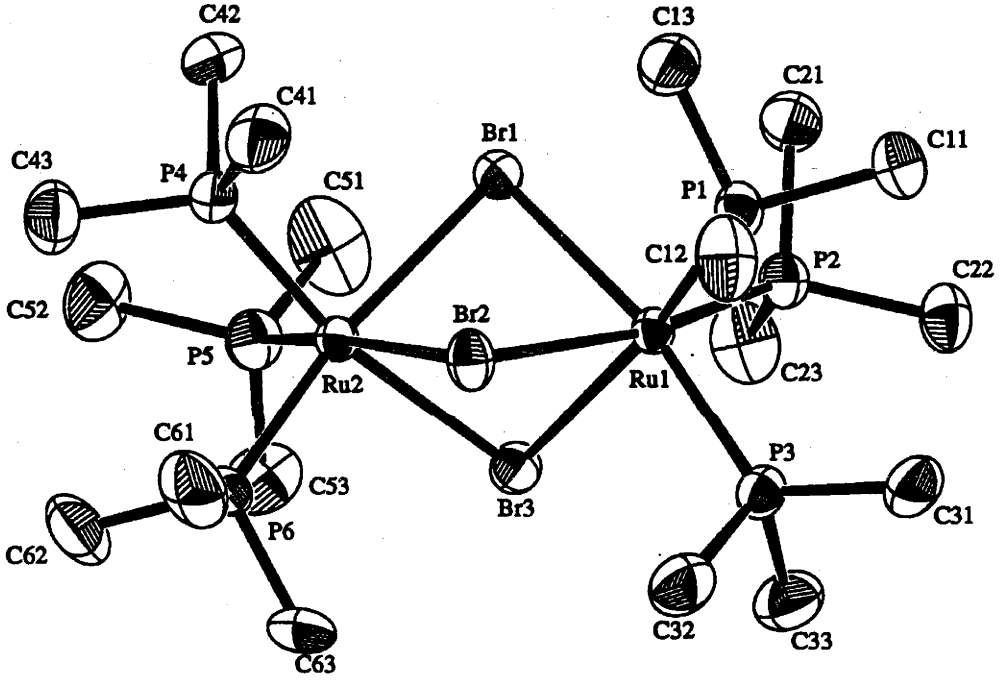

Figure A3.5 *View of the binuclear cation $[Ru_2(\mu\text{-}Br)_3(PMe_3)_6]^+$, showing atom numbering scheme. Ellipsoids are drawn at the 50 % probability level.*

Table A3.5 *Selected Bond Lengths (Å) and Angles (°) for* $[Ru_2(\mu\text{-}Br)_3(PMe_3)_6]CF_3SO_3$.

Ru(1)-P(1)	2.267(2)	Ru(2)-P(4)	2.272(2)
Ru(1)-P(2)	2.275(2)	Ru(2)-P(5)	2.266(3)
Ru(1)-P(3)	2.273(2)	Ru(2)-P(6)	2.272(2)
Ru(1)-Br(1)	2.642(1)	Ru(2)-Br(1)	2.635(1)
Ru(1)-Br(2)	2.645(1)	Ru(2)-Br(2)	2.626(1)
Ru(1)-Br(3)	2.634(1)	Ru(2)-Br(3)	2.644(1)
P(1)-Ru(1)-P(2)	95.11(9)	P(4)-Ru(2)-P(5)	94.84(9)
P(1)-Ru(1)-P(3)	94.82(8)	P(4)-Ru(2)-P(6)	95.34(9)
P(2)-Ru(1)-P(3)	95.08(9)	P(5)-Ru(2)-P(6)	95.03(10)
Br(1)-Ru(1)-Br(2)	79.62(4)	Br(1)-Ru(2)-Br(2)	80.10(4)
Br(1)-Ru(1)-Br(3)	79.80(3)	Br(1)-Ru(2)-Br(3)	79.74(3)
Br(2)-Ru(1)-Br(3)	80.22(4)	Br(2)-Ru(2)-Br(3)	80.39(4)
Ru(1)-Br(1)-Ru(2)	84.14(3)	Ru(1)-Br(2)-Ru(2)	84.26(4)
Ru(1)-Br(3)-Ru(2)	84.15(3)		

Note also that the non-bonded Ru····Ru separation is 3.5365(8) Å, reflecting the additional precision of this analysis.

CHAPTER FOUR

Diosmium and Ruthenium-Osmium Binuclear Complexes: Synthesis, Electrochemistry and Spectro-electrochemistry

---

4.1 INTRODUCTION

Like their diruthenium analogues, confacial bioctahedral diosmium complexes of the form $[Os_2(\mu\text{-}X)_3(PR_3)_6]^+$ have been known for over 30 years.[1] However, it was only recently confirmed that upon oxidation, the mixed-valence states, like the $[Ru_2(\mu\text{-}X)_3(PR_3)_6]^+$ systems, exhibit interesting near-IR spectra.[2,3] The mixed-valence properties of diosmium complexes have usually been studied in conjunction with their diruthenium analogues, and tacitly assumed to be similar to them. However, as explained below, we believe that the different optical and EPR properties displayed by diosmium complexes warrant separate consideration.

4.2 DIOSMIUM COMPLEXES, $[Os_2(\mu\text{-}X)_3(PR_3)_6]^{+/2+/3+}$

4.2.1 Synthesis

Chatt and Hayter described the first $[Os_2(\mu\text{-}Cl)_3(PR_3)_6]^+$ complexes, in the same report as their preparation of the analogous diruthenium complexes, by heating $(NH_4)_2[OsCl_6]$ with an excess of the required phosphine in aqueous alcohol.[1] Since then $[Os_2(\mu\text{-}Cl)_3(PR_3)_6]^+$ complexes have been prepared by a number of reactions,[2-6] mostly by reduction of compounds containing higher oxidation states of osmium. As with the

preparation of $[Ru_2(\mu\text{-}X)_3(PR_3)_6]^+$ complexes from $[RuCl_2(PPh_3)_3]$,[2] the triply-chloride bridged diosmium complexes can be formed by heating $[OsCl_2(PPh_3)_3]$ [7-9] with an excess of phosphine in ethanol, and those examined here (PR_3 = PMe_2Ph, PEt_3, PEt_2Ph, triphos†) were prepared by this method. The only structurally characterised complexes are $[Os_2Cl_3(PEt_3)_6]^+$ and its oxidised form, $[Os_2Cl_3(PEt_3)_6]^{2+}$.[3] Interestingly, the Os···Os separation decreased by only 0.07 Å upon oxidation (3.473(1) vs 3.406(1) Å).

In contrast, there have been few reports of triply-bromo bridged diosmium complexes. Walton *et al* prepared $[Os_2(\mu\text{-}Br)_3(PR_3)_6]^+$ (PR_3 = PEt_3, $PMePh_2$) by heating $[Os_2Br_8]^{2-}$ with the appropriate phosphine in alcoholic solvents.[5] However, the syntheses of $[Os_2Br_8]^{2-}$,[10] and of its diosmium(III) carboxylate $[Os_2(O_2CR)_4Cl_2]$ (R = Me, Pr^n) precursors,[11] are non-trivial. It has also been found that *mer*-$[OsBr_3(PMe_2Ph)_3]$ condenses to form $[Os_2(\mu\text{-}Br)_3(PMe_2Ph)_6]^+$ upon reduction,[2] like its chloride analogue.[6] However this route is not readily generalised to other phosphines. The individual *mer*-$[OsX_3(PR_3)_3]$ complexes are first required, and even then we have found that these do not always follow the same electroreductive pathway. Fortunately, $[OsBr_2(PPh_3)_3]$, readily prepared by heating $(Bu^n_4N)_2[OsBr_6]$ with PPh_3 in a mixture of Bu^tOH/H_2O (3:1 v/v),[8] has proved to be a useful starting material for the triply-bromide bridged complexes.

In general then, heating suspensions of $[MX_2(PPh_3)_3]$ (M = Ru, Os; X = Cl, Br) in ethanol (or, for the tridentate ligands triphos, 2-methoxyethanol as solvent) with the appropriate phosphine until a clear yellow solution is obtained provides a convenient route to a wide range of $[M_2(\mu\text{-}X)_3(PR_3)_6]^+$ (M = Ru, Os; X = Cl, Br) complexes (Fig. 4.1). In all cases triflate salts of $[Os_2(\mu\text{-}X)_3(PR_3)_6]^+$ were prepared by the same procedure used for $[Ru_2(\mu\text{-}X)_3(PR_3)_6]CF_3SO_3$.

† triphos = 1,1,1-tris((diphenylphosphino)methyl)ethane

$$2\,[MX_2(PPh_3)_3] + 6PR_3 \xrightarrow[(ii)\ CF_3SO_3H/MeOH,CH_2Cl_2]{(i)\ EtOH,\ \Delta} [M_2X_3(PR_3)_6]CF_3SO_3 + 6PPh_3$$

Figure 4.1 *General synthetic route to $[M_2(\mu\text{-}X)_3(PR_3)_6]CF_3SO_3$ complexes.*

4.2.2 Electrochemistry

Non-aqueous electrochemistry of $[Os_2(\mu\text{-}X)_3(PR_3)_6]^+$ complexes[2,3] (recorded for the $CF_3SO_3^-$ salt) in CH_2Cl_2/0.5 mol dm^{-3} $[Bu^n_4N][BF_4]$) has established that, like their $[Ru_2(\mu\text{-}X)_3(PR_3)_6]^+$ analogues, they undergo two one-electron oxidations, corresponding to progressive oxidation of the $\{Os(\mu\text{-}X)_3Os\}^+$ core. The electrochemical data for these complexes, collected in this laboratory, are listed in Table 4.1.

Table 4.1 *Electrochemical Data for $[Os_2X_3L_6]^+$ Complexes.*

Complex	$E_{1/2}$ / V vs Ag/AgCl [a] $E_{ox}(1)$	$E_{ox}(2)$	E_{av} / V [b]	$\Delta E_{1/2}$ / V [c]
$[Os_2Cl_3(PEt_3)_6]^+$ [d]	+0.87	+1.47	+1.17	0.60
$[Os_2Cl_3(PEt_2Ph)_6]^+$ [d]	+0.97	+1.49	+1.23	0.52
$[Os_2Br_3(PEt_2Ph)_6]^+$	+0.94	+1.44	+1.19	0.50
$[Os_2Cl_3(PMe_2Ph)_6]^+$ [d]	+1.07	+1.57	+1.32	0.50
$[Os_2Br_3(PMe_2Ph)_6]^+$ [d]	+1.05	+1.55	+1.30	0.50
$[Os_2Cl_3(triphos)_2]^+$ [d]	+1.26	+1.75	+1.51	0.49
$[Os_2Br_3(triphos)_2]^+$	+1.26	+1.75	+1.51	0.49

[a] Recorded in CH_2Cl_2 containing 0.5 mol dm^{-3} $[NBu^n_4][BF_4]$ at 213K; ferrocene is oxidised at +0.55 V vs Ag/AgCl under these conditions. [b] $E_{av} = 1/2(E_{ox}(1) + E_{ox}(2))$. [c] $\Delta E_{1/2} = (E_{ox}(2) - E_{ox}(1))$. [d] *Data taken from Ref. 2.*

Unlike the corresponding $[Ru_2(\mu\text{-}X)_3(PR_3)_6]^+$ complexes (and with the possible exception of $[Os_2Cl_3(PEt_3)_6]^+$), there does not appear to be any correlation between E_{av} and $\Delta E_{1/2}$ within the μ-Cl or μ-Br series. There is a subtle but systematic variation between the differences in E_{av} values in the three μ-Cl/μ-Br pairs. In the more easily oxidised complexes (lower E_{av}) the difference in E_{av} between the Cl and Br complexes is

40 mV and this declines to zero as E_{av} becomes more positive, *i.e.* the μ-Br complexes are very marginally easier to oxidise but this vanishes as the compounds become more electron-deficient. In contrast, the separation between oxidations ($\Delta E_{1/2}$) is ~0.50 V for all complexes except $[Os_2(\mu\text{-}Cl)_3(PEt_3)_6]^+$, and remains constant regardless of the bridging halide. If the diosmium complexes are compared with the corresponding diruthenium complexes (Table 3.1), the former are more easily oxidised (E_{av} lower by 180 to 300 mV), but as already noted no pattern is established for $\Delta E_{1/2}$. Compared to the diruthenium complexes, $\Delta E_{1/2}$ for the diosmium systems is surprisingly small and surprisingly constant.

4.2.3 UV/Vis/Near-IR Spectra of $[Os_2(\mu\text{-}X)_3(PR_3)_6]^+$ Complexes

The spectra of the closed-shell (12-e) $[Os_2(\mu\text{-}X)_3(PR_3)_6]^+$ complexes are mostly featureless below ~25 000 cm^{-1}, which helps the definition of the near-infrared bands which appear in the electrogenerated 11-e and 10-e states.

Table 4.2 *UV/Vis/Near-IR Data for $[Os_2(\mu\text{-}X)_3(PR_3)_6]^+$ Complexes.*

Complex	ν_{max} / cm^{-1} (ε / dm^3 mol^{-1} cm^{-1}) [a]
$[Os_2Cl_3(PMe_2Ph)_6]^+$ [b]	32 580 (7920)
$[Os_2Br_3(PMe_2Ph)_6]^+$ [b]	31 410 (6580)
$[Os_2Cl_3(PEt_3)_6]^+$ [b]	~32 500 (sh), 34 390 (4660), 41 050 (7550)
$[Os_2Cl_3(PEt_2Ph)_6]^+$ [b]	31 690 (5790), 37 940 (11 020)
$[Os_2Br_3(PEt_2Ph)_6]^+$	30 700 (6300), ~36 500 (sh)
$[Os_2Cl_3(triphos)_2]^+$ [b]	31 410 (8730)
$[Os_2Br_3(triphos)_2]^+$	30 500 (8170), ~37 000 (sh)

[a] *Recorded in CH_2Cl_2 containing 0.5 mol dm^{-3} $[Bu^n_4N][BF_4]$, at 213 K.* [b] *Data from Ref. 2.*

The spectra reveal a moderately intense band in the region 30-33 000 cm^{-1}, and a more intense absorption above 35 000 cm^{-1} (Table 4.2). These bands are at lower energy (by ~1000 cm^{-1}) for bromide-bridged complexes, and appear at higher energy (by ~5000 cm^{-1}) than for the corresponding diruthenium complexes, but are of similar

intensity. Although these bands are intense, these are probably d-d type promotions, between t_{2g}- and e_g-based molecular orbitals. In monomeric Os^{II} complexes (§5.4), weak d-d bands are observed below 32 000 cm^{-1}, and more intense charge-transfer bands (into the e_g orbitals) appear above 36 000 cm^{-1}. The difference between the ruthenium and osmium complexes is explained by the larger single-ion 10Dq expected for osmium, and similarly 10Dq(Br) < 10Dq(Cl).

4.2.4 UV/Vis/Near-IR Spectra of $[Os_2(\mu\text{-}X)_3(PR_3)_6]^{2+}$ Complexes

Upon electrogeneration of the $[Os_2(\mu\text{-}X)_3(PR_3)_6]^{2+}$ species, several bands develop in the near-infrared region (below 8000 cm^{-1}). Initially spectra were recorded only as far as 4000 cm^{-1} (2500 nm), revealing a weak band near 8000 cm^{-1} and a moderately intense structured band near 5000 cm^{-1}.[2,3] We have since re-recorded the spectra to 3125 cm^{-1}, revealing another narrow absorption band near 3500 cm^{-1} (Table 4.3).

Our spectra (Fig. 4.2) also show the band ~4500 cm^{-1} to be split into two components for some complexes. Whilst the spectra of the corresponding diruthenium complexes are now seen as a series of two-band spectra converging and moving to lower energy (Ch. 3), the $[Os_2(\mu\text{-}X)_3(PR_3)_6]^{2+}$ spectra are more complicated, yet more consistent. They all have the same general appearance, *i.e.* a weak band at 7-8000 cm^{-1}, and a moderately intense band near 4500 cm^{-1} and 3500 cm^{-1}. Detailed solvent-dependence studies on the 4500 cm^{-1} band of $[Os_2(\mu\text{-}Cl)_3(PEt_3)_6]^{2+}$ by Yellowlees *et al*,[3] have shown the position of this band to be invarient with solvent, which is usually indicative of a delocalised system. The unusual near-IR spectra, which appear different from their class III diruthenium counterparts, have caused us to wonder whether a trapped ($Os^{II}Os^{III}$) state prevails, however we defer discussion until we have considered the evidence of the heterobimetallic $[RuOs(\mu\text{-}X)_3(PR_3)_6]^{2+}$ complexes.

Table 4.3 *UV/Vis/Near-IR Data for* $[Os_2(\mu\text{-}X)_3(PR_3)_6]^{2+}$ *Complexes.*

Complex	ν_{max} / cm^{-1} (ε / $dm^3\ mol^{-1}\ cm^{-1}$) [a]			
$[Os_2Cl_3(PMe_2Ph)_6]^{2+}$	3410 (4140)	4410 (5950)	8800 (1150)	18 000 (1520)
		5200 (6600)		31 950 (8710)
$[Os_2Br_3(PMe_2Ph)_6]^{2+}$	3550 (3460)	4380 (3650)	8200 (200)	15 500 (980)
		4950 (4400)		31 130 (5500)
$[Os_2Cl_3(PEt_3)_6]^{2+}$	3440 (5800)	4380 (5200)	7770 (720)	19 130 (960)
		4980 (5020)		25 540 (1790)
				32 100 (4900)
$[Os_2Cl_3(PEt_2Ph)_6]^{2+}$	3450 (2730)	4360 (2350)	7510 (530)	17 800 (550)
		4850 (2300)		30 950 (5440)
$[Os_2Br_3(PEt_2Ph)_6]^{2+}$	3450 (6100)	4500 (4290)	7450 (1190)	15 400 (1060)
				19200 (1030)
				29 800 (5620)
$[Os_2Cl_3(triphos)_2]^{2+}$		4910 (5880)	7900 (600)	16 520 (1170)
				31 730 (8280)
$[Os_2Br_3(triphos)_2]^{2+}$	3600 (2900)	4900 (8600)		14 000 (1500)
				30 700 (9100)

[a] *Electrogenerated in the OSTLE cell, in* CH_2Cl_2 *containing 0.5 mol* dm^{-3} $[Bu^n_4N][BF_4]$, *at 213 K.*

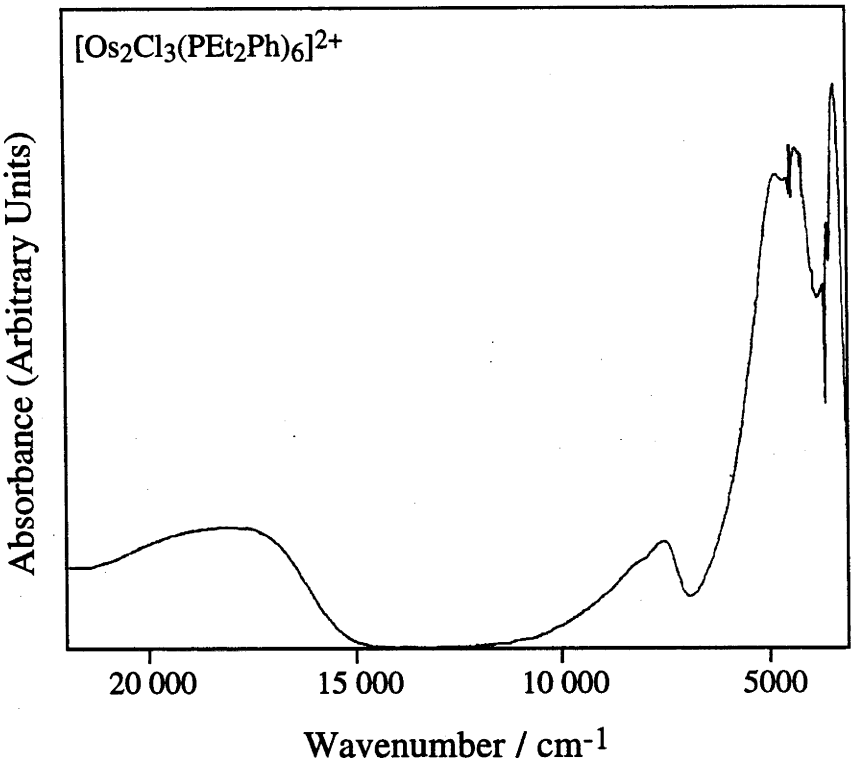

Figure 4.2 *Visible/near-IR spectrum of* $[Os_2(\mu\text{-}Cl)_3(PEt_2Ph)_6]^{2+}$.

4.2.5 UV/Vis/Near-IR spectra of $[Os_2(\mu\text{-}X)_3(PR_3)_6]^{3+}$ complexes

All of the $[Os_2(\mu\text{-}X)_3(PR_3)_6]^{2+}$ complexes were further oxidised electrochemically to the $[Os_2(\mu\text{-}X)_3(PR_3)_6]^{3+}$ state (Fig. 4.3), which were stable for several hours at -60 °C in the presence of a suitably polarised electrode. Upon oxidation, the near-IR bands associated with the mixed-valence species collapse and an intense sharp band develops near 10 000 cm^{-1} (in bold in Table 4.4). This is similar to the spectrum observed for the 10-e $[Ru_2(\mu\text{-}X)_3(PR_3)_6]^{3+}$ complexes (§3.3.4), and isoelectronic $[Ir_2Cl_9]^-$,[12] and this exceptional feature is believed to be a pairwise transition associated with a localised $d^5 \cdots d^5$ configuration.

It is reasonable that localisation takes over in higher oxidation states, as the d-orbitals contract. Thus, $[Ir_2Cl_9]^{2-}$ (11-e) is undoubtedly a trapped $Ir^{III}Ir^{IV}$ system,[12] whereas isoelectronic $[Ru_2Cl_9]^{4-}$ is delocalised.[13]

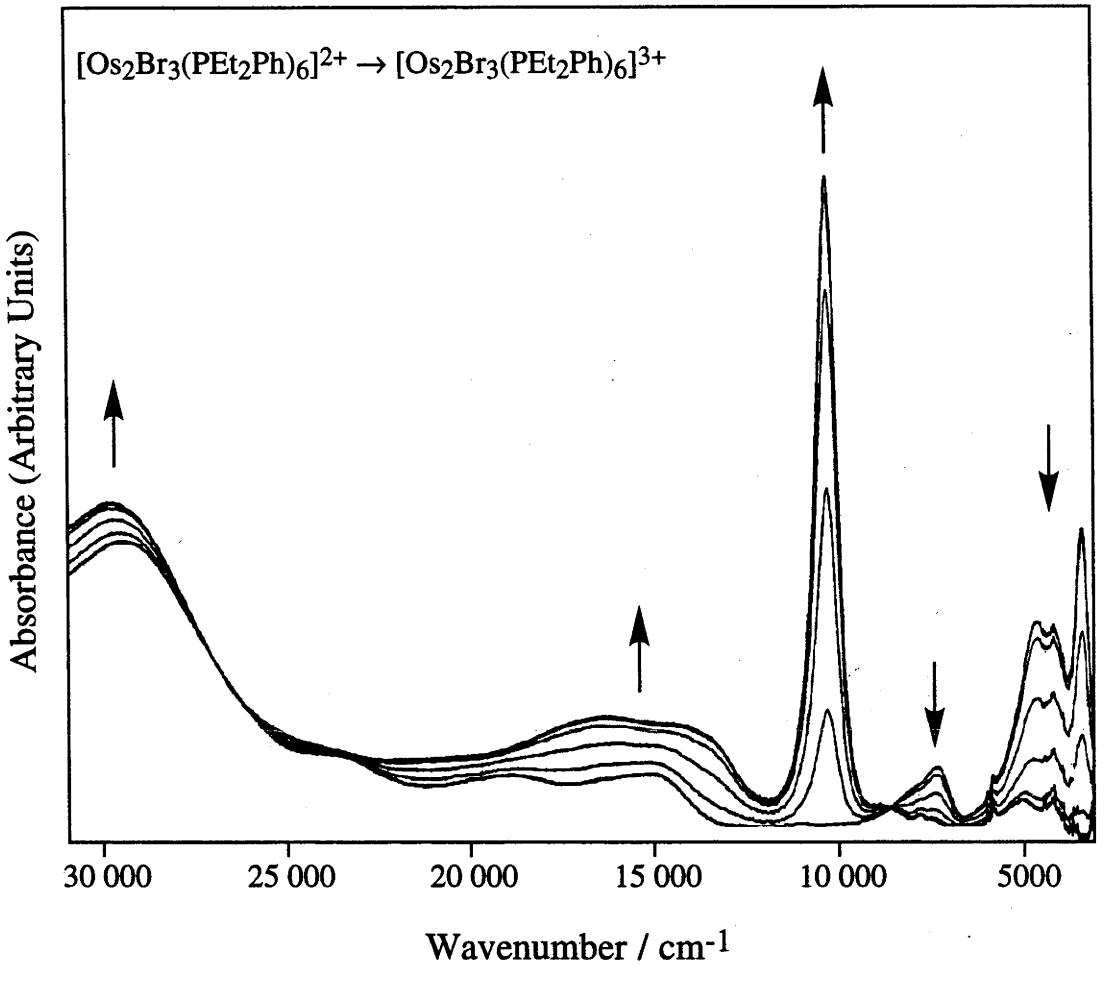

Figure 4.3 *Spectral progressions upon oxidation of* $[Os_2Br_3(PEt_2Ph)_6]^{2+}$ *to* $[Os_2Br_3(PEt_2Ph)_6]^{3+}$ *in an OSTLE cell at 213 K.*

Table 4.4 *UV/Vis/Near-IR Data for $[Os_2(\mu\text{-}X)_3(PR_3)_6]^{3+}$ Complexes.*

Complex	ν_{max} / cm^{-1} (ε / dm^3 mol^{-1} cm^{-1}) [a]
$[Os_2Cl_3(PMe_2Ph)_6]^{3+}$ [b]	5400 (330), **11 550 (11 150)**, ~15 000 (~3700), 32 400 (9500)
$[Os_2Br_3(PMe_2Ph)_6]^{3+}$ [b]	5300 (590), **10 360 (8440)**, ~14 500 (~2500), 31 600 (3660)
$[Os_2Cl_3(PEt_3)_6]^{3+}$ [b]	5100 (420), **11 930 (11 220)**, 14 950 (900), 18 460 (1320), 31 330 (4620)
$[Os_2Cl_3(PEt_2Ph)_6]^{3+}$ [b]	4450 (470), **11 260 (5350)**, 16 570 (1130), 31 500 (3660)
$[Os_2Br_3(PEt_2Ph)_6]^{3+}$	5100 (520), **10 450 (12 700)**, 30 100 (6250)
$[Os_2Cl_3(triphos)_2]^{3+}$ [b]	5300 (300), **10 820 (7000)**, 14 340 (2690)
$[Os_2Br_3(triphos)_2]^{3+}$	**10 200 (8760)**, ~14 000 (~2200)

[a] *Electrogenerated in the OSTLE cell, in CH_2Cl_2 solution containing 0.5 mol dm^{-3} $[Bu^n_4N][BF_4]$, at 213 K. The intense band near 10 000 cm^{-1} is shown in bold.* [b] *Data from Ref. 2.*

4.3 MIXED-METAL COMPLEXES, $[(PR_3)_3Ru(\mu\text{-}X)_3Os(PR_3)_3]^{+/2+}$

4.3.1 Introduction

Given the complexity of the $[Os_2(\mu\text{-}X)_3(PR_3)_6]^{2+}$ spectra, we wanted to define the properties of a truly localised mixed-valence complex, *i.e.* $\{M^{II}(\mu\text{-}Cl)_3M^{III}\}^{2+}$. Based on electrochemical evidence that $[Os_2(\mu\text{-}X)_3(PR_3)_6]^{+}$ complexes are more easily oxidised than their ruthenium analogues (by ~0.2 V), we believed that a heterobimetallic (ruthenium-osmium) complex of the type $\{Ru^{II}(\mu\text{-}X)_3Os^{II}\}^{+}$ would, upon oxidation, undoubtedly result in a trapped ($Ru^{II}Os^{III}$) state.

Of the reports detailing the formation of mixed ruthenium-osmium confacial bioctahedral complexes, only twice have mixed-metal complexes been isolated free of other species. These complexes, $[(PPh_3)_2(CO)Ru(\mu\text{-}Cl)_3OsCl(PPh_3)_2]$ [14] and $[(triphos)Ru(\mu\text{-}Cl)_3Os(triphos)](PF_6)_2$,[2] were not fully characterised on account of their poor solubilities. The reduced solubility of the latter, whilst sufficient for room-temperature measurements in acetonitrile, prevented the recording of electrochemical, optical and EPR data in dichloromethane solution at low temperature. Other known heterobimetallics, $[(\eta^6\text{-}C_6H_6)Ru(\mu\text{-}Cl)_3Os(\eta^6\text{-}C_6H_6)]^{+}$,[15] and $[(\eta^6\text{-}C_6H_6)Ru(\mu\text{-}OMe)_3Os(\eta^6\text{-}C_6H_6)]^{+}$,[16] were characterised in solution by NMR, as mixtures with their respective $[M_2(\mu\text{-}X)_3(\eta\text{-}C_6H_6)]^{+}$ (M = Ru, Os; X = Cl, OMe) counterparts. These accounts highlight the difficulty of separating mixed-metal complexes from their homobimetallic counterparts, a problem successfully addressed during this study.

4.3.2 Synthesis and Characterisation

Prior to this work, the reaction of equimolar amounts of $[RuCl_2(PPh_3)_3]$ and $[OsCl_2(PPh_3)_3]$ with an excess of the tridentate ligand triphos was investigated (Fig. 4.4).[2] Heating these materials in 2-methoxyethanol yielded, upon workup, a yellow microcrystalline solid. The $^{31}P\text{-}\{^1H\}$ NMR spectrum of the reaction products consisted

of four singlets, two of which were assigned to the homobimetallic complexes $[M_2(\mu\text{-}Cl)_3(triphos)_2]^+$, where M = Ru and Os respectively, with the remaining resonances assigned as belonging to $[(triphos)Ru(\mu\text{-}Cl)_3Os(triphos)]^+$.[2] These complexes were formed in an approximately statistical ratio ($\{Ru_2\}^+$:2$\{RuOs\}^+$:$\{Os_2\}^+$).‡ We have since tried this reaction with the appropriate bromide starting materials and found a similar ratio of products. The $^{31}P\text{-}\{^1H\}$ NMR of this bromo-bridged mixture is shown in Fig. 4.5.

$$[OsCl_2(PPh_3)_3] + [RuCl_2(PPh_3)_3] \xrightarrow[\text{(ii) } CF_3SO_3H/MeOH,CH_2Cl_2]{\text{(i) triphos, EtOH, } \Delta} [Ru_2Cl_3(triphos)_2]CF_3SO_3 + 2\,[RuOsCl_3(triphos)_2]CF_3SO_3 + [Os_2Cl_3(triphos)_2]CF_3SO_3$$

Figure 4.4 *Reaction of equal quantities of $[RuCl_2(PPh_3)_3]$ and $[OsCl_2(PPh_3)_3]$ with triphos.*

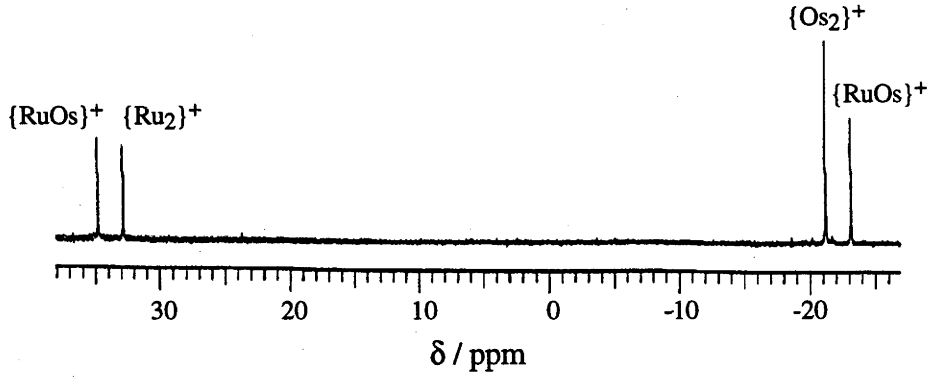

Figure 4.5 *$^{31}P\text{-}\{^1H\}$ NMR spectrum of a 1:2:1 mixture of $[Ru_2(\mu\text{-}Br)_3(triphos)_2]^+$, $[RuOs(\mu\text{-}Br)_3(triphos)_2]^+$ and $[Os_2(\mu\text{-}Br)_3(triphos)_2]^+$.*

Electrochemistry of these 1:2:1 mixtures confirmed that both the $\{Os_2\}^+$ and $\{RuOs\}^+$ complexes were oxidised more easily than $\{Ru_2\}^+$. The isolation of $[RuOs(\mu\text{-}Cl)_3(triphos)_2][PF_6]_2$ was achieved by taking advantage of this difference in oxidation potentials.[2] Performing the same reactions using a five-fold excess of $[RuCl_2(PPh_3)_3]$ (Fig. 4.6), led to a decreased yield of the heterobimetallic complex, but also had the desired effect of limiting the formation of the diosmium complex to only

‡ $\{Ru_2\}^+ = [Ru_2(\mu\text{-}X)_3(PR_3)_6]^+$; $\{Os_2\}^+ = [Os_2(\mu\text{-}X)_3(PR_3)_6]^+$; $\{RuOs\}^+ = [RuOs(\mu\text{-}X)_3(PR_3)_6]^+$.

about 1% of the total product. The $^{31}P-\{^{1}H\}$ NMR spectrum of these reaction mixtures reveal only two major products, $[Ru_2(\mu\text{-}X)_3(triphos)_2]^+$ and $[(triphos)Ru(\mu\text{-}X)_3Os(triphos)]^+$, in approximately a 2:1 ratio (Fig. 4.7). The isolation of $[RuOs(\mu\text{-}Cl)_3(triphos)_2]^{2+}$ was then achieved by exploiting the difference in the relative ease of oxidation of osmium compared with ruthenium, by selectively oxidising the $\{RuOs\}^+$ complex as anticipated, and precipitating the less soluble dication ($[RuOs(\mu\text{-}Cl)_3(triphos)_2](PF_6)_2$) in low yield.[2]

$$[OsX_2(PPh_3)_3] + 5\,[RuX_2(PPh_3)_3] \xrightarrow[\text{(ii) } CF_3SO_3H/MeOH,CH_2Cl_2]{\text{(i) } PR_3,\ EtOH,\ \Delta} \begin{array}{l}[Ru_2X_3(PR_3)_6]CF_3SO_3\ (\sim 65\%) + \\ [RuOsX_3(PR3)_6]CF_3SO_3\ (\sim 34\%) + \\ [Os_2X_3(PR_3)_6]CF_3SO_3\ (\sim 1\%)\end{array}$$

Figure 4.6 *General synthesis of mixtures containing (mostly) $\{Ru_2\}^+$ and $\{RuOs\}^+$ complexes.*

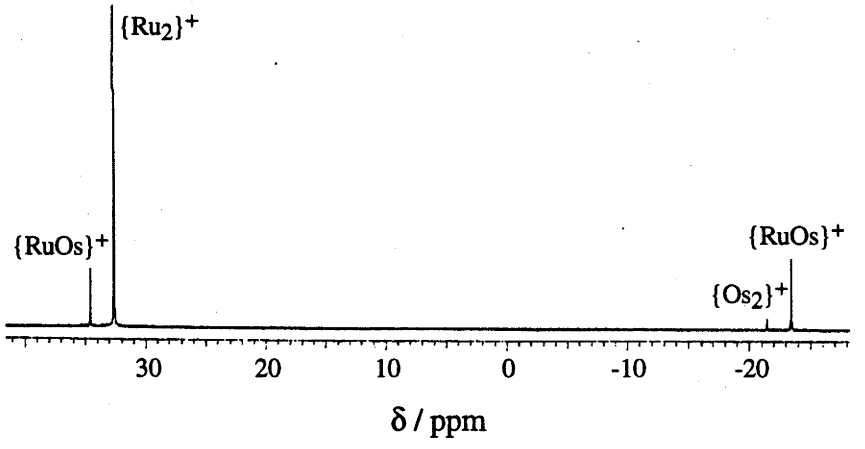

Figure 4.7 *$^{31}P-\{^{1}H\}$ NMR spectrum of a 2:1 mixture of $[Ru_2(\mu\text{-}Br)_3(triphos)_2]^+$ and $[RuOs(\mu\text{-}Br)_3(triphos)_2]^+$.*

Since the isolation and characterisation of $[RuOs(\mu\text{-}Cl)_3(triphos)_2]^{2+}$,[2] we have attempted the same procedure to separate the bromide-bridged bimetallic complexes $[MM'(\mu\text{-}Br)_3(triphos)_2]^+$ (MM' = Ru_2, RuOs). Unfortunately, despite efficient selective oxidation, the pure heterobimetallic complex has not been isolated free of homobimetallic contaminants to date.

We have also examined the outcome of analogous reactions involving monodentate phosphines. Heating mixtures of $[RuCl_2(PPh_3)_3]$, $[OsCl_2(PPh_3)_3]$ and monodentate phosphines (PR_3 = PEt_3 or PEt_2Ph) resulted in the formation of $\{RuOs\}^+$ complexes, along with their $\{Ru_2\}^+$ and $\{Os_2\}^+$ counterparts. The ratio of $\{Ru_2\}^+$:$\{RuOs\}^+$:$\{Os_2\}^+$, as determined by ^{31}P-$\{^1H\}$ NMR, was typically 65:34:1%, *i.e.* roughly 2:1 in favour of $\{Ru_2\}^+$ over $\{RuOs\}^+$ with a trace of $\{Os_2\}^+$. Interestingly, this is marginally superior to the simple statistical outcome (68:29:3%). The oxidised heterobimetallic complexes were again unable to be crystallised free of the $\{Ru_2\}^+$ complexes, however this did not prohibit using these mixtures of $\{Ru_2\}^+$ and $\{RuOs\}^+$ to obtain authentic optical and EPR spectra of the mixed-valence $\{RuOs\}^{2+}$ complexes, as discussed later. All of the components of the mixtures were converted to the redox-inert triflate salts as described previously.

The identities and approximate proportions of the reaction products were further substantiated by electrospray (ESMS) and fast atom bombardment mass spectra (FABMS), which clearly revealed peaks assignable to the molecular ions of the $\{Ru_2\}^+$, $\{RuOs\}^+$ and $\{Os_2\}^+$ complexes. Figure 4.8(a) shows the positive ion ES mass spectrum at B1 = 40 V for a mixture known to contain $[Ru_2Cl_3(PEt_2Ph)_6]CF_3SO_3$, $[RuOsCl_3(PEt_2Ph)_6]CF_3SO_3$ (approximately 2:1) and a trace of $[Os_2Cl_3(PEt_2Ph)_6]CF_3SO_3$. The peaks at m/z 1307 and 1395 are due to the intact ions of the main constituents and that due to $[Os_2Cl_3(PEt_2Ph)_6]^+$ is just detectable at m/z 1488. Figure 4.8(b) shows the ES mass spectrum at B1 = 80 V and the new peaks at m/z 1141 and 1229 are due to ions formed by loss of PEt_2Ph from the precursor ions. At B1 = 100 V (Fig. 4.8(c)) there is a small peak due to $[Ru_2Cl_3(PEt_2Ph)_4]^+$ but the base peak is at m/z 635 which is assigned to $[RuCl(PEt_2Ph)_3]^+$ and there is a smaller peak at m/z 725 assigned to $[OsCl(PEt_2Ph)_3]^+$. These ES mass spectra are consistent with cleavage of the dimeric ions within the ion source by collisionally activated decompositions as follows:

$$[Ru_2Cl_3(PEt_2Ph)_6]+ \rightarrow [RuCl(PEt_2Ph)_3]^+ + [RuCl_2(PEt_2Ph)_x]$$

$$[RuOsCl_3(PEt_2Ph)_6]^+ \rightarrow [RuCl(PEt_2Ph)_3]^+ + [OsCl_2(PEt_2Ph)_x]$$

$$\text{and} \rightarrow [OsCl(PEt_2Ph)_3]^+ + [RuCl_2(PEt_2Ph)_x]$$

in which the triple-chloride bridge is cleaved to give a neutral M^{II} fragment (not observed by ESMS) and the cationic fragments which are observed. Similar mixtures containing other $\{Ru_2\}^+$ and $\{RuOs\}^+$ complexes also gave the intact ions at low ion source energy (Table 4.5). It would be interesting to examine a pure $\{RuOs\}^+$ sample to see whether the two asymmetric fragmentations have equal importance.

Table 4.5 *ES Mass Spectral Data for Products from Reactions of $[RuCl_2(PPh_3)_3]$ and $[OsCl_2(PPh_3)_3]$ with PR_3.*

Product Mixture	Ions observed at low ion-source energy (m/z)	Fragment ions observed at higher ion-source energy (m/z)
$[Ru_2Cl_3(triphos)_2]^+$; $[RuOsCl_3(triphos)_2]^+$	$[RuOsCl_3(triphos)_2]^+$ (1647); $[Ru_2Cl_3(triphos)_2]^+$ (1558)	
$[Ru_2Br_3(triphos)_2]^+$; $[RuOsBr_3(triphos)_2]^+$	$[RuOsBr_3(triphos)_2]^+$ (1781); $[Ru_2Br_3(triphos)_2]^+$ (1691)	
$[Ru_2Cl_3(PEt_3)_6]^+$; $[RuOsCl_3(PEt_3)_6]^+$	$[RuOsCl_3(PEt_3)_6]^+$ (1107); $[Ru_2Cl_3(PEt_3)_6]^+$ (1017)	$[Ru_2Cl_3(PEt_3)_5]^+$ (898)
$[Ru_2Cl_3(PEt_2Ph)_6]^+$; $[RuOsCl_3(PEt_2Ph)_6]^+$; $[Os_2Cl_3(PEt_2Ph)_6]^+$	$[Os_2Cl_3(PEt_2Ph)_6]^+$ (1488); $[RuOsCl_3(PEt_2Ph)_6]^+$ (1395); $[Ru_2Cl_3(PEt_2Ph)_6]^+$ (1307)	$[RuOsCl_3(PEt_2Ph)_5]^+$ (1229); $[Ru_2Cl_3(PEt_2Ph)_5]^+$ (1141); $[Ru_2Cl_3(PEt_2Ph)_4]^+$ (975); $[OsCl(PEt_2Ph)_3]^+$ (725); $[RuCl(PEt_2Ph)_3]^+$ (635)

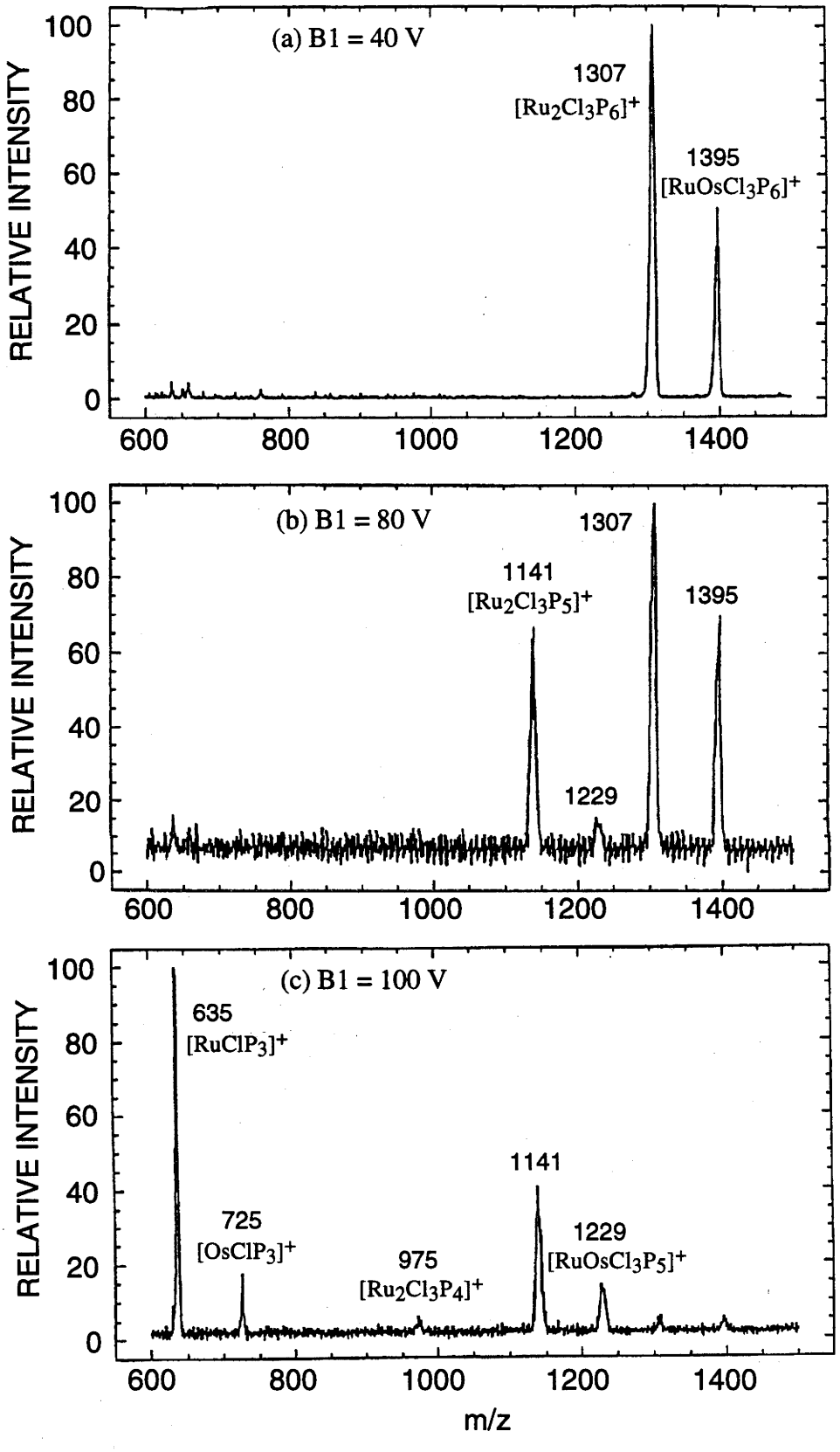

Figure 4.8 *Positive ion ES mass spectra at various ion source energies for a solution containing a mixture of* $[Ru_2Cl_3(PEt_2Ph)_6]CF_3SO_3$ *and* $[RuOsCl_3(PEt_2Ph)_6]CF_3SO_3$ *at (a) B1 = 40 V, (b) B1 = 80 V and (c) B1 = 100 V.*

4.3.3 Electrochemistry

Prior to this study, the only electrochemical study of a ruthenium-osmium bimetallic complex was of $[RuOs(\mu\text{-}Cl)_3(triphos)_2][PF_6]_2$.[2] However, this complex is only very sparingly soluble in dichloromethane, and decomposes slowly in acetonitrile. Nevertheless, the complex was found to be sufficiently stable in acetonitrile to observe two redox processes, a reduction at +1.26 V and an oxidation at +1.94 V, in accord with its isolation at the mixed-valence level. In the present work, the redox properties of the $[RuOs(\mu\text{-}X)_3(PR_3)_6]^+$ complexes were determined as their triflate salts from mixtures which also contained one or both of the parent homobimetallic $[M_2(\mu\text{-}X)_3(PR_3)_6]^+$ (M = Ru, Os) complexes. Through the use of cyclic voltammetry, alternating current voltammetry and linear sweep stirred voltammetry, and with a knowledge of the redox responses of the homobimetallic diruthenium and diosmium $[M_2(\mu\text{-}X)_3(PR_3)_6]^+$ complexes, the redox properties of the $[RuOs(\mu\text{-}X)_3(PR_3)_6]^+$ complexes could be readily established and interpreted.

The acV and stirred linear sweep voltammograms of a typical 1:2:1 mixture of $\{Ru_2\}^+$:$\{RuOs\}^+$:$\{Os_2\}^+$ complexes are shown in Fig. 4.9. The $[M_2(\mu\text{-}Cl)_3(PEt_2Ph)_6]^+$ complexes display two oxidations, at +1.09 and +1.71 V (M = Ru), and +0.87 and +1.47 V (M = Os). The stirred voltammogram of the mixture clearly reveals the presence of further major species in addition to $\{Ru_2\}^+$ and $\{Os_2\}^+$. A simple 1:1 mixture of the homobimetallic complexes would yield oxidations in the same places as those shown in Fig. 4.9, however each oxidation would involve the same number of electrons, in direct contrast to what is revealed. The larger current responses at +0.87 and +1.71 V suggests additional oxidation processes, which are assigned to the 12/11-e and 11/10-e oxidations of $[RuOs(\mu\text{-}Cl)_3(PEt_2Ph)_6]^+$. The first couple (+0.87 V) corresponds to the oxidation of the osmium centre and the second (+1.71 V) to that of ruthenium. The acV peaks in Fig. 4.9 are not obviously asymmetric, and so, remarkably enough, within the resolution limits of this technique the 12/11-e oxidations of $\{Os_2\}^+$

and $\{RuOs\}^{+}$ are coincident, and so are the 11/10-e oxidations of $\{Ru_2\}^{2+}$ and $\{RuOs\}^{2+}$.

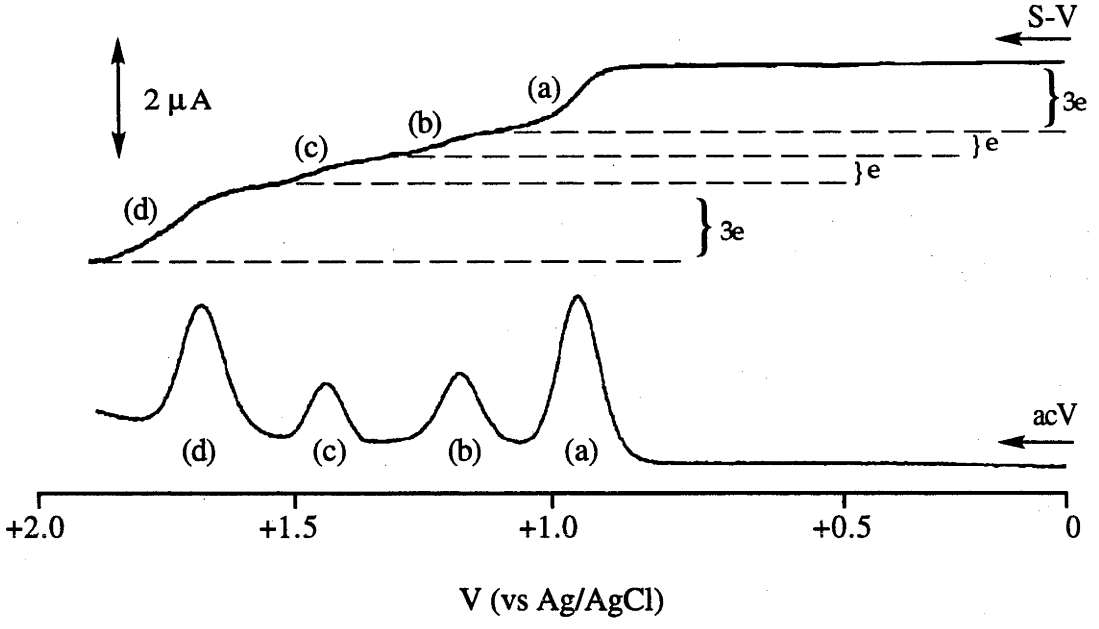

Figure 4.9 *Stirred voltammogram (S-V) and alternating current voltammogram (acV) of a 1:2:1 mixture of* $[Ru_2Cl_3(PEt_2Ph)_6]^{+}$, $[RuOsCl_3(PEt_2Ph)_6]^{+}$ *and* $[Os_2Cl_3(PEt_2Ph)_6]^{+}$. *Processes are:*
(a) $2\{RuOs\}^{+} \rightarrow 2\{RuOs\}^{2+}$ *and* $\{Os_2\}^{+} \rightarrow \{Os_2\}^{2+}$.
(b) $\{Ru_2\}^{+} \rightarrow \{Ru_2\}^{2+}$.
(c) $\{Os_2\}^{2+} \rightarrow \{Os_2\}^{3+}$.
(d) $2\{RuOs\}^{2+} \rightarrow 2\{RuOs\}^{3+}$ *and* $\{Ru_2\}^{2+} \rightarrow \{Ru_2\}^{3+}$.

The voltammetry of the 2:1 mixtures (based on NMR) of $\{Ru_2\}^{+}$ and $\{RuOs\}^{+}$ was similar, with three oxidative processes observed at +0.87, +1.09 and +1.71 V (Fig. 4.10). The processes at +1.09 and +1.71 V coincide with those observed for the diruthenium species. However, the different current responses associated with these couples in the stirred voltammogram clearly indicate the presence of an additional species, with an oxidative process coincident with the 11/10-e couple of $\{Ru_2\}^{2+}$ at +1.71V. What is most apparent from the voltammetry of this mixture is the absence of a process at +1.47 V, confirming that very little of the diosmium species is present in the mixture. The first oxidation of $\{RuOs\}^{+}$ ($Ru^{II}Os^{II} \rightarrow Ru^{II}Os^{III}$) is clearly observed at +0.87 V, whilst the second oxidation ($Ru^{II}Os^{III} \rightarrow Ru^{III}Os^{III}$) once more occurs at a potential identical with the 11/10-e oxidation of $\{Ru_2\}^{2+}$.

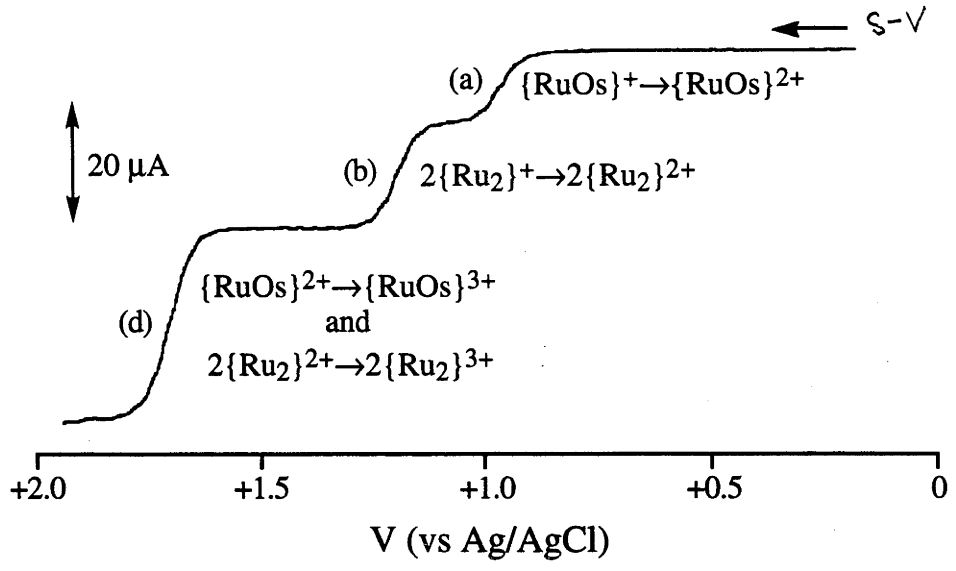

Figure 4.10 *Stirred voltammogram of a 2:1 mixture of* $[Ru_2Cl_3(PEt_2Ph)_6]^+$ *and* $[RuOsCl_3(PEt_2Ph)_6]^+$. *Process (c) of Fig. 4.9 is missing.*

For all of the mixed-metal complexes the first oxidation was found at potentials identical with that of the 12/11-e couple in the corresponding $\{Os_2\}^+$ systems, and their second oxidation was coincident with the 11/10-e couples of the $\{Ru_2\}^{2+}$ complexes. This implies that the ruthenium and osmium centres in $[(PR_3)_3Ru(\mu\text{-}Cl)_3Os(PR_3)_3]^+$ do not discriminate between ruthenium and osmium centres at the other site.

The separation of the two couples ($\Delta E_{1/2}$) in the $\{RuOs\}^+$ complexes ranges from ~0.65 V in the triphos complexes to 0.84 V in the more electron-rich (lower E_{av}) PEt_3 complex. The larger separation compared with the homobimetallic complexes represents the electronic asymmetry of the mixed-metal complexes, and is not a measure of greater metal-metal interaction as discussed in §3.7.

Table 4.6 *Electrochemical Data for $[RuOsX_3L_6]^+$ Complexes.*

Complex	$E_{1/2}$ / V vs Ag/AgCl [a] $E_{ox}(1)$ [b]	$E_{ox}(2)$ [c]	E_{av} / V [d]	$\Delta E_{1/2}$ / V [e]
$[RuOsCl_3(PEt_3)_6]^+$	+0.87	+1.71	+1.29	0.84
$[RuOsCl_3(PEt_2Ph)_6]^+$	+0.97	+1.71	+1.34	0.74
$[RuOsCl_3(triphos)_2]^+$	+1.26	+1.94	+1.60	0.68
$[RuOsBr_3(triphos)_2]^+$	+1.26	+1.91	+1.58	0.65

[a] Recorded in CH_2Cl_2 containing 0.5 mol dm^{-3} $[NBu^n_4][BF_4]$ at 213K; ferrocene is oxidised at +0.55 V vs Ag/AgCl under these conditions. [b] $E_{ox}(1) = Ru^{II}Os^{II} \rightarrow Ru^{II}Os^{III}$. [c] $E_{ox}(2) = Ru^{II}Os^{III} \rightarrow Ru^{III}Os^{III}$

4.3.4 Near-IR Spectra

Despite being unable to readily isolate pure $[(PR_3)_3Ru(\mu\text{-}X)_3Os(PR_3)_3]^z$ complexes, the informative near-IR electronic spectrum of the 11-e systems could still be collected from mixtures of $\{Ru_2\}^+$ and $\{RuOs\}^+$. Given that the $\{RuOs\}^+$ complexes were oxidised at a lower potential than their diruthenium analogues by 0.2 V or more, selective controlled-potential electrolysis in an OSTLE cell produced clean mixtures of $[Ru_2(\mu\text{-}X)_3(PR_3)_6]^+$ and the mixed-valence $[RuOs(\mu\text{-}X)_3(PR_3)_3]^{2+}$ complexes. The near-IR spectra of the 12-e $\{Ru_2\}^+$ complexes are devoid of any features below ~15 000 cm^{-1}, hence the presence of the latter does not contribute in any way to the low-energy region of the 11-e $\{RuOs\}^{2+}$ spectra.

The near-IR spectra of the 11-e heterobimetallic complexes are all very similar in profile and unmistakably different from their $\{Ru_2\}^{2+}$ or $\{Os_2\}^{2+}$ analogues. The spectra consist of a single symmetric band centred in the region 7000 - 8000 cm^{-1} (Fig. 4.11). With the four examples at hand (Table 4.7), there is an obvious relationship between ν_{max} and $\Delta E_{1/2}$, where the band energy decreases with decreasing separation of the two oxidation potentials ($\Delta E_{1/2}$). The bands are typically very broad, with a width of ~4000 cm^{-1} at half maximum intensity.

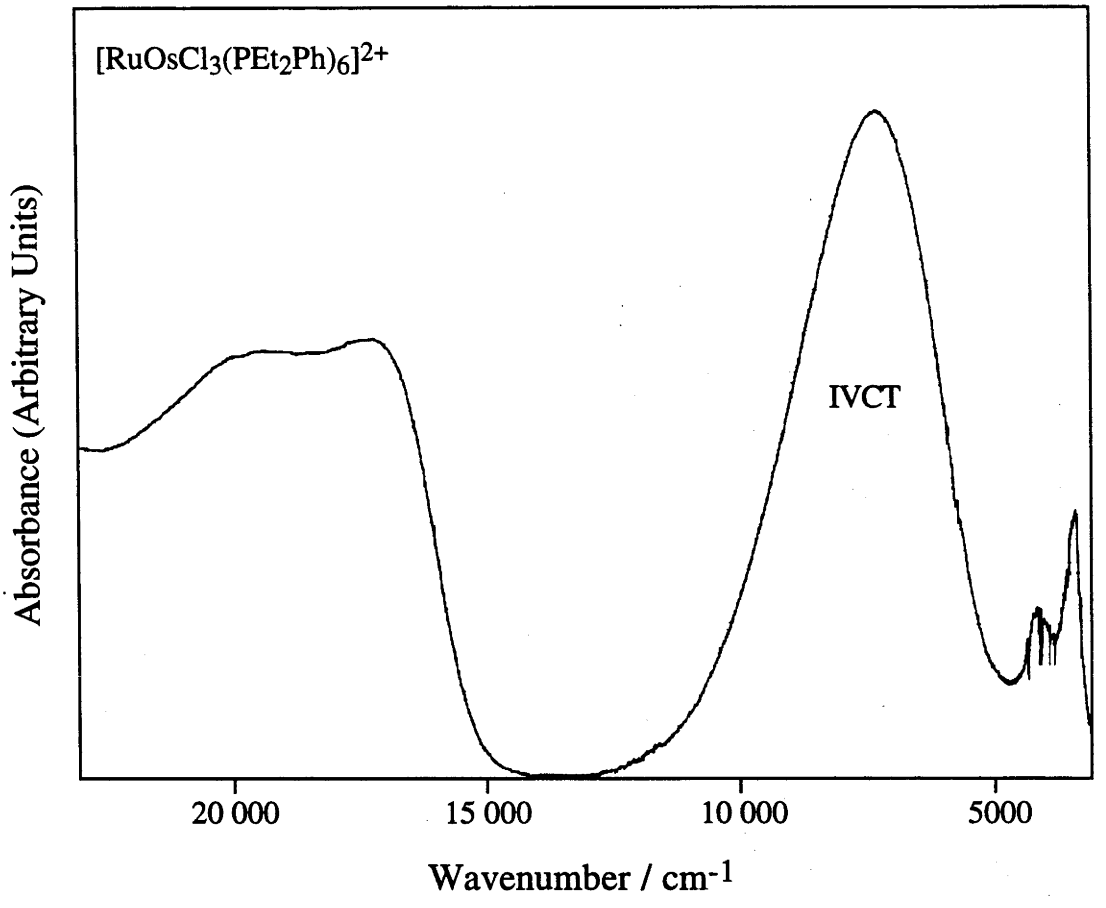

Figure 4.11 *Visible/near-IR spectrum of* $[(PEt_2Ph)_3Ru(\mu\text{-}Cl)_3Os(PEt_2Ph)_3]^{2+}$.

The broad band present in the near-IR spectra of the 11-e mixed ruthenium-osmium complexes can be assigned to a classical intervalence charge-transfer (IVCT) transition, of the type $Ru^{II}Os^{III} \rightarrow \{Ru^{III}Os^{II}\}^*$. These spectra are typical of weakly coupled class II systems, according to the Robin and Day classification scheme.[17] Hush's model for such systems relates the band position (ν_{max}) to the bandwidth at half intensity ($\Delta\nu_{1/2}$), where E_o is the energy difference between the initial ($[Ru^{II}Os^{III}]_o$) and final ($[Ru^{III}Os^{II}]_o$) states (Fig. 4.12):[18]

$$\Delta\nu_{1/2} = [16kT \ln 2(\nu_{max} - E_o)]^{1/2} \qquad (4.1)$$

In equation 4.1, the term 16kT ln 2 takes the values 2310 cm^{-1} at 300 K, and 1640 cm^{-1} at 213 K where the majority of the present spectra were determined. The bandwidth at half intensity ($\Delta\nu_{1/2}$) is usually greater than that predicted by equation 4.1.[18]

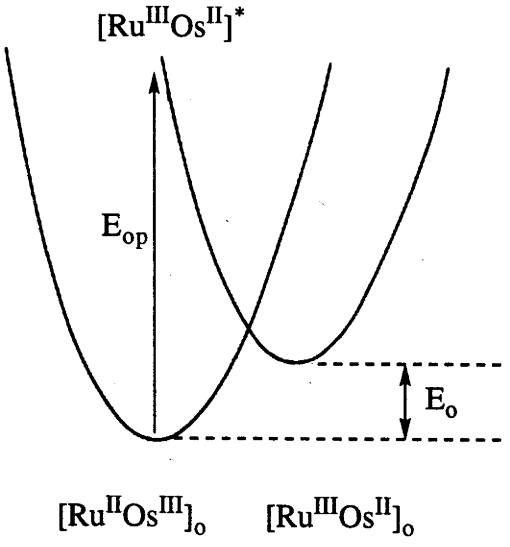

Figure 4.12 *Potential energy curve for the asymmetric $\{RuOs\}^{2+}$ systems, where E_{op} is the energy of the optical promotion (IVCT band) and E_o is the difference in energy between the $[Ru^{II}Os^{III}]_o$ and $[Ru^{III}Os^{II}]_o$ states. The horizontal axis represents the reaction coordinate connecting these states.*

It is apparent from the extraordinarily simple transferrable nature of corresponding electrode potentials in the diruthenium, diosmium and ruthenium-osmium systems that we can model the couples for the electrochemically inaccessible $\{Ru^{III}Os^{II}\}^{2+}$ complexes (Fig. 4.13).

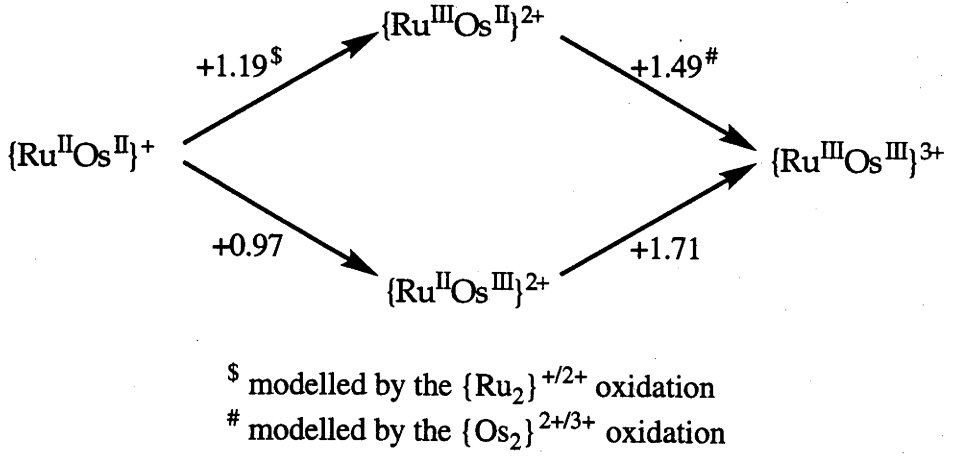

Figure 4.13 *Estimation of redox potentials for the electrochemically inaccessible and thermodynamically unstable $[Ru^{III}Os^{II}(\mu\text{-}Cl)_3(PEt_2Ph)_6]^{2+}$ complexes.*

In other words, oxidation potentials for the generation of $\{Ru^{II}Os^{III}\}^{2+}$ and $\{Ru^{III}Os^{II}\}^{2+}$ differ by ~0.22 V. This is a very reasonable estimate for E_o (~1800 cm^{-1}), the difference in equilibrium energy of the $[Ru^{II}Os^{III}]_o$ and $[Ru^{III}Os^{II}]_o$ states (Fig. 4.12).

As an example, the predicted bandwidth at half intensity ($\Delta\nu_{1/2}$) for the IVCT band in $[RuOsCl_3(PEt_3)_6]^{2+}$ (ν_{max} = 7800 cm^{-1}) is 3150 cm^{-1} at 213 K (Table 4.7). The observed value of the band width is ~4000 cm^{-1}, supporting the class II mixed-valence classification.

Table 4.7 *Energy of IVCT Band for $[RuOs(\mu\text{-}X)_3(PR_3)_6]^{2+}$ Complexes.*

Complex	ν_{IVCT} / cm^{-1} (ε / dm^3 mol^{-1} cm^{-1}) [a]	$\Delta\nu_{1/2}$ / cm^{-1} [b]	$\Delta E_{1/2}$ / V
$[RuOsCl_3(PEt_3)_6]^{2+}$	7800 (~450)	4000 (3150)	0.84
$[RuOsCl_3(PEt_2Ph)_6]^{2+}$	7300 (~1600)	3400 (3000)	0.74
$[RuOsCl_3(triphos)_2]^{2+}$ [c]	7200 (1870)	3900 (3550)	0.68
$[RuOsBr_3(triphos)_2]^{2+}$	7000 (~900)	3300 (2900)	0.65

[a] Recorded in $CH_2Cl_2/[Bu^n_4N][BF_4]$ (0.5 mol dm^{-3}) at 213 K (unless stated otherwise) in an OSTLE cell. [b] Width of the IVCT band at half of the full intensity. Approximate theoretical values, calculated from Eq. 4.1 and assuming an E_o of ~0.2 eV (~1600 cm^{-1}), are given in parentheses. [c] Recorded at room temperature (298 K).

4.4 EPR SPECTRA OF $\{Os_2\}^{2+}$ AND $\{RuOs\}^{2+}$ COMPLEXES

The EPR spectra of several mixed-valence diosmium and ruthenium-osmium complexes were recorded in frozen dichloromethane solutions (glasses) containing $[Bu^n_4N][BF_4]$ (0.5 mol dm^{-3}). The samples were generated electrochemically, due to the observation that the chemical oxidant ($NOPF_6$) led to contamination of these spectra. These spectra can be discussed in terms of the trigonal-field splitting model described in §3.4.

Consider first the EPR spectra of the localised $[L_3Ru^{II}(\mu\text{-}X)_3Os^{III}L_3]^{2+}$ complexes. Apparently only one resonance is observed, but it is likely that $g_{\|}$ cannot be seen beneath the intense $g_{\perp}$ resonance (Fig. 4.14). It is difficult to assign particular g-values given the current spectra, and it is even difficult to determine which resonance has the higher g value. What is clear, however, is that the trigonal splitting, Δ_t, in these complexes is small, and may even cross over from a positive value ($^2A_{1g}$ state lowest in energy) to negative (^2E_g lowest).

Given the presumed localised (Os^{III}) nature, the simplest comparison to be made for the $\{RuOs\}^{2+}$ complexes is with trigonally distorted *fac*-$[Os^{III}Cl_3(PR_3)_3]$ monomers. The EPR spectrum of *fac*-$[OsCl_3(PBu^n_2Ph)_3]$, recorded in an ether glass at 77 K, has been reported to have g values of $g_{\perp} = 1.83$ and $g_{\|} = 1.28$.[19,20] We have since recorded the EPR spectrum of *fac*-$[OsCl_3(PMe_2Ph)_3]$, which was prepared by the method of Levason *et al*,[21] using the same conditions as for the bimetallic complexes. Under these conditions a weak EPR signal is observed, with $g_{\perp} = 1.90$ and $g_{\|} = 1.43$. Fitting these g values to the equations 3.3 and 3.4 gives $K = 0.81$ and $\Delta_t/\lambda = 0.18$, where λ for Os^{III} is ~3000 cm^{-1}.

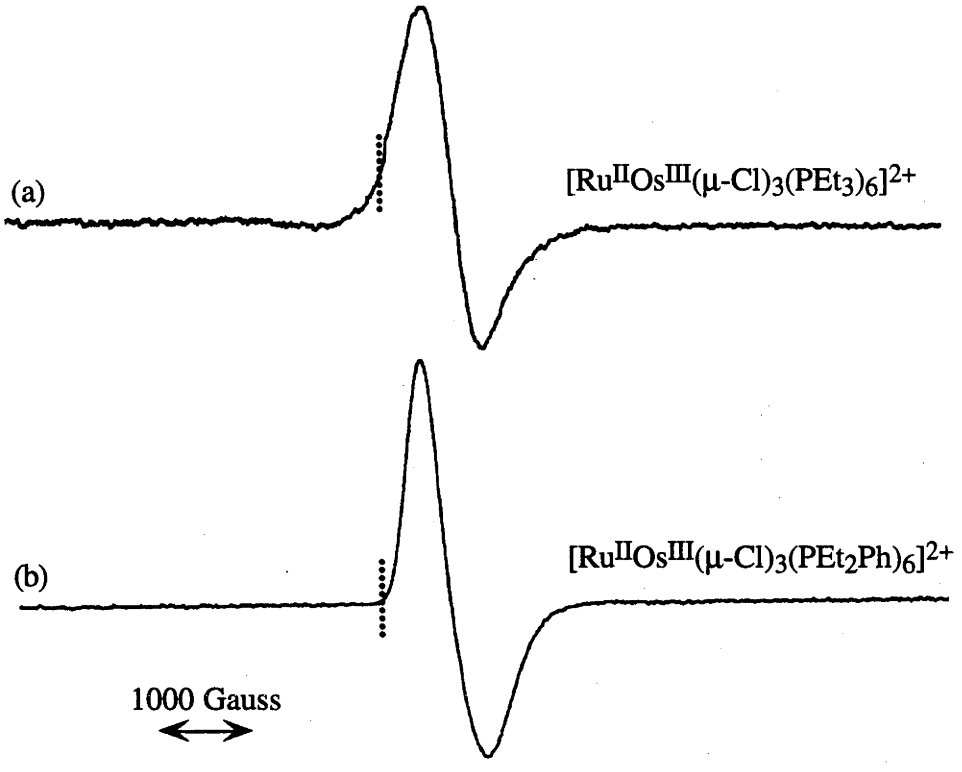

Figure 4.14 *EPR spectra of $[RuOs(\mu\text{-}Cl)_3(PR_3)_6]^{2+}$ complexes. (a) PR_3 = PEt_2Ph. (b) PR_3 = PEt_3. Possible positions for $g_{||}$ resonances are indicated by "$g_{||}$". The dotted lines represent g = 2.0.*

In these trigonally distorted mononuclear and binuclear Os^{III} centres, Δ_t is small in comparison to the binuclear ruthenium complexes discussed earlier, even considering the larger spin-orbit coupling constant associated with the osmium complexes ($\lambda_{Os} \sim 3\ \lambda_{Ru}$). In the two *mer*-$\{OsCl_3(PR_3)_3\}$ examples to hand, $\Delta_t < 0$, which is associated with a ^2E_g ($x_o^2x_\pm^3$), rather than a $^2A_{1g}$ ($x_\pm^4x_o^1$), ground state.

Table 4.8 *EPR Data for fac-$[OsCl_3(PR_3)_3]$, $[RuOs(\mu\text{-}Cl)_3(PR_3)_3]^{2+}$ and $[Os_2(\mu\text{-}Cl)_3(PR_3)_6]^{2+}$ Complexes.*[a]

Complex	$g_\perp$	$g_\parallel$
fac-$[OsCl_3(PBu^n{}_2Ph)_3]$ [b]	**1.83**	1.28
fac-$[OsCl_3(PMe_2Ph)_3]$	**1.90**	1.43
$[RuOs(\mu\text{-}Cl)_3(PEt_3)_6]^{2+}$	**~1.9** [c]	
$[RuOs(\mu\text{-}Cl)_3(PEt_2Ph)_6]^{2+}$	**~1.9** [c]	
$[Os_2(\mu\text{-}Cl)_3(PEt_3)_6]^{2+}$	1.59	**1.98**
$[Os_2(\mu\text{-}Cl)_3(PEt_2Ph)_6]^{2+}$	1.48	**1.99**
$Os_2(\mu\text{-}Br)_3(PMe_2Ph)_6]^{2+}$	1.36	**~1.8**

[a] *Recorded in frozen $CH_2Cl_2/[Bu^n{}_4N][BF_4]$ (0.5 mol dm^{-3}) solutions at 20 K unless stated otherwise. The larger g value is in bold.* [b] *Recorded in an ether glass at 77 K (Ref. 19).* [c] *These values are estimates only, as the two resonances are too close to each other to assign.*

Turning now to the EPR spectra of diosmium complexes it can be seen that these spectra (Fig. 4.15) clearly do not resemble those of the corresponding diruthenium complexes described in §3.4. If we were to assume that, like the diruthenium complexes, the diosmium systems are delocalised, the MO scheme used to describe the properties of diruthenium complexes would equally apply to the diosmium complexes. Based on the position of the mixed-valence near-IR bands, however, orbital splitting would be smaller than in the corresponding $\{Ru_2\}^{2+}$ complexes, though still of the same sign.¶ Instead, we find for the diosmium complexes that the $g_\parallel$ resonance is consistently at higher energy than $g_\perp$, *i.e.* $\Delta_t < 0$. If we held to a delocalised model this would put $\delta_\pi{}^*(x_\pm)$ above $\sigma^*(x_o)$, which is self-contradictory. The EPR of the two $\{RuOs\}^{2+}$ systems are perfectly consistent with this view of the $\{Os_2\}^{2+}$ complexes, *i.e.* both localised, with Δ_t near zero and permitted to be negative or positive.

¶ That is, the hypothetically delocalised $\{Os_2\}^{2+}$ complexes are required to have reduced Δ_t and greater λ than their $\{Ru_2\}^{2+}$ analogues. This would lead to a smaller ratio of Δ_t/λ (decreased to about 1/3 to 1/4 of the value for analogous $\{Ru_2\}^{2+}$ systems).

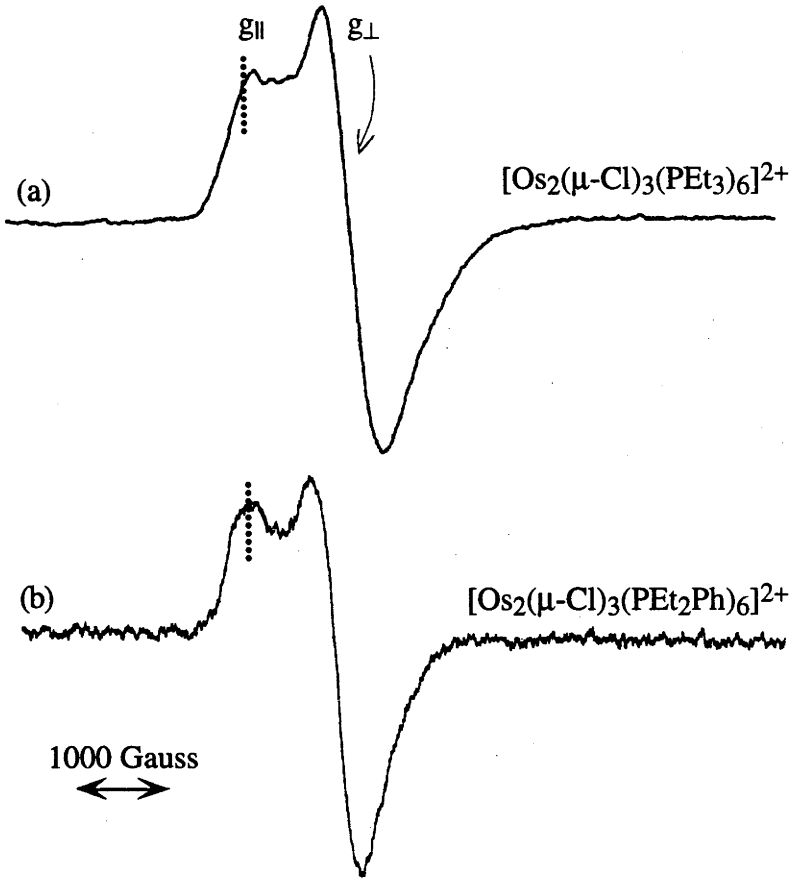

Figure 4.15 *EPR spectra of* $[Os_2(\mu\text{-}Cl)_3(PR_3)_6]^{2+}$ *complexes. (a)* $PR_3 = PEt_3$. *(b)* $PR_3 = PEt_2Ph$. *The dotted lines represent* $g = 2.0$.

In summary, the EPR spectra of the diosmium complexes, with $\Delta_t < 0$, are more similar to the localised $\{RuOs\}^{2+}$ spectra than they are to the delocalised $\{Ru_2\}^{2+}$ systems. A more detailed analysis of these results is in progress.[22] These results led us to entertain the possibility that the mixed-valence diosmium complexes are essentially localised $\{Os^{II}Os^{III}\}^{2+}$ complexes, in contrast to their delocalised $\{Ru_2\}^{2+}$ analogues.

4.5 SOLVENT DEPENDENCY OF MIXED-VALENCE SPECTRA

According to the theory developed by Hush and others for class II mixed-valence binuclear complexes,[18, 23-25] the position of the intervalence charge-transfer (IVCT)

absorption band (E_{op}) should be dependent upon solvent properties. For a weakly coupled (class II) system:

$$E_{op} = \chi_{inner} + \chi_{outer} \qquad (4.2)$$

where χ_{inner} and χ_{outer} are the inner-sphere and outer-sphere reorganisation energies respectively. The outer-sphere parameter, χ_{outer}, is related to solvent properties:

$$\chi_{outer} = (\Delta e)^2\left(\frac{1}{2r_1} + \frac{1}{2r_2} - \frac{1}{d}\right)\left(\frac{1}{n^2} - \frac{1}{D_S}\right) \qquad (4.3)$$

where Δe = the electronic charge transferred, r_1 and r_2 are the metal-ligand bond lengths for the two metal sites, d is the separation between metal centres, n^2 is the optical dielectric constant (n being the solvent refractive index) and D_S = the static dielectric constant of the solvent. For a weakly interacting mixed-valence system examined in a series of solvents, E_{op} is sensitive to solvent polarity and predicted to show a linear variation with $(1/n^2 - 1/D_S)$. Qualitatively speaking, the unfavourable outer-sphere interactions between the solvent cage and the charge-localised excited state (relative to the ground state) should lead to a blue-shift in the IVCT band as the solvent polarity increases.

There are numerous examples in the literature of class II complexes which show a rational dependence of the energy of the IVCT band with solvent.[26] On the other hand, Yellowlees *et al* have examined the near-IR band of $[Os_2(\mu\text{-}Cl)_3(PMe_2Ph)_6]^{2+}$ at ~4500 cm^{-1}, and found its position to be invariant over a range of solvents, a property usually attributable to a delocalised (class III) system.

We have repeated these experiments, examining the position of all of the near-IR bands in $[Os_2(\mu\text{-}Cl)_3(PEt_2Ph)_6]^{2+}$, in $CHCl_3$, CH_2Cl_2, $(CH_3)_2CO$ and CH_3CN, at different temperatures, with and without electrolyte present. We concur that the 4500 cm^{-1} band does not shift with differing solvents, and in fact none of the near-IR bands shifted in this range of solvents. However, we have also measured the position of the clear-cut IVCT band exhibited by the mixed-metal complex

$[RuOs(\mu\text{-}Cl)_3(PEt_2Ph)_6]^{2+}$, and have found no trend in the position of this band over the range of solvents employed. Shifts of less than 50 cm^{-1} were observed for the IVCT band of $[RuOs(\mu\text{-}Cl)_3(PEt_2Ph)_6]^{2+}$, and a mean shift of zero, in cases where variations of hundreds of wavenumbers might have been expected.

There are already examples in the literature in which the position of the IVCT band in class II complexes does not exhibit a significant dependence on $(1/n^2 - 1/D_s)$, including $[(bpy)_2(py)Ru(4,4'\text{-}bpy)Ru(py)(bpy)_2]^{5+}$ [27] and biferrocinium complexes.[28-30] Equation 4.3 assumes that the solvent cage surrounding the molecules undergoing intramolecular electron transfer has the same properties as the bulk solution, and it has been suggested that this assumption is not appropriate for the examples listed above.[30]

The IVCT band of the ruthenium-osmium complex, which we expect to be strongly valence trapped, does not exhibit solvent dependency, although we do not know the reason for this. Moreover, it is difficult to think of a more faithful test, given that the ruthenium-osmium complexes are isostructural with the diosmium systems, and have the same overall charge. This indicates that, while such experiments have commonly been utilised to determine whether a particular mixed-valence complex is trapped or delocalised, these measurements are unable to give a reliable indication of the degree of delocalisation or the nature of mixed-valence state of the confacial diosmium complexes.

4.6 INTERPRETATION OF MIXED-VALENCE SPECTRA

We have seen that close examination of the near-infrared spectra of $\{Os_2\}^{2+}$ complexes reveals an interesting series of bands which have a different appearance from their $\{Ru_2\}^{2+}$ analogues and cannot readily be explained in terms of a delocalised mixed-valence system. These observations, coupled with EPR spectroscopy, have led us to conclude that the diosmium complexes are trapped, rather than delocalised, in the 11-e state.

We expect that the near-IR spectrum of a localised $\{Os^{II}Os^{III}\}^{2+}$ complex should include an ($\{Os^{II}Os^{III}\} \rightarrow \{Os^{III}Os^{II}\}^*$) intervalence band, as well as typical single-ion (Os^{III}) absorptions. The latter transitions are intraconfigurational d-d bands, due to transitions within the t_{2g}-derived orbital set. These bands occur at low energy and are usually of low intensity, and have been observed for tetragonal and trigonal Os^{III} complexes.[21,31,32] The triplet ($^2T_2$) ground state arising in O_h geometry is split into a doublet (^2E) and singlet state ($^2A_1$) in a trigonal field, as discussed in §3.4, and further mixing occurs due to the large spin-orbit coupling constant associated with Os^{III}, giving rise to three Kramer's doublets. The two low-energy intraconfigurational transitions observed in monomeric osmium complexes are promotions from the ground state doublet to the higher energy Kramer's doublets.

To model the single-ion site of a $[Os_2(\mu\text{-}X)_3(PR_3)_6]^{2+}$ complex, the near-IR spectrum of the sparingly soluble *fac*-$[Os^{III}Cl_3(PMe_2Ph)_3]$ was recorded in dichloromethane, revealing two weak, sharp bands near 4000 cm^{-1}. The features might correspond to either the 3500 cm^{-1} or 4500 cm^{-1} band in the $\{Os_2\}^{2+}$ complex.

The other expected transition is an intervalence charge-transfer (IVCT) absorption. This involves the transfer of an electron from the Os^{II} site of the binuclear complex to an excited vibronic state of the Os^{III} centre, *i.e.* $[Os^{II}Os^{III}]_o \rightarrow [Os^{III}Os^{II}]^*$,

where the new Os^{II} site has Os^{III} geometry and the new Os^{III} centre has the geometry of the pre-existing Os^{II} site. The $[Os^{III}Os^{II}]^*$ state, like a single-ion Os^{III} centre, will be split into its own family of three Kramer's doublets, so that instead of a single IVCT band, *three* IVCT transitions can arise. We therefore expect up to five overlapping transitions in all, two from the intraconfigurational bands associated with the single Os^{III} centre, and three from intervalence transitions.

Our assignment of the bands in the trapped diosmium scenario is displayed in Fig. 4.16, showing the intraconfigurational band at 3500 cm^{-1}, the first fundamental mixed-valence band at 4500 cm^{-1} and the second and third mixed-valence bands contained within the asymmetric band at 7500 cm^{-1}. These assignments seem reasonable, as the difference in energy between the mixed-valence bands (7500 - 4500 = 3000 cm^{-1}) should be comparable to the energy of the intraconfigurational band(s), (~3500 cm^{-1}). These assignments are naturally provisional and the relative intensities of the bands are presently under theoretical investigation.[22]

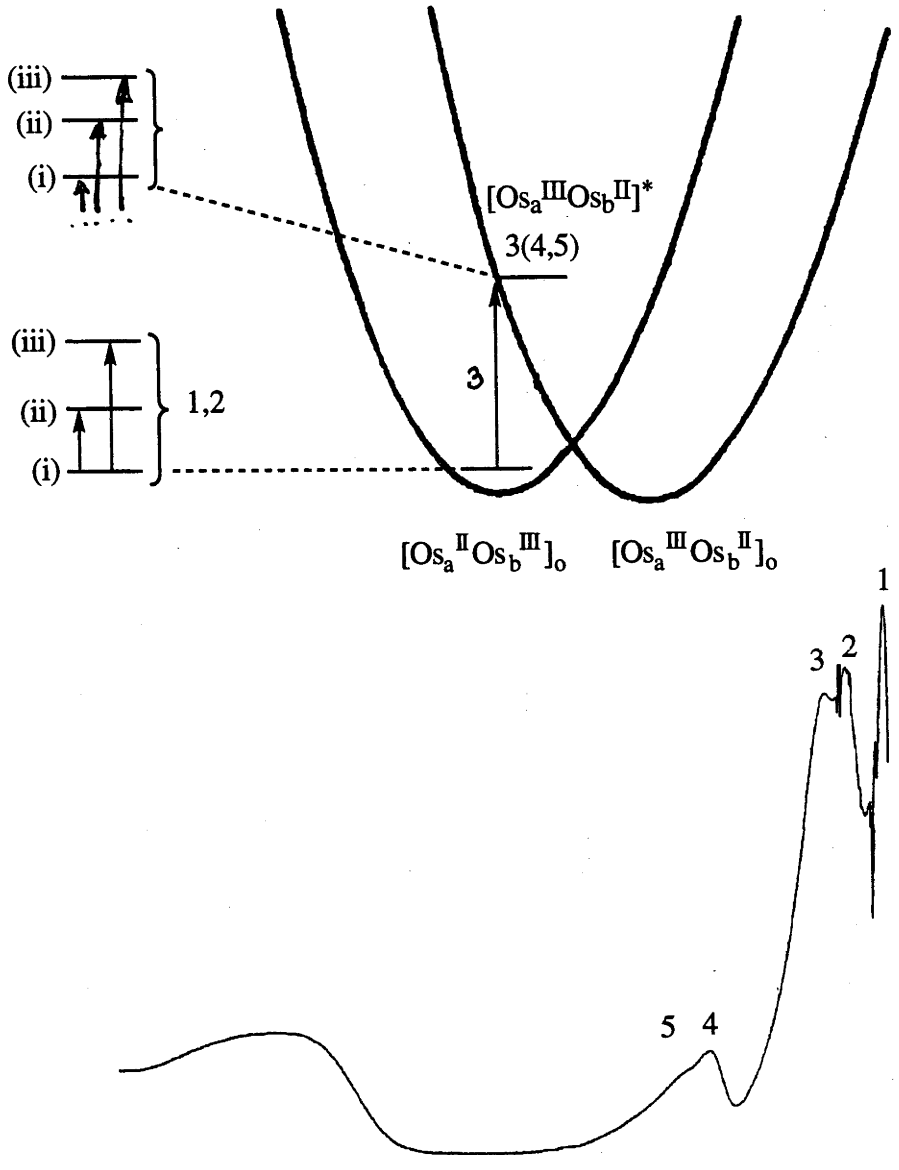

Figure 4.16 *Potential energy curves for a symmetric class-II mixed-valence system (cf p. 125). The potential energy curves of intra-configurational states are omitted for clarity. The intra-configurational states are denoted by (i), (ii) and (iii) for both* $[Os_a^{II}Os_b^{III}]_o$ *and* $[Os_a^{III}Os_b^{II}]^*$ *systems. Transitions 1 and 2 are related to single-ion intraconfigurational promotions, and 3, 4 and 5 are intervalence processes. The relationship of these bands to the spectrum of* $[Os_2(\mu\text{-}Cl)_3(PEt_2Ph)_6]^{2+}$ *is shown.*

Turning now to the spectra of the ruthenium-osmium complexes, we still expect to observe single-ion Os^{III} bands near 4000 cm^{-1}, but the mixed-valence transitions are all contained within the 7500 cm^{-1} absorption band. The spin-orbit coupling constant is

substantially less for ruthenium than osmium, so we anticipate that the mixed-valence bands will be closer in energy in the $[Ru^{III}Os^{II}]^*$ state, and not resolved.

4.7 MISSING $[Os_2(\mu\text{-}X)_3L_6]^+$ (L = PMe_3, AsR_3) COMPLEXES

The spectra of the $[Os_2(\mu\text{-}X)_3(PR_3)_6]^{2+}$ complexes are clearly more complicated than those of their diruthenium analogues discussed in §3.3. On the basis of the near-IR spectra and EPR studies, we believe that a localised $\{Os^{II}Os^{III}\}^{2+}$ structure prevails. This assignment is still far from conclusive, and to help understand the nature of the diosmium complexes, it is important to prepare an unambiguously delocalised $[Os_2(\mu\text{-}X)_3L_6]^{2+}$ system, such as an osmium equivalent of the ruthenium "blues".

Our belief is that the stabilisation of the single-ion osmium centres through greater spin-orbit coupling overcomes the σ/σ^* bonding energy. With this in mind, we chose capping ligands (L) which gave higher energy $\sigma\rightarrow\sigma^*$ bands for the corresponding $[Ru_2(\mu\text{-}X)_3L_6]^{2+}$ complexes, namely L = PMe_3, AsR_3 or NR_3. The only known complexes of this type are $[Os_2(\mu\text{-}X)_3(AsMe_2Ph)_6]H_2PO_2$,[32] prepared from $Na_2[OsX_6]$ and $AsMe_2Ph$ in EtOH, with hypophosphorous acid. Prior to this, *trans*-$[OsX_2(AsMe_2Ph)_4]$ was reported as the product from the same long-standing reaction.[33] Despite numerous attempts and variations of the conditions, we were only able to prepare monomeric complexes by this method.

Other attempts were made to prepare $[Os_2(\mu\text{-}X)_3L_6]^+$ (L = AsR_3, PMe_3) complexes, from starting materials such as $[OsX_6]^{2-}$, $[Os_2X_8]^{2-}$,[10] $[Os_2(\mu\text{-}X)_3X_6]^{3-}$,[2,34] $[Os_2(\mu\text{-}Cl)_3(\eta^6\text{-}C_6H_6)_2]^+$ and $[OsCl_2(\eta^6\text{-}C_6H_6)]_2$,[15] using a variety of reaction conditions. In these reactions, monomeric $[OsX_2L_4]$ or $[OsX_2L_4]^+$ complexes were produced, or a multitude of products resulted which were unable to be separated. Another approach would be to drive recently discovered $[Os_2(\mu\text{-}X)_3X_6]^{3-}$ (X = Cl,

Br)[2,34] to their 11-e ($[Os_2X_9]^{4-}$) states, which should be delocalised, but voltammetry shows the 10-e/11-e reduction to be irreversible under current conditions. Attempts to prepare such a diosmium complex are continuing. We predict that the long-sought $[Os_2(\mu\text{-}X)_3(NR_3)_6]^{2+}$ complexes will have a classical "blue" nature, when discovered.

Noted added when placing this Thesis in the ANU Library, October, 1996

(See reference 35)

Happily, in April, 1996, some six months after submission of the present thesis, Ware and Taube, and their colleagues announced the discovery of $[Os_2(\mu\text{-}Cl)_3(tacn)_2](PF_6)_3$ and $[Os_2(\mu\text{-}Cl)_3(Metacn)_2](PF_6)_3$.[35] These 10-e $Os_2^{III,III}$ systems show two successive reductions separated by about 1.0 V, and the mixed-valence binuclear state is described as deep red or purple in solution though visible/near-infrared spectra are yet to be reported. These physical properties are fully consistent with the prediction above, and offer excellent opportunities for detailed comparison with the contrasting $Os_2^{III,II}$ PR_3-based systems.

4.8 EXPERIMENTAL

Starting materials and general experimental procedures were as described in §2.2. All reactions were carried out under an atmosphere of N_2 and the products were handled in air. Solutions of mixed-valence complexes for EPR studies were generated by bulk electrolysis of solutions of *ca.* 10^{-2} mol dm^{-3} $[M_2(\mu\text{-}X)_3(PR_3)_6]^+$ in CH_2Cl_2 containing 0.5 mol dm^{-3} $[NBu^n_4][BF_4]$. EPR spectra of the glassy frozen electrolyte solutions at 20 K were recorded using a Varian X-band spectrometer fitted with an Oxford Instruments helium flow cryostat.

4.8.1 Diosmium Complexes, $[Os_2(\mu\text{-}X)_3(PR_3)_6]CF_3SO_3$

$[Os_2(\mu\text{-}Br)_3(PEt_2Ph)_6]CF_3SO_3$

To a suspension of $[OsBr_2(PPh_3)_3]$ (0.31 g, 0.27 mmol) in ethanol (30 cm^3) was added PEt_2Ph (0.19 g, 1.16 mmol). The mixture was heated at reflux for 44 h. The solvent was removed *in vacuo* to give a yellow residue, which was dissolved in dichloromethane (5 cm^3) and CF_3SO_3H (0.1 mol dm^{-3}) in methanol (2 cm^3, 0.2 mmol) added, and heated to reflux for 16 h. The solvent was evaporated *in vacuo* and the residue recrystallised from dichloromethane/diethyl ether. Yield of $[Os_2(\mu\text{-}Br)_3(PEt_2Ph)_6]CF_3SO_3$: 0.20 g (80%) (Found: C 43.3; H 5.5. Calculated for $C_{61}H_{90}Br_3F_3O_3Os_2P_6S$: C 41.5; H 5.1%). FAB MS(+ve ion): Found: 1619.0. Calculated for $[Os_2(\mu\text{-}Br)_3(PEt_2Ph)_6]^+$: 1617.3. $^{31}P\text{-}\{^1H\}$ NMR (CD_2Cl_2): δ -23.6 ppm.

$[Os_2(\mu\text{-}Br)_3(triphos)_2]CF_3SO_3$

To a suspension of $[OsBr_2(PPh_3)_3]$ (0.25 g, 0.22 mmol) in ethanol (30 cm^3) was added triphos (0.20 g, 0.32 mmol). The mixture was heated at reflux for 119 h. The solvent was removed *in vacuo* to give a yellow residue, which was dissolved in dichloromethane (3 cm^3) and CF_3SO_3H (0.1 mol dm^{-3}) in methanol (2 cm^3, 0.2 mmol) added, and heated to reflux for 16 h. The solvent was evaporated *in vacuo* and the

residue recrystallised from dichloromethane/diethyl ether. Yield of $[Os_2(\mu\text{-}Br)_3(triphos)_2]CF_3SO_3$: 0.20 g (91%) (Found: C 48.1; H 3.8; P 9.1. Calculated for $C_{83}H_{78}Br_3F_3O_3Os_2P_6S$: C 49.4; H 3.9; P 9.2%). FAB MS(+ve ion): Found: 1870.2. Calculated for $[Os_2(\mu\text{-}Br)_3(triphos)_2]^+$: 1869.5. $^{31}P\text{-}\{^1H\}$ NMR (CD_2Cl_2): δ -21.6 ppm.

4.8.2 Mixed-Metal Complexes, $[(PR_3)_3Ru(\mu\text{-}X)_3Os(PR_3)_3]CF_3SO_3$

For example, $[RuCl_2(PPh_3)_3]$ (0.73 g, 0.76 mmol) and $[OsCl_2(PPh_3)_3]$ (0.16 g, 0.15 mmol) were weighed into a side-arm round bottomed flask. Triphos (0.63 g, 1.01 mmol) and 2-methoxyethanol (50 cm^3) were added, and the mixture heated at reflux for 13 h. The solvent was removed *in vacuo*, to give a yellow residue. The residue was dissolved in dichloromethane (10cm^3), and heated at reflux for 16 h with a 0.1 mol dm^{-3} CF_3SO_3H in methanol solution. The solvent was removed *in vacuo* and the residue recrystallised from dichloromethane/diethyl ether to yield a yellow crystalline precipitate. $^{31}P\text{-}\{^1H\}$ NMR revealed the yellow product was a mixture of $[Ru_2(\mu\text{-}Cl)_3(triphos)_2]CF_3SO_3$ (71%), $[RuOs(\mu\text{-}Cl)_3(triphos)_2]CF_3SO_3$ (28%) and $[Os_2(\mu\text{-}Cl)_3(triphos)_2]CF_3SO_3$ (1%).

Other mixtures were similarly prepared, using the appropriate ratios of starting materials and the phosphine of choice. The ratio of products obtained, $^{31}P\text{-}\{^1H\}$ NMR and mass spectral data are listed in Table 4.9.

Table 4.9 *NMR and Mass Spectral Data for $[RuOs(\mu\text{-}X)_3(PR_3)_6]^+$ Complexes.*

Product Mixture	% complex in mixture [a]	$^{31}P\text{-}\{^1H\}$ NMR [b] Ru	Os	Mass Spectra (m/z)[c]
$[RuOsCl_3(triphos)_2]^+$	71	+38.7	-19.0	1647 (1647)
$[Ru_2Cl_3(triphos)_2]^+$	28	+36.5	-	1559 (1558)
$[Os_2Cl_3(triphos)_2]^+$	1	-	-17.4	1735 (1736)
$[RuOsBr_3(triphos)_2]^+$	56	+34.8	-23.1	1781 (1780)
$[Ru_2Br_3(triphos)_2]^+$	39	+32.9	-	1691 (1691)
$[Os_2Br_3(triphos)_2]^+$	5	-	-21.2	1869 (1870)
$[RuOsCl_3(PEt_3)_6]^+$	63	+35.9	-27.3	1107 (1107)
$[Ru_2Cl_3(PEt_3)_6]^+$	36	+33.7	-	1017 (1018)
$[Os_2Cl_3(PEt_3)_6]^+$	1	-	-25.8	1195 (1196)
$[RuOsCl_3(PEt_2Ph)_6]^+$	63	+38.1	-22.9	1395 (1395)
$[Ru_2Cl_3(PEt_2Ph)_6]^+$	36	+36.0	-	1307 (1306)
$[Os_2Cl_3(PEt_2Ph)_6]^+$	1	-	-21.3	1488 (1484)

[a] As determined by $^{31}P\text{-}\{^1H\}$ NMR [b] Chemical Shifts in ppm, referred to external 85% H_3PO_4. Recorded in CD_2Cl_2. [c] Positive-ion, as determined from mass spectral data. Mass spectra were recorded using electrospray or fast atom bombardment ionization. The former were recorded in water/methanol/acetic acid mixture (50/50/1, v/v), the latter in a 3-nitrobenzyl alcohol liquid matrix. Calculated value of positive-ion in parentheses.

4.9 REFERENCES

1. J. Chatt and R.G. Hayter, *J. Chem. Soc. (A)*, 1961, 896.
2. D.G. Humphrey, Ph.D. Thesis, Australian National University, 1992.
3. S.A. Macgregor, E. McInnes, R.J. Sorbie and L.J. Yellowlees, in *Molecular Electrochemistry of Inorganic, Bioinorganic and Organometallic Compounds*, eds. A.J.L. Pombeiro and J.A. McCleverty, Kluwer Academic Publishers, Dordrecht, 1993, pp. 503-507.
4. J. Chatt, D.P. Melville and R.L. Richards, *J. Chem. Soc. (A)*, 1971, 1169.
5. P.E. Fanwick, I.F. Fraser, S.M. Tetrick and R.A. Walton, *Inorg. Chem.*, 1987, **26**, 3786.
6. V.T. Coombe, G.A. Heath, T.A. Stephenson, J.D. Whitelock and L.J. Yellowlees, *J. Chem. Soc., Dalton Trans.*, 1985, 947.
7. P.R. Hoffman and K.G. Caulton, *J. Am. Chem. Soc.*, 1975, **97**, 4221.
8. G.V. Goeden and B.L. Haymore, *Inorg. Chim. Acta*, 1983, **71**, 239.
9. A.R. Chakravarty, F.A. Cotton and D.A. Tocher, *Acta Crystallogr., Sect. C*, 1985, **41**, 698.
10. P.E. Fanwick, S.M. Tetrick and R.A. Walton, *Inorg. Chem.*, 1986, **25**, 4546.
11. T. Behling, G. Wilkinson, T.A. Stephenson, D.A. Tocher and M.D. Walkinshaw, *J. Chem. Soc., Dalton Trans.*, 1983, 2109.
12. B.J. Kennedy and G.A. Heath, unpublished work.
13. B.J. Kennedy, G.A. Heath and T.J. Khoo, *Inorg. Chim. Acta*, 1991, **190**, 265.
14. T. Arthur, Ph.D. Thesis, University of Edinburgh, 1980.
15. T. Arthur and T.A. Stephenson, *J. Organomet. Chem.*, 1981, **208**, 369.
16. R.O. Gould, T.A. Stephenson and D.A. Tocher, *J. Organomet. Chem.*, 1984, **263**, 375.
17. M.D. Robin and P. Day, *Adv. Inorg. Chem. Radiochem.*, 1967, **10**, 247.
18. N.S. Hush, *Prog. Inorg. Chem.*, 1967, **8**, 391.
19. J. Chatt, G.J. Leigh and D.M.P. Mingos, *J. Chem. Soc. (A)*, 1969, 1674.

20. A. Hudson and M.J. Kennedy, *J. Chem. Soc. (A)*, 1969, 1116.

21. R.A. Cipriano, W. Levason, R.A.S. Mould, D. Pletcher and M. Webster, *J. Chem. Soc., Dalton Trans.*, 1990, 2609.

22. L. Dubicki, unpublished work.

23. N.S. Hush, *Electrochim. Acta*, 1968, **13**, 1005.

24. S.B. Piepho, E.R. Krausz and P.N. Schatz, *J. Am. Chem. Soc.*, 1978, **100**, 2996.

25. K.Y. Wong and P.N. Schatz, *Prog. Inorg. Chem.*, 1978, **28**, 369.

26. R.J. Crutchley, *Adv. Inorg. Chem.*, 1994, **41**, 273.

27. M.J. Powers and T.J. Meyer, *Inorg. Chem.*, 1978, **17**, 1785.

28. W.S. Hammack, H.G. Drickamer, M.D. Lowery and D.N. Hendrickson, *Chem. Phys. Lett.*, 1986, **132**, 231.

29. M.D. Lowery, W.S. Hammack, H.G. Drickamer and D.N. Hendrickson, *J. Am. Chem. Soc.*, 1987, **109**, 8019.

30. W.S. Hammack, H.G. Drickamer, M.D. Lowery and D.N. Hendrickson, *Inorg. Chem.*, 1988, **27**, 1307.

31. R.A. Cipriano, W. Levason, R.A.S. Mould, D. Pletcher and M. Webster, *J. Chem. Soc., Dalton Trans.*, 1990, 339.

32. N.R. Champness, W. Levason, R.A.S. Mould, D. Pletcher and M. Webster, *J. Chem. Soc., Dalton Trans.*, 1991, 2777.

33. F.P. Dwyer, R.S. Nyholm and B.T. Tyson, *J. Proc. R. Soc. N.S.W.*, 1947, **81**, 272.

34. G.A. Heath and D.G. Humphrey, *J. Chem. Soc., Chem. Commun.*, 1990, 672.

******

Added when placing this Thesis in the ANU Library , October, 1996 :

(see page 137)

35. D.C. Ware, M.M. Olmstead, R. Wang and H. Taube, *Inorg. Chem.*, 1996, **35**, 2576

CHAPTER FIVE

Monomeric $[MX_nL_{6-n}]^z$ Complexes (M = Ru, Os; X = Cl, Br; L = PR_3, AsR_3): Synthesis, Electrochemistry and Spectro-electrochemistry

---

5.1 INTRODUCTION

During our investigation of triply-halide bridged diruthenium and diosmium complexes, it was essential to examine related monomeric complexes, both to be able to identify them in product mixtures and to understand their properties. In the preparation of binuclear complexes, many $[MX_2L_4]$ complexes were isolated from reaction mixtures, and it was important to be able to recognise these. It was also important to have a general feel for the electronic properties (optical and redox behaviour) of relevant halide/arsine and halide/phosphine monomers as a background for assessing the behaviour of M^{II} and M^{III} centres in the binuclear complexes. The most obvious comparisons might involve *fac*-$[M^{II}X_3L_3]^-$ and *fac*-$[M^{III}X_3L_3]$ systems, together with *cis*-$[M^{II}X_2L_4]$ and *cis*-$[M^{III}X_2L_4]^+$ complexes. The construction of satisfactory models for individual metal centres in confacial bioctahedral complexes turns out to be quite challenging as explained later in the Chapter.

The monomeric complexes are also of considerable appeal in their own right, since collectively they form a series ranging stepwise in stoichiometry from MX_4L_2 to MXL_5. Such a series is important in terms of the principle of ligand-additivity, which assumes that the effects of individual ligands upon the electronic properties are additive. One example of this is the linear relationship observed for E° ($M^{IV/III}$ and $M^{III/II}$) *vs* n for

the exhaustive halide/nitrile series, $[RuCl_{6-n}(PhCN)_n]^{(n-3)}$, recently developed in this laboratory.[1] In this case, the linear dependence of E° ($M^{IV/III}$ and $M^{III/II}$) was accompanied by orderly progressions in the X to M^{III} and M^{II} to L(PhCN) charge-transfer optical spectra. It will be seen below that the extension to halide/arsine and halide phosphine series is non-trivial. It has also been shown that shifts in electrode potentials for a given substitutional series are not always linear,[2] and one of the aims of this work was to examine the electrochemistry of series of $[MX_{6-n}L_n]$ complexes, where M = Ru and Os and L = PR_3 or AsR_3, in order to further test the limits of current ligand-additivity models.[3,4]

In addition to electrochemical properties, we have examined the charge-transfer spectra of the halide/arsine and halide/phosphine monomers. It turns out that the most instructive complexes to investigate are the M^{III} *trans*-$[MX_4L_2]^-$ and *trans*-$[MX_2L_4]^+$ systems which, because of their low-spin d_π^5 configuration, have LMCT spectra of maximum simplicity, and where, because of their physical structure and tetragonal (D_{4h}) symmetry, the observed bands can largely be attributed to separate halide-to-metal and arsine/phosphine-to-metal charge-transfer.

5.2 SYNTHESIS AND CHARACTERISATION

5.2.1 General

In the sections that follow (dealing in turn with MX_4L_2, MX_3L_3, MX_2L_4 and MXL_5 systems) we first summarise the historical position before outlining the measures we have found most effective for the preparation of these complexes.

5.2.2 $[MX_4L_2]$ and $[MX_4L_2]^-$ Complexes

The synthesis of several *trans*-$[RuX_4L_2]^-$ complexes (X = Cl, L = $AsPh_3$, PPh_3, PMe_2Ph, PEt_3; X = Br, L = $AsPh_3$, PEt_3) has been described by Stephenson.[5,6] The

PPh_3 and $AsPh_3$ complexes were prepared by treating $[RuX_3L_2(MeOH)]$ with $[AsPh_4]Cl$ or $[PPh_4]Br$ and HX in acetone. The remainder of the complexes listed above were prepared by ligand exchange, achieved by stirring the tetra-halo PPh_3 (or $AsPh_3$) derivative with PR_3 at room temperature for several days. These complexes were formulated as *trans* isomers on the basis of EPR[7] and far-IR evidence.[8] More recently, additional AsR_3 complexes (X = Cl, Br, L = $AsMe_3$, $AsMe_2Ph$) have also been prepared by this method in our laboratory.[9] In coordinating solvents such as acetonitrile these ruthenium complexes are prone to loss of halide, but can be stabilised in the presence of excess halide at low temperatures (Fig. 5.1).

$$[RuX_4L_2]^- + S \underset{+X^-}{\overset{+S}{\rightleftharpoons}} [RuX_3L_2S] + X^-$$

Figure 5.1 *Solvolysis of trans-$[RuX_4L_2]^-$ complexes in solvents S = CH_3NO_2, CH_3CN.*

In the present work, the *trans*-$[RuX_4L_2]^-$ complexes were prepared by the method of Stephenson,[6] stirring *trans*-$[RuX_4(EPh_3)_2]^-$ (E = P or As) with neat ligand L for several days.

A number of preparations have been reported for the corresponding tetra-halo osmium complexes, with the compounds being isolated in both Os^{III} and Os^{IV} states. A wide variety of phosphine and arsine complexes have been prepared by reaction of the appropriate ligand with OsO_4 in ethanol/HX solution, which gives $[Os^{III}X_4L_2]^-$.[10-12] Other *trans*-$[OsX_4L_2]$ complexes have been prepared by oxidation of *mer*-$[OsX_3L_3]$ by X_2.[10,13] The anionic Os^{III} complexes have been prepared cleavage of $[Os_2X_8]^{2-}$ with a range of phosphine ligands in ethanol,[14,15] by reduction of the neutral Os^{IV} complexes by ascorbic acid[12] or $NaBH_4$,[13] and have also been reported from reaction of $[OsX_4N]^-$ (X = Cl, Br) with PEt_2Ph.[16] The *trans* configuration of the Os^{IV} complexes was determined from their far-IR spectra[8] and has since been confirmed by crystallographic

studies on *trans*-$[OsCl_4(PMe_2Ph)_4]$ [17] and *trans*-$[OsBr_4(AsPh_3)_2]$.[18] In addition, the structure of the Os^{III} complex, *trans*-$[OsCl_4(PEt_2Ph)_2]^-$, has been reported.[12]

In this work, the Os^{IV} complex, *trans*-$[OsCl_4(PMe_3)_2]$, was prepared by the method of Leigh *et al* ,[10] that is, by heating OsO_4 and PMe_3 in EtOH/HCl.

5.2.3 $[MX_2L_4]$ and $[MX_2L_4]^+$ Complexes

Many monomeric ruthenium and osmium complexes of the type *cis*- and *trans*-$[MX_2L_4]$ were prepared in this work. Some of the established synthetic routes to the *trans*- divalent ruthenium complexes containing four tertiary phosphine or arsine ligands are shown in Fig. 5.2. The $[RuX_2(PR_3)_4]$ complexes were generally prepared by reaction of $[RuCl_2(PPh_3)_{3\text{ or }4}]$ with PR_3 in *non-polar solvents*, as P-donor ligands react with ruthenium precursors in polar media to give the familiar triply-bridged diruthenium complexes, $[Ru_2(\mu\text{-}X)_3(PR_3)_6]^+$. We have found the mononuclear arsine complexes are distinctly more readily prepared, as described in Chapter 3, because the procedures which lead to binuclear phosphine complexes favour $[RuX_2(AsMe_3)_4]$ instead when arsine ligands are used. The syntheses of many *cis*-$[RuCl_2L_4]$ complexes have also been reported in the literature, starting from "$RuCl_3.xH_2O$" (L = $AsMe_2Ph$),[19] $[RuCl_2(PPh_3)_3]$ (L = $AsMePh_2$, $AsMe_2Ph$,[20] PMe_2Ph[21]) and $[RuH(\eta^2\text{-}Me_2PCH_2)(PMe_3)_3]$ (L = PMe_3).[22] The only structurally characterised complexes of this type, *cis*- and *trans*-$[RuCl_2(dppm^{\dagger})_2]$[23] and *trans*-$[RuCl_2(vdpp^{\P})_2]$,[24] have contained bidentate phosphines.

---

† dppm = bis(diphenylphosphino)methane

¶ vdpp = 1,1-bis(diphenylphosphino)ethene

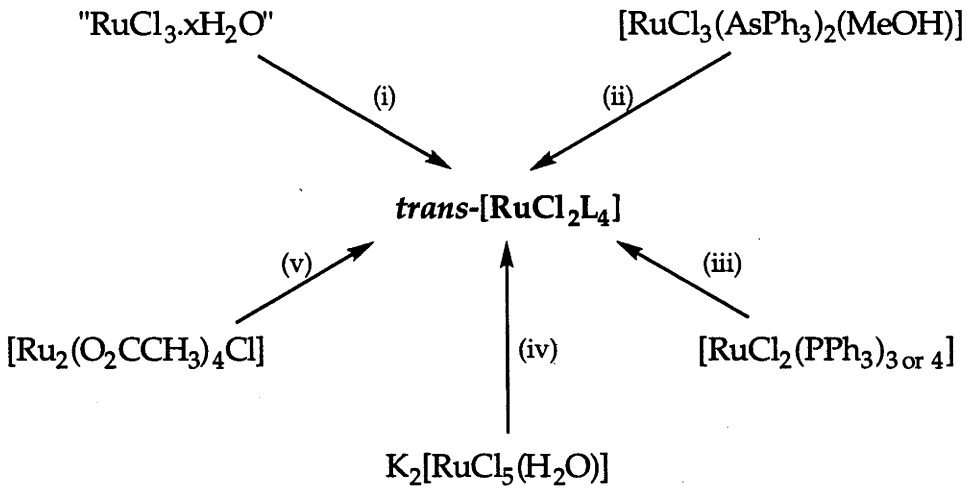

Figure 5.2 *Synthetic routes to trans-[RuCl$_2$L$_4$] complexes: (i) Boiling methanol, L = AsMe$_2$Ph,[19] AsMe$_2$(CH$_2$Ph), PMe$_2$(CH$_2$Ph),[25] P(p-tol)$_3$;[26] Boiling ethanol, L = AsMePh$_2$.[27] (ii) Treated with amalgamated zinc in methanol/benzene, L = AsMe$_2$Ph.[20] (iii) Treated with L in n-hexane or light petroleum, L = PMe$_3$,[22,28] PMe$_2$Ph, PEt$_3$,[29] PMePh$_2$, P(MeCH$_2$CH(Ph)CH$_2$)Ph$_2$;[30] (iv) Treated with hypophosphorus acid in ethanol, L = AsMePh$_2$.[31] (v) Treated with LiCl and sodium amalgam in thf at room temperature, L = PMe$_3$.[32]*

In this work, we sought a reliable general synthetic route to both *cis*- and *trans*-[MX$_2$L$_4$] complexes (M = Ru, Os; X = Cl, Br). The *trans*-[RuX$_2$L$_4$] complexes were prepared by heating organo-soluble salts of $[Ru_2X_9]^{3-}$ with L (PMe_3, $AsMe_3$, $AsMe_2Ph$ or $AsMePh_2$) and zinc amalgam in dichloromethane solution (Fig. 5.3). The *trans*-[RuX$_2$L$_4$] complexes were isolated after column chromatography and were either orange or dark pink in colour.

$$[Bu^n{}_4N]_3[Ru_2X_9] \xrightarrow{AsR_3,\ Zn/Hg,\ CH_2Cl_2} \textit{trans}\text{-}[RuX_2(AsR_3)_4]$$

$$[EPh_4][RuX_4(AsMe_3)_2] \xrightarrow{AsMe_3,\ Zn/Hg,\ CH_2Cl_2} \textit{trans}\text{-}[RuX_2(AsMe_3)_4]$$

Figure 5.3 *Synthesis of trans-[RuX$_2$L$_4$] complexes in our laboratory. EPh$_4$ = PPh$_4$ or AsPh$_4$.*

A second route to *trans*-[RuX$_2$(AsMe$_3$)$_4$] involved reduction (using zinc amalgam) of *trans*-[RuX$_4$(AsMe$_3$)$_2$]$^-$ in the presence of AsMe$_3$. In contrast, when this procedure was followed using AsMe$_2$Ph, the only isolated product was *cis*-[RuCl$_2$(AsMe$_2$Ph)$_4$]. Other *cis* isomers studied in this work, *cis*-[RuCl$_2$(AsMe$_3$)$_4$]

and *cis*-[$RuBr_2(AsMe_2Ph)_4$], were obtained as readily-isolated by-products in the synthesis of triply-bridged diruthenium complexes (§3.1). Heating "$RuCl_3.xH_2O$" and $AsMe_3$ in ethanol/HCl resulted in a mixture containing *cis*-[$RuCl_2(AsMe_3)_4$], *trans*-[$RuCl_2(AsMe_2Ph)_4$] and [$Ru_2(\mu\text{-}Cl)_3(AsMe_3)_6$]Cl. After removal of the *trans* isomer, the *cis* monomer was isolated by extraction into diethyl ether. Turning to the bromo complex, *cis*-[$RuBr_2(AsMe_2Ph)_4$] was isolated from the reaction of $K_3[Ru_2Br_9]$ with $AsMe_2Ph$ in $EtOH/H_2O$ (4:1). In contrast, we have found reactions of $K_3[Ru_2X_9]$ with all other arsine ligands in this solvent system (to prepare binuclear complexes) gave *trans*-[$RuX_2(AsR_3)_4$] complexes as the favoured by-product. These reactions are summarised in Fig. 5.4.

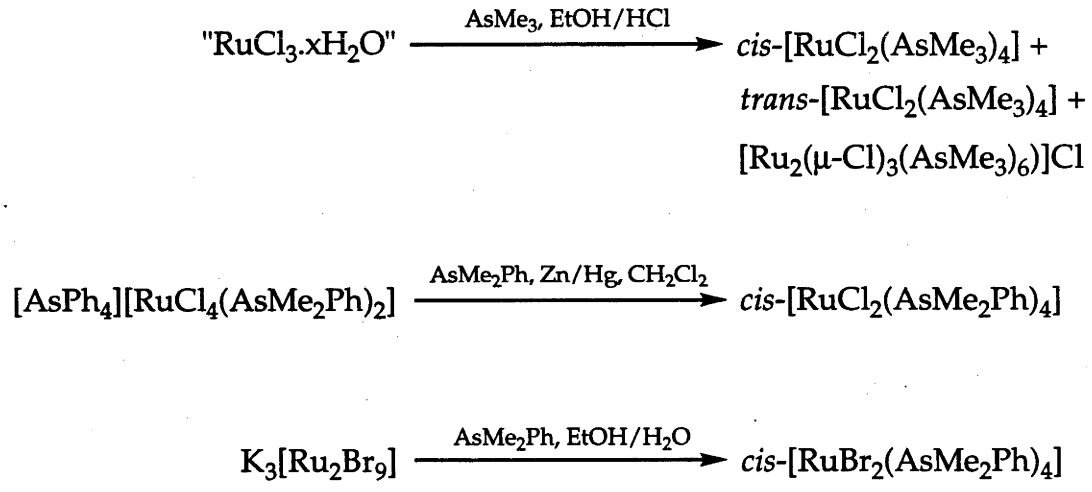

Figure 5.4 *Synthesis of cis-[RuX_2L_4] complexes in our laboratory.*

The *trans*-[$RuX_2(AsR_3)_4$] complexes were readily converted to the corresponding Ru^{III} cations by chemical oxidation. Red/pink dichloromethane solutions of neutral Ru^{II} complexes were stirred with $NOPF_6$ for about 1 hour, over which time the solutions turned dark green. The addition of diethyl ether followed by cooling of the solution led to the isolation of the dark green *trans*-[$RuCl_2(AsR_3)_4$]PF_6 salts (Fig. 5.5). The *cis* isomers, even given their higher oxidation potentials, should also be able to be oxidised using NO^+, although we have not attempted to do so. Aside from these chemical

oxidations, alternative oxidation states (M^{III} and M^{IV}) were generated as required by spectro-electrochemistry, as described later.

$$trans\text{-}[RuX_2(AsR_3)_4] \xrightarrow{NOPF_6,\ CH_2Cl_2} trans\text{-}[RuX_2(AsR_3)_4]PF_6$$

Figure 5.5 *Oxidation of trans-[RuX2L4] complexes.*

Osmium complexes, *cis*- and *trans*-$[Os^{II}X_2L_4]$ and *trans*-$[Os^{III}X_2L_4]^+$, have been mostly reported with L being phosphine rather than arsine ligands. Some of the preparative routes to Os^{II} phosphine complexes include reduction of OsO_4 or $Na_2[OsCl_6]$ in the presence of PR_3,[33-35] heating $[Os_2Cl_8]^{2-}$ with PR_3 in ethanol[15] and exchange between $[OsX_2(PPh_3)_3]$ and PMe_3 to give *trans*-$[OsX_2(PMe_3)_4]$.[22,36,37] These complexes are readily oxidised to Os^{III} cations in air or with HNO_3.[35] Fewer AsR_3 complexes are known, with the only report of $[Os^{II}X_2(AsR_3)_4]$ complexes being from heating $[OsCl_6]^{2-}$ with AsR_3 in ethanol, with hypophosphorous acid added as a reducing agent.[38] This early paper characterised the complexes only by halide analyses and the geometry was not specified. Cationic Os^{III} complexes have been reported by the reduction of *mer*-$[OsX_3(AsMe_3)_3]$ in the presence of $AsMe_3$, followed by oxidation to isolate *trans*-$[OsX_2(AsMe_3)_4]PF_6$.[35] Several *cis*-$[OsX_2(PR_3)_4]$ complexes have been prepared, by reduction of *mer*-$[OsX_3L_3]$ in the presence of L (X = Cl, Br; L = PMe_2Ph),[34,35] isomerisation of *trans* isomers (by standing in dichloromethane solution for several days; L = PMe_3),[35] and by treatment of $[OsH(\eta^2\text{-}Me_2PCH_2)(PMe_3)_3]$ with HX.[22] Osmium complexes which have been structurally characterised include *trans*-$[Os^{III}Cl_2(PMe_3)_4]BF_4$, and divalent complexes with bidentate phosphines, *trans*-$[OsCl_2(vdpp)_2]$ [24] and *cis*-$[OsCl_2(dppm)_4]$.[23]

The *trans*-$[OsX_2L_4]$ and *trans*-$[OsX_2L_4]^+$ complexes examined in this work were prepared by methods described above, heating $[OsX_6]^{2-}$ or $[OsX_2(PPh_3)_3]$ with excess L in alcoholic solvents. Reaction of $[OsCl_2(PPh_3)_3]$ with a limited quantity of $AsMe_2Ph$ (3

equivalents instead of excess) in ethanol led to *cis*-$[OsCl_2(AsMe_2Ph)_4]$, rather than the expected *trans* isomer.

Positive-ion electrospray (ES) mass spectra of the isolated Ru^{III} salts were examined. At low ion source energy (B1 = 40 V) the dominant peak in the ES mass spectrum of *trans*-$[RuCl_2(AsMe_3)_4]PF_6$ is at m/z 652, which is due to the intact ion $[RuCl_2(AsMe_3)_4]^+$, but there are also weak peaks at m/z 617 and 532. As the ion source energy is increased, the intensities of these peaks, especially that at m/z 532, increase relative to that of the intact ion, showing that they are formed by collisional activation. These peaks are assigned to $[RuCl(AsMe_3)_4]^+$ and $[RuCl_2(AsMe_3)_3]^+$ respectively, formed by loss of Cl or $AsMe_3$ from the precursor ion. At higher ion source energies further collisional activation gives $[RuCl(AsMe_3)_3]^+$ (m/z 497), $[RuCl_2(AsMe_3)_2]^+$ (m/z 412) and $[RuCl_2(AsMe_3)]^+$ (m/z 292). Entirely analogous ES mass spectra were obtained for *trans*-$[RuBr_2(AsMe_3)_4]PF_6$, but in the case of *trans*-$[RuCl_2(AsMe_2Ph)_4]PF_6$ there is an additional peak at m/z 748 which is assigned to a nitrosyl derivative, $[RuCl_2(NO)(AsMe_2Ph)_3]^+$, which presumably arises from the NO^+ oxidant. The presence of the nitrosyl moiety was confirmed by the observation of an infrared absorption at 1866 cm^{-1}, characteristic of a coordinated NO^+ group. The nitrosyl impurity was removed from this sample by slow recrystallisation of *trans*-$[RuCl_2(AsMe_2Ph)_4]PF_6$. We have since repeated this and other oxidations using NO^+, but have not observed any impurities from nitrosyl complexes. Despite this being a seemingly isolated example, the possibility of side reactions such as that leading to $[RuCl_2(NO)(AsMe_2Ph)_3]^+$, should be considered when attempting to oxidise compounds using NO^+. Investigation of Os^{III} monomers by ESMS is presently under investigation.

Table 5.1 *ES Mass Spectral Data for trans-[$RuX_2(AsR_3)_4$]$^+$ Complexes.*

Cation	Ions observed at low ion source energies (m/z)	Ions observed at higher ion source energies (m/z)
$[RuCl_2(AsMe_3)_4]^+$	$[RuCl_2(AsMe_3)_4]^+$ (652); $[RuCl(AsMe_3)_4]^+$ (617); $[RuCl_2(AsMe_3)_3]^+$ (532)	$[RuCl(AsMe_3)_3]^+$ (497); $[RuCl_2(AsMe_3)_2]^+$ (412); $[RuCl_2(AsMe_3)]^+$ (292)
$[RuBr_2(AsMe_3)_4]^+$	$[RuBr_2(AsMe_3)_4]^+$ (741); $[RuBr(AsMe_3)_4]^+$ (663); $[RuBr_2(AsMe_3)_3]^+$ (621)	$[RuBr(AsMe_3)_3]^+$ (543); $[RuBr_2(AsMe_3)_2]^+$ (501)
$[RuCl_2(AsMe_2Ph)_4]^+$	$[RuCl_2(AsMe_2Ph)_4]^+$ (900); $[RuCl(AsMe_2Ph)_4]^+$ (865); $[RuCl_2(NO)(AsMe_2Ph)_3]^+$ (748); $[RuCl_2(AsMe_2Ph)_3]^+$ (718)	$[RuCl_2(AsMe_2Ph)_2]^+$ (565)

5.2.4 $[MXL_5]^+$ Complexes (X = Cl, L = $AsMe_3$)

To the best of our knowledge there are no previously reported complexes of tertiary phosphines or arsines having the stoichiometry $[MXL_5]^+$ (M = Ru, Os). The novel $[RuCl(AsMe_3)_5]CF_3SO_3$ complex was prepared by heating "$RuCl_3.xH_2O$" and $AsMe_3$ in ethanol followed by treatment with triflic acid. The solution was cooled at 4 °C for several days, after which pale green crystals of $[RuCl(AsMe_3)_5]CF_3SO_3$ were collected. The penta-arsine product was characterised by ^1H NMR, ESMS, voltammetry and spectro-electrochemistry. An attempted X-ray crystal structure determination confirmed the proposed structure (Fig. 5.6), but the data set was unable to be fully refined. Unfortunately we have been unable to repeat this reaction, with *trans*-$[RuCl_2(AsMe_3)_4]CF_3SO_3$ being the only isolated product from several subsequent attempts. It may be that *cis*-$[RuCl_2(AsMe_3)_4]$ proves to be a preferable starting material, as it is less readily oxidised than trans-$[Ru^{II}Cl_2(AsMe_3)_4]$.

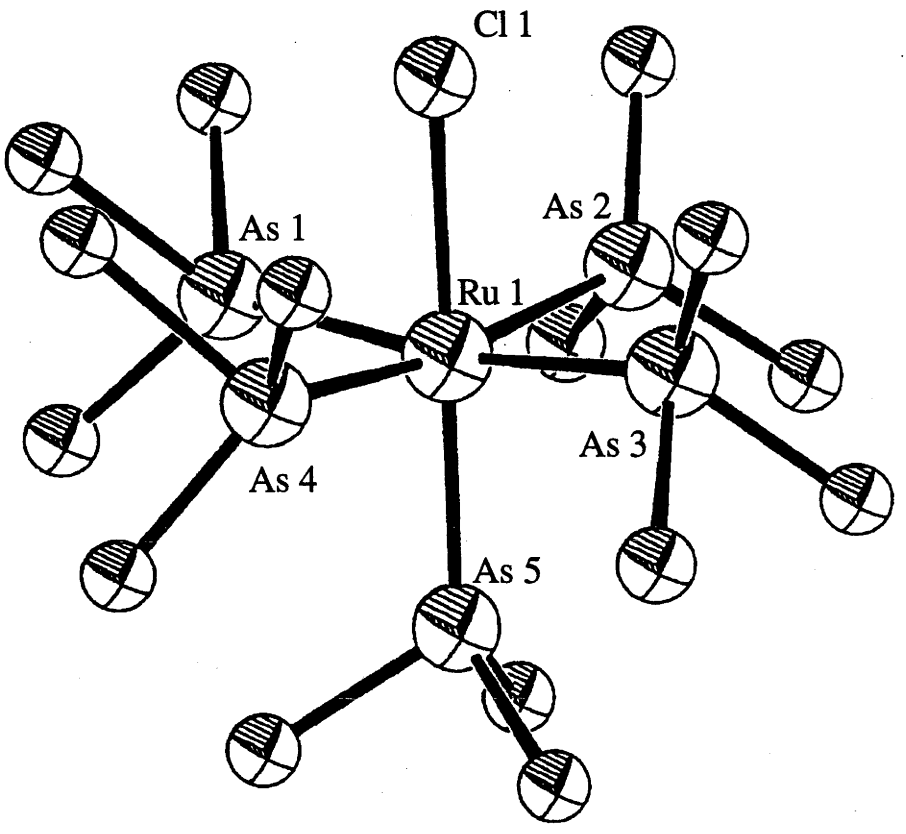

Figure 5.6 *Molecular structure of* $[RuCl(AsMe_3)_5]^+$ *(preliminary structure determination).*

The corresponding osmium complex, $[OsCl(AsMe_3)_5]CF_3SO_3$, was prepared by heating $[OsCl_2(PPh_3)_3]$ with $AsMe_3$ in ethanol, followed by treatment with dilute triflic acid to yield pale pink crystalline $[OsCl(AsMe_3)_5]CF_3SO_3$ (Fig. 5.7). In contrast to the preparation of $[RuCl(AsMe_3)_5]CF_3SO_3$, this reaction is reproducible with typical yields of 60-80%.

$$\text{"}RuCl_3.xH_2O\text{"} \xrightarrow[\text{(ii) } CF_3SO_3H \text{ (0.1 M), MeOH/}CH_2Cl_2]{\text{(i) } AsMe_3\text{, EtOH}} [RuCl(AsMe_3)_5]CF_3SO_3 \quad \text{(once only)}$$

$$[OsCl_2(PPh_3)_3] \xrightarrow[\text{(ii) } CF_3SO_3H \text{ (0.1 M), MeOH/}CH_2Cl_2]{\text{(i) } AsMe_3\text{, EtOH}} [OsCl(AsMe_3)_5]CF_3SO_3$$

Figure 5.7 *Preparation of* $[MCl(AsMe_3)_5]CF_3SO_3$ *complexes.*

Figure 5.8 shows the positive ion ES mass spectra of $[RuCl(AsMe_3)_5]CF_3SO_3$ at various ion source energies (B1 voltages). With B1 = 30 V the strongest peak in the ES mass spectrum at m/z 739 is due to the intact ion $[RuCl(AsMe_3)_5]^+$. At B1 = 40 V, the base peak at m/z 617 is due to $[RuCl(AsMe_3)_4]^+$ formed by loss of one $AsMe_3$ ligand within the ion source by collisionally activated decomposition of ligands. This is a very low ion source energy for dissociation of ligands in ES mass spectra and suggests that the intact ion is fragile. As the ion source energy is increased to 90 V, further decomposition of the precursor ion occurs to give $[RuCl(AsMe_3)_3]^+$ (m/z 497).

The corresponding Os^{II} complex, $[OsCl(AsMe_3)_5]CF_3SO_3$, gives similar ES mass spectra but it is rather more robust. At B1 = 40 V the only significant peak in the mass spectrum is that due to the intact ion at m/z 827, but at higher ion source energies the ions $[OsCl(AsMe_3)_4]^+$ (m/z 707) and $[OsCl(AsMe_3)_3]^+$ (m/z 587) are observed. At B1 = 120 V, the highest m/z peak observed is that at 587, but considerable fragmentation occurs to give several peaks containing osmium at lower m/z values, however the only one identified is due to $[OsCl(AsMe_3)_2]^+$ (m/z 467).

Table 5.2 *ES Mass Spectral Data for* $[MX(AsMe_3)_5]CF_3SO_3$ *Complexes.*

Compound	Ions observed at low ion source energies (m/z)	Ions observed at higher ion source energies (m/z)
$[RuCl(AsMe_3)_5]CF_3SO_3$	$[RuCl(AsMe_3)_5]^+$ (737); $[RuCl(AsMe_3)_4]^+$ (617)	$[RuCl(AsMe_3)_3]^+$ (497)
$[OsCl(AsMe_3)_5]CF_3SO_3$	$[OsCl(AsMe_3)_5]^+$ (827)	$[OsCl(AsMe_3)_4]^+$ (707); $[OsCl(AsMe_3)_3]^+$ (587); $[OsCl(AsMe_3)_2]^+$ (467)

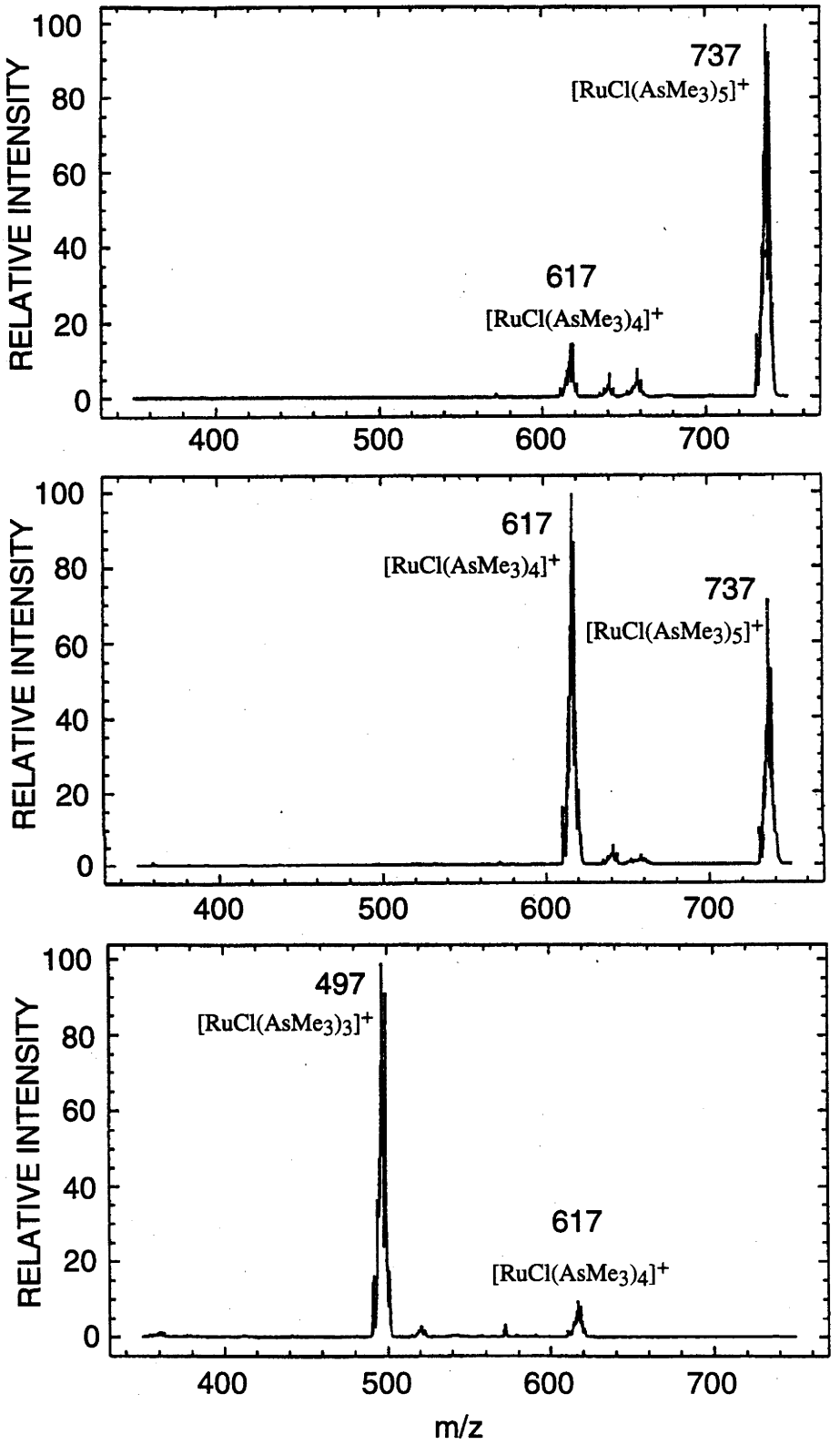

Figure 5.8 *Positive ion ES mass spectra at various ion source energies for a solution of [RuCl(AsMe3)5]CF3SO3. (a) B1 = 30 V. (b) B1 = 40 V. (c) B1 = 90 V.*

Presumably the fragile nature of the $[RuCl(AsMe_3)_5]^+$ cation, as observed in the electrospray mass spectrometric study, is due to the steric constraints of five trimethylarsine ligands about the Ru^{II} centre, which could explain why the initial fortuitous isolation of the penta-arsine complex has not yet been repeated. The preparation of $[OsCl(AsMe_3)_5]CF_3SO_3$ has been repeated a number of times, and this complex is stable in solution over several days.

5.3 ELECTROCHEMISTRY

The electrochemical behaviour of ruthenium and osmium halo-arsine and halo-phosphine complexes were first investigated in 1979,[39] with the investigation of $[RuX_4L_2]^-$ and $[RuX_2L_4]$ complexes, where L = PR_3. Since then, most reports have been for osmium complexes, such as $[OsX_4L_2]$,[12,15,40] $[OsX_3L_3]$ [15,34,41] and $[OsX_2L_4]$.[15,34,35,40] Whilst there have been systematic electrochemical investigations of sequentially substituted ruthenium (*e.g.* $[RuCl_{6-n}(RCN)_n]^{z+}$ (R = CH_3, Ph)[1,42]) and osmium (*e.g.* $[OsCl_{6-n}(py)_n]^{z+}$ [43]) complexes, there does not appear to have been such studies of arsine or phosphine substituted systems. We have studied a range of complexes, from $[MX_4L_2]$ to $[MX_2L_4]$ and extended the study to the new $[MXL_5]^+$ systems.

The monomeric complexes were examined at -60 °C in dichloromethane solutions containing $[Bu^n_4N][BF_4]$ (0.5 mol dm^{-3}). In the case of the *trans*-$[RuX_4L_2]^-$ complexes $[Bu^n_4N]X$ (0.05 mol dm^{-3}) was added to suppress halide dissociation, especially upon reduction to Ru^{II}. This reduced the potential window for the measurements due to oxidation of X^- at ~1.2 - 1.4 V, but the oxidation to Ru^{IV} (near +1.0 V) was still observable. The voltammetry of *trans*-$[OsBr_2(AsMe_3)_4]^+$ is shown in Fig. 5.9.

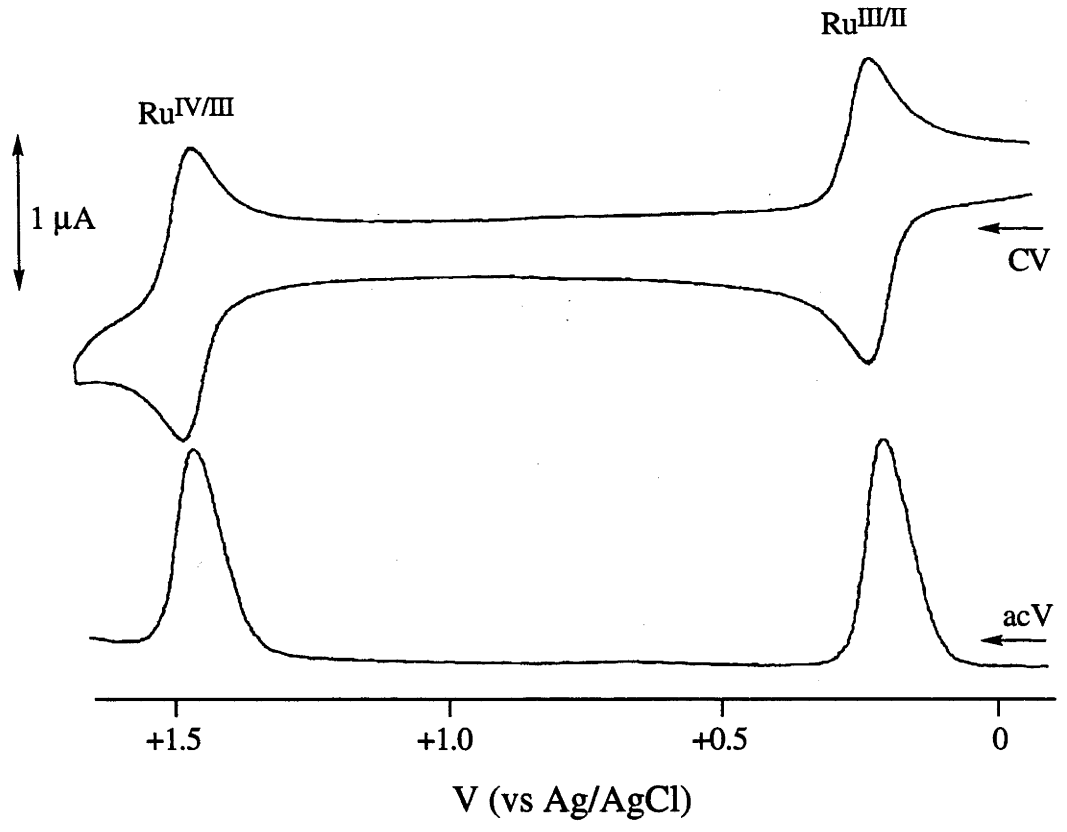

Figure 5.9 *Cyclic volvammetry (CV) and alternating current voltammetry (acV) for trans-[$OsBr_2(AsMe_3)_4$]$^+$, recorded in CH_2Cl_2/[Bu^n_4N][BF_4] (0.5 mol dm^{-3}) at 213 K.*

Most of the redox processes reported in Tables 5.3 and 5.4 were reversible, with one interesting exception being *cis*-[$OsCl_2(AsMe_2Ph)_4$]. This complex underwent an irreversible $Os^{IV/III}$ oxidation, and two daughter waves (both from the one rearrangement product) were observed at +1.56 and +0.25 V; these correspond to the *trans* isomer. This isomerisation was subsequently confirmed by spectro-electrochemistry, as the one-electron oxidation of *cis*-[$Os^{III}Cl_2(AsMe_2Ph)_4$]$^+$ was observed to yield the *trans*-[$Os^{IV}Cl_2(AsMe_2Ph)$]$^{2+}$ species. It would be interesting to explore whether the corresponding ruthenium complexes (*cis*-[RuX_2L_4]$^+$) isomerise upon oxidation to the Ru^{IV} level, however the potential required is > +2.0 V.

Table 5.3 *Electrochemical Data for Monomeric Ruthenium Complexes.*

Stoichiometry	Complex	$E_{1/2}$ / V vs Ag/AgCl [a]		$\Delta E_{1/2}$ [b]
		$Ru^{IV/III}$	$Ru^{III/II}$	
$[RuX_6]^{3-}$	$[RuCl_6]^{3-}$	0.22	-1.51	1.73
	$[RuBr_6]^{3-}$	0.14	-1.46	1.60
trans-$[RuX_4L_2]^-$ [c]	*trans*-$[RuCl_4(AsMe_3)_2]^-$	+0.99	-0.65	1.64
	trans-$[RuCl_4(AsMe_2Ph)_2]^-$	+1.03	-0.59	1.62
	trans-$[RuCl_4(PMe_2Ph)_2]^-$	+1.05	-0.62	1.67
	trans-$[RuBr_4(AsMe_3)_2]^-$	+1.01	-0.53	1.54
mer-$[RuX_3L_3]$	*mer*-$[RuCl_3(PMe_2Ph)_3]$	+1.34[d]	+0.11[d]	1.23
trans-$[RuX_2L_4]$	*trans*-$[RuCl_2(AsMe_3)_4]$	+1.74	+0.51	1.23
	trans-$[RuCl_2(AsMe_2Ph)_4]$	+1.83	+0.59	1.24
	trans-$[RuCl_2(PMe_3)_4]$	+1.63	+0.47	1.16
	trans-$[RuBr_2(AsMe_3)_4]$	+1.72	+0.52	1.20
	trans-$[RuBr_2(AsMe_2Ph)_4]$	+1.79	+0.62	1.17
	trans-$[RuBr_2(AsMePh_2)_4]$	+1.87[d]	+0.72	1.15
cis-$[RuX_2L_4]$	*cis*-$[RuCl_2(AsMe_3)_4]$	*e*	+0.76	-
	cis-$[RuCl_2(AsMe_2Ph)_4]$	*e*	+0.89	-
	cis-$[RuCl_2(PMe_2Ph)_4]$	*e*	+0.97	-
	cis-$[RuBr_2(AsMe_2Ph)_4]$	*e*	+0.88	-
$[RuXL_5]^+$	$[RuCl(AsMe_3)_5]^+$	*e*	+1.40	-

[a] Recorded in CH_2Cl_2/$[Bu^n_4N][BF_4]$ (0.5 mol dm^{-3}) at 213 K. Ferrocene is oxidised at +0.55 V under these conditions. [b] $\Delta E_{1/2} = E_{1/2}(Ru^{IV/III}) - E_{1/2}(Ru^{III/II})$. [c] Solutions contained 0.05 mol dm^{-3} $[Bu^n_4N]X$. [d] Irreversible process. [e] Not observed to +2.0 V.

Within a particular group of complexes it can be seen that the the effects of changing phosphines for similarly substituted arsines is marginal. Moreover, the bromo complexes are similar to their chloro counterparts, with the main difference being a smaller separation (~0.1 V) between the $Ru^{IV/III}$ and $Ru^{III/II}$ couples.

Table 5.4 *Electrochemical Data for Monomeric Osmium Complexes.*

Stoichiometry	Complex	$E_{1/2}$ / V vs Ag/AgCl [a]		$\Delta E_{1/2}$ [b]
		$Os^{IV/III}$	$Os^{III/II}$	
$[OsX_6]^{2-}$	$[OsCl_6]^{2-}$	-0.56	-	-
	$[OsBr_6]^{2-}$	-0.37[c]	-2.28[c]	1.91
trans-$[OsX_4L_2]$	*trans*-$[OsCl_4(PMe_3)_2]$	+0.49	-1.16	1.65
mer-$[OsX_3L_3]$	*mer*-$[OsCl_3(AsMe_3)_3]$	+0.99	-0.41	1.40
	mer-$[OsCl_3(AsMe_2Ph)_3]$	+1.04	-0.34	1.38
	mer-$[OsCl_3(AsMePh_2)_3]$	+1.12	-0.23[d]	1.35
	mer-$[OsCl_3(PMe_2Ph)_3]$	+1.08	-0.27[d]	1.35
trans-$[OsX_2L_4]$	*trans*-$[OsCl_2(AsMe_3)_4]^+$	+1.44	+0.13	1.31
and	*trans*-$[OsCl_2(AsMe_2Ph)_4]$	+1.56	+0.25	1.31
trans-$[OsX_2L_4]^+$	*trans*-$[OsCl_2(PMe_3)_4]^+$	+1.42	+0.15	1.27
	trans-$[OsBr_2(AsMe_3)_4]^+$	+1.45	+0.20	1.25
	trans-$[OsBr_2(AsMe_2Ph)_4]$	+1.54	+0.31	1.23
	trans-$[OsBr_2(PMe_3)_4]^+$	+1.46	+0.19	1.27
cis-$[OsX_2L_4]$	*cis*-$[OsCl_2(AsMe_2Ph)_4]$	+1.76[d]	+0.62	1.14
$[OsXL_5]^+$	$[OsCl(AsMe_3)_5]^+$	[e]	+1.19	-

[a] *Recorded in CH_2Cl_2/$[Bu^n_4N][BF_4]$ (0.5 mol dm^{-3}) at 213 K. Ferrocene is oxidised at +0.55 V under these conditions.* [b] $\Delta E_{1/2} = E_{1/2}(Os^{IV/III}) - E_{1/2}(Os^{III/II})$. [c] *Data from Ref. 2.* [d] *Irreversible process.* [e] *Not observed to +2.0 V.*

Comparing these series of compounds we find that, as expected, the electrode potentials become more positive upon substitution of a phosphine or arsine in place of a halide ligand. The potentials are geometry-dependent, as there are differences in $E_{1/2}$ of 250 - 370 mV between the *cis* and *trans* isomers of $[MX_2L_4]$, with the *cis* isomer being more difficult to oxidise. Also, comparing ruthenium and osmium complexes, the osmium complexes are easier to oxidise, by ~0.5 V in $[MX_4L_2]$, a gap that narrows to ~0.2 V in $[MCl(AsMe_3)_5]^+$. There is also evidence of the $M^{IV/III}$ and $M^{III/II}$ electrode potentials converging (Tables 5.3 and 5.4). These effects will be discussed in greater detail below (§ 5.5).

5.4 UV/VIS/NEAR-IR SPECTRA

5.4.1 General - M^{II} (d^6) Systems

For monomeric coordination complexes, the two distinct types of optical charge-transfer transitions are ligand-to-metal charge-transfer (LMCT) and metal-to-ligand charge-transfer (MLCT). The MLCT bands occur most readily in lower-valent transition metal complexes having a large complement of d_π (maximally, t_{2g}^6) electrons. The UV/Visible spectra of the M^{III} (t_{2g}^5) and M^{IV} (t_{2g}^4) complexes studied here are dominated by ligand-to-metal charge-transfer (LMCT) transitions, where an electron is promoted from ligand-based orbitals into unoccupied metal-based orbitals.

In the closed shell M^{II} complexes studied here, the optical spectra are free of intense features in the visible range, implying that the allowed charge-transfer into the empty metal e_g level must be well into the ultraviolet region, typically above 35 000 cm^{-1} (see Table 5.5). For the majority of these $M^{II}(d_\pi^6)$ complexes, two d-d transitions are observed (Fig. 5.10).

Table 5.5 *UV/Vis Spectral Data for M^{II} Complexes.*

Complex	ν_{max} / cm^{-1} (ε / dm^3 mol^{-1} cm^{-1}) [a]	
	d-d bands	Charge-transfer bands
trans-$[RuCl_2(AsMe_3)_4]$	21 000 (630), 28 650 (490)	
trans-$[RuCl_2(AsMe_2Ph)_4]$	20 600 (340)	33 900 (2410), 40 800 (42 300)
trans-$[RuCl_2(PMe_3)_4]$	22 200 (520), 32 500 (790)	40 700 (7760)
trans-$[RuBr_2(AsMe_3)_4]$	20 160 (280), 32 230 (560)	36 960 (3900)
trans-$[RuBr_2(AsMe_2Ph)_4]$	20 800 (370)	35 950 (14 000), 39 900 (44 800)
trans-$[RuBr_2(PMe_3)_4]$	21 240 (400), 32 200 (610)	37 450 (6010)
cis-$[RuCl_2(AsMe_3)_4]$	24 500 (400), 27 100 (500)	43 000 (18 600)
cis-$[RuCl_2(AsMe_2Ph)_4]$	25 600 (650), 29 200 (400)	38 000 (25 600)
cis-$[RuCl_2(PMe_2Ph)_4]$	26 200 (700)	38 700 (23 000)
cis-$[RuBr_2(AsMe_2Ph)_4]$	24 600 (850), 28 000 (580)	
$[RuCl(AsMe_3)_5]^+$	27 060 (630), 32 230 (560)	
trans-$[OsCl_2(AsMe_3)_4]$	25 370 (750), 32 900 (sh)	36 640 (1970)
trans-$[OsCl_2(AsMe_2Ph)_4]$	24 600 (290), 35 100 (sh)	38 500 (6390)
trans-$[OsCl_2(PMe_3)_4]$	27 100 (250)	
trans-$[OsBr_2(AsMe_3)_4]$	17 600 (220), 24 180 (270)	36 600 (3880)
trans-$[OsBr_2(AsMe_2Ph)_4]$	24 000 (200)	40 800 (sh), 43 780 (12 900)
$[OsCl(AsMe_3)_5]^+$	26 000 (sh), 31 470 (610), 36 300 (570)	

[a] *Recorded in CH_2Cl_2 containing $[Bu^n_4N][BF_4]$ (0.5 mol dm^{-3}) at 213 K.*

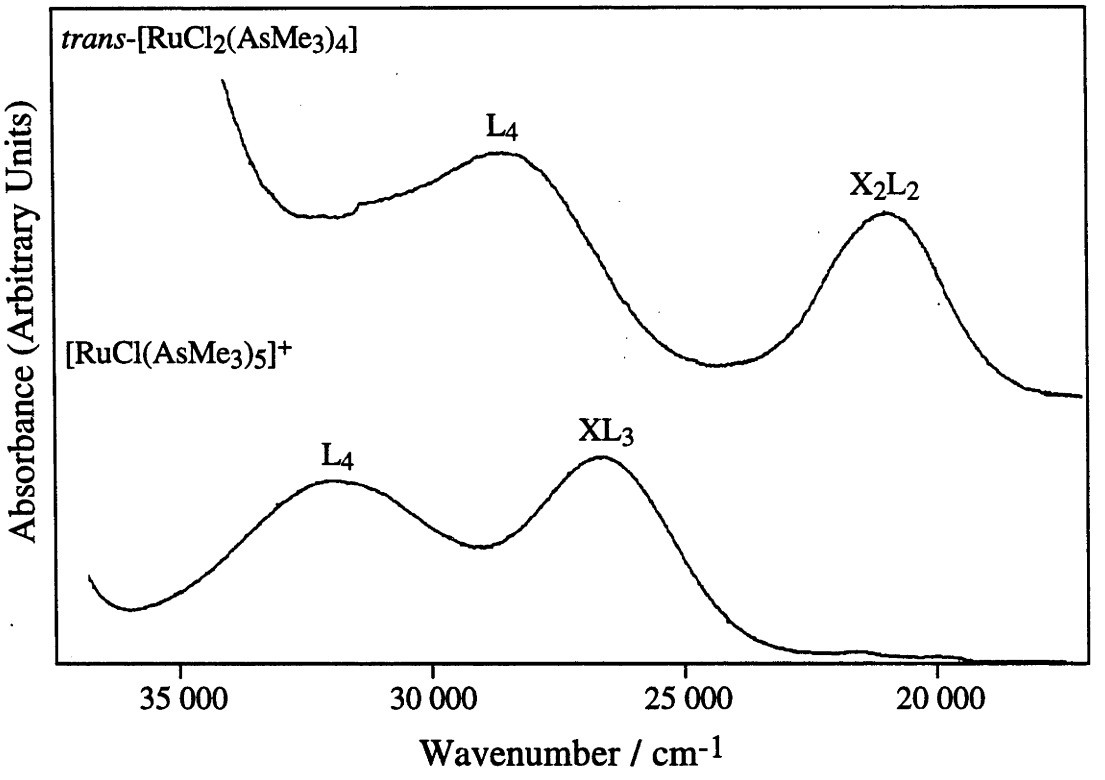

Figure 5.10 *UV/Vis spectra of trans-[RuCl$_2$(AsMe$_3$)$_4$] and [RuCl(AsMe$_3$)$_5$]$^+$, recorded in CH$_2$Cl$_2$/[Bu^n$_4$N][BF$_4$] (0.5 mol dm^{-3}) at 213 K.*

For the majority of M^{II} complexes two d-d transitions are observed due to splitting of the ^1T state into ^1E and ^1A terms. These transitions can be viewed as in-plane ligand-field transitions ($d_{xy} \rightarrow d_{x^2-y^2}$ style transitions) with a 10Dq value characteristic of the planar ligand array. For *trans*-[MX_2L_4] there is one band characteristic of the unique ML_4 plane, and one band characteristic of the MX_2L_2 planes. Assuming L has a larger 10Dq than X, then 10 Dq for $L_4 > XL_3 > X_2L_2 > X_3L > X_4$. Examining Table 5.5, we can see an orderly pattern to the two weak UV/Vis bands between 20 000 and 32 000 cm^{-1} (Ru) or 36 000 cm^{-1} (Os). Comparing *trans*-[$RuCl_2(AsMe_3)_4$] and [$RuCl(AsMe_3)_5$]$^+$, the former has one band associated with the L_4 plane transition (28 600 cm^{-1}) and one with the X_2L_2 plane (21 000 cm^{-1}). The penta-arsine complex has transitions characteristic of L_4 (moved to higher energy than in *trans*-[$RuCl_2(AsMe_3)_4$], at 32 200 cm^{-1}) and XL_3 (27 000 cm^{-1}) planes. As expected from this analysis, the separation between the XL_3 and L_4 bands is less than between the X_2L_2 and

L_4 bands in these two complexes. Values of 10Dq for the various planes in the $Ru/Cl/AsMe_3$ series are listed in Table 5.6, based on values in Table 5.6. A complementary pattern is formed for the weak d-d bands of the corresponding Os^{II} complexes.

Table 5.6 *Energies of In-Plane Ligand-Field Transitions in the Ru/Cl/AsMe3 Series.*

Plane	Energy / cm^{-1}	
$Ru(AsMe_3)_4$	32 230	from $[RuCl(AsMe_3)_5]^+$
	28 650	from *trans*-$[RuCl_2(AsMe_3)_4]$
$RuCl(AsMe_3)_3$	27 060	from $[RuCl(AsMe_3)_5]^+$
	27 100	from *cis*-$[RuCl_2(AsMe_3)_4]$
$RuCl_2(AsMe_3)_2$	24 500	from *cis*-$[RuCl_2(AsMe_3)_4]$
	21 000	from *trans*-$[RuCl_2(AsMe_3)_4]$

5.4.2 General - M^{III} (d^5) Systems

An early study of the UV/Vis spectra of d^n heavy metal hexahalide complexes by Jørgensen[44,45] found that the energy of $\pi(X) \rightarrow M$ charge-transfer is qualitatively dependent upon how easily each metal is reduced. That is, hν(XMCT) decreases with increasing atomic number across the second and third rows, and increases in going from a 4d ion to the corresponding 5d ion. Equally, hν(XMCT) depends on how easily the ligand is oxidised (*i.e* XMCT for F >> Cl > Br > I). Transient one-electron photo-reduction of the central metal ion is a good description of the XMCT process,[44] so the correlation between XMCT energy and the reducibility of the metal is reasonable.

In what follows we focus on tervalent *trans*-$[MX_4L_2]^-$ and electrogenerated *trans*-$[MX_2L_4]^+$. The complexes of D_{4h} symmetry have axial ligands which do not interact with the equatorial halides to any great extent, so that distinct charge-transfer transitions are expected from the halides (XMCT) and from the phosphines or arsines (LMCT). Complexes of lower symmetry, such as *cis*-$[M^{III}X_2L_4]^+$ and *mer*-$[M^{III}X_3L_3]$

are expected to have greater mixing of the π(X) and σ(L) orbitals, hence spectral assignments become more complicated.[41,46,47]

5.4.3 Spectra of *trans*-$[MX_4L_2]^-$ Complexes

The intense optical spectra of *trans*-$[MX_4L_2]^-$ complexes are dominated by the planar MX_4 chromophore. Duff and Heath,[42] in their study of halide-to-Ru^{III} charge-transfer in the series from $[RuCl_6]^{3-}$ to $[RuCl(RCN)_5]^-$, showed that the important halide donor orbitals are those set up by the filled π-orbitals of the planar halides, giving rise to three halide π-levels, A_{2g}, E_u and B_{2g}. The singly-occupied metal acceptor orbital is the particular t_{2g}-derived orbital which experiences the greatest destabilisation from interaction with halide ligands, in this case d_{xy} (assuming the x and y axes lie in the MX_4 plane), giving a B_{2g} metal ground state. The handsome band near 27 000 cm^{-1} for the $AsMe_3$ ruthenium complexes is the transition from $E_u \rightarrow B_{2g}$ (Fig. 5.11). This band is intense as it involves a u/g transition from ligand-orbitals co-planar with the d_{xy} acceptor orbital,[42] and usually appears as a characteristic doublet due to noticeable splitting of the E_u state through halide-based spin-orbit coupling. The splitting is substantially larger in the corresponding bromo complexes because of the larger spin-orbit coupling constant (~650 cm^{-1} for Cl^-, 2200 cm^{-1} for Br^-). In addition, the position of this doublet band consistently decreases by *ca.* 6000 cm^{-1} in replacing Cl by Br, as anticipated for a XMCT band. Associated with the same $\{X_4\}\rightarrow M$ manifold, there is also a characteristic weaker band at lower energy (~23 000 cm^{-1}), assigned as the forbidden (g/g transition) $A_{2g}\rightarrow B_{2g}$. Just discernible in the $[RuCl_4(AsMe_3)_2]^-$ spectrum at higher energy (~31 000 cm^{-1}) is a weaker band at higher energy, assigned as $B_{2g} \rightarrow B_{2g}$, which is not always observed. In the bis-MeCN complex, the clearly defined band near 33 000 cm^{-1} represents promotion (into d_{xy}) from the chloride σ-dative lone pairs.[42]

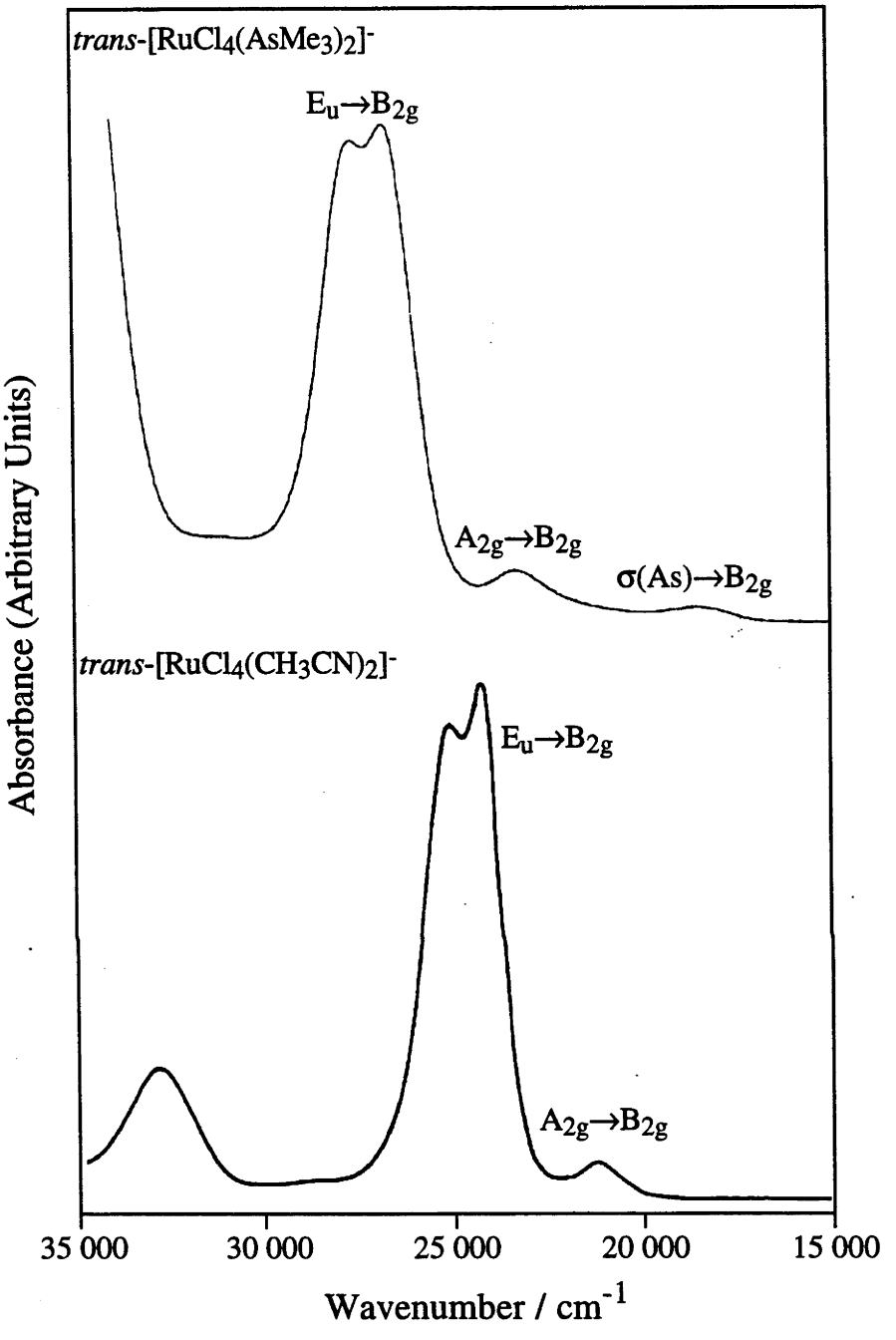

Figure 5.11 *UV/Vis spectra of trans-[RuCl4L2]-, where L = AsMe3 and CH3CN.*[42]

The other major feature of these spectra is the low-intensity band near 17 000 - 18 000 cm^{-1}. These bands are expected to be σ(L)→M charge-transfer (L = PR_3 or AsR_3), as similar bands are not present in spectra of $[MX_4(RCN)_2]^-$, and their position does not alter upon changing chloride for bromide. In this case, there being no non-bonding pairs on PR_3 or AsR_3 ligands, we know the dative lone-pairs of the As→M or

P→M bond are the ones involved in excitation. There is little difference in altering the donor atom, as there is a shift of only ~700 cm^{-1} between *trans*-$[RuCl_4(AsMe_2Ph)_2]^-$ and *trans*-$[RuCl_2(PMe_2Ph)_4]^+$, with the As→M CT being at higher energy.

Table 5.7 *UV/Vis Spectral Data for trans-*$[M^{III}X_4L_2]^-$ *Complexes.*

Complex	ν_{max} / cm^{-1} (ε / dm^3 mol^{-1} cm^{-1}) [a]		
	$\sigma(L) \rightarrow t_{2g}(M)$	$\pi(X) \rightarrow t_{2g}(M)$	
		$A_{2g} \rightarrow B_{2g}$	$E_u \rightarrow B_{2g}$
trans-$[RuCl_4(AsMe_3)_2]^-$	18 440 (160)	23 210 (540)	26 530 (5600), 27 370 (5420)
trans-$[RuCl_4(AsMe_2Ph)_2]^-$	18 360 (200)	22 830 (570)	26 140 (5390), 26 900 (5730)
trans-$[RuCl_4(PEt_3)_2]^-$	16 950 (130)	23 300 (430)	26 440 (5000), 27 200 (5000)
trans-$[RuCl_4(PMe_2Ph)_2]^-$	17 960 (130)	22 700 (510)	26 070 (5320), 26 910 (5270)
trans-$[RuBr_4(AsMe_3)_2]^-$			20 270 (4790), 23 070 (4480)
trans-$[OsCl_4(PMe_3)_2]^-$	22 400 (300)	27 900 (700)	31 150 (2960), 32 130 (3110)

[a] *Recorded in* CH_2Cl_2 *containing* $[Bu^n_4N][BF_4]$ *(0.5 mol* dm^{-3}*) at 213 K.*

Comparing a series of *trans*-$[RuX_4L_2]^-$ complexes (Table 5.8), it can be seen that the position of the XMCT bands for the $\{RuX_4\}$ chromophore decreases systematically in energy with the increasing ease of reduction of the Ru^{III} centre. The same distinctive pattern of XMCT bands is seen for all of these complexes, as shown in the examples of L = $AsMe_3$ and MeCN (Fig. 5.11).

Table 5.8 *Position of XMCT Bands in trans-[$Ru^{III}Cl_4LL']^z$ Complexes.*

Complex	XMCT	$E_{1/2}$ ($Ru^{III/II}$)	Ref.
trans-$[RuCl_4(AsMe_3)_2]^-$	27 000	-0.65	tw
trans-$[RuCl_4(CH_3CN)_2]^-$	24 700	-0.38	42
trans-$[RuCl_4(CO)Cl]^{2-}$	21 600	+0.41	48
trans-$[RuCl_4(NO)Cl]^{t-}$	15 200	+1.60	48

tw = this work

Our data for the Ru^{III} complexes can be compared with that for *trans*-$[OsCl_4(PMe_3)_2]^-$, spectro-electrochemically generated here from $[OsCl_4(PMe_3)_2]$, and with the spectral data reported by Levason *et al*[12] for a range of related Os^{III} complexes. The LMCT transitions invariably occur at higher energy, by about 4000 cm^{-1}, for the corresponding $[OsX_4L_2]^-$ complexes, which is as expected since each osmium centre is some 0.5 V more difficult to reduce than its ruthenium analogue.

5.4.4 Spectra of *trans*-$[MX_2L_4]^+$ Complexes

The spectra of the *trans*-$[RuX_2L_4]^+$ complexes were generally obtained spectro-electrochemically, from the neutral Ru^{II} precursors. Where both the Ru^{II} and Ru^{III} complexes had been prepared, the spectra of the Ru^{III} complexes confirmed those obtained by *in situ* electrogeneration. Similarly, those osmium complexes isolated in the in the Os^{II} state were electrochemically oxidised (Fig. 5.12). The osmium complexes were further oxidised to Os^{IV}, however all attempts to produce Ru^{IV} species resulted in unspecified decomposition. The Os^{IV} spectra show much the same features as the Os^{III} complexes but shifted to lower energy.

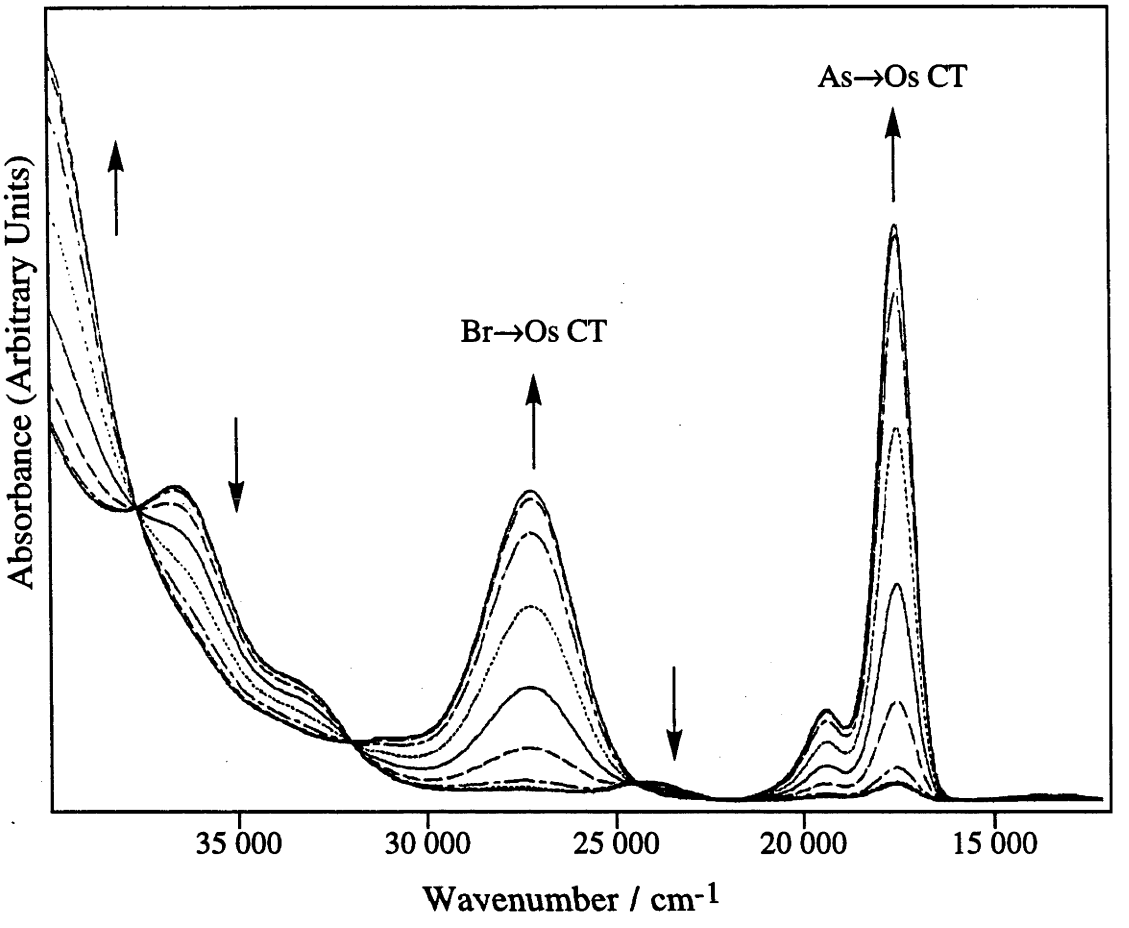

Figure 5.12 *Spectral progressions upon re-generation of trans-[Os^{III}Br$_2$(AsMe$_3$)$_4$]$^+$ from trans-[Os^{II}Br$_2$(AsMe$_3$)$_4$], recorded in CH$_2$Cl$_2$/[Bu$^n_4$N][BF$_4$] (0.5 mol dm^{-3}) at 213 K.*

In these *trans*-$[MX_2L_4]^+$ complexes, the highest lying t_{2g}-derived orbitals are those which interact with the two axial halides, *i.e.* the d_{xz} and d_{yz} orbitals (where the z axis coincides with X-Ru-X), hence the ground state is doubly-degenerate (E_g) and the π(L) electron is promoted from the halide to the $(d_{xy}, d_{yz})^3$ level. The major chloride-to-metal charge transfer band ($E_u \rightarrow E_g$[42,49]) near 28 000 cm^{-1} in the Ru/Cl systems red-shifts by ~4000 cm^{-1} for the bromo complexes, and the σ(L) $\rightarrow$ Ru charge-transfer band also decreases in energy, by about 1500 cm^{-1}, indicating there is some degree of mixing of the halide and phosphine or arsine orbitals. There is virtually no shift in the position of either band when the four phosphines are replaced by arsine ligands. All of these bands are moved to higher energy (~5000 cm^{-1}) in the analogous Os^{III} complexes, where the

underlying $E_{1/2}(M^{III/II})$ is 0.3 to 0.4 V higher. The UV/Vis spectra of *trans*-$[RuCl_2(AsMe_3)_4]^+$ and *trans*-$[OsCl_2(AsMe_2Ph)_4]^+$ are shown in Fig. 5.13 and 5.14 respectively.

Table 5.9 *UV/Vis Spectral Data for trans-$[MX_2L_4]^+$ Complexes.*

	ν_{max} / cm^{-1} (ε / dm^3 mol^{-1} cm^{-1}) [a]	
Complex	$\sigma(L) \rightarrow t_{2g}(M)$ [b]	$\pi(X) \rightarrow t_{2g}(M)$
trans-$[RuCl_2(AsMe_3)_4]^+$	15 600 (1220)	28 140 (3060)
trans-$[RuCl_2(AsMe_2Ph)_4]^+$	14 600 (1170)	27 200 (2400)
trans-$[RuCl_2(PMe_3)_4]^+$	15 880 (880)	27 750 (4070)
trans-$[RuBr_2(AsMe_3)_4]^+$	14 210 (2320)	23 950 (1750)
trans-$[RuBr_2(AsMe_2Ph)_4]^+$	13 360 (3290)	22 750 (1720)
trans-$[RuBr_2(PMe_3)_4]^+$	14 360 (3370)	23 600 (4320)
trans-$[OsCl_2(AsMe_3)_4]^+$	19 120 (1490)	31 180 (2280)
trans-$[OsCl_2(AsMe_2Ph)_4]^+$	18 040 (2070)	31 320 (2730)
trans-$[OsCl_2(PMe_3)_4]^+$	18 910 (1590)	30 940 (2790)
trans-$[OsBr_2(AsMe_3)_4]^+$ [c]	17 500 (7050), 19370 (960)	27 140 (3680)
trans-$[OsBr_2(AsMe_2Ph)_4]^+$	16 540 (1560)	27 400 (590)

[a] Recorded in CH_2Cl_2 containing 0.5 mol dm^{-3} $[Bun_4N][BF_4]$ at 213 K. [b] All $\sigma(L) \rightarrow M$ CT bands have a high energy shoulder. [c] See Fig. 5.12.

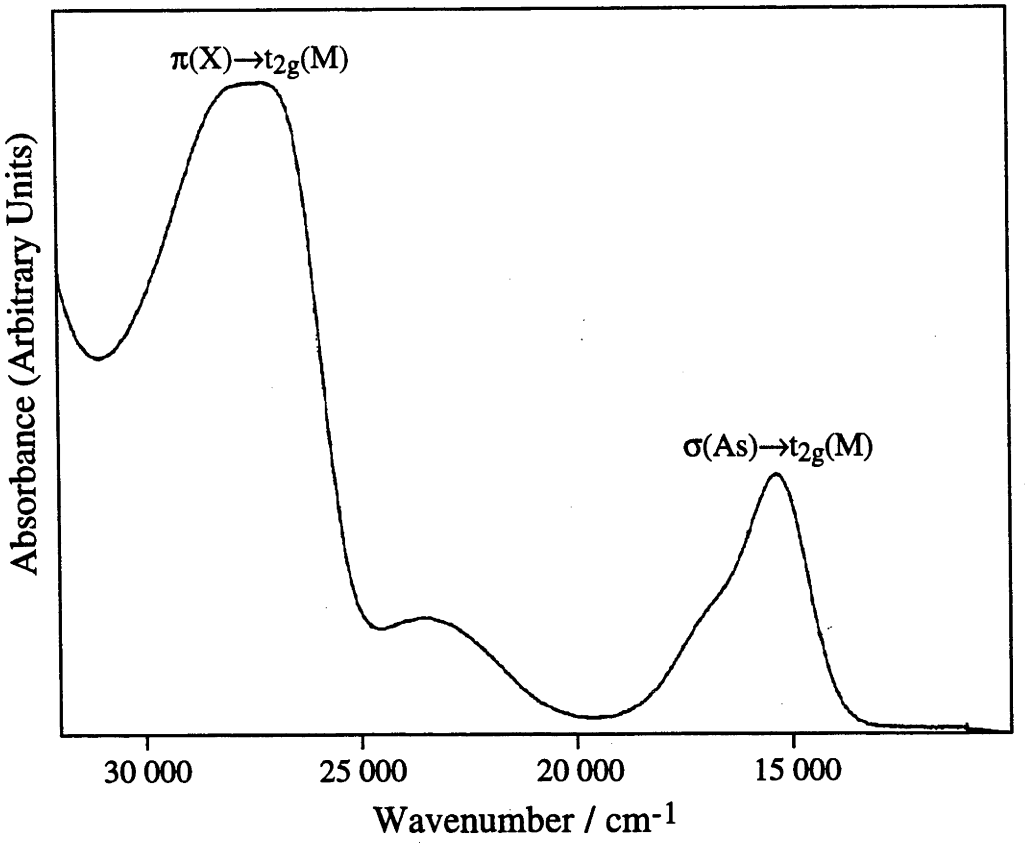

Figure 5.13 *UV/Vis spectrum of trans-$[RuCl_2(AsMe_3)_4]^+$, recorded in $CH_2Cl_2/[Bu^n_4N][BF_4]$ (0.5 mol dm^{-3}) at 213 K.*

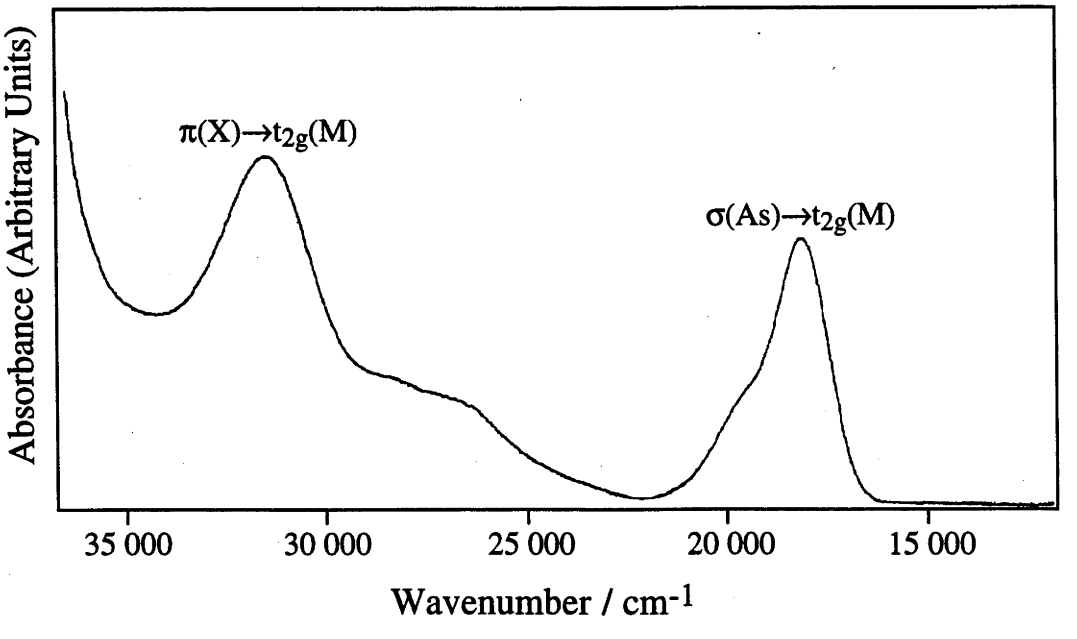

Figure 5.14 *UV/Vis spectrum of trans-$[OsCl_2(AsMe_2Ph)_4]^+$, recorded in $CH_2Cl_2/[Bu^n_4N][BF_4]$ (0.5 mol dm^{-3}) at 213 K.*

5.4.5 Spectra of Other Complexes

The $[M^{III}Cl(AsMe_3)_5]^{2+}$ complexes were generated electrochemically, in the OSTLE cell, in CH_3CN solution, rather than CH_2Cl_2 (Fig. 5.15 and 5.16). Whilst these M^{III} complexes were sufficiently soluble in CH_2Cl_2 to give a fully reversible voltammetric response, the dication precipitated upon bulk electrogeneration in the OSTLE cell.

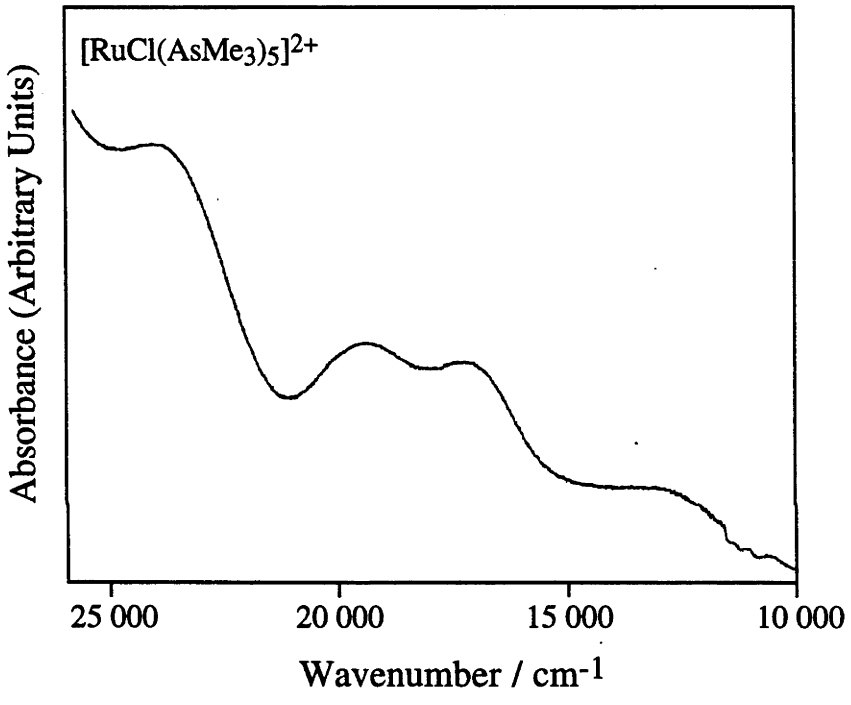

Figure 5.15 *UV/Vis spectrum of* $[RuCl(AsMe_3)_5]^{2+}$, *recorded in* $CH_3CN/[Bu^n_4N][BF_4]$ *(0.1 mol* dm^{-3}*) at 243 K.*

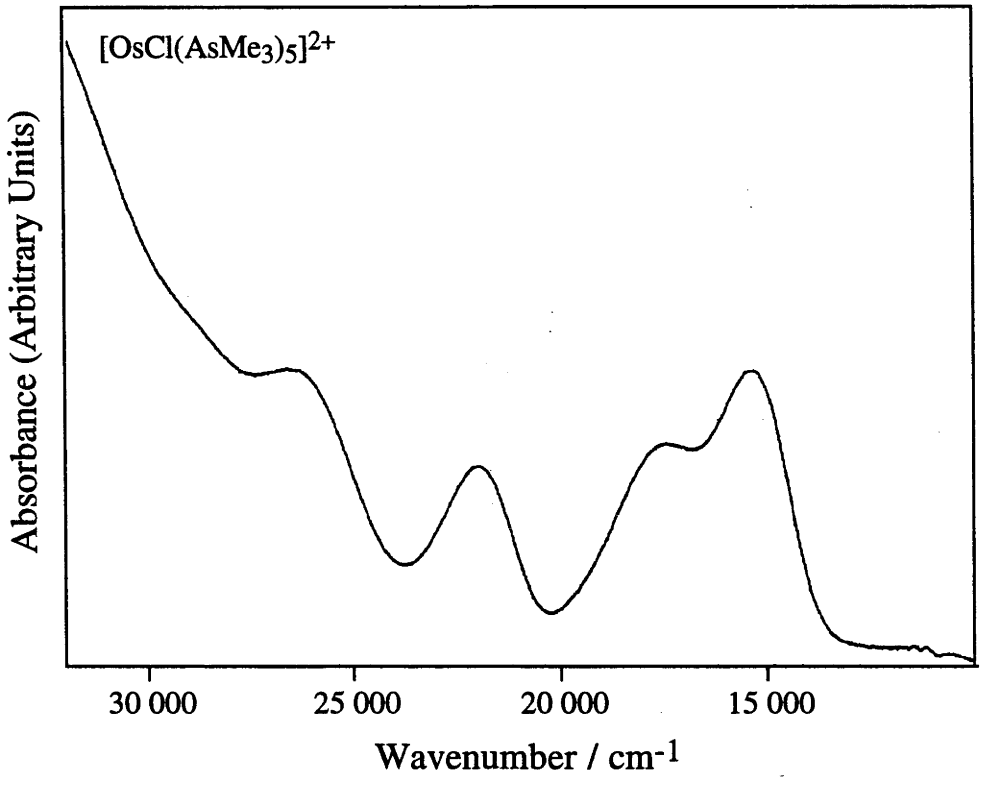

Figure 5.16 *UV/Vis spectrum of* $[OsCl(AsMe_3)_5]^{2+}$, *recorded in* $CH_3CN/[Bu^n_4N][BF_4]$ *(0.1 mol* dm^{-3}*) at 243 K.*

The complexities of the charge-transfer spectra are increased upon departure from D_{4h} symmetry. For example, replacing one axial chloride of *trans*-$[MCl_2(AsMe_3)_4]^+$ to give $[MXL_5]^{2+}$ retains the equatorial {4 x $AsMe_3$} arrangement, however the lack of a centre of symmetry corresponds with the emergence of more bands. Four transitions are observed, the one with highest energy clearly being XMCT and the remainder being As→M CT, or possibly charge-transfer transitions from mixed X/As orbitals.

Table 5.10 *UV/Vis Spectral Data for* $[MCl(AsMe_3)_5]^{2+}$ *Complexes.*

Complex	ν_{max} / cm^{-1} (ε / $dm^3\ mol^{-1}\ cm^{-1}$) [a]	
	$\sigma(L) \rightarrow t_{2g}(M)$	$\pi(X) \rightarrow t_{2g}(M)$
$[RuCl(AsMe_3)_5]^{2+}$	13 000 (290) 17 250 (680) 19 330 (740)	24 040 (1350)
$[OsCl(AsMe_3)_5]^{2+}$	15 400 (550) 17 390 (390) 22 020 (340)	26 640 (550)

[a] *Recorded in* CH_3CN *containing* $[Bu^n_4N][BF_4]$ *(0.1 mol* dm^{-3}*) at 213 K.*

The complications upon departure from D_{4h} symmetry are also highlighted in the optical spectra of *mer*-$[MX_3L_3]$ complexes, where three bands are observed in the visible region. The lowest and highest bands are essentially $\sigma(L)$ and $\pi(X)$ to $t_{2g}(M^{III})$ charge-transfer respectively, and the intermediate band involves mixed X/L donor orbitals.[41,46,47] Similarly, the optical spectra of the *cis*-$[MX_2L_4]^+$ systems are more complex than the *trans*-$[MX_4L_2]^-$ and *trans*-$[MX_2L_4]^+$ spectra. Also, many of the transitions from mixed orbitals are of similar energy and intensity to the weak d-d bands, as shown in the M^{II} complexes. Consequently the spectra of these complexes are not discussed in detail here.

An important and as yet unknown compound in the complete series would be homoleptic $[Os^{III}(AsMe_3)_6]^{3+}$, where the problems of X-As mixing would be removed, resulting in charge-transfer from pure arsine-based orbitals. Such a hypothetical complex, which would normally exist as the Os^{II} cation, would hopefully not have an impossibly high potential for spectro-electrochemical oxidation to the Os^{III} state (see §5.7).

5.4.6 Trends in Charge-Transfer Spectra of M^{III} (d^5) Systems

The energies of arsine (or phosphine)-to-metal and halide-to-metal charge transfer bands are collected in Table 5.11. For $[MCl(AsMe_3)_5]^{2+}$ and *trans*-$[MX_2L_4]^+$ systems, the lowest energy bands are listed, as these bands are most likely to be "pure" As→M charge-transfer.

Table 5.11 *Comparison of σ(L) and π(X) to Metal Charge-Transfer Bands in* $[MCl_{6-n}L_n]^{z+}$ *Complexes.*[a]

Complex	ν_{max} / cm^{-1} (ε / dm^3 mol^{-1} cm^{-1})		$E_{1/2}(M^{III/II})$
	σ(L) → t_{2g}(M)	π(X) → t_{2g}(M)	
$[RuCl_6]^{3-}$ *b*	-	30 500	-1.51
trans-$[RuCl_4(AsMe_3)_2]^-$	18 440	27 000	-0.65
trans-$[RuCl_2(AsMe_3)_4]^+$	15 600	28 140	+0.51
$[RuCl(AsMe_3)_5]^{2+}$	13 000	24 040	+1.40
$[OsCl_6]^{3-}$	-	37 000	-2.28
trans-$[OsCl_4(PMe_3)_2]^-$	22 400	31 700	-1.16
trans-$[OsCl_2(AsMe_3)_4]^+$	19 120	31 180	+0.13
$[OsCl(AsMe_3)_5]^{2+}$	15 400	26 600	+1.19

[a] Only the tetragonal systems (MX_4L_2, MX_2L_4, MXL_5) are shown. [b] Values from Ref. 45.

The data in this table show that the σ(L)→M charge-transfer band shifts to lower energy upon replacement of halides for arsine or phosphine ligands, as expected by the increasing ease of Ru^{III} reduction across this series. There is, however, no systematic shift in π(X)→M CT between $[MX_4L_2]^-$ and $[MX_2L_4]^+$, but further substitution leads to a sharp decrease in the XMCT energy. This is an interesting contrast to the structurally related RCN substituted complexes,[42] where the position of the XMCT band steadily decreases in energy upon replacement of halides by nitrile ligands, and reflects the ease of reduction of the Ru^{III} ion. The invariance of the XMCT band in the arsine series suggests that the energy of the orbital involving the remaining halide donor orbitals decreases nearly as rapidly as the energy of the central metal ion, making the difference between the two nearly constant.

5.4.7 Comparisons with Optical Spectra of Binuclear Complexes.

The charge-transfer spectra of monomeric complexes discussed in this section have highlighted the complexities involved in the interpretation of such spectra. Even the relatively simple spectra of *fac*-$[OsCl_3(PR_3)_3]$ complexes,[41,50] which as a class show a $\sigma(P)\rightarrow t_{2g}(Os)$ charge-transfer band near 19 000 cm^{-1} and $\pi(Cl)\rightarrow t_{2g}(Os)$ near 32 700 cm^{-1} and resemble energetically the $[OsCl_2L_4]^+$ systems (Table 5.9), cannot adequately model the more intricate UV/Visible spectra of $[Os_2(\mu\text{-}Cl)_3(PR_3)_6]^{2+}$ complexes. The latter have a broad band near 18 000 cm^{-1}, likely to be P→M CT as in the *fac* monomer, but the binuclear complex also has higher energy bands not observed in the monomer. Rather than relying on *fac*-$[OsX_3(PR_3)_3]$ complexes as the sole comparison for binuclear complexes, a better model would be a hypothetical $[Os(0.5X)_3(PR_3)_3]^{1.5+}$ complex, where the sharing of the bridging halides with the second Os centre is taken into account. This emphasises the value of the spectrum of the mixed-metal $[Ru^{II}Os^{III}(\mu\text{-}Cl)_3(PR_3)_6]^{2+}$ to model an isolated Os^{III} site in the confacial bioctahedral environment. The best model for a Ru^{III} site in such a complex requires development of a system where the Ru^{III} ion is adjacent to a closed-shell non-interacting metal ion such as 11-e (d^5d^6) $\{Ru^{III}(\mu\text{-}X)_3Rh^{III}\}^{3+}$ or $\{Ru^{III}(\mu\text{-}X)_3Ir^{III}\}^{3+}$.

5.5 LIGAND ADDITIVITY

The concept of ligand additivity requires that individual ligands have a simple cumulative effect upon the electronic properties of a given complex. For example, in $[MX_{6-n}L_n]^z$ (L = AsR_3, PR_3), the electrode potentials become more positive upon increasing substitution of L in place of X, but can this effect be quantified or systematised?

In relation to central ion electrode potentials, Pickett *et al* established the concept of a ligand-specific parameter, P_L (defined by the shift in E° for the $Cr^{I/0}$ (d^5/d^6) couple as L' replaces L in $[Cr(CO)_5L]^+$), in order to quantify the overall electron-donor capabilities of a range of ligands replacing one another on a fixed binding site.[51] The P_L values define the effect of one displaceable ligand on a constant site ($[Cr(CO)_5L]^+$), and are not applicable to further substitution or different sites, unless the relative polarisability of the new site is defined. Since then, the possibility of correlating electrode potentials with HOMO energies has been developed, and was the subject of a review by Bursten and Green.[3] This relies on an Angular Overlap Model (AOM) analysis of the effect of the ligand assembly on the HOMO in passing along a substitutional series. Bursten's treatment assumes a fixed contribution from each ligand regardless of the stoichiometry or the identity of the co-ligands. Recently, Lever defined ligand parameters, E_L (derived from the $Ru^{III/II}$ couple in $[Ru(bpy)_nL_{6-2n}]^{z+}$ complexes), for over 200 ligands,[4] and suggested these parameters can be used to predict redox potentials for a given metal ion containing *any* combination of these ligands coordinated on a given metal ion. The difference between P_L and E_L should be emphasised; P_L values are rigorously restricted to introduction of *one* displaceable ligand on a *constant site*, and are not applicable to further substitution or to different sites unless the polarisability of the new site is parameterised, whereas the E_L parameter is suggested to be transferable to a wide range of metal sites. More recently, Heath and Humphrey have shown that Lever's model is

not applicable for all systems,[2] essentially through its explicit neglect of variation in polarisability of the binding site in a sequentially substituted series.

Moreover, Lever's ligand additivity model generally disregards a correction factor for different isomers, which was originally developed by Bursten[52] to explain the different redox potentials of isomeric pairs of low-spin d^5/d^6 and also of d^0/d^1 complexes. This distinction emerges naturally under AOM theory. Lever's model acknowledges the work of Bursten, but gives no correction terms for ligands other than CO and RNC, and the corrections given for these ligands are specific to particular metals and redox couples. Lever recommends no correction for the $Ru^{III/II}$ couple, and all of his $Ru^{III/II}$ data are fitted to the basic additivity equation which ignores *cis-trans* and *mer-fac* isomerism.

Bursten argued that the relative energy of the redox-active t_{2g} orbital (the HOMO) depends only on the number of each ligand interacting π-wise with the HOMO, and that these individual contributions are arithmetically additive.[52] In a series of complexes $[MX_{6-n}L_n]$, where X is a poorer π-accepting ligand than L, $E_{1/2}$ was predicted to vary with n (an isotropic, electrostatic effect) and with x_{HOMO}, where x is the number of ligands L suitably positioned to interact π-wise with the redox-active orbital:

$$E_{1/2} = A + B\,n + C\,x_{HOMO} \qquad (5.1)$$

Here, A is characteristic of the metal and its oxidation state, B measures the isotropic effect of changing a single X for L upon M, and C measures the difference in the π-bonding interaction of X and L with the uppermost (redox-active) t_{2g}-based orbital. For such a series, the predicted $E_{1/2}$ values are listed in Table 5.12. In the complexes under investigation in this Chapter, L = AsR_3 or PR_3 and X = Cl or Br. Bursten employed the symbols L and L' for L and X respectively.

Table 5.12 *Predicted $E_{1/2}$ Values for a Series of $MX_{6-n}L_n$ Compounds, where X is a poorer π-acceptor than L.*[52]

Compound	n	x_{HOMO}	Predicted E_L
MX_6	0	0	A
MX_5L	1	0	A + B
trans-MX_4L_2	2	0	A + 2B
cis-MX_4L_2	2	1	A + 2B + C
mer-MX_3L_3	3	1	A + 3B + C
fac-MX_3L_3	3	2	A + 3B + 2C
trans-MX_2L_4	4	2	A + 4B + 2C
cis-MX_2L_4	4	2	A + 4B + 2C
MXL	5	3	A + 5B + 3C
ML_6	6	4	A + 6B + 4C

From this analysis, a plot of $E_{1/2}$ vs n should be linear with slope B for the truncated series n = 0, 1 and *trans*-2. Similarly, for n = *mer*-3, 4, 5 and 6 the plot should be linear with slope B + C. For n = 4, it is predicted that both *cis* and *trans* isomers of $[RuX_2L_4]$ interact equally with the redox-active orbital, and therefore they should have the same electrode potentials.

Table 5.13 *Electrochemical Data for $[MCl_{6-n}L_n]^{z/z-}$ Complexes.*[a]

	$[RuCl_{6-n}(CH_3CN)_n]^{z/z-}$		$[RuCl_{6-n}(AsMe_3)_n]^{z/z-}$		$[OsCl_{6-n}(AsMe_3)_n]^{z/z-}$	
n	IV/III	III/II	IV/III	III/II	IV/III	III/II
0	+0.22	-1.51	+0.22	-1.51	-0.37[b]	-2.28[b]
1	+0.82	(-0.95)[c]	-	-	-	-
trans-2	+1.45	-0.38	+0.99	-0.65	+0.49[d]	-1.16[c]
mer-3	+1.89	+0.29	+1.34	+0.11	+0.99	-0.41
trans-4	-	+0.84	+1.70	+0.48	+1.44	+0.13
cis-4	-	-	-	+0.79	-	-
5	-	(+1.40)[c]	-	+1.40	-	+1.19

[a] *Data from Tables 5.3, 5.4 or Ref. 1.* [b] *Values are for $[OsBr_6]^{2-}$, from Ref. 2.* [c] *These values have been extrapolated from other points in the linear series, assuming $E_L(CH_3CN)$ = +0.34 V and $E_L(Cl)$ = -0.22 V.* [d] *Values for $[OsCl_4(PMe_3)_2]$, but we do not expect much difference for $[OsCl_4(AsMe_3)_2]$.*

Firstly, let us consider the region where n = 0, 1 and *trans*-2. A useful comparison is with the $[Ru^{III}Cl_{6-n}(MeCN)_n]^{(n-3)}$ series,[1,42] as E_L for MeCN and $AsMe_3$ are likely to be almost the same, and the MeCN series gives a linear correlation of $E_{1/2}$ vs n.‡ (Inspection of Table 5.13 shows that for the $AsMe_3$ series, the $Ru^{IV/III}$ and $Ru^{III/II}$ $E_{1/2}$ values are lower than in the MeCN series, *i.e.* lower than predicted. Without data for $[RuCl_5(AsMe_3)]^z$ (n = 1) we cannot say whether the n = 0, 1 and *trans*-2 series is linear upon successive substitution of Cl for $AsMe_3$, with a steady but anomalously low shift of $E_{1/2}$, of if the progression in $E_{1/2}$ will prove to be non-linear. An example of non-additivity is the iso-electronic series $[OsBr_6]^{2-} \rightarrow [OsBr_5(CO)]^- \rightarrow$ *trans*-$[OsBr_4(CO)_2]$, where there is a shift of +1.8 V for the first substitution, but only 0.63 V for the second step.[2] The lower shift of $E_{1/2}$ upon second substitution is due to the two *trans* π-acceptor carbonyl ligands "competing" for the same d_π electrons, with the result that the net effect of the two CO ligands is severely attenuated. We suspect that a similar, although not so dramatic, effect is observed in the $AsMe_3$ series, leading to lower than anticipated oxidation potentials. It is likely (see below) that the n = 1 datum lies ~0.15 V above the dashed line shown in Fig. 5.17 (at ~ -0.95 V for $Ru^{III/II}$) but that the second substitution shifts $E_{1/2}$ by only 0.43 V, rather than the 2 x 0.55 V shift for a stepwise linear progression.

Looking at further substitution of $AsMe_3$ (Fig. 5.17), it is most noticeable that the *cis*- and *trans*-$[RuCl_2(AsMe_3)_4]$ complexes have different $Ru^{III/II}$ electrode potentials. This contradicts both Bursten's model, which takes into account symmetry-differentiated π-covalency and nevertheless predicts equal E° values for *cis*- and *trans*-$[MX_2L_4]$, and Lever's model which explicitly ignores geometric dependence (other than for isonitrile and carbonyl ligands). In our view this is the result of the *trans* arrangement of the arsine ligands. Because they are competing with each other, the redox-active orbitals are not

‡ The difference between E_L(MeCN) and $E_L(PMe_3)$ is listed as 0.01 V, and we expect $E_L(AsMe_3)$ to be similar to $E_L(PMe_3)$.

stabilised by the π-acceptor ligands to the same extent as in the *cis* isomer, and therefore the $Ru^{II} \rightarrow Ru^{III}$ oxidation becomes easier.

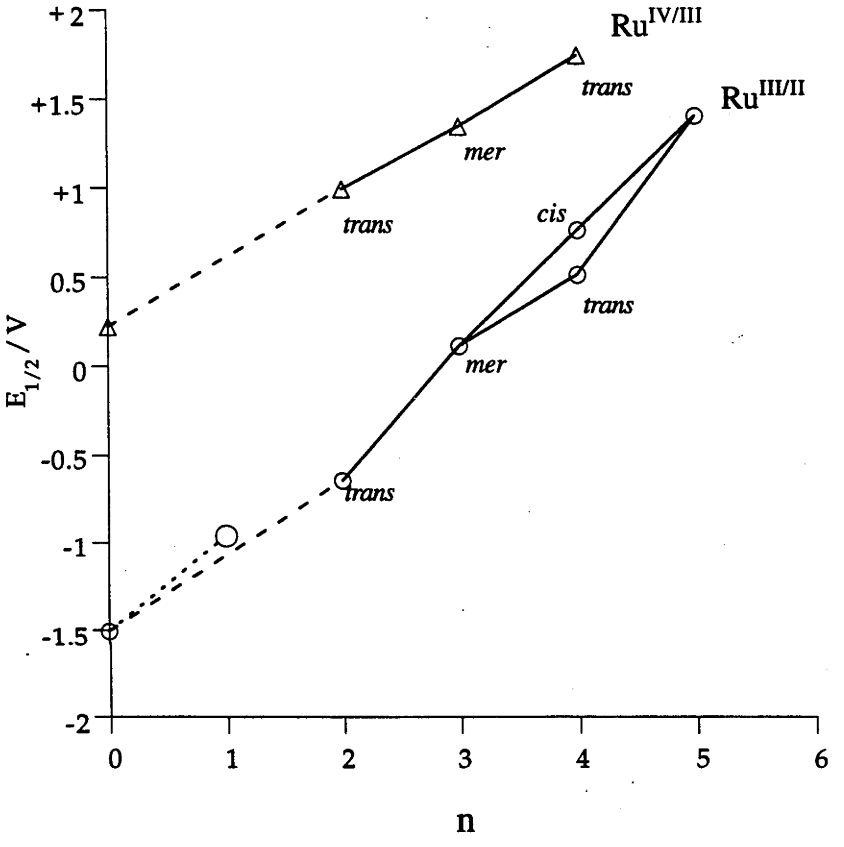

Figure 5.17 *Plot of $E_{1/2}$ vs n for $[RuCl_{6-n}(AsMe_3)_n]^{z/z-}$. It should not be assumed that the unknown couples for n = 1 lie on the dashed line. The large circle for n = 1 represents the predicted postion of $E_{1/2}$ for $E_L(AsMe_3)$ = +0.33 V and $E_L(Cl)$ = -0.22 V.*

The systematic non-linearity of $E_{1/2}$ vs n for these complexes is further confirmed and emphasised in the analogous osmium series. As explained, the currently accepted models predict the plot for *mer*-3, 4, 5 and 6 should be linear (Table 5.12), but it is clear from Fig. 5.17 that this is not so. It can also be seen that $E_{1/2}$ values for analogous ruthenium and osmium complexes converge as further arsine ligands are incorporated, and are *not* separated by a constant value of 0.4 V as suggested by Lever. The increased substitution of π-acid AsR_3 or PR_3 ligands leads to increased covalency of the metal d-

electrons, hence the redox-active electrons are less metal-based, and less susceptible to changes in ionisation energy related to the identity of the metal.

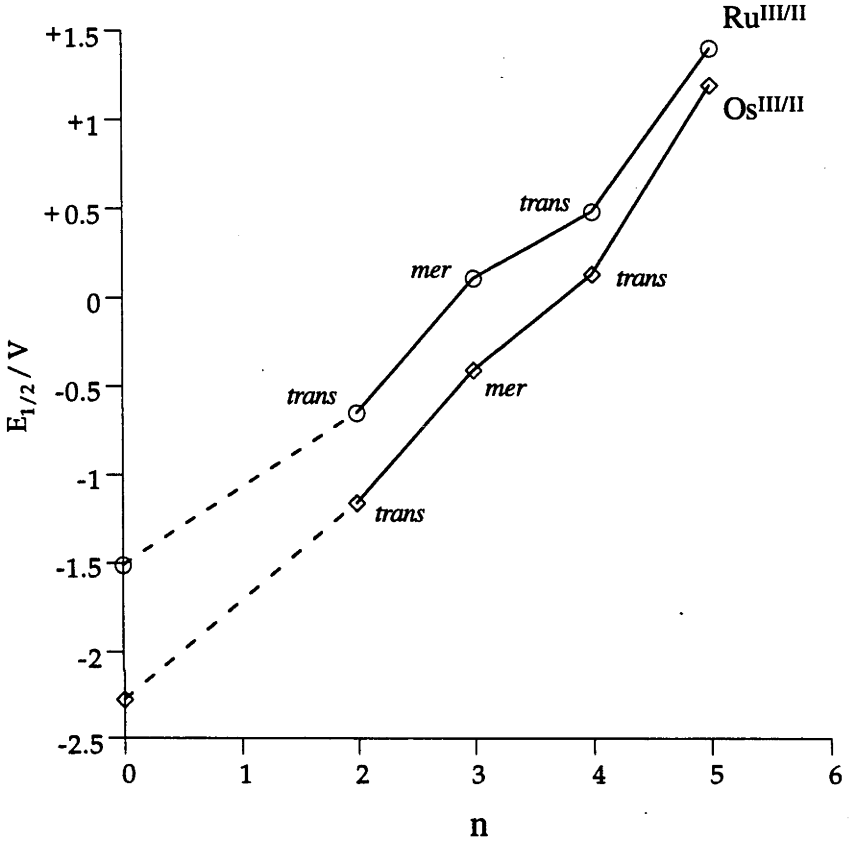

Figure 5.18 *Plot of $E_{1/2}$ vs n for $[MCl_{6-n}(AsMe_3)_n]^{z/z-}$ (M = Ru, Os).*

5.6 FUTURE WORK ON MONOMERS

This ligand-additivity story would be much improved by achieving the synthesis of both $[M^{III}X_5(AsR_3)]^{2-}$ and $[M^{II}(AsR_3)_6]^{2+}$, and oxidising the latter to the $[M^{III}(AsR_3)_6]^{3+}$, where the problem of halide/arsine electronic mixing is removed. The preparation of $[RuCl_5(PhCN)]^{2-}$,[42] by reduction of $[RuCl_6]^{2-}$ in the presence of PhCN, may provide a model for the formation of $[RuCl_5(AsMe_3)]^{2-}$. The preparation of $[OsCl(AsMe_3)_5]^{+}$ is very encouraging and invites attempts at halide abstraction to eventually isolate $[Os^{II}(AsMe_3)_6]^{2+}$.

5.7 EXPERIMENTAL

5.7.1 General

Ruthenium and osmium starting materials were prepared as described in §2.2 and liquid zinc amalgam according to standard procedures.[53] All reactions were carried out under N_2, but the products were handled in air. Microanalytical data for new complexes are listed in Table 5.14.

5.7.2 *trans*-$[M^{III}X_4L_2]^-$

trans-$[RuX_4L_2]^-$

The *trans*-$[RuX_4L_2]^-$ compounds were prepared previously in this laboratory, using the method described by Stephenson.[6] This procedure involved stirring *trans*-$[RuX_4(AsPh_3)_2]^-$ or *trans*-$[RuX_4(PPh_3)_2]^-$ with neat phosphine or arsine for several days. The compounds were isolated as either $[PPh_4]^+$ or $[AsPh_4]^+$ salts, in quantitative yield.

5.7.3 *trans*-$[M^{IV}X_4L_2]$

trans-$[OsCl_4(PMe_3)_2]$

To a solution containing OsO_4 (0.25 g, 1.0 mmol) in ethanol (25 cm^3) was added PMe_3 (0.27 g, 3.5 mmol) and conc. HCl (1 cm^3), and the solution was heated to reflux for 2 h. The solution was cooled, filtered and refrigerated (4 °C) for 7 days, after which time dark green needles of *trans*-$[OsCl_4(PMe_3)_2]$ were collected and washed with cold ethanol. Yield: 87 mg (18 %).

5.7.4 *mer*-$[M^{III}X_3L_3]$

mer-$[RuCl_3(PMe_2Ph)_3]$

This compound was prepared by the literature method,[10] heating an ethanol/conc. HCl (10:1 v/v) solution containing "$RuCl_3.xH_2O$" and PMe_2Ph for 5 min.

mer-[OsX$_3$L$_3$] (X = Cl; L = AsMe$_3$, AsMe$_2$Ph, AsMePh$_2$)

These complexes were prepared by the standard method for similar complexes,[41] heating OsO_4 and L in ethanol/conc. HCl (10:1 v/v) for 2 h. The desired complexes precipitated upon evaporation of the solvent. Typical yields were ~50%.

5.7.5 *trans*-[M^{II}X$_2$L$_4$]

trans-[RuCl$_2$(AsMe$_3$)$_4$]

METHOD A: To dichloromethane (50 cm^3) was added [Bu$^n_4$N]$_3$[Ru$_2$Cl$_9$] (0.18 g, 0.14 mmol), $AsMe_3$ (0.17 g, 1.42 mmol) and zinc amalgam (5 g). The mixture was heated at reflux for 19 h, then filtered through celite to give an orange solution. The solvent was removed *in vacuo* to leave an orange residue, which was recrystallised from hot hexane. Yield of *trans*-[$RuCl_2(AsMe_3)_4$]: 64 mg (34%).

METHOD B: A mixture of [PPh_4][$RuCl_4(AsMe_3)_2$] (0.20 g, 0.23 mmol), $AsMe_3$ (0.10 g, 0.83 mmol) and amalgamated zinc (5 g) were added to dichloromethane (30 cm^3), and heated at reflux for 16 h. The solution was filtered through celite and the filtrate evaporated to dryness *in vacuo*. The residue was recrystallised from hot hexane to produce orange crystalline *trans*-[$RuCl_2(AsMe_3)_4$]. Yield: 40 mg (27%).

trans-[RuCl$_2$(AsMe$_2$Ph)$_4$]

This compound was prepared by heating [Bu$^n_4$N]$_3$[Ru$_2$Cl$_9$] (0.20 g, 0.16 mmol), $AsMe_2Ph$ (0.25 g, 1.37 mmol) and amalgamated zinc (5 g) in dichloromethane (50 cm^3) for 17 h. The solution was filtered through celite and the solvent evaporated to dryness *in vacuo*. The residue was dissolved in a minimal volume of dichloromethane and passed through an alumina (activity I) column, eluting the pink band with dichloromethane. The solvent was evaporated *in vacuo* and the residue was stirred with a small volume of hexane to give an orange-pink powder, which was collected and washed with hexane. Yield of *trans*-[$RuCl_2(AsMe_2Ph)_4$]: 0.15 g (53%).

trans-[$RuCl_2(PMe_3)_4$]

To a suspension of [$RuCl_2(PPh_3)_3$] (0.48 g, 0.50 mmol) in ethanol (60 cm^3) was added PMe_3 (0.16 g, 2.1 mmol). The mixture was then heated at reflux for 16 h, producing a yellow solution. The solvent was removed *in vacuo* to give a yellow residue which was purified by chromatography on alumina, eluting with dichloromethane. Evaporation of the solvent yielded a yellow powder, which was collected and washed with hexane. Yield: 1.03 g (87%).

trans-[$RuBr_2(AsMe_3)_4$]

METHOD A: This compound was prepared by the method described for *trans*-[$RuCl_2(AsMe_2Ph)_4$], heating [$Bu^n_4N]_3[Ru_2Br_9$] (0.15 g, 0.091 mmol), $AsMe_3$ (0.10 g, 0.83 mmol) and amalgamated zinc (5 g) in dichloromethane (40 cm^3) for 16 h. Following column chromatography and evaporation of the solvent, the residue was recrystallised from hot methanol. Yield of *trans*-[$RuBr_2(AsMe_3)_4$]: 60 mg (50%).

METHOD B: A mixture of [$AsPh_4$][$RuBr_4(AsMe_3)_2$] (0.20 g, 0.19 mmol), $AsMe_3$ (0.10 g, 0.83 mmol) and amalgamated zinc (5 g) were added to dichloromethane (40 cm^3), and heated at reflux for 1 h. The solution was filtered through celite and the filtrate evaporated to dryness *in vacuo*. The residue was recrystallised from methanol/petroleum spirit (80 - 100 °C) to produce pink crystals of *trans*-[$RuBr_2(AsMe_3)_4$]. Yield: 70 mg (50%).

trans-[$RuBr_2(AsMe_2Ph)_4$]

This compound was prepared by the method described for *trans*-[$RuCl_2(AsMe_2Ph)_4$], heating [$Bu^n_4N]_3[Ru_2Br_9$] (0.17 g, 0.10 mmol), $AsMe_2Ph$ (0.20 g, 1.1 mmol) and amalgamated zinc (5 g) in dichloromethane (30 cm^3) for 22 h. Following column chromatography, the residue was stirred with a small volume of methanol to yield a pink powder, which was collected and washed with cold methanol. Yield of *trans*-[$RuBr_2(AsMe_2Ph)_4$]: 0.11 g (56%).

trans-[RuBr$_2$(PMe$_3$)$_4$]

This compound was prepared by the method described for *trans*-[RuCl$_2$(AsMe$_2$Ph)$_4$], heating [Bu$^n_4$N]$_3$[Ru$_2$Br$_9$] (0.30 g, 0.18 mmol), PMe$_3$ (0.20 g, 2.7 mmol) and amalgamated zinc (5 g) in dichloromethane (50 cm^3) for 3 h. Following column chromatography, the residue was stirred with a small volume of methanol to yield a yellow powder, which was collected and washed with cold methanol. Yield of *trans*-[RuBr$_2$(PMe$_3$)$_4$]: 0.14 g (69 %).

trans-[OsCl$_2$(PMe$_3$)$_4$]

To a suspension of [OsCl$_2$(PPh$_3$)$_3$] (0.25 g, 0.24 mmol) in 2-methoxyethanol (30 cm^3) was added PMe$_3$ (0.10 g, 1.3 mmol) and the mixture heated at reflux until the solution was yellow in colour (~2 h). The solvent was evaporated to ~ 2 cm^3 *in vacuo* to precipitate *trans*-[OsCl$_2$(PMe$_3$)$_4$] as a yellow powder, which was collected and washed with cold diethyl ether. Yield: 57 mg (42%).

trans-[OsBr$_2$(AsMe$_2$Ph)$_4$]

To [NH$_4$]$_2$[OsBr$_6$] (0.15 g, 0.21 mmol) and AsMe$_2$Ph (0.25 g, 1.4 mmol) in methanol (10 cm^3) was added zinc amalgam (5 g) and the mixture heated at reflux for 16 h. A yellow precipitate (*trans*-[OsBr$_2$(AsMe$_2$Ph)$_4$]) which had formed was collected and washed with methanol. Yield: 0.16 g (70%).

5.7.6 *trans*-[M^{III}X$_2$L$_4$]$^+$

trans-[RuCl$_2$(AsMe$_3$)$_4$]PF$_6$

To a solution of *trans*-[RuCl$_2$(AsMe$_3$)$_4$] (49 mg, 75 μmol) in freshly distilled dichloromethane (10 cm^3) was added excess NOPF$_6$ and the solution stirred at room temperature for 1 h. The solution was filtered and then evaporated to dryness *in vacuo*. The resulting residue was recrystallised from acetone/diethyl ether. Yield of *trans*-[RuCl$_2$(AsMe$_3$)$_4$]PF$_6$: 26 mg (43%).

trans-[$RuCl_2(AsMe_2Ph)_4$]PF_6

This compound was prepared by the method described for *trans*-[$RuCl_2(AsMe_3)_4$]PF_6, in 75 % yield.

trans-[$RuBr_2(AsMe_3)_4$]PF_6

This compound was prepared by the method described for *trans*-[$RuCl_2(AsMe_3)_4$]PF_6, in 75% yield.

trans-[$OsCl_2(AsMe_2Ph)_4$]CF_3SO_3

Zinc amalgam (5 g) was added to a solution containing $Na_2[OsCl_6]$ (0.15 g, 0.33 mmol) and $AsMe_2Ph$ (0.30 g, 1.7 mmol) in ethanol/conc. HCl (4:1 v/v, 10 cm^3), and the solution was heated at reflux for 16 h. The solution was filtered through celite to give a pink filtrate, which was evaporated to dryness *in vacuo*. The residue was dissolved in dichloromethane (5 cm^3), CF_3SO_3H (0.1 mol dm^{-3}) in methanol (2 cm^3, 0.2 mmol) was added, and the mixture was heated at reflux for 8 h. The solvent was evaporated *in vacuo* and the purple residue recrystallised from dichloromethane/diethyl ether to give crystals of *trans*-[$OsCl_2(AsMe_2Ph)_6$]CF_3SO_3. Yield: 50 mg (13%).

trans-[$OsBr_2(AsMe_3)_4$]CF_3SO_3

To methanol (10 cm^3) was added $[NH_4]_2[OsBr_6]$ (0.15 g, 0.21 mmol) and $AsMe_3$ (0.30 g, 3.5 mmol), and the mixture heated at reflux for 16 h. The solvent was evaporated *in vacuo* and the residue dissolved in dichloromethane (10 cm^3), CF_3SO_3H (0.1 mol dm^{-3}) in methanol (4 cm^3, 0.4 mmol) added, and heated at reflux for 20 h. The solvent was evaporated *in vacuo* and the residue recrystallised from acetone/diethyl ether to give purple crystals of *trans*-[$OsBr_2(AsMe_3)_4$]CF_3SO_3. Yield: 42 mg (20%).

5.7.7 *cis*-[$M^{II}X_2L_4$]

cis-[$RuCl_2(AsMe_3)_4$]

To "$RuCl_3.xH_2O$" (0.10 g, 0.42 mmol) in a solution of ethanol/conc. HCl (20 cm^3, 20:1 v/v) was added $AsMe_3$ (0.30 g, 2.5 mmol), and the solution heated at reflux for 48 h. The solvent was reduced to ~3 cm^3 *in vacuo* and sufficient water added dropwise to precipitate *trans*-[$RuCl_2(AsMe_3)_4$], which was collected. The filtrate was evaporated to dryness *in vacuo* and the *cis* isomer was extracted into diethyl ether. Upon partial evaporation of diethyl ether, yellow crystalline *cis*-[$RuCl_2(AsMe_3)_4$] precipitated. Yield: 80 mg (29%).

cis-[$RuCl_2(AsMe_2Ph)_4$]

To a solution of [PPh_4][$RuCl_4(AsMe_2Ph)_2$] (0.27 g, 0.27 mmol) in dichloromethane (25 cm^3) was added $AsMe_2Ph$ (0.15 g, 0.82 mmol) and zinc amalgam (5 g). The mixture was heated at reflux for 2 h, filtered through celite and the solvent removed from the filtrate *in vacuo*. The residue was dissolved in hot methanol, and orange crystals of *cis*-[$RuCl_2(AsMe_2Ph)_4$] formed upon cooling the solution. Yield: 50 mg (21%).

cis-[$RuCl_2(PMe_2Ph)_4$]

Prepared by the method of Yellowlees *et al*,[34] heating *mer*-[$OsCl_3(PMe_2Ph)_3$] and PMe_2Ph in 2-methoxyethanol for 30 min.

cis-[$RuBr_2(AsMe_2Ph)_4$]

To a mixture of ethanol (45 cm^3) and distilled water (15 cm^3) was added $K_3[Ru_2Br_9]$ (0.30 g, 0.29 mmol) and $AsMe_2Ph$ (0.50 g, 2.7 mmol), and the mixture was heated at reflux for 16 h. The yellow precipitate which had formed was collected and washed with diethyl ether. Yield of *cis*-[$RuBr_2(AsMe_2Ph)_4$]: 0.16 g (28%).

cis-[$OsCl_2(AsMe_2Ph)_4$]

To a suspension of [$OsCl_2(PPh_3)_3$] in ethanol (25 cm^3) was added $AsMe_2Ph$ (0.10 g, 0.55 mmol). The mixture was heated at reflux for 16 h and the solvent evaporated in vacuo. Diethyl ether was added to the residue, and a yellow precipitate was collected and washed with diethyl ether. Yield of *cis*-[$OsCl_2(AsMe_2Ph)_4$]: 50 mg (37%).

5.7.7 $[M^{II}XL_5]^+$

[$RuCl(AsMe_3)_5$]CF_3SO_3

Commercial "$RuCl_3.xH_2O$" (0.10 g, 0.41 mmol) and $AsMe_3$ (0.5 g, 4.2 mmol) were dissolved in ethanol (40 cm^3) and heated at reflux for 70 h, at which point the solution was yellow-orange in colour. The solvent was removed *in vacuo* and the residue dissolved in dichloromethane (5 cm^3). A solution of CF_3SO_3H (0.1 mol dm^{-3}) in methanol (4 cm^3, 0.4 mmol) was added, and the mixture heated gently at reflux for 3 h. The solvent was removed *in vacuo* and the residue dissolved in minimal acetone. Diethyl ether was added until the solution started became cloudy, at which point it was refrigerated for several days. Pale green crystals of [$RuCl(AsMe_3)_5$]CF_3SO_3 were collected and washed with diethyl ether. Yield: 30 mg (17%). Several attempts to obtain more material by repetition of this procedure have been unsuccessful but the constitution of the orginal sample has been confirmed by X-ray crystallography.

[$OsCl(AsMe_3)_5$]CF_3SO_3

To a suspension of [$OsCl_2(PPh_3)_3$] (0.26 g, 0.25 mmol) in ethanol (40 cm^3) was added $AsMe_3$ (0.5 g, 4.2 mmol) and the mixture heated at reflux for 40 h. The solvent was removed *in vacuo* and the residue dissolved in dichloromethane (5 cm^3). A solution of CF_3SO_3H (0.1 mol dm^{-3}) in methanol (3 cm^3, 0.3 mmol) added, and heated gently at reflux for 16 h. The solvent was removed *in vacuo* and the pink residue recrystallised from dichloromethane/diethyl ether to give pink needles of [$OsCl(AsMe_3)_5$]CF_3SO_3. Yield: 0.13 g (54%).

Table 5.14 *Analytical data for monomeric ruthenium and osmium complexes.*

Complex	Analytical Data [a] (%)		
	C	H	Cl/Br
trans-$[RuCl_2(AsMe_3)_4]$	21.7 (22.1)	5.4 (5.6)	11.6 (10.9)
trans-$[RuCl_2(AsMe_2Ph)_4]$	42.5 (42.7)	4.6 (4.9)	8.0 (7.9)
trans-$[RuCl_2(PMe_3)_4]$	30.2 (30.3)	7.7 (7.6)	16.1 (14.9)
trans-$[RuBr_2(AsMe_3)_4]$	19.3 (19.5)	4.7 (4.9)	21.6 (21.6)
trans-$[RuBr_2(AsMe_2Ph)_4]$	38.1 (38.85)	4.4 (4.5)	16.2 (16.15)
trans-$[RuBr_2(PMe_3)_4]$	26.1 (25.5)	6.5 (6.4)	28.0 (28.3)
trans-$[RuCl_2(AsMe_3)_4]PF_6$	17.8 (18.1)	4.3 (4.55)	8.6 (8.9)
trans-$[RuBr_2(AsMe_3)_4]PF_6$	16.0 (16.3)	4.3 (4.1)	18.1 (18.0)
trans-$[RuCl_2(AsMe_2Ph)_4]PF_6$	36.5 (36.8)	4.2 (4.2)	7.0 (6.8)
cis-$[RuCl_2(AsMe_3)_4]$	22.2 (22.1)	6.0 (5.6)	10.9 (10.9)
cis-$[RuCl_2(AsMe_2Ph)_4]$	42.5 (42.7)	5.1 (4.9)	7.9 (7.9)
cis-$[RuBr_2(AsMe_2Ph)_4]$	38.2 (38.85)	4.5 (4.5)	16.2 (16.15)
$[RuCl(AsMe_3)_5]CF_3SO_3$	21.6 (21.7)	5.1 (5.1)	4.2 (4.0)
trans-$[OsCl_4(PMe_3)_2]$	14.7 (14.6)	3.5 (3.75)	
trans-$[OsCl_2(PMe_3)_4]$	24.9 (25.5)	6.7 (6.4)	
trans-$[OsBr_2(AsMe_2Ph)_4]$	39.3 (38.8)	4.2 (4.5)	
trans-$[OsCl_2(AsMe_2Ph)_4]CF_3SO_3$	34.8 (34.8)	3.8 (3.9)	6.4 (6.2)
trans-$[OsBr_2(AsMe_3)_4]CF_3SO_3$	15.8 (15.95)	3.5 (3.7)	
cis-$[OsCl_2(AsMe_2Ph)_4]$	36.7 (38.8)	4.8 (4.5)	
$[OsCl(AsMe_3)_5]CF_3SO_3$	19.7 (19.7)	4.5 (4.65)	4.0 (3.7)

[a] *Calculated values in parentheses.*

5.8 REFERENCES

1. C.M. Duff and G.A. Heath, *Inorg. Chem.*, 1991, **30**, 2528.
2. G.A. Heath and D.G. Humphrey, *J. Chem. Soc., Chem. Commun.*, 1991, 1668.
3. B.E. Bursten and M.R. Green, Prog. Inorg. Chem., 1988, **36**, 393.
4. A.B.P. Lever, *Inorg. Chem.*, 1990, **29**, 1271.
5. T.A. Stephenson and G. Wilkinson, *J. Inorg. Nucl. Chem.*, 1966, **28**, 945.
6. T.A. Stephenson, *J. Chem. Soc. (A)*, 1970, 889.
7. A. Hudson and M.J. Kennedy, *J. Chem. Soc. (A)*, 1969, 1116.
8. J. Chatt, G.J. Leigh and D.M.P. Mingos, *J. Chem. Soc. (A)*, 1969, 1674.
9. T.J. Khoo and G.A. Heath, unpublished work.
10. J. Chatt, G.J. Leigh, D.M.P. Mingos and R.J. Paske, *J. Chem. Soc. (A)*, 1968, 2636.
11. J.E. Armstrong and R.A. Walton, *Inorg. Chem.*, 1983, **22**, 1545.
12. R.A. Cipriano, W. Levason, R.A.S. Mould, D. Pletcher and M. Webster, *J. Chem. Soc., Dalton Trans.*, 1990, 339.
13. P.G. Douglas and B.L. Shaw, *J. Chem. Soc. (A)*, 1970, 334.
14. P.E. Fanwick, M.K. King, S.M. Tetrick and R.A. Walton, *J. Am. Chem. Soc.*, 1985, **107**, 5009.
15. P.E. Fanwick, I.F. Fraser, S.M. Tetrick and R.A. Walton, *Inorg. Chem.*, 1987, **26**, 3786.
16. D. Pawson and W.P. Griffith, *J. Chem. Soc., Dalton Trans.*, 1975, 417.
17. L. Aslonov, R. Mason, A.G. Wheeler and P.O. Whimp, *J. Chem. Soc., Chem. Commun.*, 1970, 30.
18. C.C. Hinkley, M. Matusz and P.D. Robinson, *Acta Crystallogr. Sect. C*, 1988, **44**, 371.
19. J. Chatt, B.L. Shaw and A.E. Field, *J. Chem. Soc.*, 1964, 3466.
20. M.M. Taqui Khan and K. Veera Reddy, *J. Coord. Chem.*, 1982, **12**, 71.

21. P.W. Armit, A.S.F. Boyd and T.A. Stephenson, *J. Chem. Soc., Dalton Trans.*, 1975, 1663.

22. J. Gotzig, R. Werner and H. Werner, *J. Organomet. Chem.*, 1985, **290**, 99.

23. A.R. Chakravarty, F.A. Cotton and W. Schwotzer, *Inorg. Chim Acta*, 1984, **84**, 179.

24. F.A. Cotton, M.P. Diebold and M. Matusz, *Polyhedron*, 1987, **6**, 1131.

25. R.L. Bennett, M.I. Bruce and F.G.A. Stone, *J. Organomet. Chem.*, 1972, **38**, 325.

26. W.H. Knoth, *J. Am. Chem. Soc.*, 1972, **94**, 104.

27. K.G. Srinivasamurthy, N.M. Nanje Gowda and G.K.N. Reddy, *J. Inorg. Nucl. Chem.*, 1977, **39**, 1977.

28. H. Singer, E. Hademer, U. Oehmichen and P. Dixneuf, *J. Organomet. Chem.*, 1979, **178**, C13.

29. S.D. Chappell, D.J. Cole-Hamilton, A.M.R. Galas and M.B. Hursthouse, *J. Chem. Soc., Dalton Trans.*, 1982, 1867.

30. B.R. James, D.K.W. Wang and R.F. Voigt, *J. Chem. Soc., Chem. Commun.*, 1975, 574.

31. F.P. Dwyer, J.E. Humpoletz and R.S. Nyholm, *J. Proc. R. Soc. N. S. W.*, 1946, **80**, 217.

32. R.A. Jones, F. Mayor Real, G. Wilkinson, A.M.R. Galas, M.B. Hursthouse and K.M.A. Malik, *J. Chem. Soc., Dalton Trans.*, 1980, 511.

33. B. Bell, J. Chatt and G.J. Leigh, *J. Chem. Soc., Dalton Trans.*, 1973, 997.

34. V.T. Coombe, G.A. Heath, T.A. Stephenson, J.D. Whitelock and L.J. Yellowlees, *J. Chem. Soc., Dalton Trans.*, 1985, 947.

35. N.R. Champness, W. Levason, R.A.S. Mould, D. Pletcher and M. Webster, *J. Chem. Soc., Dalton Trans.*, 1991, 2777.

36. A.S. Alves, D.S. Moore, R.A. Andersen and G. Wilkinson, *Polyhedron*, 1982, **1**, 83.

37. H. Werner and J. Gotzig, *J. Organomet. Chem.*, 1985, **284**, 73.

38. F.P. Dwyer, R.S. Nyholm and B.T. Tyson, *J. Proc. R. Soc. N.S.W.*, 1947, **81**, 272.

39. R.A. Contreras, G.A. Heath, A.J. Lindsay and T.A. Stephenson, *J. Organomet. Chem.*, 1979, **179**, C55.

40. N.R. Champness, C.S. Frampton, W. Levason and S.R, Preece, *Inorg. Chim. Acta*, 1995, **233**, 43.

41. R.A. Cipriano, W. Levason, R.A.S. Mould, D. Pletcher and M. Webster, *J. Chem. Soc., Dalton Trans.*, 1990, 2609.

42. C.M. Duff and G.A. Heath, *J. Chem. Soc., Dalton Trans.*, 1991, 2401.

43. K.G. Taylor and L.J. Yellowlees, in *Molecular Electrochemistry of Inorganic, Bioinorganic and Organometallic Compounds*, eds. A.J.L. Pombeiro and J.A. McCleverty, Kluwer Academic Publishers, Dordrecht, 1993, pp. 69-75.

44. C.K. Jørgensen, *Mol. Phys.*, 1959, **2**, 309.

45. C.K. Jørgensen, *Prog. Inorg. Chem.*, 1970, **12**, 101.

46. G.J. Leigh and D.M.P. Mingos, *J. Chem. Soc. (A)*, 1970, 587.

47. A.J. McCaffery and M.D. Rowe, *J. Chem. Soc., Faraday Trans. 2*, 1973, **69**, 1767.

48. G.A. Heath and D. Menglet, unpublished work.

49. E. Verdonck and L.G. Vanquickenborne, *Inorg. Chem.*, 1974, **13**, 762.

50. A.J. McCaffery and M.D. Rowe, *J. Chem. Soc., Faraday Trans. 2*, 1973, **69**, 1779.

51. J. Chatt, C.T. Kan, G.J. Leigh, C.J. Pickett and D.R. Stanley, *J. Chem. Soc., Dalton Trans.*, 1980, 2032.

52. B.E. Bursten, *J. Am. Chem. Soc.*, 1982, **104**, 1299.

53. G. Brauer, *Handbook of Preparative Inorganic Chemistry*, Academic Press, 2nd edn., 1965, vol. II, p. 1806.

CONCLUSIONS

During this work we have developed a reliable general synthetic route to triply-halide bridged binuclear complexes, $[Ru_2(\mu\text{-}X)_3L_6]^+$ (X = Cl, Br; L = AsR_3, PR_3), starting from diruthenium nonahalides, $K_3[Ru_2X_9]$. Through the investigation of the electrochemistry, near-IR spectra and EPR spectra of the electrogenerated mixed-valence binuclear systems, we find that these complexes with various AsR_3 and PR_3 terminal ligands clearly belong within a continuum of electronic behaviour. Within this series of $[Ru_2(\mu\text{-}X)_3L_6]^{2+}$ complexes, the energy of the $\sigma \rightarrow \sigma^*$ transition spans a remarkable range from 17 000 cm^{-1} to below 5000 cm^{-1}, with the capping ligands ranked as follows: L = NR_3 (and Me_3tacn) > H_2O > Cl, Br > AsR_3 > PR_3. This work has placed the long-standing mixed-valence PR_3 systems in a proper context as delocalised mixed-valence complexes and it has clarified the implications of their non-classical near-IR spectra.

There is considerable circumstantial evidence that the $[Ru_2(\mu\text{-}X)_3(PR_3)_6]^{2+}$ complexes are close to the point of being localised mixed-valence systems. This evidence includes the smooth progression in electrochemical behaviour connecting $[Ru_2(\mu\text{-}X)_3(PR_3)_6]^{2+}$ with compounds of the more general stoichiometry $[(PR_3)_{3-x}Cl_xRu(\mu\text{-}Cl)_3RuX_y(PR_3)_{3-y}]$, even though the latter are localised whenever $y \neq x$. In addition, the spectra of the 10-e $[Ru_2(\mu\text{-}X)_3(PR_3)_6]^{3+}$ complexes exhibit an intense, narrow band near 10 000 cm^{-1} which is associated with a localised binuclear $d^5 \cdots d^5$ configuration. It is not surprising that localisation occurs in the higher oxidation state, as the d-orbitals contract. However, the characteristic band at 10 000 cm^{-1} is not observed for the corresponding AsR_3-capped complexes (whose spectra resemble those

of the delocalised 10-e $[Ru_2(\mu\text{-}X)_3(NR_3)_6]^{3+}$ complexes), where the $\sigma \rightarrow \sigma^*$ band is still observed, but shifted to greater than 20 000 cm^{-1} due to additional electron-electron correlation energy.

The voltammetric properties of $[(PR_3)_3Ru(\mu\text{-}X)_3Os(PR_3)_3]^+$ complexes compared with those of the corresponding $\{Ru_2\}^+$ and $\{Os_2\}^+$ systems provide separate evidence of the marginal influence of Ru···Ru interaction. In each $\{RuOs\}^+$ complex, the first (osmium centred) oxidation coincides with $E_{ox}(1)$ in the $\{Os_2\}^+$ analogue while the more difficult (ruthenium centred) oxidation coincides with $E_{ox}(2)$ in the $\{Ru_2\}^+$ analogue. The heterobimetallic complexes are necessarily localised in the 11-e state, so the simple, transferrable nature of the electrode-potentials confirms the marginal influence of the prospective hemi-bond in the parent $\{Ru_2\}^{2+}$ phosphine-capped systems. It would be interesting to investigate the behaviour of NR_3- or AsR_3-capped heterobimetallic complexes, particularly as to whether the presence of these ligands shift the redox potentials compared with analogous $\{Ru_2\}^+$ and (hypothetical) $\{Os_2\}^+$ complexes.

Contrary to expectations we believe that the diosmium phosphine complexes are electronically trapped. The added stabilisation of much greater single-ion spin-orbit coupling on Os^{3+} provides a driving force to resist delocalisation and transform the $\{Os_2\}^{2+}$ species from class III to class II systems. The absence of a three-electron hemi-bond would explain the unexpected similarity of the metal-metal separation in the crystal structures of $[Os_2(\mu\text{-}Cl)_3(PEt_3)_6]^+$ and $[Os_2(\mu\text{-}Cl)_3(PEt_3)_6]^{2+}$, where the Os···Os separation is 3.473(1) Å and 3.406(1) Å respectively. It would also explain the unexpected contraction in $\Delta E_{1/2}$ for the $\{Os_2\}^{2+}$ systems, relative to their $\{Ru_2\}^{2+}$ analogues, noted earlier. The electronic spectra of the 11-e diosmium species is then dominated by single-ion inter-configurational bands characteristic of the localised Os^{III} centre, and multiple IVCT bands (as a result of transitions into inter-configurational bands of the excited $[Os^{II}Os^{III}]^*$ state).

This proposition (that the 11-e diruthenium systems are delocalised whereas their osmium analogues may be trapped) underscores the electronic subtlety of this general class of confacial binuclear complexes. Given the enforced proximity of the two halide-bridged metal ions, the limiting physical properties of such notionally trapped confacial systems are of keen interest. Inevitably, there will be a domain which is transitional between the two descriptions. It should be possible to generate genuine diosmium "blues", with classical near-IR spectra, by replacing PR_3 by NR_3 (or possibly by AsR_3), though these targets have proved synthetically elusive to date.† Equally, it may be possible to induce electronic trapping in symmetric diruthenium systems by the introduction of more electron-withdrawing ligands. Oxidation to the 11-e state becomes more difficult as more electron-withdrawing ligands are introduced, but our projections suggest the trapped state might be approached without an impossibly high elecrogeneration potential.

This thesis embodies the integration of strategic synthesis with voltammetry, optical spectra, EPR spectra, crystallography and electronic-structure computation. In this way the research has brought about the integration of wide-ranging information on a large and instructive family of compounds, and has resolved long-standing difficulties. The 11-e confacial bioctahedral system provides an ideal framework for the systematic modulation of mixed-valency. It is hoped that these findings will form part of continued investigations into mixed-valence systems.

---

†See especially pages 136 - 137